

Identification and functional analysis of
proteins involved in host cell cytosol
uptake of the human malaria parasite
Plasmodium falciparum

-DISSERTATION-

with the aim of achieving a doctoral degree at the Faculty of
Mathematics, Informatics and Natural Sciences
Department of Biology
University Hamburg

submitted by
Ricarda Sabitzki

Hamburg, 2022



Datum der Disputation: 01.07.2022

1. Gutachter der Dissertation: Dr. Tobias Spielmann

2. Gutachter der Dissertation: Prof. Dr. Tim-Wolf Gilberger

Vorsitz der Prüfungskommission: Prof. Dr. Julia Kehr

Eidesstattliche Versicherung

Hiermit erkläre ich an Eides statt, dass ich die vorliegende Dissertationsschrift selbst verfasst und keine anderen als die angegebenen Quellen und Hilfsmittel benutzt habe.



Hamburg, den 20.05.2022

Ricarda Sabitzki

Language certificate

I am a native speaker, have read the present PhD thesis and hereby confirm that it complies with the rules of the English language.



Hamburg, den 20.05.2022

Isabelle Henshall

Summary

Malaria is a life-threatening disease caused by apicomplexan parasites. *Plasmodium falciparum* is the causative agent of the severest form of human malaria and is responsible for most malaria-related deaths. The pathology of human malaria is caused exclusively by the asexual blood cycle of the parasite and is based on the development of these parasites within red blood cells of the host. Although significant strides have been made toward malaria eradication over the past two decades, progress has stalled recently. In particular, the rise and spread of resistance against antimalarial drugs are of great concern. Critical to the mode of action of several antimalarial drugs (e.g. artemisinin) is an intact endocytosis process by which the parasite takes up host cell hemoglobin and transports it to its site of degradation, the digestive vacuole (DV). This host cell cytosol uptake (HCCU) process is crucial for the parasite to obtain nutrients, as hemoglobin is an important source of amino acids. HCCU is also important to generate space for parasite growth within red blood cells and to maintain osmotic stability. However, endocytosis in blood stages encounters special challenges arising from the unique environment in which the parasite resides. The parasites develop surrounded by a milieu of high protein density consisting mainly of hemoglobin, from which they are separated not only by their plasma membrane but also by an additional membrane, the parasitophorous vacuolar membrane. Although HCCU has long been known to be a crucial endocytic process, it is hitherto poorly understood. Only recently, the first proteins involved in this process have been identified, leaving the exact mechanism of HCCU still speculative.

Work from model organisms established that endocytosed material gets transported along the endosomal pathway. After initiation of endocytosis which results in an endocytic vesicle, the internalized material is transported via early and late endosomes to the lysosome for degradation. Each of these steps is distinct in terms of associated structures and molecules. In this work, proteins of different steps of HCCU of the malaria parasite were identified, characterized, and functionally analyzed.

An unusual structure called the cytostome, an invagination of both membranes surrounding the parasite and filled with host cell cytosol, is associated with the initiation of endocytosis in the parasite. Interestingly, the artemisinin resistance-associated Kelch13 (K13) protein and its K13-interacting candidates (KICs) are present in the

same cellular compartment and several of them were linked to endocytosis. K13 colocalizes with some proteins that are typical for the initiation of endocytosis, such as AP-2 μ . The adaptin AP-2 μ is part of a heterotetrameric adaptor complex typically involved in Clathrin-mediated endocytosis. However, Clathrin is absent from the initiation site in *P. falciparum* parasites, indicating AP-2-dependent but Clathrin-independent initiation, a type of endocytosis that hitherto has been rarely described.

In this work, the adaptins AP-2 α , AP-2 β 1/2, and AP-2 σ of *P. falciparum* were investigated and differences in the protein domains compared to model organisms were identified. Inactivation of the individual adaptins by the use of different conditional systems showed their essentiality for the growth of blood stages and indicated that the AP-2 complex is required for HCCU, as suggested by previous work with AP-2 μ . The β -adaptin, which typically mediates the binding to Clathrin, was found to localize at the K13 compartment as well as at the Golgi apparatus. This confirms its suspected dual localization as part of AP-2 and the Golgi trafficking-associated AP-1 complex and it hence can be designated as AP-1/2 β . While Clathrin is absent from the early endocytosis site, it is present at the Golgi- apparatus of the parasite. In AP-1/2 β , a Clathrin binding motif was identified. However, this region was not within the hinge region, where it is typically located, but within the trunk domain of the protein. This could possibly account for the different Clathrin binding affinities of AP-1/2 β in the two different adaptor complexes. Another peculiarity are unconventional hydrophobic regions predicted as potential transmembrane domains present in AP-2 α and AP-2 σ . A resultant stronger association of the AP-2 complex with the plasma membrane than usual was supported by the inability of complete mislocalization of AP-2 σ from its site of action with our conditional inactivation system and may indicate a more permanent association at endocytosis initiation sites, due to a lacking need for reversible membrane association regulating cargo dependent uptake.

The first essential protein identified in the parasite's HCCU, termed *PVPS45*, is part of a complex fusion-machinery located at early endosomes in mammals, where it is linked to Rab5 via the Rab5 effector protein Rabenosyn5 (Rbsn5). Previous work showed that conditional inactivation of *PVPS45* and *PfRab5b*, but not *PfRab5a*, in the parasites leads to the accumulation of hemoglobin-filled vesicles with endosomal features in the parasite cytosol, suggesting that both proteins play a role in the same HCCU step downstream of endocytosis initiation. In this work, a putative plasmodial Rbsn5 was identified, which up to now had been elusive in malaria parasites when searched using

computational methods. Conditional inactivation of *PfRbsn5* in trophozoite-stage parasites resulted in the accumulation of hemoglobin-filled vesicular structures positive for the early endosomal marker PI3P, prevented the transport of internalized host cell cytosol to the DV, and led to parasite death. Overall, a phenotype similar to that previously observed after the inactivation of *PfVPS45* and *PfRab5b* was evident. Localization studies revealed that *PfVPS45*, together with *Rbsn5*, was located at *PfRab5b*-positive membranes within the parasite and that localization of these proteins was altered by the inactivation of *PfRbsn5*. Co-immunoprecipitation experiments showed that *PfRab5b* and *PfVPS45* are interaction partners of *PfRbsn5*. These data provide strong evidence that the Rab5-Rbsn5-VPS45-SNARE fusion complex in *P. falciparum* - and thus this step of the canonical endosomal pathway - is evolutionarily conserved. A newly established system that enables simultaneous conditional inactivation of the endosomal protein *Rbsn5* together with the early endocytosis protein *KIC7* provided evidence that the host cell cytosol content of these vesicles originated from the Kelch13-defined compartment that feeds into a more conserved endosomal delivery process to the DV. These findings for the first time establish a possible link between endocytosis initiation and early endosomal structures in the parasite. However, experiments with late-stage parasites indicated that *VPS45* was additionally repurposed for functions in the secretory pathway in schizonts and seemed to be critical for IMC formation. This suggests that the Rab5-Rbsn5-VPS45-SNARE complex may have additional functions.

In a next step, it was attempted to establish the route of endocytic transport using a potential marker. It is known that the aspartic protease Plasmepsin II (PMII) is involved in proteolytic hemoglobin degradation in the DV. It was previously proposed that PMII is trafficked via the secretory pathway to the cytostome, from where it gets transported alongside hemoglobin to the DV. However, no evidence was found in this work that the plasma membrane or cytostome are involved in the delivery process. Inactivation of *Rbsn5* and *VPS45* indicated that PMII is present in or at the accumulating endosomal structures and led to a reduction of PMII reaching the DV. While the assays used may not have been sensitive enough to see transport via the cytostome, the data obtained nevertheless favored the hypothesis that PMII gets transported from the Golgi/ER to the DV directly via the endosomes. This raised the possibility that proteins destined for the DV use a more direct transport route than previously suspected. It also indicated that PMII may not be suitable to visualize the full endocytic route.

The maturation model states that early endosomes mature into late endosomes and a key step in endosome maturation is the conversion from Rab5 to Rab7 at the endosomal compartment. However, Rab7 is also assumed to regulate the autophagosome-lysosome fusion step during autophagy. Here *P. falciparum* Rab7 was analyzed. Rab7 displayed circular signals, near the DV in trophozoites that surrounded structures visible in the DIC images. These structures potentially could represent late endosomes or autophagosomes. Localization of Kelch13 in the proximity of this compartment might indicate an interception of early endocytosis and late endocytosis or autophagy. Although conditional inactivation by mislocalization of Rab7 was incomplete, it revealed an essential function, at least for schizont formation, hinting at a potential repurposed function of Rab7 in late-stage parasites.

The data in this thesis provides insights for a broader understanding of the HCCU process at different steps and revealed that a hybrid of unconventional and conserved components contributes to the endosomal pathway in *P. falciparum* parasites.

Zusammenfassung

Malaria ist eine lebensbedrohliche Krankheit, die durch zu den Apikomplexa gehörenden Parasiten verursacht wird. *Plasmodium falciparum* ist der Erreger der schwersten Form der menschlichen Malaria und ist für die meisten malariabedingten Todesfälle verantwortlich. Die Pathologie der menschlichen Malaria wird ausschließlich durch den asexuellen Blutzyklus des Parasiten verursacht und beruht auf der Entwicklung dieser Parasiten in den roten Blutkörperchen des Wirts. Obwohl in den letzten zwei Jahrzehnten erhebliche Fortschritte bei der Ausrottung der Malaria erzielt wurden, sind die Fortschritte in letzter Zeit ins Stocken geraten. Insbesondere die Zunahme und Ausbreitung von Resistenzen gegen Malariamittel geben Anlass zu großer Sorge. Entscheidend für die Wirkungsweise mehrerer Malariamittel (z. B. Artemisinin) ist ein intakter Endozytoseprozess, durch den der Parasit Hämoglobin aus der Wirtszelle aufnimmt und zu seinem Abbauort, der Nahrungsvakuole (DV), transportiert. Diese Aufnahme des Wirtszellzytols (HCCU) ist für den Parasiten von entscheidender Bedeutung, um Nährstoffe zu erhalten, da Hämoglobin eine wichtige Quelle für Aminosäuren darstellt. HCCU ist auch wichtig, um Platz für das Wachstum des Parasiten im roten Blutkörperchen zu schaffen und die osmotische Stabilität aufrechtzuerhalten. Die Endozytose in Blutstadien stößt jedoch auf besondere Herausforderungen, die sich aus der einzigartigen Umgebung ergeben, in der sich der Parasit aufhält. Die Parasiten entwickeln sich in einem Milieu mit hoher Proteindichte, das hauptsächlich aus Hämoglobin besteht und von dem sie nicht nur durch ihre Plasmamembran, sondern auch durch eine zusätzliche Membran, die parasitophore Vakuolenmembran, getrennt sind. Obwohl HCCU seit langem als entscheidender endozytotischer Prozess bekannt ist, wurde er bisher nur unzureichend verstanden. Erst vor kurzem wurden die ersten an diesem Prozess beteiligten Proteine identifiziert, so dass der genaue Mechanismus von HCCU noch spekulativ ist.

Arbeiten mit Modellorganismen haben gezeigt, dass endozytiertes Material über den endosomalen Weg transportiert wird. Nach der Initiation der Endozytose, die zur Bildung eines endozytotischen Vesikels führt, wird das internalisierte Material über frühe und späte Endosomen zum Lysosom transportiert und dort abgebaut. Jeder dieser Schritte unterscheidet sich in Bezug auf die damit verbundenen Strukturen und Mole-

küle. In dieser Arbeit wurden die Proteine der verschiedenen Schritte des HCCU des Malariaparasiten identifiziert, charakterisiert und funktionell analysiert.

Eine ungewöhnliche Struktur, das so genannte Zytostom, eine Einstülpung der beiden Membranen, die den Parasiten umgeben und mit dem Zytosol der Wirtszelle gefüllt ist, wird mit der Initiation der Endozytose im Parasiten in Verbindung gebracht. Interessanterweise wurde das Artemisinin-Resistenz-assoziierte Kelch13 (K13)-Protein und sich im selben zellulären Kompartiment befindende K13 Interaktionskandidaten Proteine (KICs) mit Endozytose in Verbindung gebracht. K13 kolokalisiert mit einigen Proteinen, die für die Einleitung der Endozytose typisch sind, wie z. B. AP-2 μ . Das Adaptin AP-2 μ ist Teil eines heterotetrameren Adaptorkomplexes, der typischerweise an der Clathrin-vermittelten Endozytose beteiligt ist. In *P. falciparum* Parasiten fehlt jedoch Clathrin an der Initiationsstelle, was auf eine AP-2-abhängige, aber Clathrin-unabhängige Initiation hinweist, eine Art der Endozytose, die bisher nur selten beschrieben wurde.

In dieser Arbeit wurden die Adaptine AP-2 α , AP-2 β 1/2 und AP-2 σ von *P. falciparum* untersucht und Unterschiede in den Proteindomänen im Vergleich zu Modellorganismen identifiziert. Die Inaktivierung der einzelnen Adaptine durch die Verwendung verschiedener konditionaler Systeme zeigte ihre Unverzichtbarkeit für das Wachstum der Blutstadien und deutete darauf hin, dass der AP-2-Komplex für HCCU erforderlich ist, wie frühere Arbeiten mit AP-2 μ nahelegten. Das β -Adaptin, das normalerweise die Bindung an Clathrin vermittelt, wurde sowohl im K13-Kompartiment als auch im Golgi-Apparat lokalisiert. Dies bestätigt seine vermutete duale Lokalisierung als Teil des AP-2 und des Golgi-Trafficking-assoziierten AP-1-Komplexes und es kann daher als AP-1/2 β bezeichnet werden. Während Clathrin am Ort der frühen Endozytose fehlt, ist es hingegen am Golgi-Apparat des Parasiten vorhanden. In AP-1/2 β wurde ein Clathrin-Bindungsmotiv identifiziert. Allerdings befand sich diese Region nicht in der Scharnierregion, wo sie normalerweise zu finden ist, sondern in der Rumpfdomäne des Proteins. Dies könnte möglicherweise eine Erklärung für die unterschiedlichen Clathrin-Bindungsaffinitäten von AP-1/2 β in den beiden verschiedenen Adaptorkomplexen sein. Eine weitere Besonderheit sind unkonventionelle hydrophobe Regionen, die als potentielle Transmembrandomänen in AP-2 α und AP-2 σ vorhergesagt wurden. Eine daraus resultierende stärkere Assoziation des AP-2-Komplexes mit der Plasmamembran als üblich wurde durch die Unmöglichkeit einer vollständigen Fehllokalisierung von AP-2 σ von seinem Wirkungsort mit unserem konditionalen Inaktivierungssystem unterstützt

und könnte auf eine dauerhaftere Assoziation an der Initiationsstellen der Endozytose hindeuten, da die Notwendigkeit einer reversiblen Membranassoziation zur Regulierung der Fracht-abhängigen Aufnahme fehlt.

Das erste im HCCU des Parasiten identifizierte essenzielle Protein, *PfVPS45*, ist Teil einer komplexen Fusionsmaschine, die bei Säugetieren an frühen Endosomen lokalisiert ist, wo es über das Rab5-Effektorprotein Rabenosyn5 (Rbsn5) mit Rab5 verlinkt ist. Frühere Arbeiten haben gezeigt, dass die konditionale Inaktivierung von *PfVPS45* und *PfRab5b*, nicht aber von *PfRab5a*, in den Parasiten zur Anhäufung von Hämoglobin gefüllten Vesikeln mit endosomalen Merkmalen im Zytosol der Parasiten führt, was darauf hindeutet, dass beide Proteine eine Rolle in dem auf die Endozytose-Initiierung folgenden HCCU-Schritt spielen. In dieser Arbeit wurde ein putatives plasmodiales Rbsn5 identifiziert, das bisher in Malariaparasiten bei der Suche mit computergestützten Methoden nicht auffindbar gewesen war. Die konditionale Inaktivierung von *PfRbsn5* in Parasiten im Trophozitenstadium führte zur Anhäufung von mit Hämoglobin gefüllten vesikulären Strukturen, die positiv für den frühen endosomalen Marker PI3P waren, verhinderte den Transport von internalisiertem Wirtszellzytosol zur DV und führte zum Tod des Parasiten. Insgesamt zeigte sich ein ähnlicher Phänotyp wie der, der zuvor nach der Inaktivierung von *PfVPS45* und *PfRab5b* beobachtet wurde. Lokalisierungsstudien zeigten, dass *PfVPS45* zusammen mit Rbsn5 an *PfRab5b*-positiven Membranen innerhalb des Parasiten lokalisiert war und dass die Lokalisierung dieser Proteine durch die Inaktivierung von *PfRbsn5* verändert wurde. Ko-Immunopräzipitationsexperimente zeigten, dass *PfRab5b* und *PfVPS45* Interaktionspartner von *PfRbsn5* sind. Diese Daten sind ein starker Hinweis dafür, dass der Rab5-Rbsn5-VPS45-SNARE-Fusionskomplex in *P. falciparum* - und damit dieser Schritt des kanonischen endosomalen Weges - evolutionär konserviert ist. Ein neu etabliertes System, das die gleichzeitige konditionale Inaktivierung des endosomalen Proteins Rbsn5 zusammen mit dem frühen Endozytoseprotein KIC7 ermöglicht, lieferte Evidenz, dass diese induzierten Vesikel aus dem von Kelch13 definierten Kompartiment stammt, welches in einen konservierteren endosomalen Transportprozess zur DV gebracht wird. Diese Ergebnisse stellen erstmals eine mögliche Verbindung zwischen der Einleitung der Endozytose und frühen endosomalen Strukturen im Parasiten her. Experimente mit späten Blutstadien des Parasiten (Schizonten) zeigten jedoch, dass VPS45 in diesen Stadien zusätzlich für Funktionen im sekretorischen Weg umfunktioniert wurde und für die IMC-Bildung entscheidend zu sein scheint. Dies deutet darauf hin, dass der Rab5-Rbsn5-VPS45-SNARE-Komplex zusätzliche Funktionen haben könnte.

In einem nächsten Schritt wurde versucht, den Weg des endozytären Transports mit Hilfe eines potentiellen Markers zu verfolgen. Es ist bekannt, dass die Aspartatprotease Plasmepepsin II (PMII) am proteolytischen Hämoglobinabbau in der DV beteiligt ist. Früher wurde vorgeschlagen, dass PMII über den sekretorischen Weg zum Zytostom transportiert wird, von wo aus sie zusammen mit Hämoglobin in die DV gelangt. In dieser Arbeit wurden jedoch keine Hinweise dafür gefunden, dass die Plasmamembran oder das Zytostom am Transportprozess von PMII beteiligt sind. Die Inaktivierung von Rbsn5 und VPS45 deutete darauf hin, dass PMII in oder an den sich ansammelnden endosomalen Strukturen auftaucht, und führte zu einer Verringerung der PMII-Menge, die die DV erreicht. Obwohl die verwendeten Testverfahren möglicherweise nicht empfindlich genug waren, um den Transport über das Zytostom zu erkennen, sprachen die erhaltenen Daten dennoch für die Hypothese, dass PMII direkt über die Endosomen vom Golgi/ER zur DV transportiert wird. Dies deutete auf die Möglichkeit hin, dass Parasitenproteine, die für die DV bestimmt sind, einen direkteren Transportweg nutzen als bisher angenommen. Es deutet auch darauf hin, dass PMII möglicherweise nicht geeignet ist, den gesamten endozytotischen Weg zu visualisieren.

Das Reifungsmodell besagt, dass frühe Endosomen zu späten Endosomen reifen, und ein wichtiger Schritt bei der Endosomenreifung ist die Umwandlung von Rab5 in Rab7 im endosomalen Kompartiment. Es wird jedoch angenommen, dass Rab7 auch den Schritt der Autophagosom-Lysosom-Fusion während der Autophagie reguliert. Hier wurde das *P. falciparum* Rab7 analysiert. Rab7 zeigte kreisförmige Signale in der Nähe der DV in Trophozoiten, die Strukturen umgaben, die in den DIC-Bildern sichtbar waren. Bei diesen Strukturen könnte es sich um späte Endosomen oder Autophagosomen handeln. Die Lokalisierung von Kelch13 in der Nähe dieses Kompartiments könnte auf eine Kreuzung der Wege der frühen Endozytose und der späten Endozytose oder Autophagie hinweisen. Obwohl die konditionale Inaktivierung durch Fehllokalisierung von Rab7 unvollständig war, zeigte sie eine für den Parasiten wichtige Funktion, zumindest für die Schizontenbildung, was auf eine potentielle neue Funktion von Rab7 bei Parasiten in späten Blutstadien hindeutet.

Die in dieser Arbeit gewonnenen Daten liefern Einblicke, die ein umfassenderes Verständnis des HCCU-Prozesses in verschiedenen Schritten ermöglichen und zeigen, dass sowohl unkonventionelle als auch konservierte Komponenten zum endosomalen Transportweg in *P. falciparum* Parasiten beitragen.

Table of contents

Eidesstattliche Versicherung	III
Language certificate	IV
Summary	V
Zusammenfassung	IX
Table of contents	XIII
List of figures	XIX
List of tables	XXI
Abbreviations	XXII
1 Introduction	25
1.1 Malaria- Overview	25
1.2 Epidemiology	26
1.3 Life cycle of <i>Plasmodium falciparum</i>	29
1.3.1 Mosquito stages	30
1.3.2 Liver stages	30
1.3.3 Blood stages.....	31
1.4 Pathophysiology and clinical presentation	32
1.4.1 Asymptomatic and uncomplicated malaria.....	33
1.4.2 Severe malaria	33
1.4.3 Malaria high-risk groups	34
1.5 Diagnostics	36
1.6 Anti-malarial drugs and drug resistance	37
1.6.1 Drugs.....	37
1.6.2 Drug resistance	38
1.7 Vaccine development	39
1.7.1 Pre-erythrocytic anti-infection vaccines.....	39
1.7.1.1 Subunit vaccines: RTS,S and R21/Matrix-M	40
1.7.1.2 Whole sporozoite vaccines	42
1.7.2 Blood-stage vaccines	43
1.7.3 Transmission-blocking vaccines	44
1.8 Cell Biology	44
1.8.1 Systematic classification.....	44
1.8.2 Specific organelles of <i>Plasmodium</i> spp.	44

1.8.3	Apical complex and inner membrane complex.....	45
1.8.4	Parasitophorous vacuole	46
1.8.5	Apicoplast.....	46
1.8.6	Digestive vacuole	47
1.9	Endocytosis.....	48
1.9.1	Endosomal pathway	48
1.9.1.1	Different endocytosis mechanisms	49
1.9.1.2	Early endosome.....	52
1.9.1.3	Late endosome.....	54
1.9.1.4	Lysosome	54
1.10	Endocytosis in <i>P. falciparum</i> parasites	55
1.10.1	Host cell cytosol uptake in <i>P. falciparum</i> parasites	55
1.10.1.1	Initiation of endocytosis associated structures and proteins in HCCU.....	57
1.10.1.2	Early endosome associated structures and proteins in HCCU	60
1.10.1.3	Late endosome associated structures and proteins in HCCU	62
1.11	Aim of Thesis.....	63
2	Materials and Methods.....	64
2.1	Materials.....	64
2.1.1	Chemicals.....	64
2.1.2	Kits.....	67
2.1.3	DNA and protein ladders	67
2.1.4	Solutions, buffer and media	68
2.1.4.1	Microbiological culture	68
2.1.5	Solutions and buffers for molecular biology analyses	70
2.1.5.1	DNA gel electrophoresis	70
2.1.5.2	DNA precipitation.....	70
2.1.5.3	Gibson assembly	71
2.1.6	Media and solutions for cell biology experiments.....	71
2.1.6.1	<i>P. falciparum</i> in vitro culture.....	71
2.1.6.2	Solutions for cell biology and biochemical assays.....	74
2.1.7	Buffers and solutions for protein analyses	75
2.1.7.1	SDS-Page and Western Blot	75
2.1.8	Bacterial and <i>Plasmodium</i> strains.....	77
2.1.9	Enzymes and antibodies.....	78
2.1.9.1	Polymerases.....	78
2.1.9.2	Restriction enzymes	78
2.1.9.3	Primary antibodies	79
2.1.9.4	Secondary antibodies	80
2.1.9.5	Streptavidin beads	80
2.1.9.6	Oligonucleotides	80
2.1.9.7	General plasmids.....	81

2.1.10	Sequencing	81
2.1.11	Technical devices	82
2.1.12	Labware and disposables	84
2.1.13	Computer Software.....	85
2.1.14	Databases and online sources.....	86
2.2	Methods	87
2.2.1	Molecular biology methods	87
2.2.1.1	Polymerase chain reaction (PCR).....	87
2.2.1.2	Purification of PCR products and digested vectors	88
2.2.1.3	Digestion of PCR products and vectors	88
2.2.1.4	Gibson assembly	88
2.2.1.5	Colony PCR screen to detect bacterial clones	89
2.2.1.6	Sequencing of plasmid DNA	89
2.2.1.7	Isolation of genomic DNA	89
2.2.1.8	PCR to verify genome integration	90
2.2.1.9	Agarose gel electrophoresis	90
2.2.2	Microbiological methods	90
2.2.2.1	Transformation of <i>E.coli</i> chemo competent cells.....	90
2.2.2.2	Cultivation and storage of <i>E. coli</i> transgenic cells	91
2.2.2.3	Purification of bacterial plasmids (Mini Prep and Midi Prep).....	91
2.2.3	Cell biological methods.....	91
2.2.3.1	Cell culture of <i>P. falciparum</i>	91
2.2.3.2	Blood smears and Giemsa staining.....	92
2.2.3.3	<i>P. falciparum</i> cryo-stabilates	92
2.2.3.4	Parasite synchronization with Sorbitol.....	92
2.2.3.5	Differential purification of <i>P. falciparum</i> infected erythrocytes in a Percoll gradient.....	93
2.2.3.6	Transfection of <i>P. falciparum</i>	93
2.2.3.7	Selection linked integration (SLI)	94
2.2.3.8	Knock-sideway of target protein using the FKBP-FRB* system.....	95
2.2.3.9	SLI-based conditional deletion using <i>diCre-mediated gene excision</i>	96
2.2.3.10	Growth assays with synchronized parasites using conditional inactivation systems.....	98
2.2.3.11	Flow cytometry growth assay.....	98
2.2.3.12	Vesicle accumulation assay	99
2.2.3.13	Bloated food vacuole assay	99
2.2.3.14	Preloading of red blood cells and infection of preloaded cells	99
2.2.3.15	IFAs with formaldehyde- and glutaraldehyde-fixed cells performed in suspension.....	100
2.2.3.16	Hemoglobin Immunofluorescence Assay	100
2.2.3.17	Isolation of parasites by saponin lysis and protein extraction	101
2.2.4	Biochemical methods	101

2.2.4.1	Sodium dodecyl sulphate- polyacrylamide gel electrophoresis (SDS PAGE).....	101
2.2.4.2	Western blot	102
2.2.4.3	Immunodetection of proteins.....	102
2.2.4.4	Dimerization induced in vitro proximity biotinylation of interacting proteins (DiQ-BioID)	103
2.2.4.5	In-cell DSP cross-linking and co-immunoprecipitation (CoIP)	104
2.2.5	Microscopy	105
2.2.5.1	Optical light microscope.....	105
2.2.5.2	Fluorescence microscope	105
2.2.5.3	Transmission electron microscopy (TEM)	105
3	Results	106
3.1	Early- endocytosis associated proteins in HCCU	106
3.1.1	The heterotetrameric AP-2 complex in <i>P. falciparum</i>	106
3.1.1.1	AP-1/2 β of <i>P. falciparum</i>	108
3.1.1.2	AP-2 α of <i>P. falciparum</i>	114
3.1.1.3	AP-2 σ of <i>P. falciparum</i>	122
3.2	Early endosome associated structures and proteins in HCCU	129
3.2.1	Identification of the putative <i>P. falciparum</i> Rbsn5	129
3.2.2	Subcellular localization of <i>PfRbsn5</i>	132
3.2.3	Rbsn5 co-localizes with VPS45 to Rab5b positive membranes	132
3.2.4	Conditional inactivation of Rbsn5 leads to an accumulation of vesicular structures and parasite death	135
3.2.5	<i>PfRbsn5</i> is involved in HCCU	137
3.2.6	Accumulating vesicular structures upon Rbsn5 inactivation are positive for the early endosomal marker PI3P.....	139
3.2.7	Rbsn5 is essential for the delivery of internalized HCC to the DV.....	142
3.2.8	<i>PfRbsn5</i> , <i>PfRab5b</i> , and <i>PfVPS45</i> inactivation leads to the accumulation of hemoglobin filled vesicles that possess no continuous connection to the host cell	144
3.2.9	A modification of the SLI plasmid enables endogenous tagging and inactivation of Rbsn5 by a single plasmid	146
3.2.10	Inactivation of Rbsn5 ^{endo} affects VPS45 ^{epi} and Rab5b ^{epi} localization ...	148
3.2.11	Rab5b and VPS45 are interaction partners of Rbsn5	150
3.2.12	Conditional double inactivation of Rbsn5 and KIC7 leads to less vesicle accumulation	151
3.2.13	Localization of the early endocytosis associated proteins K13 and AP-2 σ is not affected upon Rbsn5 inactivation	155
3.2.14	Plasmeprin II accumulates within or at forming vesicles induced upon Rbsn5 inactivation	157
3.2.15	Evidence for the transport route of PMII to the DV.....	161
3.2.16	Biotinylation of proteins within vesicles induced upon Rbsn5 inactivation	163

3.2.17	Conditional inactivation of VPS45 in schizonts affects IMC biogenesis and indicates the presence of HCCU in the late stages of <i>P. falciparum</i>	166
3.3	Late endosome associated structures and proteins in HCCU	168
3.3.1	Rab7 of <i>P. falciparum</i> shares high similarity to its orthologue in <i>H. sapiens</i>	168
3.3.2	Subcellular localization of Rab7 in blood stages of <i>P. falciparum</i>	170
3.3.3	Rab7 is important for the development of parasite blood stages.....	172
3.3.4	Inactivation of Rab7 affects schizont formation.....	173
3.3.5	K13 is localizing close to Rab7 positive circular structures adjacent to the DV.	175
3.3.6	Rab7 positive circular structures adjacent to the DV do not overlap with hemoglobin signal.	176
4	Discussion	177
4.1	New improved tools to investigate endocytosis	177
4.2	Initiation of endocytosis in <i>P. falciparum</i> parasites.....	179
4.2.1	Components of the AP-2 adaptor complex in <i>P. falciparum</i> parasites display unique features.....	180
4.2.1.1	AP-2 α and AP-2 σ of <i>P. falciparum</i> parasites possess unusual hydrophobic regions predicted to be transmembrane domains	180
4.2.1.2	AP-2 β shows a translocated Clathrin binding box	183
4.3	Early endosome associated structures and proteins in HCCU of <i>P. falciparum</i>.....	184
4.3.1	<i>P. falciparum</i> parasites possess an evolutionarily conserved Rbsn5-VPS45-SNARE fusion complex	184
4.3.2	KIC7 is necessary for processes upstream of those resulting in the vesicles accumulating upon Rbsn5 inactivation	185
4.3.3	Plasmeprin II is transported to the DV via endosomal structures.....	186
4.3.4	VPS45 is relevant for IMC biogenesis in schizonts and HCCU is present in the late stages of <i>P. falciparum</i> parasites.....	188
4.4	Late endosome associated structures and proteins in HCCU	189
4.5	Proposed working model of HCCU in <i>P. falciparum</i> parasites.....	192
	References.....	195
	Appendix A- Oligonucleotides and Plasmids.....	221
A.1	Oligonucleotides for cloning	221
A.2	Oligonucleotides to assess correct integration	228
A.3	Plasmids.....	229
	Appendix B- Flow cytometry growth curves	231
	Appendix C- Sequence alignment.....	233
	Appendix D- Live cell images	234

Appendix E- Co-IP	235
Appendix F- Functional analysis of VPS45 in schizonts	237
List of publications	238
Danksagung.....	239

List of figures

Figure 1 Geographical distribution of malaria.	26
Figure 2 Life cycle of <i>Plasmodium falciparum</i> parasites.	29
Figure 3 Development of asexual blood stages of <i>P. falciparum</i> parasites.	31
Figure 4 Intravascular sequestrations of <i>P. falciparum</i> parasites.	34
Figure 5 Vaccine candidates that target different stages of the <i>Plasmodium</i> life cycle.	39
Figure 6 Schematic representation and comparison of RTS,S, and R21 vaccine particle design.	41
Figure 7 Schematic of organelle organization of two different <i>Plasmodium</i> spp. blood stages.	45
Figure 8 Generic scheme of the endosomal pathway.	49
Figure 9 Overview of endocytosis mechanisms.	50
Figure 10 AP-2 in Clathrin-mediated endocytosis.	52
Figure 11 Complexity of the fusion machinery of the early endosome.	53
Figure 12 Structures and proteins in HCCU of <i>P. falciparum</i> blood stages.	56
Figure 13 Localization and functional data of AP-2 μ	60
Figure 14 Scheme of PVPS45 function in <i>Plasmodium</i> blood-stage parasites.	63
Figure 15 Scheme of selection linked integration strategy and knock-sideway (Birnbaum et al., 2017).	95
Figure 16 Scheme of knock-sideway experiment.	96
Figure 17 Conditional deletion of a target gene using the diCre-based excision system.	97
Figure 18 AP-2 complex.	107
Figure 19 Comparison of predicted protein domains and motifs of PfAP-1/2 β and its orthologues.	109
Figure 20 Subcellular localization of AP-1/2 β -2xFKBP-GFP-2xFKBP ^{endo}	110
Figure 21 AP-1/2 β ^{endo} foci of <i>P. falciparum</i> co-localize with K13 ^{epi} , Grasp ^{epi} , and Clathrin-LC ^{epi} foci.	112
Figure 22 AP-1/2 β is important for the survival of <i>P. falciparum</i> blood-stage parasites.	113
Figure 23 AP-2 α of <i>P. falciparum</i> contains unusual predicted transmembrane domains.	115

Figure 24 Subcellular localization of AP-2 α -3xHA ^{endo}	117
Figure 25 Subcellular localization of N-GFP-AP-2 α ^{endo} (loxP).....	118
Figure 26 AP-2 α is important for the survival of <i>P. falciparum</i> blood-stage parasites.....	119
Figure 27 AP-2 α loss leads to a growth defect in trophozoite-staged parasites.	121
Figure 28 AP-2 σ of <i>P. falciparum</i> contains an unusual predicted transmembrane domain.....	123
Figure 29 Subcellular localization of AP-2 σ -3xHA ^{endo}	124
Figure 30 Subcellular localization of AP-2 σ -2xFKBP-GFP ^{endo}	125
Figure 31 AP-2 σ is important for the survival of <i>P. falciparum</i> blood-stage parasites.....	127
Figure 32 AP-2 σ is involved in the HCCU of <i>P. falciparum</i> blood stages.	128
Figure 33 Identification of a putative <i>P. falciparum</i> Rbsn5 protein and comparison to its homologs.....	131
Figure 34 Subcellular localization of <i>Pf</i> Rbsn5.....	133
Figure 35 Rbsn5 co-localizes with VPS45 to Rab5b positive membranes.	135
Figure 36 Inactivation of <i>Pf</i> Rbsn5 leads to accumulation of vesicular structures in the parasite cell and subsequent parasite death.	136
Figure 37 Vesicular structures after Rbsn5 or Rab5b inactivation contain material with an electron density resembling that of the host cell cytosol.....	138
Figure 38 Vesicular structures induced by inactivation of Rbsn5 contain host cell cytosol.....	139
Figure 39 Accumulating vesicular structures upon Rbsn5 inactivation are positive for the early endosomal marker PI3P.	142
Figure 40 Rbsn5, but not Sand1 and Rab5a are involved in the HCCU of <i>P. falciparum</i> blood stages.	143
Figure 41 Rbsn5, VPS45, and Rab5b inactivation induced vesicular structures are filled with hemoglobin and are not connected to the host cell cytosol.....	145
Figure 42 Modified SLI-sandwich plasmid enables endogenous tagging and mislocalization of POI.....	147
Figure 43 Inactivation of Rbsn5 ^{endo} affects VPS45 ^{epi} and Rab5b ^{epi} localization.	149
Figure 44 Rab5b and VPS45 are interacting partners of Rbsn5.	150
Figure 45 Conditional double inactivation strategy.....	153
Figure 46 Conditional double inactivation of Rbsn5 and KIC7 leads to less vesicle accumulation.....	154

Figure 47 Inactivation of Rbsn5 does not affect the localization of early endocytosis proteins K13 and AP-2 σ	156
Figure 48 PMII localizes to the DV and the ER.	158
Figure 49 PMII is enriched upon conditional inactivation of VPS45 and Rbsn5 in the region of accumulating vesicles.	161
Figure 50 Plasmepsin II does not co-localize with the early endocytosis-associated protein AP-2 σ	162
Figure 51 Biotinylation of proteins within vesicles induced upon Rbsn5 inactivation.	165
Figure 52 VPS45 plays a role in IMC biogenesis.	167
Figure 53 Rab7 of <i>P. falciparum</i> shares high similarity to its orthologue in <i>H. sapiens</i>	169
Figure 54 Analysis and subcellular localization of N-2xFKBP-GFP-2xFKBP-Rab7 ^{endo}	171
Figure 55 Rab7 is important for the survival of <i>P. falciparum</i> blood-stage parasites.	172
Figure 56 Synchronous parasites with partially mislocalized Rab7 develop to malformed schizont-stages and fail to enter the next cycle.	174
Figure 57 K13 localizes in close proximity to Rab7 positive circular structures at the DV.	176
Figure 58 Rab7 positive circular structures adjacent to the DV do not overlap with hemoglobin signal.	176
Figure 59 Proposed working model of HCCU in <i>P. falciparum</i>	194

List of tables

Table 1 Standard mix for preparative and analytical PCRs and thermocycling settings.	87
Table 2 Standard mix for preparative DNA digestion.	88
Table 3 Standard mix for Gibson DNA assembly.	89

Abbreviations

ACTs	Artemisinin Combination Therapies
AMA1	antigen 1
AP-2	adaptor protein 2 complex
ART	Artemisinin
ATG8	autophagy-related-protein-8
CME	Clathrin-mediated endocytosis
CPS	sporozoites applied under chemoprophylaxis
CQ	chloroquine
CSA	chondroitin sulfate A
diCre	dimerisable Cre-recombinase
DV	digestive vacuole
EBA-175	erythrocyte-binding antigen 175
EE	early
EEA1	early endosomal antigen 1
EMA	European Medicine Agency
ER	endoplasmic reticulum
ESCRT	endosomal sorting complex required for transport
EV	endocytic vesicles
FCP	FYVE-containing protein
FV	food vacuole
GAS	genetically attenuated sporozoites
GEF	guanine exchange factor

GSK	GlaxoSmithKline
Hb	hemoglobin
h.p.i.	hours post-invasion
HRP2	histidine-rich protein 2
HZ	hemozoin
ILVs	intraluminal vesicles
iRBC	infected RBC
IRS	indoor residual spraying
ITNs	insecticide-treated nets
K13	Kelch13
KICs	K13-interacting candidates
L	lysosome
LE	late endosomes
LIR	LC3-interacting region
MVB	multivesicular body
MVIP	Malaria Vaccine Implementation Program
NLS	Nuclear localization signal
PCR	polymerase chain reaction
<i>pfcr</i>	chloroquine resistance transporter gene
<i>PfEMP1</i>	<i>Plasmodium falciparum</i> erythrocyte membrane protein 1
<i>pfmdr1</i>	<i>Plasmodium falciparum</i> multidrug resistance gene 1
<i>PfSPZ</i>	<i>P. falciparum</i> sporozoites
PI3P	phosphatidylinositol-3-phosphate
PIP2	phosphatidylinositol 4,5-bisphosphate
PM	plasma membrane

PMII	plasmepsin II
PPM	plasma membrane
proPMII	plasmepsin II proenzyme
PV	parasitophorous vacuole
PVM	parasitophorous vacuole membrane
PYR	pyrimethamine
RAS	radiation attenuated sporozoites
RBC	red blood cell
Rbsn5	Rabenosyn-5
RDTs	rapid diagnostic tests
RE	recycling endosome
Rh5	reticulocyte-binding protein homolog 5
SIPL	Serum Institute of India Pvt Ltd.
SM	Sec1/Munc18-like
SNARE	soluble N-ethylmaleimide-sensitive factor protein receptors - mediated fusion events
TGN	trans-Golgi network
TVN	tubovesicular network
uRBCs	uninfected red blood cells
WRAIR	Walter Reed Army Institute of Research
WSV	whole sporozoite vaccines

1 Introduction

1.1 Malaria- Overview

Malaria is a mosquito-borne tropical disease caused by apicomplexan protozoan parasites of the genus *Plasmodium*. The unicellular eukaryote is transmitted through the bite of a female *Anopheles* mosquito to vertebrate hosts that range from reptiles and birds to mammals. Out of 200 described *Plasmodium* species only five - *P. falciparum*, *P. vivax*, *P. malariae*, *P. ovale*, and *P. knowlesi* - can infect humans. Out of those, *Plasmodium falciparum* is the most virulent species, responsible for most malaria-related complications and deaths.

The causative agent of malaria was identified in 1880 by Alphonse Charles Laveran after he for the first time microscopically observed the parasites in the blood of soldiers in Algeria who were suffering from a febrile disease, previously assumed to be caused among other ideas by 'bad air' ('*mal'aria*' in Medieval Italian) in marshy districts. However, knowledge of malaria is even older than its name. Clinical symptoms suggestive of malaria have already been reported as a severe health problem since the earliest ancient times and malaria has since had a devastating impact on numerous individual lives, families, and entire societies. Until today malaria remains endemic in 87 countries throughout the tropical and subtropical zones. With 94% of malaria cases and deaths in 2019, Africa carries a disproportionately high global malaria burden (WHO, 2020b).

Although substantial improvement has been made in the last two decades in reducing the incidence and mortality of malaria, progress has recently stalled and the emergence and spread of parasite drug and mosquito insecticide resistance have become a global concern. In addition, the ongoing COVID-19 pandemic and climate change could pose a threat to the already gained achievements (WHO, 2020a). Therefore, malaria continues to be a major global public health and substantial socio-economic burden, stressing the necessity of continued efforts in prevention and control and highlighting the importance of further malaria research.

1.2 Epidemiology

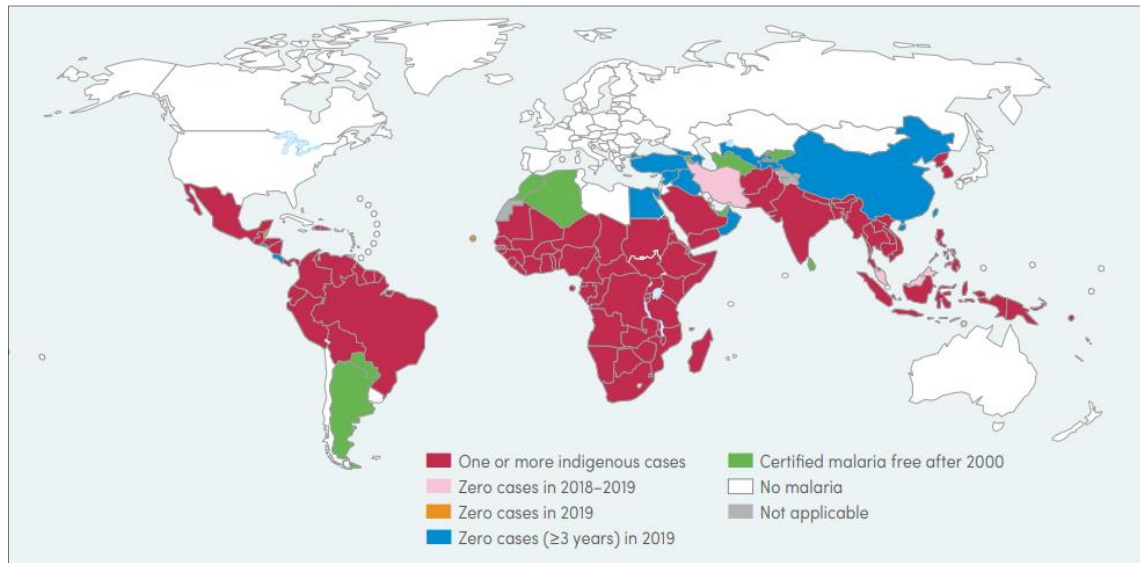


Figure 1 | Geographical distribution of malaria. Countries with indigenous cases in 2000 and their status by 2019 (WHO, 2020b).

Even though malaria is a preventable and mostly treatable disease, it still claims numerous lives each year. According to the latest global malaria report, 229 million malaria cases were estimated worldwide in 2019, resulting in 409 000 deaths (WHO, 2020b). Malaria can only occur in parts of the world that provide suitable climate conditions for both, the replication of its *Anopheles* vector species and for the successful development of the malaria parasites in those mosquitoes. As warm temperature, high humidity, and sufficient rainfalls are crucial factors (Mohammadkhani et al., 2016) malaria is mainly transmitted in tropical and subtropical areas (Figure 1). It is primarily endemic in large parts of Africa, South-East Asia, Eastern Mediterranean, and Central, and South America (Figure 1). In 2019 almost half of the world's population was at risk of contracting malaria. However, by far the most affected region was sub-Saharan Africa, with 82% of all global malaria cases and 94% of all malaria-related deaths. In that year approximately half of the malaria-related deaths worldwide occurred in just six African countries: Nigeria (23%), the Democratic Republic of the Congo (11%), the United Republic of Tanzania (5%), Burkina Faso (4%), Mozambique (4%) and Niger (4%) (WHO, 2020b). A combination of different factors is responsible for Africa's high susceptibility. Africa is home to the most effective and efficient vector species of human malaria, *Anopheles gambiae*. In addition to the high transmission rate, local climatic conditions usually allow the transmission to occur perennially. Moreover, high socio-economic

instability in many parts of these regions hampers efficient malaria control measures (CDC, 2021). This is a reciprocal effect since the consequences of high caseloads also severely hinder socio-economic development.

The major factor for the high mortality rate of malaria in Africa is the fact that the predominant parasite species on this continent is *Plasmodium falciparum*, the most virulent of the five *Plasmodium* species that can infect humans and the species responsible for the vast majority of malaria-related deaths worldwide. While *P. falciparum* leads to the most severe clinical outcomes, *Plasmodium vivax* is the most geographically widespread malaria species (Howes et al., 2016). Its development is more tolerant of lower ambient temperatures and can hence complete its lifecycle also in cooler regions of the world (Gething et al., 2011). *P. vivax* shows the highest prevalence in Southeast Asia, Latin America, and the South Pacific (Koepfli et al., 2015). However, since *P. vivax* parasites require the Duffy antigen on the red blood cell (RBC) surface for invasion and Africa has a high frequency of the Duffy-negative mutation across the human population, infections with this parasite on the African continent are infrequent (Howes et al., 2011).

Another *Plasmodium* species able to infect humans is *P. ovale*, which is most prevalent in sub-Saharan Africa but also has been reported in Asia and islands in the Western Pacific (Collins and Jeffery, 2005). *P. ovale* and *P. vivax* in general cause less severe symptoms, but share the tendency of relapsing infections. This characteristic is caused by the ability of these parasites to persist as dormant forms, called hypnozoites, in the human liver for many months, leading to reappearing infections months or even years later (Campo et al., 2015). *P. ovale* and *P. vivax* are historically referred to as 'tertian malaria', causing febrile spikes with a 48-hour rhythm. A fourth human-infecting species, *P. malariae*, is responsible for 'quartan malaria' with the typical fever interval observed every 72 hours. These fever episodes are initiated by the periodic lysis of infected RBCs (iRBC) caused by the synchronous life cycle of those parasite species (Bartoloni and Zammarchi, 2012). *P. malariae* has a low incidence but is widely distributed in most tropical and sub-tropical areas, such as the southwest Pacific, and with overlapping occurrence with *P. falciparum*, particularly in sub-Saharan Africa (Grande et al., 2019). However, due to the generally lower parasitemia of *P. malariae* and the lack of molecular techniques as a diagnostic tool (particularly in regions with high prevalence such as in sub-Saharan Africa), many infections likely stay unnoticed, and case numbers can be assumed to be underestimated (Abdulraheem et al., 2021, Lo et al.,

2017). An infection with *P. malariae* is often asymptomatic and seldom leads to severe clinical manifestations, such as the nephrotic syndrome (Bartoloni and Zammarchi, 2012).

Plasmodium knowlesi is the fifth malaria parasite causing human malaria. It occupies a unique position amongst the human-infecting *Plasmodium* species because it is adapted to Southeast Asian macaques. As a zoonotic disease, its geographical distribution is limited to the occurrence of its natural host. For this reason, it is found in Southeast Asia, especially in Myanmar. *P. knowlesi* was long assumed to rarely cross the species barrier to infect humans but is now known to account for 70% of all malaria infections in some areas. So far no transmission between human-mosquito-human has ever been reported (Davidson et al., 2019). *P. knowlesi* infection can result in severe malaria in ~10-12% of cases, resembling severe malaria caused by *P. falciparum*. Morphological similarity of *P. knowlesi* with the more benign *P. malariae* can cause misdiagnosis by routine microscopy and this can lead to delayed treatment, resulting in preventable fatality (Oresegun et al., 2021, Cox-Singh et al., 2008).

While today malaria is confined to tropical and subtropical areas, in previous times it was also prevalent in temperate areas of the northern hemisphere, including West Europe and North America. Extensive eradication programs in the middle of the last century succeeded in eliminating malaria from these zones. These programs employed a combination of insecticide spraying, drug therapy, and environmental engineering. However, it took several decades for distinct progress to be made in other parts of the world affected by malaria. Since 2000, an expansion of malaria interventions, in parallel with overall health system advances, better infrastructure, housing improvements, and rapid urbanization, has led to a tremendous global decline in malaria cases (WHO, 2020b). Vector control measures such as insecticide-treated nets (ITNs) or indoor residual spraying (IRS) were a major contributor to the success of these efforts, perhaps because they provide both, personal protection and transmission reduction (WHO, 2021a). By the end of 2019, about 1.5 billion malaria cases and nearly 7.6 million deaths had been averted since 2000. Since the beginning of the century, 21 countries have eliminated malaria and 11 have been certified malaria-free by the WHO (Figure 1). However, at the global level, progress has stagnated, and no distinct progress has been made in reducing overall malaria cases over the past five years (WHO, 2020b).

1.3 Life cycle of *Plasmodium falciparum*

During the life cycle of *Plasmodium* spp. (Figure 2), the parasites alternate between sexual development in the primary mosquito host and asexual development in the intermediary vertebrate host. *Plasmodium* parasites reside and develop not only in different species but also in distinct organs and cell types, resulting in a life cycle of great complexity. It can be subdivided into three main sections: the mosquito stages (Section 1.3.1), the human liver stages (Section 1.3.2), and the human blood stages (Section 1.3.3).

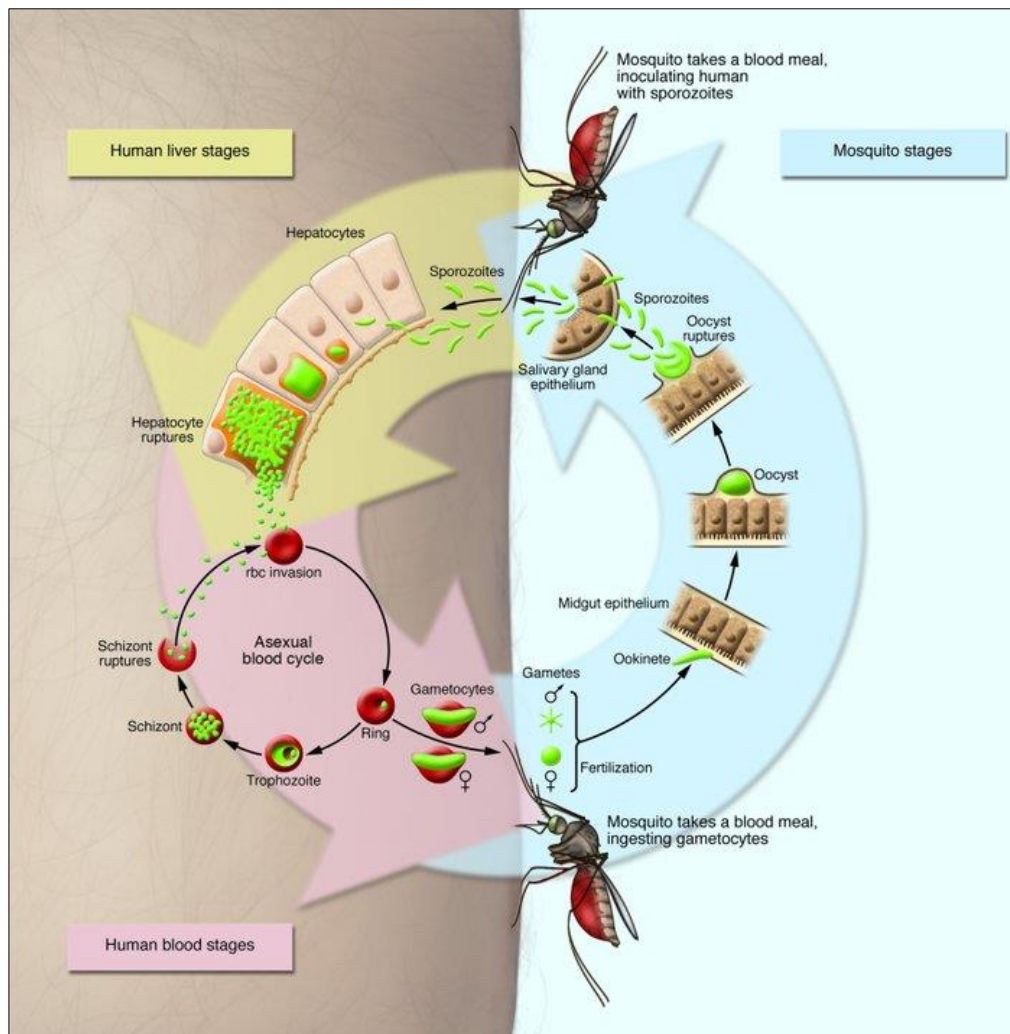


Figure 2 | Life cycle of *Plasmodium falciparum* parasites. Mosquito stages (blue arrow): Gametocytes are ingested during the blood meal of a female *Anopheles* mosquito. In the mosquito midgut, the parasites (green) undergo sexual replication, resulting in ookinetes penetrating the midgut wall. The ookinete develops into an oocyst that forms sporozoites that reach the salivary glands of the mosquito. Human liver stages (yellow arrow): Sporozoites are injected into the human host and invade hepatocytes, wherein they develop into thousands of merozoites that are released into the blood circulation (yellow arrow). Human

blood stages (pink arrow): Merozoites invade RBCs and develop from ring to trophozoite to schizont stages and new infectious merozoites are formed. A small subpopulation of parasites develops into male and female gametocytes (Neill, 2011) modified from (Greenwood et al., 2008).

1.3.1 Mosquito stages

A female *Anopheles* mosquito takes up transmissible sexual stages of the parasite, called gametocytes while feeding on an infected human. In the mosquito midgut, the male (microgametocytes) and female gametocytes (macrogametocytes) further mature into gametes and mate. The fertilized female gametes develop from a diploid zygote that undergoes meiotic division into an actively moving tetraploid stage, termed ookinete (Janse et al., 1986, Bennink et al., 2016). These elongated ookinete cells penetrate the epithelium of the mosquito's midgut and form round sessile oocysts beneath the gut basal lamina (Bennink et al., 2016). Inside the oocyst, thousands of sporozoites develop which upon rupture of the oocyst wall enter the hemolymph. Some of the sporozoites reach and invade the salivary gland of the mosquito. Upon the next blood meal of the mosquito, the sporozoites can be transmitted to the next host (Figure 2; blue arrow) (Kojin and Adelman, 2019, Frischknecht and Matuschewski, 2017).

1.3.2 Liver stages

During the blood meal of the infected mosquito, fewer than a hundred motile sporozoites are inoculated into the skin of the human host (Jin et al., 2007, Hopp et al., 2019, Rosenberg et al., 1990). The sporozoites migrate towards a blood capillary and enter the blood circulation (Amino et al., 2008, Frischknecht and Matuschewski, 2017, Prudêncio and Mota, 2007). Once they reach the liver sinusoids, the sporozoites invade a hepatocyte after transmigration through multiple cells (Mota et al., 2001) and thereby escape host immunity or drainage through the lymphatic system. Within the hepatocyte, the parasites establish a parasitophorous vacuole (Section 1.8.4) and undergo asexual replication cycles that result in a multinucleated exo-erythrocytic liver schizont containing thousands of daughter merozoites. Thereafter, the merozoites egress the host cell and enter the bloodstream via the liver sinusoids in so-called 'merosomes', bundles of merozoites in membrane-bound sacs (Sturm et al., 2006). Once ruptured, the released merozoites invade red blood cells and thus initiate the intra-erythrocytic cycle (Sturm et al., 2006, Baer et al., 2007) (Figure 2; yellow arrow).

Notably, sporozoites of *P. vivax* and *P. ovale* do not necessarily have to develop into schizonts immediately but can persist as non-replicating hypnozoites for several months or even years. These stages ensure the parasite's long-term survival during periods of poor transmission and can lead to recurring relapses of the disease (Richter et al., 2010, Mueller et al., 2009).

1.3.3 Blood stages

In the blood of the human host, the parasites undergo repeating cycles of asexual replication (Figure 2; pink arrow). In the case of *Plasmodium falciparum*, the duration of one cycle takes 48 hours. After the invasion of a red blood cell (duration: ~1 min), the parasites develop from ring (~0-18 hours post-invasion (h.p.i.)) to trophozoite (~18-36 h.p.i.) and to schizont (~36-48 h.p.i) stages. Mature schizonts rupture and release up to 32 merozoites into the blood circulation that immediately invade new RBCs and thus initiate another replication cycle (Figure 3) (Bannister et al., 2000a, Gruring et al., 2011).

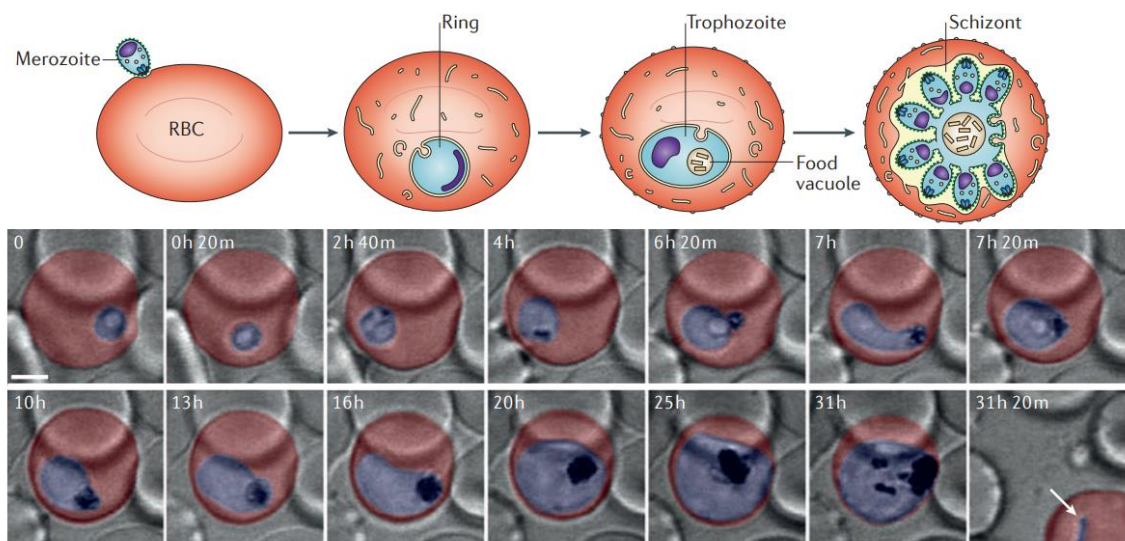


Figure 3 | Development of asexual blood stages of *P. falciparum* parasites. Top panel: Schematic of the main asexual developmental stages of *P. falciparum* blood stages. Bottom panel: 4D imaging of a complete intraerythrocytic cycle of a *P. falciparum* parasite (blue) in an RBC (red) using time-lapse imaging. Single z-slices of elected time points in hours post-infection are shown. The arrow in the last picture indicates a ring-stage parasite derived from reinvasion after rupture (De Niz et al., 2017).

The blood cycle is responsible for all the symptoms of the disease (Section 1.4). One major pathogenic mechanism of *P. falciparum* is based on the ability of the parasite to induce cytoadherence of iRBCs to the endothelial cells of blood vessels and uninfected erythrocytes (rosetting) which can cause cerebral and placental malaria (Figure 4) (Kamaliddin et al., 2019, Bernabeu and Smith, 2017, Wassmer and Grau, 2017, Pain et al., 2001). Only trophozoites and schizonts adhere to blood vessels and sequester, whereas iRBCs containing ring-stage parasites remain in circulation (David et al., 1983) and this is a diagnostic feature of *P. falciparum* malaria. In contrast to the biconcave shape of uninfected RBCs and ring-stage iRBCs, these later-stage iRBCs are spherical and less deformable and thus their cytoadherence is a mechanism to prevent splenic clearance of the iRBC (Venugopal et al., 2020).

A small subpopulation of asexual blood-stage parasites commits to sexual development and turns into gametocytes, an obligate step for parasite transmission and hence crucial for parasite survival. The immature gametocyte stages, classified into stages I-IV, sequester in the bone marrow before developing to mature crescent-shaped stage V gametocytes that are released in the peripheral blood circulation. These stage V gametocytes can be transmitted during a blood meal to a mosquito vector and start sexual reproduction (Section 1.3.1) (Venugopal et al., 2020, Baker, 2010, Dixon et al., 2012).

1.4 Pathophysiology and clinical presentation

Malaria is a febrile disease that can be categorized as uncomplicated (Section 1.4.1) or severe malaria (Section 1.4.2) since the symptoms can vary from asymptomatic and flu-like symptoms that may remain undiagnosed to severe manifestations like coma, multiple organ failure, and death (WHO, 2014). The range of clinical manifestations differs with *Plasmodium* species, strain, epidemiology, genetics, innate and acquired immunity of the host, timing and efficacy of treatment, general health status, and age of the infected individual (WHO, 2014). Consequently, different population groups also have a different risk potential for severe courses of the disease (Section 1.4.3.) (WHO, 2021c).

1.4.1 Asymptomatic and uncomplicated malaria

Malaria typically begins as uncomplicated malaria characterized by non-specific symptoms of the infected individual after a few days to weeks (*P. falciparum*: ~7-10 days) after the initial mosquito bite (Phillips et al., 2017). Most clinical manifestations are the result of the immune response, triggered mainly by the rupture of iRBCs and with it the release of antigens, phospholipid, and parasite toxins, such as hemozoin (Section 1.8.6) at the end of each *Plasmodium* erythrocytic development cycle (Section 1.3.3) (Buçsan and Williamson, 2020). The resulting symptoms can include fever, chills, sweat, headache, muscle pains, fatigue, nausea, vomiting, diarrhea, splenomegaly, icterus, and anemia (Bartoloni and Zammarchi, 2012), a clinical picture shared with several other infectious diseases. This can make a rapid definitive diagnostic challenging, particularly in countries with poor health care and diagnostic systems. Diagnosed uncomplicated malaria is usually easily treated with antimalarials (Section 1.6) and the majority of patients overcome the infection without difficulty if treated appropriately (Milner, 2018). Asymptomatic malaria usually occurs in individuals with an exposure-related acquired partial immunity typically found in highly endemic areas (Doolan et al., 2009, Mendonça and Barral-Netto, 2015). Although often subpatent, such individuals can still transmit the parasite, making eradication of malaria in areas with high transmission rates difficult (Slater et al., 2019).

1.4.2 Severe malaria

Severe malaria can be the result of failure or delay to treat uncomplicated malaria (Mousa et al., 2020, WHO, 2012) and is defined by clinical or laboratory evidence of vital organ dysfunction (WHO, 2012). It is mostly caused by an infection with *P. falciparum* and it is often the result of the ability of late developmental stages to attach to the vascular endothelium of the host to avoid splenic clearance (Lee et al., 2019). This capability is mainly given by the *Plasmodium falciparum* erythrocyte membrane protein 1 (PfEMP1) (Turner et al., 2013), encoded by the clonally variant var gene family with approximately 60 members per parasite genome (Wang and Zhang, 2020). Cytoadherence leads to the sequestration of iRBCs, rosetting of iRBCs with uninfected red blood cells (uRBCs), and platelet-mediated clumping, in several tissues and organs (Figure 4), disturbing the microcirculation and causing vascular occlusion, hypoxia, and inflammation (Kamaliddin et al., 2019, Bernabeu and Smith, 2017, Wassmer and Grau, 2017, Pain et al., 2001). One of the severest complications is cerebral malaria, result-

ing in impaired consciousness, coma, and death (Schiess et al., 2020). Further frequent severe clinical manifestations are anemia, convulsions, pulmonary complications, metabolic acidosis, hemoglobinuria, hypoglycemia, acute kidney damage, and spontaneous bleeding (Trampuz et al., 2003). Next to cerebral malaria, severe malarial anemia (SMA) is a major cause of severe malaria. SMA, typically a normocytic and normochromic anemia with an absence of reticulocytes (Lamikanra et al., 2007) is defined by hemoglobin blood levels less than 5.0 g/dL (or a hematocrit <15.0 %) in the presence of malaria infection. It is often the result of multiple factors such as hemolysis, splenic sequestration of RBCs, dyserythropoiesis, and erythropoietic suppression (Raja et al., 2019, Perkins et al., 2011). All types of severe malaria are often associated with hyperparasitemia and high mortality (WHO, 2014).

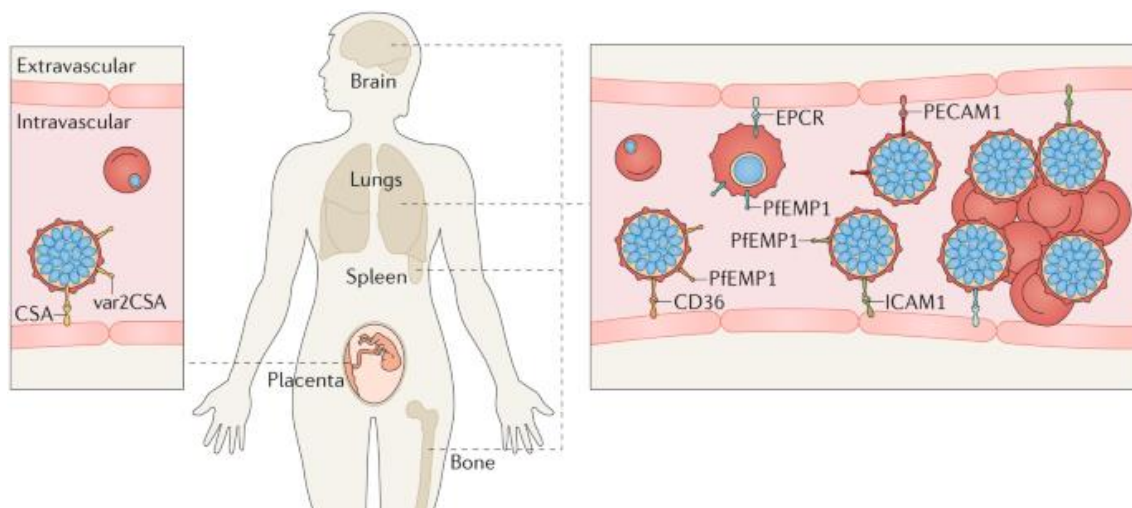


Figure 4 | Intravascular sequestrations of *P. falciparum* parasites. Cytoadherence of iRBCs (red: RBC/ blue: parasite) to endothelial cells of blood vessels and to uninfected red blood cells (rosetting) enables sequestration of the parasites in the capillaries of several organs, including the brain (cerebral malaria), lung, spleen and bone marrow. Different variants of *PfEMP1* interact with diverse endothelial cell receptors, such as ICAM1 and CD36 (right box). The parasites can also adhere to the blood vessels of the placenta of pregnant women through the *PfEMP1* variant VAR2CSA and the placental receptor CSA (placental malaria, left box) (Venugopal et al., 2020).

1.4.3 Malaria high-risk groups

Certain population groups have an increased risk of contracting malaria and taking a severe course of the disease when compared to others (WHO, 2021c). An important factor for the likelihood of severe manifestations of malaria is the immune status of the

infected individual. After surviving repeated malaria exposure, adults in high-endemic regions can acquire partial immunity which can protect them from severe and fatal malaria (Doolan et al., 2009). Thus, the most vulnerable groups are non-immune humans such as children under five years of age, migrants and travelers from non-endemic regions, as well as persons with a lower immune response such as pregnant women and AIDS patients (WHO, 2021c).

Children under five years of age, including infants, accounted for 67% (274 000) of all malaria-related deaths globally in 2019, highlighting that this group is disproportionately affected (WHO, 2020b). In regions of high transmission, severe malaria is negatively correlated with age since children in these areas, unlike adults, have not yet developed an exposure-related partial immunity (Laishram et al., 2012, Mendonça and Barral-Netto, 2015) and at six months of age, maternally transferred antibodies have vanished (Dobbs and Dent, 2016). Malaria caused by *P. falciparum* in children younger than five years has the worst prognosis. The rapid proliferation of *P. falciparum*, combined with the small blood volume in young children, a tendency for hypoglycemia, poor tolerability of oral medications, and the difficulty in assessing the severity of infection would require hospitalization for almost all malaria cases in this age group (Kuhn and McCarthy, 2006). However, due to a lack of resources in most African hospitals, few children are treated in intensive care units, and this is one major contributor to the high mortality rate in this age group (Maitland, 2015). Additionally, children who survived cerebral malaria often have neurological or cognitive sequelae at hospital discharge, with long-term negative effects on the individual and community level (Schiess et al., 2020, Langfitt et al., 2019).

Severe malaria also heavily affects pregnant women and poses a great risk to the mother and her fetus. Malaria infections during pregnancy often lead to complications such as maternal and fetal anemia, spontaneous abortion, stillbirth, intrauterine growth retardation, low birth weight, and neonatal death (Sharma and Shukla, 2017). One reason for the high susceptibility of pregnant women to severe malaria is an alteration in the maternal immune system during pregnancy, such as the halted cell-mediated immunity. This degree of immunosuppression is a necessity for the immune tolerance towards the 'foreign' fetus and placenta but it also renders pregnant women more vulnerable to intracellular pathogens (Jamieson et al., 2006, McLean et al., 2015). Another reason is the fact that the placenta is a niche for *P. falciparum* parasites. The placenta is a highly vascularized organ and thus an additional tissue for sequestration of *P. fal-*

ciparum parasites. This phenomenon occurs when the parasites express the *PfEMP1* variant VAR2CSA on the surface of the iRBCs that binds to chondroitin sulfate A (CSA) in the placental intervillous spaces (Figure 4) (Milner, 2018). VAR2CSA is thought to be antigenically different from all other *PfEMP1* types typically expressed during infection in non-pregnant individuals (Tomlinson et al., 2021, Bull and Abdi, 2016, Zakama et al., 2020) and while maternal antibodies - if present - can destroy non-CSA-binding parasites, VAR2CSA-positive parasites can replicate in the protected space of the placenta (Milner, 2018). As a consequence, women cannot acquire protective immunity against VAR2CSA before the first pregnancy and hence first-time mothers have a much higher risk of contracting placental malaria than multigravida. In low transmission regions, immunity in the population is generally low due to the reduced exposure to the parasite and all pregnancies are at risk for placental malaria (Zakama et al., 2020, Ofori et al., 2018).

1.5 Diagnostics

Rapid and accurate diagnosis is critical for the effective treatment of malaria (Tangpukdee et al., 2009). Early diagnosis can prevent further progression of the disease, reduce its severity and avert death (Mbanefo and Kumar, 2020). A solely clinical diagnosis of malaria has very low sensitivity and specificity since the symptoms are usually nonspecific (Section 1.4) (Oleribe et al., 2017). However, most malaria cases in Africa are still diagnosed presumptively, leading to overdiagnosis of malaria, inappropriate treatment, and drug mismanagement (Falade et al., 2016). Specific diagnostic techniques, such as microscopy, rapid diagnostic tests (RDTs), and polymerase chain reaction (PCR) are required to distinguish malaria from other febrile diseases (Mbanefo and Kumar, 2020). Microscopic examination of Giemsa-stained thick and thin blood smears remains the current 'gold standard'. It permits the relatively inexpensive identification and quantification of the causative pathogen and can additionally be used to monitor treatment. However, the supply of electricity for microscopes may be unreliable in many parts of sub-Saharan Africa. Additionally, well-trained laboratory personnel is rare. This is a critical factor, as the sensitivity and specificity of Giemsa-stained smear-based diagnostics vary and depend on the skill of the operator (Mbanefo and Kumar, 2020, Falade et al., 2016). Rapid diagnostic tests can circumvent those obstacles. They involve the use of an immunochromatographic lateral flow device to detect

parasite antigens, such as the histidine-rich protein 2 (HRP2) of *P. falciparum* in the blood of patients. RDTs are affordable, relatively easy to use, and provide a rapid (< 30 min), point-of-care diagnosis (Cunningham et al., 2019). However, the quantification of parasitemia and thus therapy-monitoring is difficult based on TRDs. Additionally, false-positive or false-negative results can lead to incorrect treatment (Mbanefo and Kumar, 2020). For instance, the reliability of HRP2-based RDTs is severely threatened by the emergence of *P. falciparum* parasites with deleted HRP2 and/or HRP3 antigen-encoding genes (Gatton et al., 2020). PCR-based methods have a much higher sensitivity than RDTs and microscopy and allow the definitive discrimination of *Plasmodium* species, as well as the detection of mixed infections (Leski et al., 2020). However, PCR is often not feasible in field settings, since it is expensive and needs highly skilled personnel and specialized equipment (Mbanefo and Kumar, 2020).

1.6 Anti-malarial drugs and drug resistance

Antimalarial drugs can be used for both the treatment and the prevention of malaria infection. Currently, drugs with only a limited mode of action range (Section 1.6.1) are available, and emerging drug resistance (Section 1.6.2) poses a threat to the capability of malaria control and treatment.

1.6.1 Drugs

Most antimalarial drugs target the erythrocytic stages of the parasite since this part of the parasite's life cycle is responsible for the clinical symptoms. Quinine extracted from cinchona bark in 1820 was the first commercially used antimalarial drug. Quinine and its derivatives, such as chloroquine, mefloquine, and piperaquine accumulate in the digestive vacuole (DV) of the parasite (Section 1.8.6), the site to which the parasite transports and digests host cell derived hemoglobin (Section 1.10). These drugs inhibit the sequestration of free heme that is released during the hemoglobin degradation process, an important detoxification process and thus a necessary step for parasite survival (Fitch, 1986, Sullivan et al., 1996). Antifolates, such as proguanil, trimethoprim, and pyrimethamine target purine and pyrimidine synthesis, which is important for DNA synthesis (Gregson and Plowe, 2005) and Atovaquone inhibits the electron transport chain in the mitochondria of the parasite (Goodman et al., 2016). At present, the most widely used antimalarial drug is Artemisinin and its derivatives (ART), including artemether, artesunate, and dihydroartemisinin. Artemisinin was initially used in traditional

Chinese medicine and can be extracted from the leaves, stems, and flowers of the plant *Artemisia annua* (Klayman et al., 1984). ART has a short half-life of approximately 1h and is activated by degradation products of hemoglobin digestion in the parasite's food vacuole (Klonis et al., 2013, Xie et al., 2016). Artemisinin Combination Therapies (ACTs) consisting of an artemisinin derivative plus a slower-acting partner drug with a longer half-life, such as mefloquine, piperaquine, and lumefantrine are at present the first-line malaria drug treatment recommended by the WHO (Davis et al., 2005).

1.6.2 Drug resistance

Drug resistance is a major threat to malaria control. It leads to an increased frequency of treatment failures, and thus to higher mortality. *P. falciparum* parasites acquired resistance to all of the currently available antimalarial drugs. The parasites independently developed resistance to chloroquine in Southeast Asia, Oceania, and South America in the late 1950s (Payne, 1987). Chloroquine resistance has since spread to almost all areas of the world where *P. falciparum* malaria is transmitted. Resistance is associated with point mutations in the chloroquine resistance transporter gene (*pfcr1*), which encodes a transporter in the food vacuole membrane (Fidock et al., 2000, Goldberg et al., 1990, Fitch, 1970). The mutated transporter is able to efflux the drug out of the DV and thus remove chloroquine from its site of action (Bray et al., 1998). Alterations in another food vacuole transporter, multidrug resistance gene 1 (*pfmdr1*), are linked to resistance to mefloquine and quinine (Sidhu et al., 2006, Cowman et al., 1994). Artemisinin resistance has emerged and spread in South-East Asia and is associated with mutations in the parasite's Kelch13 (K13) protein (Straimer et al., 2015, Ariey et al., 2014). Recently a role of K13 in hemoglobin uptake along with other proteins in a K13-defined compartment has been identified (Birnbaum et al., 2020). Mutations in K13, lead to a reduced hemoglobin uptake in ring-stage parasites and it is assumed that this results in a decreased artemisinin activation (Birnbaum et al., 2020).

1.7 Vaccine development

The development of an effective malaria vaccine could be a crucial element in the control and eradication of malaria to reduce the burden of this disease. However, the complexity of the parasite life cycle and its various strategies to evade recognition by the host immune system, make vaccine development a major challenge (Arama and Troye-Blomberg, 2014). However, while vaccine development efforts had been largely unsuccessful over decades, there are currently multiple promising malaria vaccines that are under development. Malaria vaccines can be classified by the developmental stages they target and therefore be simplified into three categories: Pre-erythrocytic anti-infection vaccines (Section 1.7.1), blood-stage vaccines (Section 1.7.2), and transmission-blocking vaccines (Section 1.7.3) (Figure 5). Some vaccines target several developmental stages.

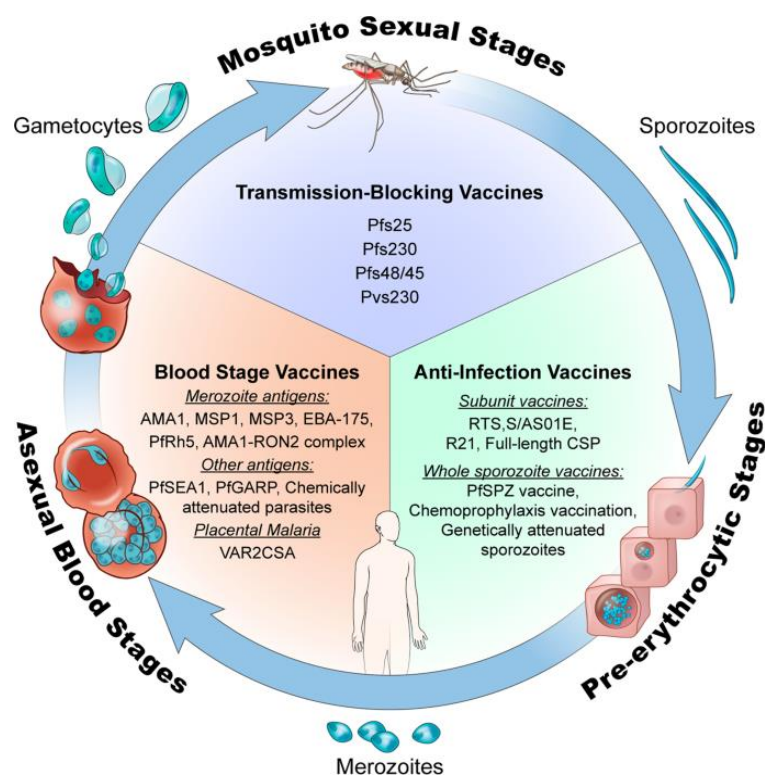


Figure 5 | Vaccine candidates that target different stages of the *Plasmodium* life cycle. (Duffy and Patrick Gorres, 2020).

1.7.1 Pre-erythrocytic anti-infection vaccines

The most efficacious vaccination strategies so far target the pre-erythrocytic stage (Figure 5) via a range of subunit (Section 1.7.1.1) or whole-sporozoite vaccine (Section

1.7.1.2) approaches. Pre-erythrocytic vaccines could target both, the sporozoite stages and the liver stages of the parasite. A block in these clinically silent phases could prevent progression to the symptomatic blood phase and subsequent transmission.

1.7.1.1 Subunit vaccines: RTS,S and R21/Matrix-M

Subunit vaccines have the advantage of generating defined immune responses to specific targets and can easily be manufactured cost-effectively on a large scale (Goh et al., 2019).

RTS,S/AS01 (Mosquirix®), initially developed by GlaxoSmithKline (GSK) in collaboration with the Walter Reed Army Institute of Research (WRAIR) in the 1980s (Gordon et al., 1995), is the first malaria vaccine approved by the European Medicine Agency (EMA) (Mullard, 2015) and so far the most clinically advanced malaria vaccine. It targets the sporozoite stage of the parasites, a strategy achieved by using virus-like particles formed by the viral envelope hepatitis B surface antigen (HBsAg) as a platform to present epitopes of the major sporozoite surface protein, termed circumsporozoite protein (CSP), to the immune system (Figure 6) (Casares et al., 2010, Kurtovic et al., 2020). The vaccine consists of a recombinant truncated CSP, containing parts of its central repeat region (**R**) and its C-terminus comprising T-cell epitopes (**T**) fused to the viral HBsAg (**S**) and the addition of the chemical adjuvant AS01 (Figure 6A). The RTS fusion protein is co-expressed in yeast with free HBsAg, which spontaneously self-assemble into RTS,S particles approximately 22 nm in size (Figure 6B) (Laurens, 2020, Collins et al., 2017). RTS,S/AS01 induces high antibody production and a moderate CD4+ T-cell response in humans (Collins et al., 2017) and was the first candidate to pass a phase III clinical trial, testing from 2009–2014 in 7 sub-Saharan African countries with 15,459 participants. The trial showed that RTS,S/AS01 protected against malaria in African children 5–17 months of age with a vaccine efficacy of approximately 55% for up to 1 year. Extended follow-up revealed an efficacy of 28% against all malaria episodes over a median of 4 years, and 36% for those who had received a booster dose (RTS, 2015). Despite its only partial protection RTS,S/AS01 entered a pilot program in areas of Ghana, Kenya, and Malawi in 2019 through national immunization programs in the outline of the WHO-commissioned Malaria Vaccine Implementation Program (MVIP). The program aims to vaccinate about 360,000 children per year from 2019 to 2023 and will examine the safety, reduction in mortality, and operational feasibility of administering four vaccine doses (WHO, 2021b).

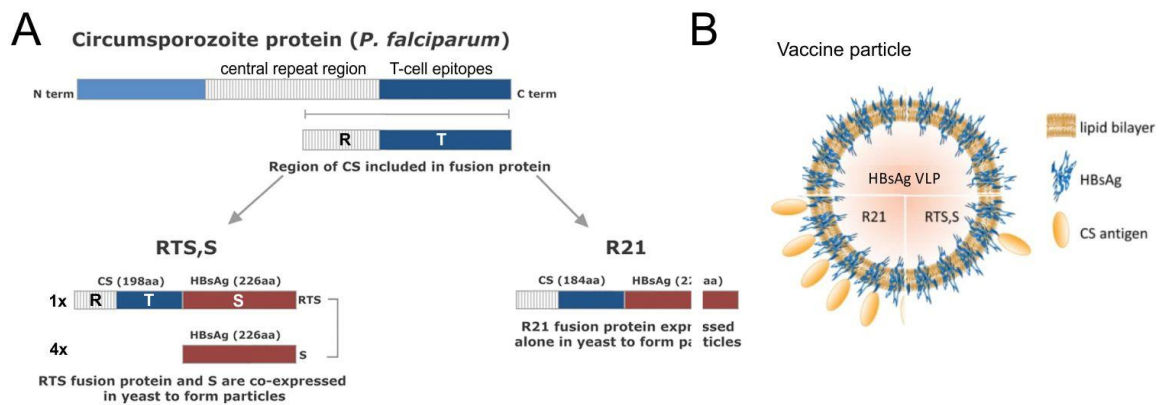


Figure 6 | Schematic representation and comparison of RTS,S, and R21 vaccine particle design.

A Composition of CSP-HBsAg fusion proteins. Modified from (Collins et al., 2017). **B** Scheme of differences in vaccine particle composition. Modified from (Collins et al., 2021).

However, the low efficacy and limited durability of the RTS,S/AS01 vaccine demonstrates that further improvement is still necessary. One possibility is an enhancement of the RTS,S vaccine strategy. The most promising next-generation RTS,S-like vaccine candidate is R21/Matrix-M, a vaccine developed at the Jenner Institute of the University of Oxford, the same institute that also worked on AstraZeneca's Covid-19 vaccine. R21 presents CSP at a higher proportion on its particle surface than RTS,S (Figure 6B). Both vaccines are based on using a fusion protein as a scaffold that enables particle formation and presentation of the CSP antigen (Figure 6A). However, RTS,S has a four-fold molar excess of HBsAg relative to the CSP-HBsAg fusion protein (Collins et al., 2021), and consequently, the virus-like particle contains only 20% of CSP-fusion protein with the remaining proportion consisting of HBsAg monomers (Datoo et al., 2021, Collins et al., 2017) (Figure 6B). As a result, much of the antibody response induced by RTS,S is directed against the HBsAg and may interfere with the induction of CSP-specific immunity (Collins et al., 2017). The excess of HBsAg in RTS,S is required for spontaneous particle formation in *S. cerevisiae*. However, in the case of the R21 vaccine, it is possible to use solely CSP-HBsAg (Figure 6A). This is achieved by expressing the fusion protein in *Pichia pastoris*, a yeast species capable of very high-density growth in combination with a strong, tightly regulated, inducible (AOX1) promoter for recombinant protein expression. The high protein densities combined with the strong promoter allow expression of a CSP-HBsAg fusion protein at sufficiently high concentrations for particles to form even without the excess of HBsAg with the conse-

quence of more CSP antigen per virus-like-particle surface (Figure 6B). With this strategy, high anti-CSP antibody and only minimal anti-HBsAg titers were induced (Collins et al., 2017). The vaccine includes Novavax's patented saponin-based Matrix-M™ adjuvant which is also a component in Novavax's protein-based COVID-19 vaccine, NVX-CoV2373 (Tian et al., 2021). A Phase IIb trial in 450 children in Burkina Faso demonstrated an efficacy of 77% against infection in the higher-dose adjuvant group over 12-months of follow-up and thus R21/Matrix-M is the first vaccine to meet the WHO's Malaria Vaccine Technology Roadmap goal of at least 75% efficacy (Dattoo et al., 2021). A Phase III trial has started and will assess efficacy and safety in 4800 children across five sites in Burkina Faso, Kenya, Mali, and Tanzania (<https://clinicaltrials.gov/NCT04704830>). The University of Oxford has already partnered with Serum Institute of India Pvt Ltd. (SIPL) which has confirmed its commitment to the provision of >200 million doses per year in the case of successful licensure.

1.7.1.2 Whole sporozoite vaccines

Vaccines using whole sporozoites contain the entire set of the parasite stage-specific antigens and therefore can also elicit a different and broader range of immune responses than subunit vaccines (Goh et al., 2019). At present whole sporozoite vaccines (WSV) with three different basic principles are under development: radiation attenuated sporozoites (RAS), genetically attenuated sporozoites (GAS), and wildtype sporozoites applied under chemoprophylaxis (CPS). These different approaches determine how far the parasite can develop until its arrest into the life cycle and consequently also lead to different immune responses. RAS and GAS both arrest in liver stages while CPS can progress to the initial blood stages where they get eliminated by an applied antimalarial drug. The further the parasite can develop, the broader the spectrum of antigens that can be presented to the immune system, and the fewer sporozoites are required to establish protection (Itsara et al., 2018). Several sporozoite vaccine candidates showed good homologous protection but failed to challenge heterologous parasites. However, recently a small early-stage trial at the US National Institutes of Health showed promising results using Sanaria's optimized CPS approaches (Sanaria® PfSPZ-CVac). In this approach, *P. falciparum* sporozoites (PfSPZ) were inoculated under prophylactic cover with pyrimethamine (PYR) (directed against liver-stage parasites) or chloroquine (CQ) (directed against blood stages). Three months after immunization participants showed a vaccine efficiency of 87.5% against a homologous (n=8) and of 77.8% against a heterologous (n=9) controlled malaria infection in

the case of PYR treatment and 100 % (n=6) efficacy against heterologous malaria infection in the case of CQ treatment (Mwakingwe-Omari et al., 2021). A larger trial has begun in Mali to test the vaccine in adults in a field setting ([https://clinicaltrials.gov/ ID NCT03952650](https://clinicaltrials.gov/ID/NCT03952650)).

Despite these promising results, the use of whole sporozoite vaccines holds many challenges. So far, to obtain the vaccine, sporozoites must be extracted from mosquito salivary glands, a complicated process that limits large-scale vaccine production and also carries high costs. Additionally, the sporozoites have to be stored in liquid nitrogen, which makes them difficult to distribute in poor areas such as sub-Saharan Africa and raises questions about their usability in the field. In addition, failed chemoprophylaxis could lead to symptomatic malaria infection in the case of unattenuated sporozoite applications.

1.7.2 Blood-stage vaccines

Blood-stage vaccines (Figure 5) target the disease-causing stage of the *Plasmodium* life cycle and can be divided into those that aim to target the iRBC and those that target the merozoite (Illingworth et al., 2019). Most of the blood-stage antigen candidates are essential invasion proteins of merozoites such as merozoite surface protein (MSP1) and MSP3, apical membrane antigen 1 (AMA1), and erythrocyte-binding antigen 175 (EBA-175) (Cai et al., 2021). However, there are several challenges in developing vaccines against merozoites, like the short period (seconds) in which free merozoites are accessible to antibodies, antigenic polymorphism, redundant invasion pathways, and a large number of parasites to target (Duffy and Patrick Gorres, 2020). So far, targeting merozoite invasion proteins showed only low efficacy in clinical trials (Sahly et al., 2010, Koram et al., 2016, Sagara et al., 2009, Payne et al., 2016, Sirima et al., 2009, Salamanca et al., 2019). Novel or improved antigens targeting non-redundant merozoite invasion pathways, such as the reticulocyte-binding protein homolog 5 (Rh5) could lead to improvement (Ndwiga et al., 2021, Payne et al., 2017). In addition, vaccines against other targets such as infected erythrocyte surface proteins, schizont egress antigens, or intact attenuated iRBCs are under development or are in preclinical and clinical trials (Duffy and Patrick Gorres, 2020). Distinct types of blood-stage vaccines are under development that are directed against VAR2CSA, expressed by iRBCs sequester in the placental intervillous space of pregnant women (Section 1.4.3), and thus are specifically designed to protect against placental malaria (Gamain et al., 2021).

1.7.3 Transmission-blocking vaccines

Transmission-blocking vaccines (Figure 5) target antigens of sexual stages to prevent parasite development in the mosquito midgut (Arama and Troye-Blomberg, 2014) and thus interrupt parasite transmission through the vector. These vaccines elicit antibodies against surface antigens which are taken up along with gametocytes into the mosquito during blood feeding. Those antibodies can either bind to gametocyte antigens, such as P230 or P48/45 (Singh et al., 2019, Marin-Mogollon et al., 2018, van Dijk et al., 2001) or ookinete antigens, such as P25 (Sala et al., 2018) or to a mosquito receptor, such as AnAPN1 (Armistead et al., 2014, Atkinson et al., 2015) that the ookinete needs to enter the mosquito midgut epithelium. The aim of these vaccines is not to protect the recipient from contracting malaria but could contribute to preventing the spread of the disease which results in ethical problems if given alone. To solve this problem, they could be co-administered with pre-erythrocytic vaccines (McCoy et al., 2021).

1.8 Cell Biology

1.8.1 Systematic classification

Parasites of the genus *Plasmodium* belong to the family Plasmodiidae in the order of Haemosporida and are part of the phylum Apicomplexa. Alongside *Plasmodium* spp. other Apicomplexan parasites are *Toxoplasma gondii*, *Cryptosporidium* spp., *Eimeria* spp., and *Theileria* spp.. Combined with Dinoflagellata and Ciliata, the Apicomplexa form the superphylum of the Alveolata.

1.8.2 Specific organelles of *Plasmodium* spp.

Plasmodium parasites possess the basic set of eukaryotic cell organelles such as the nucleus, the endoplasmic reticulum (ER), the Golgi-apparatus, and the mitochondrion (van Dooren et al., 2005, Bannister et al., 2000b, Struck et al., 2005). However, to enable invasion and development inside of another cell, the evolution of the parasite has resulted in some modified or unique and parasite-specific structures and organelles, such as the apical complex (Section 1.8.3), the parasitophorous vacuole (Section 1.8.4), the apicoplast (Section 1.8.5), and the digestive vacuole (Section 1.8.6) (Figure 7).

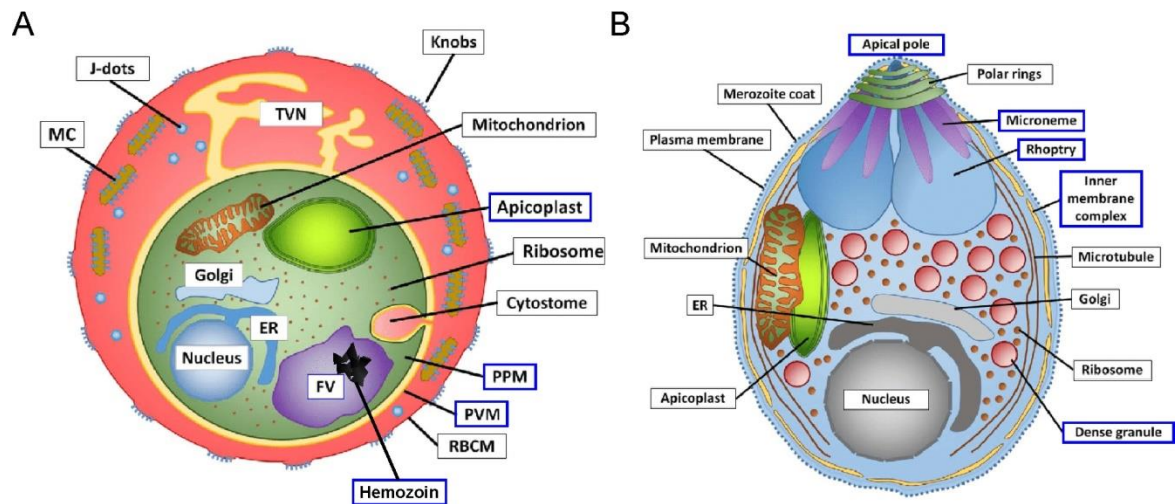


Figure 7 | Schematic of organelle organization of two different *Plasmodium* spp. blood stages. **A** A trophozoite stage parasite within a red blood cell. **B** Free merozoite. The organelles and structures referred to in the text are highlighted by blue boxes. Modified from (Flammersfeld et al., 2018)

1.8.3 Apical complex and inner membrane complex

The classification of *Plasmodium* spp. to the phylum Apicomplexa was defined by the presence of the apical complex (Figure 7B), a structure that coordinates interactions with and penetration of the respective host cell by the obligate intracellular parasites (Katris et al., 2014). It is composed of secretory organelles and specific cytoskeletal elements at the apical pole of invasive parasite cell stages (termed zoites) and is potentially evolutionarily derived from elements of the flagellar apparatus (Portman et al., 2014, de Leon et al., 2013). During the invasion process the secretory organelles, including the rhoptries, the dense granules, and the micronemes, release invasion factors that enable the zoites to adhere selectively to the host cell, alter the cell membrane, actively enter the cell in a non-destructive manner, and establish the parasitophorous vacuole (PV) (Section 1.8.4) (Blackman and Bannister, 2001, Katris et al., 2014).

The inner membrane (IMC) complex (Figure 7B) is, next to the secretory organelles, one of the key components for host cell invasion. The IMC underlies the parasite plasma membrane and consists of flattened membrane sacs (alveoli), supported by a sys-

tem of filaments (alveolin), called the subpellicular network (Harding and Meissner, 2014). The IMC functions as an anchor for the actin-myosin motor complex, which plays a central role in parasite motility. In merozoites, the motor complex is important in the erythrocyte invasion process (Harding and Meissner, 2014). Next to its role in invasion and motility, the IMC is important for cell stability and shape and it serves as a scaffold during cytokinesis (Wichers et al., 2021). The secretory organelles and the IMC are generated de novo from Golgi-derived material in each replication cycle of the parasite (Bannister et al., 2000a) and IMC development is associated with nuclear division (Harding and Meissner, 2014).

1.8.4 Parasitophorous vacuole

During host cell invasion, the apicomplexan parasites invaginate the host cell membrane so that the parasite ends up surrounded not only by its parasite plasma membrane (PPM) but also by an additional host-cell-derived membrane, called the parasitophorous vacuole membrane (PVM) (Figure 7A). The PVM, extensively re-modeled by parasitic proteins and rhoptry-derived lipids (Spielmann et al., 2012, Geoghegan et al., 2021), provides an interface between the parasite and the host cell and creates a vacuolar compartment containing the parasite, termed the parasitophorous vacuole (Lingelbach and Joiner, 1998). Within the PV the intracellular parasite resides and develops throughout the entire blood cycle until its egress into the bloodstream under the destruction of the host cell (Matz et al., 2020). The additional presence of the PV and the PVM poses a challenge to cellular processes such as nutrient uptake and protein export and consequently these compartments have additional functionalities that may not be present in model organisms.

1.8.5 Apicoplast

Apicomplexan parasites such as *Plasmodium* spp. possess a vestigial plastid that has been termed the apicoplast (apicomplexan plastid) and is present in all life cycle stages (Figure 7A; B) (McFadden and Yeh, 2017). The apicoplast resembles the chloroplasts of algae and plants but lost its photosynthetic function. Its four surrounding membranes indicate that it is a product of secondary endosymbiosis of a red algal, which was engulfed before dinoflagellates and Apicomplexa diverged several hundred million years ago (Moore et al., 2008, Janouskovec et al., 2010, van Dooren and Striepen, 2013). Since then, the endosymbiont has drastically minimized and lost its nucleus, cyto-

plasm, wall, and cytoskeleton (McFadden and Yeh, 2017). Most genome parts were transferred to the nucleus of the parasite and the resulting gene products need to be transported back to the apicoplast (Foth and McFadden, 2003). The apicoplast is the site of fatty acid, heme, and isoprenoid biosynthesis. However, only the isoprenoid synthesis seems to be essential as an external supply of the isoprenoid precursor isopentenyl pyrophosphate is sufficient to restore growth after the loss of the apicoplast (Yeh and DeRisi, 2011).

1.8.6 Digestive vacuole

Plasmodium parasites possess a unique and highly specialized lysosomal-like compartment called the digestive vacuole (DV), also referred to as the food vacuole (FV) (Figure 7A). The FV is the site of degradation for the host-cell-derived hemoglobin that is taken up by the parasite during its development within erythrocytes (Francis et al., 1997b) and is the target of several antimalarial drugs (Section 1.6). The FV is an acidic compartment surrounded by a singular membrane and is believed to be formed de novo in ring-stage parasites after each completed blood cycle (Ehlgen et al., 2012). In *P. falciparum* parasites it is assumed that initially multiple small DVs are established in ring stages which fuse into a singular large food vacuole in later stages (Abu Bakar et al., 2010).

Hemoglobin degradation occurs through a pathway of proteolytic events within the FV, involving Plasmepsin I, II, and IV, cysteine proteases, such as falcipain, metalloproteases, and aspartic proteases (Goldberg et al., 1990, Goldberg et al., 1991, Sijwali and Rosenthal, 2004). Besides the release of free amino acids, a process essential for parasite growth (Klemba et al., 2004b), hemoglobin digestion also generates reactive free heme, a toxic byproduct of the hemoglobin degradation mechanism. The parasite sequesters the heme as a crystalline, brown pigment called hemozoin (HZ), a non-toxic metabolite that accumulates in the FV, a detoxification process crucial for parasite survival (Egan, 2008, Sherman, 1977).

Although it has been known for a long time that host-cell-derived hemoglobin ends up in the parasite's food vacuole, the required endocytosis mechanism is still not well understood.

1.9 Endocytosis

Eukaryotic cells internalize extracellular macromolecules, such as extracellular fluids or specific cargoes (e.g., low-density lipoprotein, and growth factors) by a process called endocytosis. In the process, they also internalize parts of the cell such as receptors and lipid membranes. Endocytosis is fundamental for many cellular functions like nutrient intake, cell adhesion, junction formation, migration, cell polarity, and signal transduction (Basturea, 2019).

1.9.1 Endosomal pathway

Endocytosis initiates at the plasma membrane by vesicle formation through various endocytic mechanisms (Section 1.9.1.1). The formed endocytic vesicles (EV) bud from the plasma membrane, engulfing the endocytosed material destined for the endosomal pathway (Figure 8). After initial internalization, the extracellular molecules are trafficked through and sorted by endosomes, a pleiomorphic network of tubulovesicular compartments (Elkin et al., 2016). These endosomal compartments mature from early (EE) (Section 1.9.1.2) to late endosomes (LE) (Section 1.9.1.3), which includes an alteration in recruitment and activation of Rab-family GTPases, a conversion in the phosphatidylinositol lipid composition of their membranes, and a drop of the luminal pH. Internalized macromolecules in maturing endosomes can have diverse destinations. They can be recycled back to the plasma membrane, undergo retrograde transport to the *trans*-Golgi network or the material is degraded. In the latter case, the late endosome fuses with the lysosome (L) (Section 1.9.1.4), an acidic and lytic compartment, capable to digest the endosomal content.

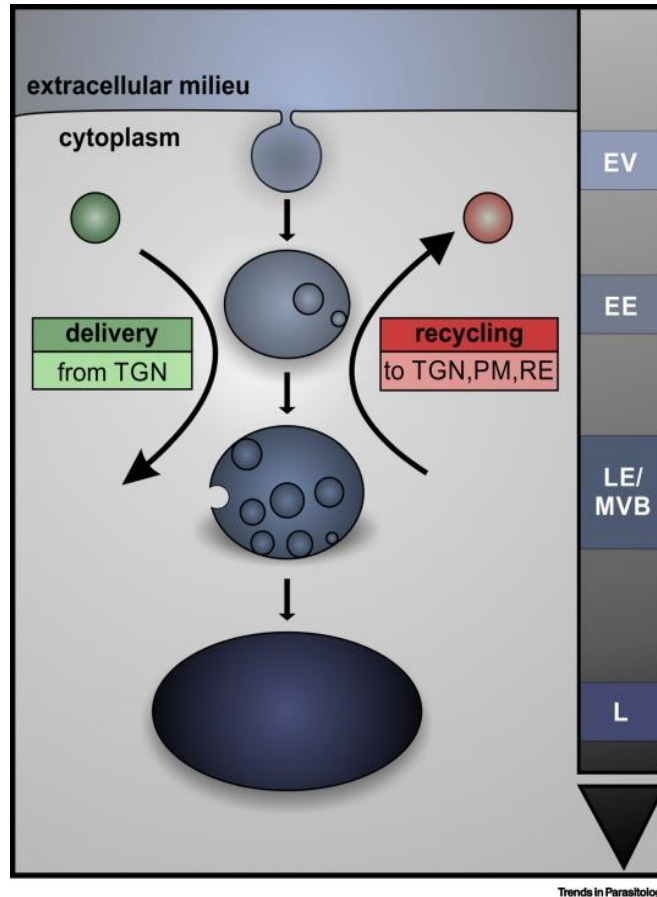


Figure 8 | Generic scheme of the endosomal pathway. Endocytic vesicles (EV) bud from the plasma membrane (PM) and are trafficked to the early endosome (EE), which matures to a late endosome (LE). From the LE the endocytosed material can be transported back to the PM, undergo retrograde transport to the TGN or, gets degraded by fusion of the LE with the lysosome. L, lysosome; MVB, multivesicular body; PM, plasma membrane; RE, recycling endosome; TGN, trans-Golgi network. Figure from (Sabitzki et al., 2020).

1.9.1.1 Different endocytosis mechanisms

Over the years, various entry routes of endocytic uptake have been discovered that can differ in the cargoes they transport and in the protein machinery that enables the endocytic process (Rennick et al., 2021). Endocytic pathways are broadly classified into Clathrin-dependent (Section 1.9.1.1.1) and Clathrin-independent and can be further subdivided according to their dynamin dependency (Figure 9A; B). The endocytosis mechanisms are cell type dependent but multiple endocytic mechanisms can occur simultaneously in one cell.

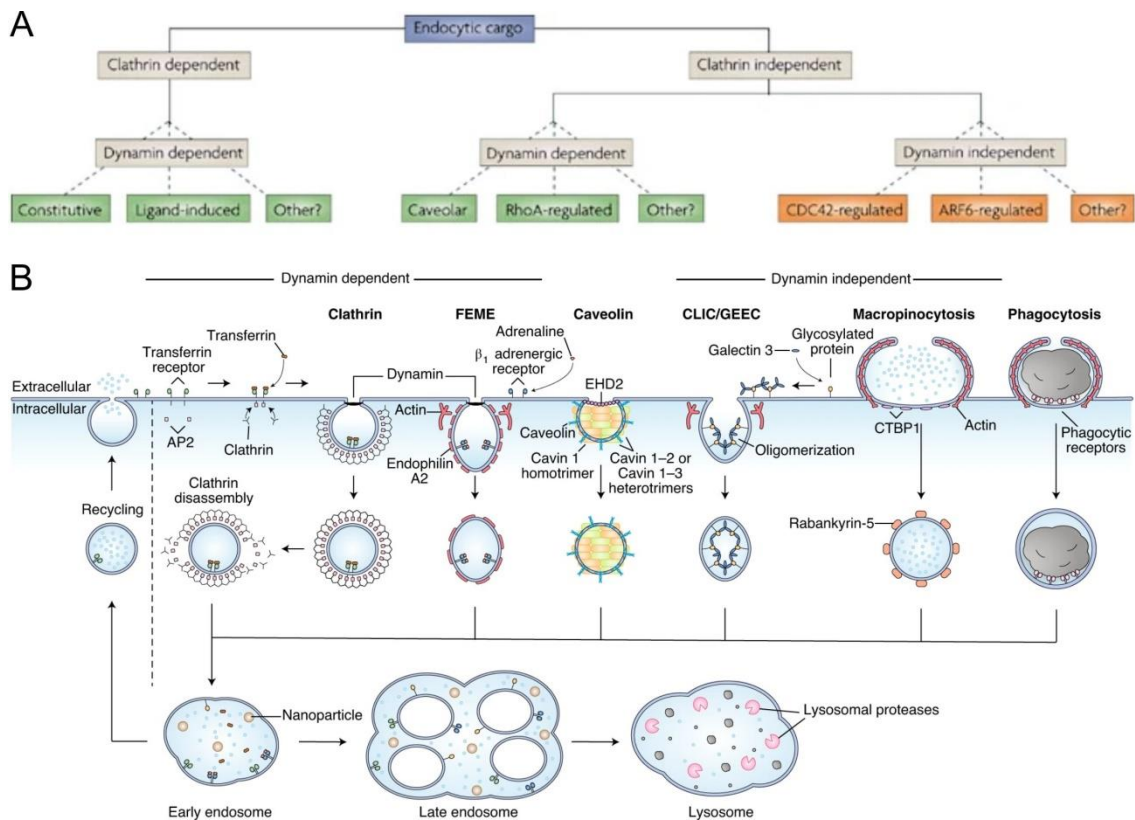


Figure 9 | Overview of endocytosis mechanisms. **A** Classification of endocytosis pathways according to dependency on Clathrin and dynamin (Mayor and Pagano, 2007). **B** Schematic representation of various endocytosis pathways with some of the main proteins characteristic for each pathway (Rennick et al., 2021).

1.9.1.1 Clathrin-mediated endocytosis

The best characterized endocytic mechanism and the major pathway by which receptors and their ligands are taken up is Clathrin-mediated endocytosis (CME) (Figure 9B and Figure 10B) (Elkin et al., 2016, Kadlecova et al., 2017). Clathrin, a triskelion-shaped complex of three small (Clathrin light chains) and three large subunits (Clathrin heavy chains) can assemble and mature into polygonal lattices forming Clathrin-coated pits that concentrate cargo concomitant with invagination of the plasma membrane to form the endocytic vesicle. The GTPase dynamin assembles into collar-like structures at the neck of the Clathrin-coated pits and catalyzes membrane fission and release of Clathrin-coated vesicles (Mettlen et al., 2018, Azarnia Tehran et al., 2019, Kadlecova et al., 2017). CME is a tightly orchestrated, multistep process involving numerous factors (Joseph et al., 2020, Loerke et al., 2009) and since Clathrin cannot bind itself to membranes or cargo molecules, accessory proteins are required for its recruitment to

endocytic sites (Azarnia Tehran et al., 2019). A fundamental role in the initiation of CME is played by the adaptor protein 2 complex AP-2), a heterotetramer that belongs to a family of adaptors (AP-1 to AP-5) that are involved in vesicle-mediated membrane trafficking (Gulbranson et al., 2019). AP-2 links the endocytic machinery, including the Clathrin scaffold, to the membrane bilayer and the transmembrane cargo. It consists of four subunits, the two large adaptin subunits (~70 kDa) α and β 2, the medium-sized μ 2-subunit (~50 kDa), and a small σ 2-subunit (~17 kDa) (Figure 10A) (Jackson et al., 2010b). The complex forms a large globular central core, composed of μ 2, σ 2, and the N-terminal trunk domains of the two large adaptins, that is connected via long flexible linkers ('hinge') to folded C-terminal appendage ('ear') domains of α and β 2 adaptin (Traub and Bonifacino, 2013). AP-2 exists in at least two functionally distinct conformations, termed the closed/inactive and the open/active state. Cytosolic inactive/closed AP-2 is assumed to be initially recruited to endocytic sites through positively charged amino acid patches that bind phosphatidylinositol 4,5-bisphosphate (PIP₂) a hallmark of the plasma membrane. AP-2 undergoes conformational changes to an open/active conformation that leads to the exposure of further PIP₂ binding sites, of binding pockets for the two most common cargo motifs (tyrosin motifs: Yxx Φ and dileucine motifs: [ED]xxxL[LI]) on the AP-2 core, of a phosphorylation site on the AP-2 μ subunit and of the Clathrin-binding box (L Φ X Φ [DE]) on the β 2 hinge region (Partlow et al., 2019, Beacham et al., 2019, Jackson et al., 2010b, Kadlecova et al., 2017). The appendage domains act as binding platforms for numerous Clathrin accessory proteins, such as epsin, AP180, and Eps15 (Owen et al., 2000, Chen and Schmid, 2020). All together these interactions allow AP-2 to function as the central regulatory hub of Clathrin-coated vesicle formation for which the cooperativity of interactions ensures that productive endocytic vesicle formation is dependent on the presence of cargo (Figure 10B) (Beacham et al., 2018, Loerke et al., 2009). However, recently it was discovered in the filamentous fungus *Aspergillus nidulans* that AP-2 also plays a role in a Clathrin-independent endocytic mechanism (Martzoukou et al., 2017).

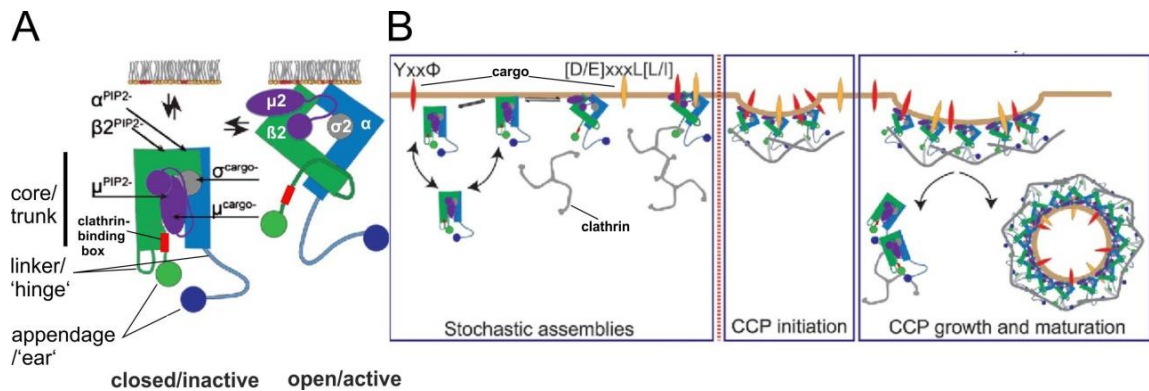


Figure 10 | AP-2 in Clathrin-mediated endocytosis. **A** Conversion of a closed/inactive state of AP-2 in the cytosol to an open/active conformation at the plasma membrane leads to exposure of PIP2, cargo, and Clathrin-binding sites. **B** Clathrin-coated pit (CCP) assembly, initiation, growth, and maturation lead to the formation of a Clathrin-coated vesicle. Modified from (Kadlecova et al., 2017).

1.9.1.2 Early endosome

The EE is the first endocytic compartment in the endosomal pathway that receives the internalized material by vesicle fusion. Its main function is the sorting of internalized material to their subsequent cellular destinations (Jovic et al., 2010). The EE membrane has a specific protein and lipid composition that provides a unique organelle identity, a requirement to regulate specific interactions with effector proteins.

One of the key proteins that regulates EE function is the small GTPase Rab5. Proteins of the Rab-family are small reversibly membrane-associated proteins that switch between an active GTP-bound state and an inactive GDP-bound state (Stroupe and Brunger, 2000). Upon activation by a specific guanine exchange factor (GEF), called Rabex5 (Horiuchi et al., 1997), Rab5 localizes to the EE membrane via its isoprenylated C-terminus (Bos et al., 2007). This leads to the recruitment of several Rab effector proteins to the early endosome, which mediates specific downstream functions, such as endosome biogenesis, maturation, and fusion (Mishra et al., 2010).

A central Rab5 effector is the type III PI3P-kinase Vps34, which mediates the conversion of phosphatidylinositol (PI) on the membrane to phosphatidylinositol-3-phosphate (PI3P) (Murray et al., 2002, Christoforidis et al., 1999). As a hallmark of early endosome membranes, PI3P is an important signal for further Rab5 effector proteins containing a FYVE zinc finger domain, a specific PI3P-binding site. FYVE-domain-containing Rab5 effector proteins such as the early endosomal antigen 1 (EEA1) (Mills

et al., 1998, Raiborg et al., 2001) and the Rabenosyn-5-hVPS45 complex (Nielsen et al., 2000) promote early endosome hetero- and homotypic SNARE (soluble N-ethylmaleimide-sensitive factor protein receptors) -mediated fusion events (Figure 11).

Rabenosyn-5 (Rbsn5), a mammalian functional homolog of yeast Vac1p bridges the interaction between Rab5 and Vps45, a member of the Sec1/Munc18-like (SM) protein family that can bind to various syntaxins (Nielsen et al., 2000, Gengyo-Ando et al., 2007). The importance of these components in the endosomal maturation process is for instance demonstrated by the fact that a knockout of VPS45 in yeast results in a vacuolar-sorting phenotype (Cowles et al., 1994).

The trafficking connection of the EEs with the TGN through bidirectional vesicle exchange is responsible for the delivery of lysosomal and removal of endosomal components during endosome maturation. Interestingly, plants lack an independent EE compartment and the functions of EEs are assumed to be performed by an organelle that combines EEs and TGN functions (Huotari and Helenius, 2011, Dettmer et al., 2006).

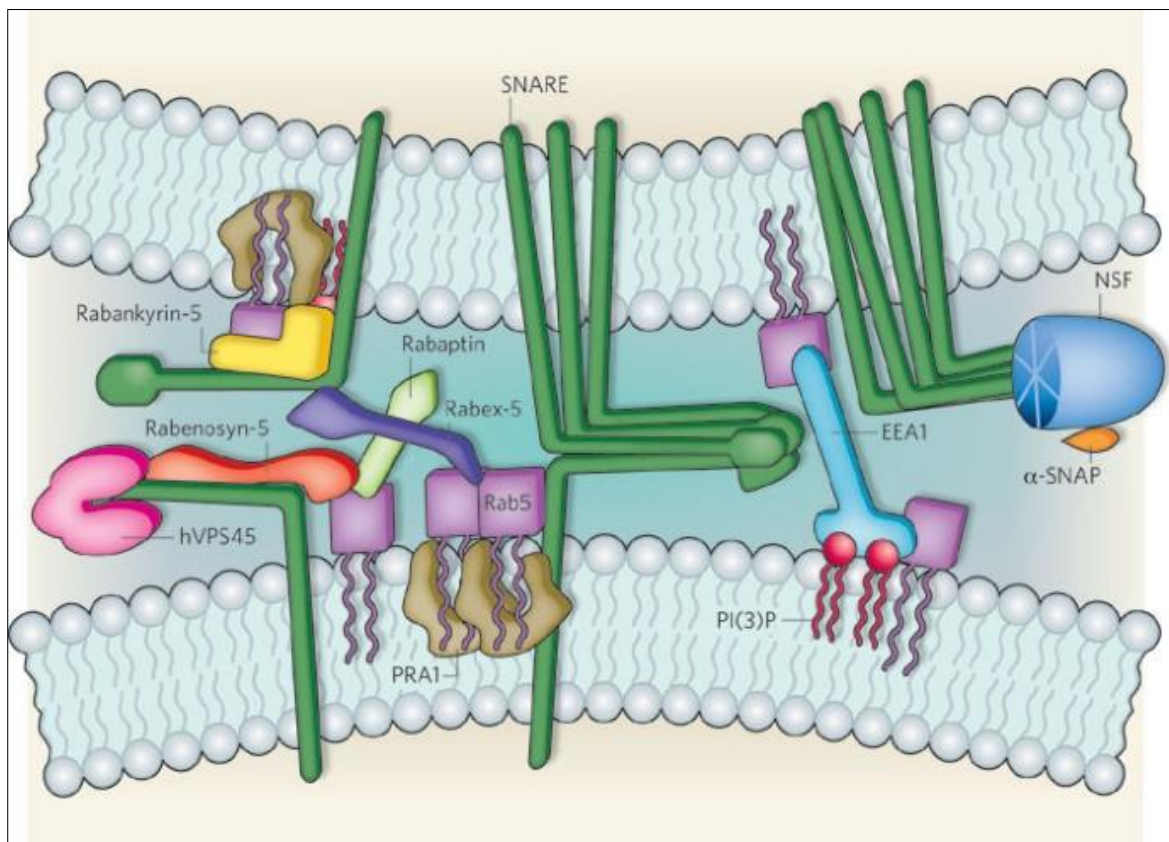


Figure 11 | Complexity of the fusion machinery of the early endosome. Rab5 and SNARE proteins drive endosomal fusion a process regulated by effector proteins such as Rabenosyn-5, hVPS45, Rabaptin, Rabex-5, and EEA1. (Collins and Zimmerberg, 2009)

1.9.1.3 Late endosome

The maturation model states that early endosomes mature into late endosomes. This process involves the exchange of membrane components, formation of intraluminal vesicles (ILVs), a decrease in luminal pH, incorporation of lysosomal components, and a change in morphology (Huotari and Helenius, 2011).

A key step in endosome maturation is a conversion from Rab5 to Rab7 at the endosomal compartment (Rink et al., 2005), a process that is assumed to involve the GEF and Rab5 effector protein complex SAND-1/Mon1 and Ccz1 (Langemeyer et al., 2020, Pfeffer, 2013, Stroupe, 2018). The Rab-switch alters the association of effector proteins and thus reshapes many of the endosomal features. It facilitates endosome maturation, trafficking, lysosome biogenesis, and positioning (Kuchitsu and Fukuda, 2018, Fujiwara et al., 2016). However, the function of Rab7 in the endocytic pathway remains controversial (Vanlandingham and Ceresa, 2009). Additionally, Rab7 is located to autophagosomes and it is widely assumed that it regulates the autophagosome-lysosome fusion step during autophagy (Kuchitsu and Fukuda, 2018). Besides the Rab GTPase-switch with maturation to the late endosome, the phosphoinositol of the endosomal membrane is converted from PI3P to phosphatidylinositol 3,5-bisphosphate (PI(3,5)P2) (Marat and Haucke, 2016).

LEs pack membrane proteins and lipids destined for the lysosome into multiple ILVs, a critical selective sorting process that already starts in early endosomes. The number of ILVs increases with endosome maturation and leads to the formation of a multivesicular body (MVB). The biogenesis of ILVs is dependent on a molecular-machinery known as the 'endosomal sorting complex required for transport' (ESCRT) and accessory proteins such as the AAA-type ATPase VPS4, which act on Clathrin-containing plaques found on the cytosolic surface of the endosome membrane and generates inward-budding vesicles (Jeger, 2020). The sorting of cargo into ILVs is based on the presence of ubiquitin-tags in the cytosolic domains of membrane proteins (Huotari and Helenius, 2011).

1.9.1.4 Lysosome

The lysosome is the terminal, acidic organelle in the endosomal pathway and is involved in the degradation of macromolecules received through endocytosis, phagocytosis, or autophagy. Increasing acidification of the content destined for the lysosome

already takes place through endosome maturation. The function of the lysosome depends on its acidic property which is at the same time a control measure of its spatio-temporally-defined lytic activity. In comparison to a cytoplasmic pH of about 7.0, the pH of the endosomal and lysosomal lumen is in the range of 6.5 to 4.5 and this difference is generated through the activity of ATP-dependent proton pumps present in their membranes. This generates optimal conditions for the activity of their degenerative hydrolases, and lipases, and mediates the uncoupling of ligands from internalized receptors. The resulting breakdown products become building blocks for cellular protein and lipid synthesis (Hu et al., 2015, Matte and Pasqualim, 2016, Wang et al., 2017).

1.10 Endocytosis in *P. falciparum* parasites

Even though it is assumed that most eukaryotic cells are capable of endocytosis, there is only limited knowledge about endocytosis in apicomplexan parasites. While in *Toxoplasma gondii* an active endocytosis process was only recently discovered (McGovern et al., 2021, Dou et al., 2014), host cell cytosol uptake (HCCU) in malaria blood-stage parasites (Section 1.10.1) is already long known as a crucial and so far the solely investigated endocytic process in *Plasmodium* spp.. The connection of HCCU and the subsequent degradation process of the internalized hemoglobin with the mechanisms of action of several antimalarial drugs (Section 1.6), such as chloroquine and artemisinin, demonstrate the high relevance of comprehending this cellular process in detail. Nevertheless, HCCU is still poorly understood and it was only recently that proteins involved in this process could be identified. We recently reviewed the current state of knowledge about HCCU in *P. falciparum* (Sabitzki et al., 2020) and this is in part summarized and extended with a focus on the topics relevant to this thesis in the following section (Section 1.10.1).

1.10.1 Host cell cytosol uptake in *P. falciparum* parasites

During its life cycle, the parasite takes up and digests in its food vacuole (Section 1.8.6) more than two-thirds of the host cell cytosol, which mainly consists of hemoglobin (Francis et al., 1997b). This is necessary for the parasite to receive nutrients, as hemoglobin is an important source of amino acids, but is also needed to generate space while growing inside of the red blood cell and simultaneously maintaining osmotic sta-

bility (Lew et al., 2003). Interestingly, the amino acids derived from hemoglobin digestion exceed the metabolic needs of the parasite to an extent that only up to one-fifth of them are used while the surplus is released into the extracellular milieu (Dalal and Klemba, 2015, Krugliak et al., 2002, Sherman, 1977).

An intracellular life cycle within the red blood cell has the consequence that endocytosis has to occur tailored to a very unique environment. Most unicellular eukaryotic cells are surrounded by an extracellular fluid with low protein density and only by a single membrane bilayer. Blood stages of malaria parasites, however, are surrounded by a high-density protein environment consisting of hemoglobin from which the parasites are separated not only by their plasma membrane but also by an additional membrane, the parasitophorous vacuolar membrane. In consideration of these special challenges, different models of HCCU have been postulated (Figure 12A). However, the exact mechanism remains so far speculative.

Host cell cytosol uptake in malaria parasites is here subdivided into initiation (Section 1.10.1.1), early endosome (Section 1.10.1.2), and late endosome (Section 1.10.1.3) associated endocytosis steps, each of which is distinct in terms of associated structures and molecules.

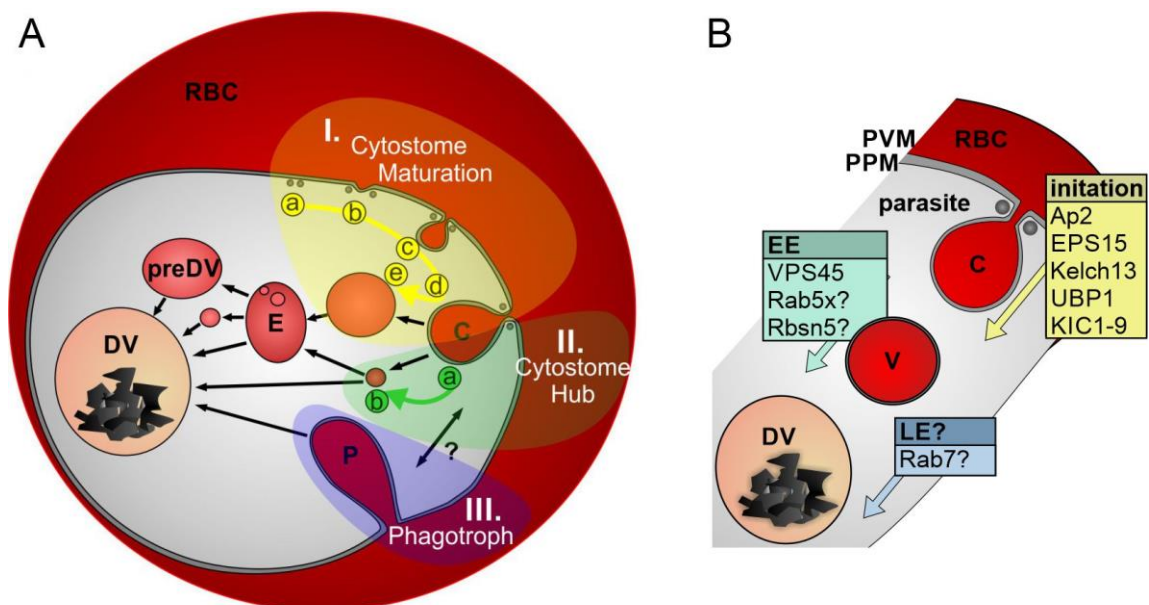


Figure 12 I Structures and proteins in HCCU of *P. falciparum* blood stages. **A** Different possible HCCU routes in a malaria parasite within a RBC. I. Cytostome maturation; II. Cytostome hub; III. Phagotroph **B** Known or suspected (indicated by a question mark) proteins associated with initiation, early endosome

dosome (EE), or late endosome (LE) of HCCU. Rab5x stands for Rab5b or Rab5c. Abbreviations: RBC: red blood cell; C: cytostome; P: phagotroph; E: endosome; DV: digestive vacuole; V: HCC-containing vesicle; PPM: parasite plasma membrane; PVM: parasitophorous vacuolar membrane. Modified from (Sabitzki et al., 2020).

1.10.1.1 Initiation of endocytosis associated structures and proteins in HCCU

HCCU is assumed to be a bulk uptake process that, in a non-discriminative manner, internalizes host cell cytosol in large portions without a need for specific cargo-ligand interactions. To initiate this process, host cell cytosol-filled invaginations of both membranes, the PVM and PPM, are generally expected to be involved. Two different structures, the cytostome, and the phagotroph, both consistently and exclusively observable by electron microscopy, exhibit this characteristic so that their participation in early endocytosis steps can be hypothesized (Abu Bakar et al., 2010, Aikawa et al., 1966, Milani et al., 2015, Elliott et al., 2008). While the invaginations of the generally smaller cytostomes have an electron-dense collar present at their narrow neck (neck diameter of ~100nm) (Milani et al., 2015, Liu et al., 2019), this is absent at the broader neck (>200nm) (Milani et al., 2015, Elliott et al., 2008) of the larger phagotrophs. However, the dynamic processes of the development and subsequent fate of these types of invaginations in the course of endocytosis remain obscure, as they have so far only been visualized by static ultrastructural methods. Hence, a variety of possible routes can be imagined for HCCU originating from these structures but there is to date little experimental data giving tangible evidence to any of them (Figure 12A; Sabitzki et al., 2020). The cytostome, as well as the phagotroph, could either be regularly formed and maturing structures that pinch off entirely or they could represent permanent structures serving as a hub from which small vesicles are budding off for subsequent transport. Also, a direct interaction, with the food vacuole without intermediate endocytosis steps has been discussed (Lazarus et al., 2008). Moreover, phagotrophs and cytostomes could be structures that merge from one to another or that possess no common function at all. At present, most studies assume that the cytostome is the initial structure involved in HCCU.

Recently, proteins involved in the initial steps of HCCU have been identified (Figure 12B). Interestingly, the artemisinin resistance-associated K13 protein and its K13-interacting candidates (KICs) were shown to be present in the same cellular compartment and several of them were linked to endocytosis (Birnbaum et al., 2020). Inactiva-

tion of K13 complex proteins, such as K13, led to impaired delivery of host cell cytosol to the food vacuole. Consequently, it can be assumed that fewer hemoglobin degradation products are present to activate artemisinin and its derivatives. This suggests a mechanism of artemisinin resistance based on a reduced HCCU. The absence of accumulation of host cell cytosol-filled intermediates of HCCU upon inactivation of K13 and the fact that K13 co-localizes with typical early endocytosis proteins such as AP-2 μ (Figure 13A) and an Eps15-like protein at the parasite plasma membrane indicates an association of the complex with an early step in endocytosis (Birnbbaum et al., 2020, Henrici et al., 2019a, Sabitzki et al., 2020). Additionally, recent work suggests that the K13 structures observed in the cell may represent cytotosomal collars, as super-resolution images revealed a K13-positive ring-shaped structure comparable in diameter to that of cytotosomal necks (Yang et al., 2019). Interestingly, while Eps15 and AP-2 usually play a role in CME (Section 1.9.1.1.1), Clathrin seems to be absent from this compartment (Figure 13A) (Henrici et al., 2020, Birnbbaum et al., 2020). This is considered unusual since the majority of described Clathrin-independent endocytosis initiation mechanisms do not involve AP-2 and a comparable observation of an endocytic process containing AP-2 but not Clathrin was so far only made in *Aspergillus nidulans* (Martzoukou et al., 2017).

The involvement of an altered AP-2 function in reduced susceptibility to artemisinin was revealed for the first time by whole genome sequencing of an artemisinin-resistant parasite lineage of the rodent malaria parasite *P. chabaudi*. Genome-wide association analysis *in vitro* identified an I568T mutation in AP-2 μ (Henriques et al., 2013), which, also later introduced at the orthologous position I592T in *P. falciparum*, displayed decreased artemisinin susceptibility of the parasites (Henrici et al., 2019b). *In vivo* the mutations causing the S160N/T change in the *P. falciparum* AP-2 μ gene were found in parasites of Kenyan malaria patients, showing a reduced response to an artemisinin-based combination therapy (Henriques et al., 2014). Transgenic parasites carrying the S160N mutation showed significantly less susceptibility to artemisinin as well as quinine *in vitro* (Henriques et al., 2015). Conditional inactivation of AP-2 μ revealed its essentiality for the parasite life cycle (Figure 13B), leading to reduced delivery of host cell cytosol to the DV (Figure 13C) and increased tolerance of ring-stage *P. falciparum* parasites to artemisinin (Figure 13D) (Birnbbaum et al., 2020). These data demonstrate AP-2 μ 's involvement in HCCU of the parasites and validate the relevance of an impaired HCCU in artemisinin resistance. In addition to mutations in AP-2 μ , also a mutation in AP-2 α (H817P) was found in artemisinin-resistant parasite lines although this mutation

was not further analyzed and it is at present unclear if it is causal for resistance (Rocamora et al., 2018). Further, inactivation of AP-2 μ has been described to lead to disrupted schizont organization, schizont maturation, and mislocalization of key merozoite proteins (Henrici et al., 2020).

Although AP-2 μ co-localizes with proteins of the K13 complex, no interaction was detected neither by K13-proximity-based biotinylation (Birnbaum et al., 2020) nor AP-2 μ immunoprecipitation (Henrici et al., 2020) studies. However, the latter found an interaction of AP-2 μ with the K13 interactor KIC7, which could indicate an indirect interaction of these proteins mediated via KIC7. Surprisingly, DIQ-BIO-ID experiments of Eps15 (Birnbaum et al., 2020), a typical Clathrin-accessory protein that binds to the appendage domains of AP-2, did not reveal an interaction with AP-2, whereas it was found to interact with K13 in co-immunoprecipitation studies. Furthermore, while Clathrin is absent, an additional adaptin-like protein, termed KIC4, is present at this compartment (Birnbaum et al., 2020).

Actin, dynamin, and myosin might be involved in HCCU. A long-term study of *in vitro* selection with artemisinin of two West African parasite isolates indicated that mutations in the WD40 propeller domain of the actin-binding protein coronin could mediate resistance (Demas et al., 2018). Based on the structural similarity to the propeller domain of K13, in which resistance-mediating mutations are found, it was hypothesized that there may be similarities in the molecular mechanism of resistance.

Overall, initiation of HCCU in *Plasmodium* parasites appears to occur by a so-far unknown and unusual endocytic mechanism.

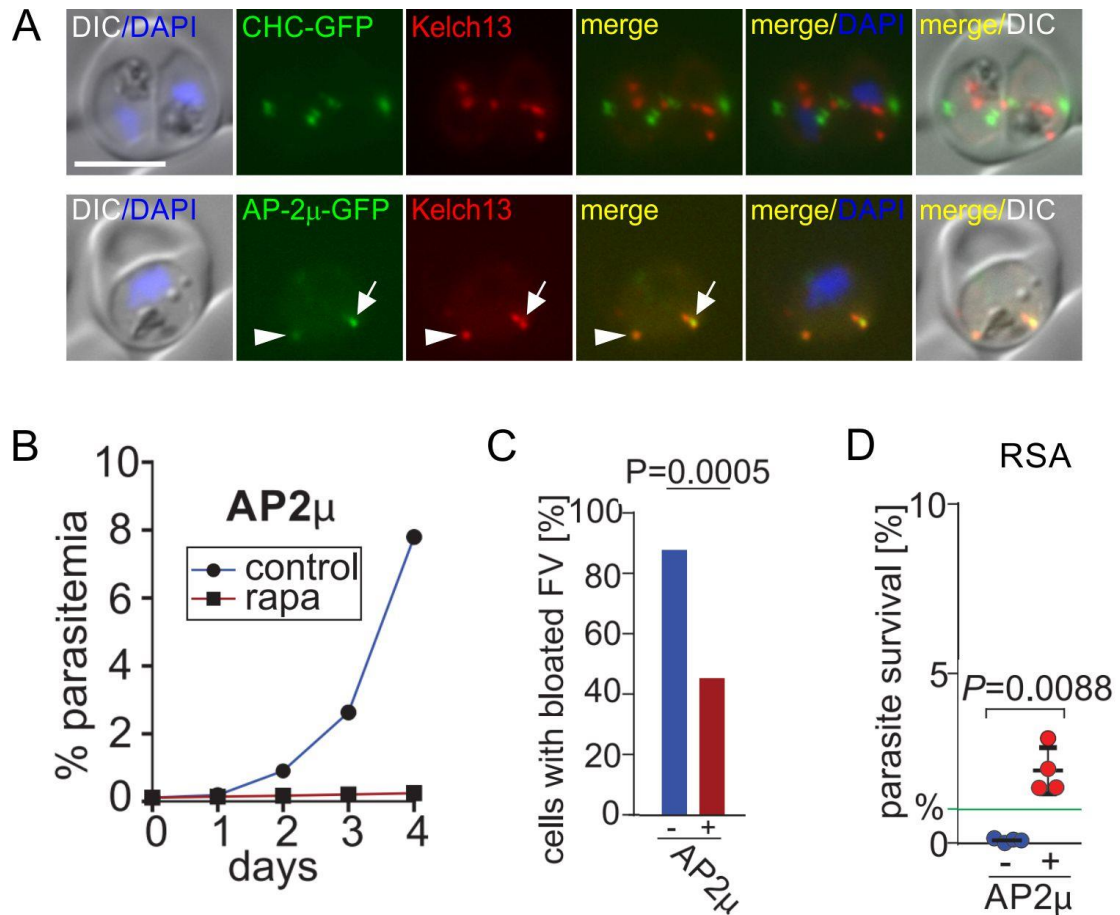


Figure 13 | Localization and functional data of AP-2 μ . **A** Fluorescence microscopy images of parasites endogenously expressing 2xFKBP-GFP-tagged Clathrin heavy chain (CHC) or AP-2 μ with episomal mCherry-Kelch13. Arrows mark co-localization, and arrowheads mark similar regions of AP-2 μ with Kelch13 foci. Merge: merge of the green and red channels; DAPI (nuclei). The scale bar is 5 μ m. **B** Growth curves based on flow cytometry measured parasitemia of control (blue) parasites and with conditional inactivation of AP-2 μ (red) over a time period of 5 days. **C** Quantification of the number of parasites with bloated food vacuoles after E64 treatment (indicative of active endocytosis) for control (blue; -) and with conditional inactivation of AP-2 μ (red;+) for 8 hours. **D** RSA of control (blue) parasites and with conditional inactivation of AP-2 μ (red). Modified from (Birnbau et al., 2020).

1.10.1.2 Early endosome associated structures and proteins in HCCU

The first essential protein identified in the parasite's HCCU termed *PVPS45* (Jonscher et al., 2019) is the orthologue of VPS45 in other eukaryotic organisms. Yeast cells lacking VPS45 show a vacuolar sorting defect (Cowles et al., 1994) and in mammalian cells, VPS45 is part of a complex fusion-machinery located at early endosomes (Section 1.9.1.2) (Collins and Zimmerberg, 2009). A similar role in intermediate steps of

endocytosis for *PfVPS45* (Figure 12B) in *Plasmodium* parasites is plausible. Its inactivation leads to an accumulation of PI3P-positive and hemoglobin-filled vesicles with endosomal characteristics in the parasite cytosol (Figure 14) (Jonscher et al., 2019). VPS45 is typically found in a complex with Rab5 (Nielsen et al., 2000, Gengyo-Ando et al., 2007). Malaria parasites possess three Rab5 proteins, termed Rab5a-c (Quevillon et al., 2003).

However, Rab5a, initially assumed to be part of the endocytosis process (Elliott et al., 2008), was shown to be only essential for schizont formation and displays no involvement in HCCU (Birnbaum et al., 2017). Rab5b lacks the conventional C-terminal cysteine residue but possesses an N-terminal myristoylation site (Quevillon et al., 2003), which might indicate an atypical function (Elliott et al., 2008). *PfRab5b* has been shown to localize to the parasite food vacuole and the plasma membrane (Ezougou et al., 2014) and has been speculated to be transported to the tubovesicular network (TVN) (Ebine et al., 2016, Taku et al., 2021). Yet, functional data indicating the involvement of Rab5b or Rab5c in HCCU have to date not been published. Rab5b was analyzed by the work of Sven Flemming (Flemming, 2015) and Marius Schmitt (Schmitt, 2020) and found to be important for the growth of parasite blood stages. Its inactivation led to a milder but similar phenotype (accumulation of vesicles in the parasite's cytosol) to that observed after VPS45 inactivation. Although ultrastructural work on Rab5b inactivation is still missing, a role in endocytosis, therefore, seems likely. However, whether Rab5b is in a functional complex with *PfVPS45* in *P. falciparum* is not known yet. In mammalian cells, VPS45 is typically linked to Rab5 through the Rab5 effector protein Rabenosyn5. However, Rabenosyn5 has not been identified in the genome of the parasite. Additionally, various endosomal proteins in Apicomplexa are assumed to have been repurposed to function in trafficking processes associated with the secretory organelles required for invasion, which makes an assignment to the endosomal pathway solely based on sequence similarity difficult (Tomavo et al., 2013b, Bisio et al., 2020b, Tomavo et al., 1991).

1.10.1.3 Late endosome associated structures and proteins in HCCU

In comparison to the remainder of the endosomal pathway, the host cell cytosol degradation mechanisms in the lysosomal-like compartment of HCCU, the DV, is well studied and is described in more detail in section 1.8.6. However, the pathway transporting host cell cytosol-filled intermediates to the DV is poorly understood and the individual steps and connection to other vesicular trafficking in the parasite are not known. In model organisms (Section 1.9.1.3; 1.9.1.4) a switch of phosphoinositides and Rabs is thought to be relevant for the maturing process in the endosomal pathway. Of note is, that in contrast to late endosomes and lysosomes of other eukaryotic cells, a switch of phosphoinositides in later HCCU steps seems not to occur since the lysosome-like DV is positive for PI3P, while PI(3,5)P₂ was not been detected in *Plasmodium* parasites. Additionally, the enzyme PIKfyve/Fab kinase, mediating PI(3,5)P₂ synthesis could not be identified in the parasite's genome (Tawk et al., 2010b). Next to Rab5, *Plasmodium* parasites possess also a Rab7 protein (Quevillion et al., 2003), raising the possibility of a Rab5 to Rab7 switch. In *P. falciparum* Rab7 was found to co-localize with a possible retromer complex near the DV and in close proximity to the Golgi-apparatus and therefore its role in recycling processes from a putative late endosome to the Golgi apparatus has been suggested (Siddiqui et al., 2020, Krai et al., 2014). Moreover, the co-localization of Rab7 with autophagy-related-protein-8 (ATG8)-positive acidic structures induced under starvation conditions may indicate a function in autophagy (Tomlins et al., 2013). It is so far unclear if any of these processes are connected to HCCU and there is so far no evidence of direct involvement of Rab7 in HCCU. Overall, the late steps involved in endosome to DV transport in *P. falciparum* parasites, therefore, remain obscure.

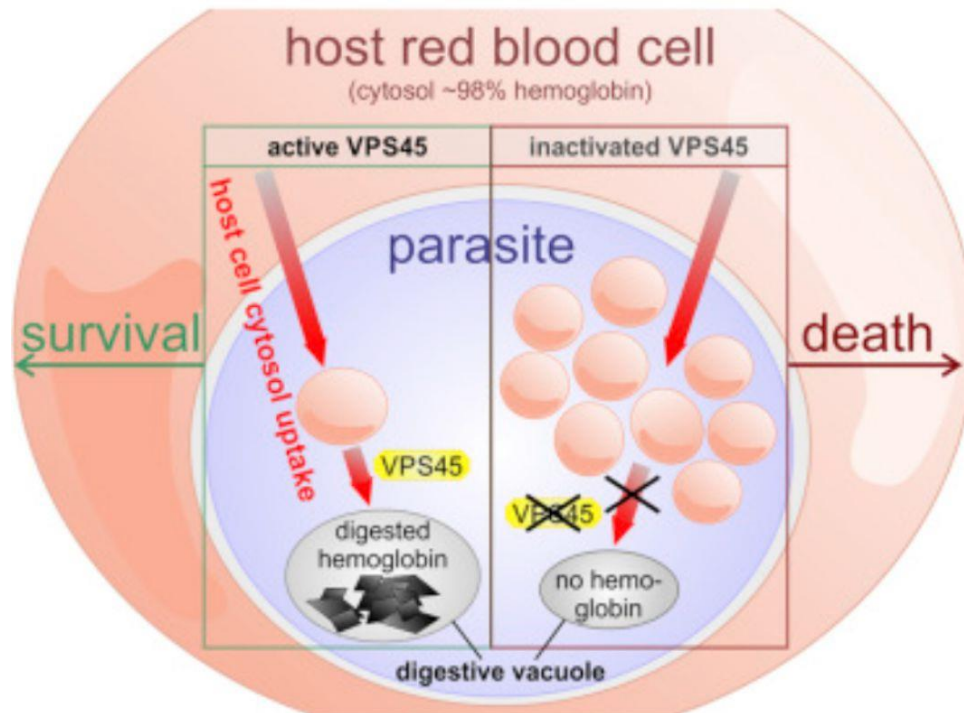


Figure 14 | Scheme of PfVPS45 function in Plasmodium blood-stage parasites. Inactivation of PfVPS45 leads to an accumulation of host cell cytosol-filled vesicles, resulting in an impaired hemoglobin delivery to the food vacuole and the subsequent death of the parasite (Jonscher et al., 2019).

1.11 Aim of Thesis

The proteins involved and the molecular mechanism of HCCU in blood stages of *P. falciparum* parasite represent a hitherto poorly understood endocytic process that has major relevance for the mechanism of action of and resistance to the antimalarial drug Artemisinin. This thesis has the aim to identify, characterize, and functionally analyze proteins in HCCU and determine their potential involvement in the early, mid or late steps of HCCU. For the early steps, the focus will be on the adaptors of the heterotetrameric AP-2 complex. For the endosomal transport steps, the aim is to explore the potential involvement of a canonical pathway alluded to by the recently discovered function of VPS45 by studying Rab5 variants, Rab7, and a potential plasmodial Rbsn5.

2 Materials and Methods

2.1 Materials

2.1.1 Chemicals

Reagent	Company
Agar-Agar	BectonDickinson, Heidelberg
Acetic acid	Roth, Karlsruhe
Aceton	Roth, Karlsruhe
Acrylamide/Bisacrylamide solution (40%)	ROTH, Karlsruhe
Agarose	Invitrogen, Karlsruhe
Albumax II	GIBCO, LIFE TECHNOLOGIES, USA
Ammonium persulfate (APS)	Applichem, Darmstadt
Ampicillin	Roche, Mannheim
Biotin	Sigma-Aldrich, Steinheim
Blasticidin	LIFE TECHNOLOGIES, USA
Concovalin A (ConA)	Sigma-Aldrich, Steinheim
Desoxynucleotides (dNTPs)	Thermo Scientific, Lithuania
Developer solution G150 (Western Blot)	Agfa, Leverkusen
Dextran, Alexa Fluor 647 labelled (10,000 MW)	Invitrogen Cat. No. 200314
4', 6-diamidino-2-phenylindole (DAPI)	Roche, Mannheim
Dihydroethidium (DHE)	Cayman, Ann Arbor, USA
Dulbecco`s Phosphate Buffered Saline (DPBS)	PAN, Biotech, Aidenbach
Dimethyl sulfoxide (DMSO)	SIGMA ALDRICH, USA
DSM1	BEI resources
1,4-dithiothreitol (DTT)	BIOMOL, Hamburg

Ethanol (EtOH)	Roth, Karlsruhe
Ethidium bromide (EtBr)	Sigma-Aldrich, Steinheim
Ethylenediaminetetraacetic acid (EDTA)	BIOMOL, Hamburg
E64 protease inhibitor	Sigma Aldrich
	Cat. No. E3132
Fixation solution G334 (Western Blot)	Agfa, Leverkusen
Formaldehyde	Polysciences
	Warrington/USA
Glutaraldehyde (25%)	Roth, Karlsruhe
Gentamycin	RATIOPHARM, Ulm
G418 disulfate salt	Sigma-Aldrich, Steinheim
Giemsa's azur, eosin, methylene blue solution	Merck, Darmstadt
Glycerol	Merck, Darmstadt
D-Glucose	MERCK, Darmstadt
Hoechst33342	Cheomdex, Switzerland
Hydrochloric acid (HCl)	MERCK, Darmstadt
Hypoxanthine	SIGMA ALDRICH, Steinheim
Isopropanol	Roth, Karlsruhe
Magnesium chloride (MgCl ₂)	Merck, Darmstadt
Methanol	Roth, Karlsruhe
Milk powder	Roth, Karlsruhe
2-[N-(7-nitrobenz-2-oxa-1,3-diazol-4-yl)amino]-2-deoxy-D-glucose (2-NBDG)	INVITROGEN, USA
N, N, N, N-tetramethylethylenediamin (TEMED)	MERCK, Darmstadt
β-Nicotinamide adenine dinucleotide hydrate (NAD)	SIGMA ALDRICH, Steinheim
Percoll	GE Healthcare, Sweden
Piperazine-N,N'-bis(2-ethanesulphonic acid) (PIPES)	SIGMA ALDRICH, Steinheim
Polyethylene glycol 8000 (PEG-8000)	ROTH, Karlsruhe
Potassium chloride (KCl)	MERCK, Darmstadt

Potassium di-hydrogen phosphate (KH ₂ PO ₄)	MERCK, Darmstadt
Potassium hydroxide (KOH)	ROTH, Karlsruhe
Protease inhibitor cocktail ("Complete Mini")	Roche, Mannheim
Rapalog (A/C Heterodimerizer AP21967)	Clontech, Mountain View, USA
RPMI (Roswell Park Memorial Institute)-Medium	Applichem, Darmstadt
Saponin	Sigma, Steinheim
Sodium acetate (NaOAc)	Merck, Darmstadt
Sodium hydrogen carbonate (NaHCO ₃)	Merck, Darmstadt
di-Sodium hydrogen phosphate (Na ₂ HPO ₄)	ROTH, Karlsruhe
Sodium di-hydrogen phosphate (NaH ₂ PO ₄)	ROTH, Karlsruhe
Sodium hydroxide (NaOH)	Merck, Darmstadt
Sodium chloride (NaCl)	GERBU, Gaiberg
Sodium dodecyl sulfate (SDS)	Applichem, Darmstadt
Sorbitol	SIGMA ALDRICH, Steinheim
Triton X-100	Biomol, Hamburg
Tris base	ROTH, Karlsruhe
Tris-EDTA (TE)	INVITROGEN, Karlsruhe
Water for molecular biology (Ampuwa)	Fresenius Kabi Bad, Homburg
WR99210 (WR)	Jacobus Pharmaceuticals Washington, USA
OsO ₄	Electron Microscopy Sciences
Uranyl Acetate	Agar Scientific LTD
Yeast extract	SIGMA ALDRICH, Steinheim
6x DNA-loading dye purple	NEB, Ipswich/USA
10x Fire-polymerase buffer	SOLIS BIODYNE
10x Cutsmart buffer	NEB, Ipswich/USA
5x Phusion HF reaction buffer	NEB, Ipswich/USA

2.1.2 Kits

Kit	Company
NucleoSpin® Plasmid Kit	Macherey-Nagel, Düren
NucleoSpin® Gel and PCR Clean-up Kit	Macherey-Nagel, Düren
QIAamp DNA Mini Kit	Qiagen, Hilden
QIAGEN® Plasmid Midi Kit	Qiagen, Hilden
Western Blot ECL – SuperSignal West Pico	Thermo Scientific, Schwerte
Western Blot ECL – Clarity Detection Kit	Bio-Rad, USA

2.1.3 DNA and protein ladders

Product	Company
GeneRuler™ 1kb DNA ladder	Thermo Scientific, Schwerte
PageRuler™ prestained protein ladder	Thermo Scientific, Schwerte
PageRuler™ plus prestained protein ladder	Thermo Scientific, Schwerte

2.1.4 Solutions, buffer and media

2.1.4.1 Microbiological culture

Ampicillin stock solution	100 mg/ml in 70 % ethanol
Glycerol freezing solution	50 % (v/v) glycerol in 1x LB medium
10x Luria-Bertani (LB) medium stock solution	10 % NaC 5 % peptone 10 % yeast extract in dH ₂ O, autoclaved
LB medium working solution	1 % (w/v) NaCl, 0.5% (w/v) peptone 1% (w/v) yeast extract in dH ₂ O
LB-Amp working solution	0.1% ampicillin in 1x LB medium working solution
LB agar plate solution	1.5% Agar-agar 1x LB mediu
Transformation buffer for ultra-competent cells	10 mM PIPES 15 mM CaCl ₂ 250 mM KCl pH 6.7 (with 10 N KOH)

SOB medium for ultra-competent cells

55 mM MnCl₂

0.05 % NaCl (w/v)

2 % tryptone (w/v)

0.5 % yeast extract (w/v)

deionized H₂O, to 950 ml

1 % 250 mM KCl (v/v)

pH 7.0 (with 5 N NaOH)

ad deionized H₂O to 1000 ml, autoclaved

0.5% 2 M MgCl₂ (v/v) (sterile)

2.1.5 Solutions and buffers for molecular biology analyses

2.1.5.1 DNA gel electrophoresis

50x TAE buffer

2 M Tris base

1 M Pure acetic acid

50 mM EDTA

pH 8.5

1x TAE buffer

40 mM Tris base

20 mM pure acetic acid

1 mM EDTA

pH 8.5

in dH₂O

6x Loading buffer

40 % Glycerol (v/v)

2.5% (w/v) Xylene cyanol

2.5% (w/v) Bromophenol blue,

in dH₂O

2.1.5.2 DNA precipitation

Sodium acetate

3 M NaAc, pH 5.2

Ethanol (EtOH)

100 % and 70%

Tris-EDTA (TE) buffer

10 mM Tris-HCl pH 8.0

1 mM EDTA

pH 8.0

2.1.5.3 Gibson assembly

5x isothermal reaction buffer (6 ml)

3 ml 1 M Tris-HCl pH 7.5

150 μ l 2 M MgCl₂

60 μ l each of 100 mM dGTP/dATP/dTTP/
dCTP

300 μ l 1 M DTT

1.5 g PEG-8000

300 μ l 100 nM NAD

ad 6 ml dH₂O

Assembly master mixture (1.2 ml)

320 μ l 5x isothermal reaction buffer

0.64 μ l 10 U/ μ l T5 exonuclease

20 μ l 2 U/ μ l Phusion DNA polymerase

160 μ l 40 U/ μ l Taq DNA ligase

ad 1.2 ml dH₂O

2.1.6 Media and solutions for cell biology experiments

2.1.6.1 *P. falciparum* in vitro culture

RPMI complete medium

1.587 % (w/v) RPMI 1640

12 mM NaHCO₃

	6 mM D-Glucose
	0.5 % (v/v) Albumax II
	0.2 mM Hypoxanthine
	0.4 mM Gentamycin
	pH 7.2
	in dH ₂ O, sterile filtered
10 % Giemsa solution	10 ml Giemsa`'s azure, eosin methylene blue solution
	90 ml dH ₂ O
Amaza transfection buffer	90 mM NaPO ₄
	5 mM KCl
	0.15 mM CaCl ₂
	50 mM HEPES
	pH 7.6, sterile filtered
Transfection buffer (Cytomix)	120 mM KCl
	150 μM CaCl ₂
	2 mM EGTA
	5 mM MgCl ₂
	10 mM KH ₂ PO ₄
	25 mM HEPES
	pH 7.6
Malaria freezing solution (MFS)	4.2 % D-sorbitol

Malaria thawing solution (MTS)	0.9 % NaCl 28% Glycerol in dH ₂ O, sterile filtered 3.5 % NaCl in dH ₂ O, sterile filtered
WR99210 stock solution	20 mM WR99210 in 1 ml DMSO, sterile filtered
WR99210 working solution	1:1000 dilution of stock solution in RPMI complete medium, sterile filtered
G418 working solution	50 mg/ml in RPMI complete medium, sterile filtered
DHE stock solution (10x)	5 mg DHE in 1 ml DMSO
DHE working solution (1x)	0.5 mg DHE in 1 ml DMSO
DSM1 stock solution (50x)	187,5 mM DSM1 in DMSO
DSM1 working solution	100 µl DSM1 stock solution ad 5 ml in 95%

	DMSO / 5 % 1xPBS solution
Blasticidin S (BS) working solution	5 mg/mL BS in RPMI complete medium, sterile filtered
FACS stop solution	0.5 µl Glutaraldehyde (25 %) in 40 ml RPMI complete medium
Hoechst33342 stock solution (10x)	4.5 mg Hoechst33342 in 1 ml DMSO
Hoechst33342 working solution (1x)	0.45 mg Hoechst33342 in 1 ml DMSO
Rapalog (AP21967) stock solution	500 mM in ethanol
Rapalog working solution	1:20 dilution of stock solution in RPMI complete medium
Human red blood cells	sterile concentrate, blood group 0+, Blood bank, Universitäts-klinikum Eppendorf (UKE), Hamburg

2.1.6.2 Solutions for cell biology and biochemical assays

Parasite lysis buffer	4 % SDS 0.5 % Triton X-100
-----------------------	-------------------------------

	0.5x PBS in H ₂ O
Percoll stock solution	90% (v/v) Percoll 10 % (v/v) 10x PBS
80% Percoll solution	8.9 ml 90% Percoll stock solution 1.1 ml RPMI complete medium 0.8 g Sorbitol sterile filtered
60% Percoll solution	6.7 mM Percoll stock solution 3.3 mM RPMI complete medium 0.8 g Sorbitol, sterile filtered
40% Percoll solution	4.4 ml 90% Percoll stock solution 5.6 ml RPMI complete medium, 0.8 g Sorbitol sterile filtered
Saponin solution	Saponin 0.03 % (w/v) in DPBS

2.1.7 Buffers and solutions for protein analyses

2.1.7.1 SDS-Page and Western Blot

Ammonium persulfate (APS)	10 % (w/v) in dH ₂ O
---------------------------	---------------------------------

Blocking solution	5% (w/v) milk powder in 1xPBS
10x Running buffer	250 mm Tris base 1.92 M Glycine 1 % (w/v) SDS in dH ₂ O Separating gel buffer 1.5 M Tris-HCl, pH 8.8 in dH ₂ O
Stacking gel buffer	1M Tris-HCl, pH 6.8 in dH ₂ O
Stacking gel (for two gels, 5%)	0.75 ml stacking gel buffer 4.35 ml dH ₂ O 750 µl Acryl amide (40 %) 60 µl SDS (10 %) 60 µl APS (10 %) 6 µl TEMED
Separating gel (for two gels, 12%)	2.5 ml running gel buffer 4.2 ml dH ₂ O 3 ml Acryl amide (40 %) 100 µl SDS (10 %) 100 µl APS (10 %) 4 µl TEMED

6x SDS sample buffer	375 mM Tris-HCl pH 6.8 12 % (w/v) SDS 60 % (v/v) Glycerol 0.6 M DTT 0.06% (w/v) Bromophenol blue
10x Western blot transfer buffer	250 mM Tris-Base 1.92M glycerol 0.1% (w/v) SDS in dH ₂ O
1x Western blot transfer buffer	10% 10x Western transfer buffer 20% Methanol in dH ₂ O

2.1.8 Bacterial and *Plasmodium* strains

Escherichia coli XL-10 Gold	Tetr Δ(mcrA)183 Δ(mcrCB-hsdSMR-mrr) 173 endA1 supE44 thi-1 recA1 gyrA96 relA1 lac Hte [F' proAB lacIqZΔM15 Tn10 (Tetr) Amy Camr]
-----------------------------	---

Plasmodium falciparum 3D7 clone of NF54 isolated from an airport malaria patient, near Schipol Airport, Amsterdam, Netherlands

2.1.9 Enzymes and antibodies

2.1.9.1 Polymerases

Enzyme	Concentration	Company
FirePol [®] DNA Polymerase	[5 U/ μ l]	Solis BioDyne, Taipei, Taiwan
Phusion [®] High-Fidelity DNA Polymerase	[2 U/ μ l]	NEB, Ipswich, USA

2.1.9.2 Restriction enzymes

Restriction	Company
AgeI-HF [®]	NEB, Ipswich, USA
AvrII	NEB, Ipswich, USA
BamHI-HF [®]	NEB, Ipswich, USA
BclI-HF [®]	NEB, Ipswich, USA
BglI	NEB, Ipswich, USA
BsII	NEB, Ipswich, USA
DpnI	NEB, Ipswich, USA
EaeI	NEB, Ipswich, USA
HindIII-HF [®]	NEB, Ipswich, USA
KpnI-HF [®]	NEB, Ipswich, USA
MfeI-HF [®]	NEB, Ipswich, USA
MluI-HF [®]	NEB, Ipswich, USA
NaeI	NEB, Ipswich, USA
NotI-HF [®]	NEB, Ipswich, USA
PmeI	NEB, Ipswich, USA
PstI-HF [®]	NEB, Ipswich, USA
SacI-HF [®]	NEB, Ipswich, USA
Sall-HF [®]	NEB, Ipswich, USA

SmaI	NEB, Ipswich, USA
SpeI-HF [®]	NEB, Ipswich, USA
XbaI	NEB, Ipswich, USA
XhoI	NEB, Ipswich, USA
XmaI	NEB, Ipswich, USA

2.1.9.3 Primary antibodies

Antigen	Organism	IFA dilution	Western blot dilution	Source
Aldolase	Rabbit	-	1:2000	
BIP	Rabbit	-	1:2000	Struck et al. 2005
GFP	mouse	1:500	1:1000	ROCHE, Mannheim
HA	rat	1:500	1:1000	ROCHE, Mannheim
Hemoglobin	Rabbit	1:2000	-	Sigma Cat. No. H4890
RFP	rat	1:500	1:2000	CHROMOTEK, Germany

2.1.9.4 Secondary antibodies

Antigen	Conjugate	Organism	IFA dilution	Western blot dilution	Source
mouse	Alexa 488	goat	1:2000	-	LIFE TECHNOLOGIES, USA
mouse	Alexa 594	goat	1:2000	-	LIFE TECHNOLOGIES, USA
mouse	HRP	goat	-	1:3000	DIANOVA, Hamburg
Rabbit	Alexa 488	donkey	1:2000	-	INVITROGEN, Molecular probes Leiden
Rabbit	Alexa 594	donkey	1:2000	-	INVITROGEN, Molecular probes Leiden
Rabbit	HRP	donkey	-	1:2500	DIANOVA, Hamburg
Rabbit	Alexa 647	goat	1:2000	-	Life Technologies Cat. No. A-21244
rat	Alexa 594	goat	1:2000	-	INVITROGEN, Molecular probes Leiden
rat	HRP	goat	1:2000	1:3000	DIANOVA, Hamburg

2.1.9.5 Streptavidin beads

Name	Antigen	Conjugate	Antibody	Source
GFP-Trap® Agarose	GFP	coupled agarose beads	GFP Nanobody/ V _H H	Chromotek, Munich

2.1.9.6 Oligonucleotides

Oligonucleotides were synthesized by Sigma-Aldrich, Steinheim and are shown in Appendix A.1 and A.2..

2.1.9.7 General plasmids

General plasmids were either used unmodified or served as a basis for cloning. New cloned plasmids are shown in Appendix A.3..

General plasmids	Source
pSkip-Flox	(Birnbaum et al., 2017)
<i>nmd3</i> '1xNLS-FRB-mCherry	(Birnbaum et al., 2017)
Clathrin-LC-mCh ^{epi}	Ulrike Fröhlke
P40-mCh ^{epi}	(Birnbaum et al., 2017)
pSkip-Flox	(Birnbaum et al., 2017)
GRASP-mCh ^{epi}	(Birnbaum et al., 2017)
K13-mCh ^{epi}	(Birnbaum et al., 2017)
pSLI-3xHA-T2A-Neo	Mesen-Ramirez
pSLI-2xFKBP-GFP-2xFKBP-T2A-Neo	(Birnbaum et al., 2017)
pSLI-2xFKBP-GFP-T2A-Neo	(Birnbaum et al., 2017)
p-N-GFP-2xFKBP-loxP	(Birnbaum et al., 2017)
pSLI-TGD	(Birnbaum et al., 2017)
p-N-GFP-loxP	(Birnbaum et al., 2017)
p-N-GFP-2xFKBP-loxP-2xFKBP	(Birnbaum et al., 2017)
pSLI2A-mSca-T2A-DHODH	(Naranjo Prado, 2020, Stäcker, 2021)

2.1.10 Sequencing

Sequencing was performed by the company SeqLab in Göttingen (Germany) using the Sanger DNA sequencing method. For the sequencing approach (in total 9 µl) up to 600 – 700 ng plasmid DNA and 20 pmol sequencing oligonucleotide were used.

2.1.11 Technical devices

Device	Article description	Company
Agarose gel chamber	Sub Cell GT basic	Bio-Rad, München
Analytical Balance	870	Kern
Laboratory balance	Atilon	ACCULAB SARTORIUS, Göttingen
Centrifuge	Megafuge 1.0R	HERAUES, Hanover
Table centrifuge	Eppendorf 5415 D	Eppendorf, Hamburg
Cooling Unit Centrifuge	Rotor JA-12	Beckman Coulter, Krefeld
	Avanti J-26S XP	
	Rotor JA-14	
Microcentrifuge	Butterfly	THERMO SCIENTIFIC, Schwerte
Electrophoresis chamber	Mini Protean 67s	Bio-Rad, München
Electroporator	Nucleofector II AAD-1001N	Amaxa Biosystems, Germany
Electroporator	Gene Pulser XCell	BIO-RAD, Munich
Flow cytometry cell analyser	LSR II	BECTON DICKINSON, Franklin Lakes/USA
Gel holder cassette	Mini Protean Tetra	Bio-Rad, München
Ice machine	EF 156 easy fit	Scotsman, Vernon Hills, USA
Bacterial incubator	Thermo function line	Heraeus, Hannover
Incubator for <i>P. falciparum</i> cell culture	Heratherm IGS400	Thermo Scientific, Langens- selbold
Shaking incubator	MaxQ4000	Barnstead, Iowa, USA
Shaking incubator	Innova 40	NEW BRUNSWICK SCI- ENTIFIC, Edison/USA
Light microscope	Axio Lab A1	Zeiss, Jena
Fluorescence microscope	Axio Lab A1	Zeiss, Jena
		Zeiss, Jena
Microscope digital camera	Orca C4742-95	HAMAMATSU PHOTO-

Microwave	Micro 750W	TONICS K. K., Japan
Microwave	900 & Grill MW7869	Whirlpool, China
Molecular imager	ChemiDoc™ XRS+	SEVERIN, Sundern
Laboratory scale	Atilon	BIO-RAD, Munich
		Acculab Sartorius, Göttingen
PCR Mastercycler	epgradient	Eppendorf, Hamburg
PCR Thermal cycler	C1000 Touch	BIO-RAD, Munich
pH-meter	SevenEasy	METTLER-TOLEDO, Giessen
Pipettes	0.2-2, 1-10, 100, 200, 1000 µl	Gilson, Middleton, USA
Pipettor	Pipetboy acu	IBS, USA
Pipettor	Cell Mate II™	THERMO SCIENTIFIC, Langenselbold
Power Supply	Power Source 300 V	VWR, Taiwan
Power Supply	E835 300 V	CONSORT, Belgium
Power Supply	EV231	CONSORT, Belgium
Roller Mixer	STR6	STUART, Staffordshire/UK
Roller Mixer	SU1400	SUN LAB, Germany
Sterile laminar flow bench	Sterilguard III Advance	Baker Company, Stanford, USA
Sterile laminar flow bench	Safe 2020™	THERMO SCIENTIFIC, Pinneberg
Thermoblock	Thermomixer compact	Eppendorf, Hamburg
Vacuum pump	BVC Control	Vacuubrand, Germany
Vortexer	Genie 2	Scientific Industries, USA
Waterbath	1083	GFL, Burgwedel

2.1.12 Labware and disposables

Product	Specification	Company
Chromatography paper		Whatman, UK
Conical falcon tubes	15 ml, 50 ml	Sarstedt, Nümbrecht
Cryotubes	1.6 ml	Sarstedt, Nümbrecht
Culture bottles	50 ml	Sarstedt, Nümbrecht
Disposable pipette tips	1-10/20-200/100-1000 µl	Sarstedt, Nümbrecht
Eppendorf reaction tubes	1.5 ml/2 ml	Sarstedt, Nümbrecht/ Eppendorf, Hamburg
Flow cytometry tubes	55.1579: 5 ml, 75x 12 mm	Sarstedt, Nümbrecht/
Glass beads	2.85 – 3.45 mm	Roth, Karlsruhe
Glass cover slips	2.85 – 3.45 mm	Roth, Karlsruhe
Glass cover slips	24 x 65 mm thickness, 0.13-0.16 mm	R. Langenbrinck, Em- mendingen
Glass slides		Engelbrecht, Edermünde
Gloves, latex EcoShield		Kimtech Science
Gloves, purple nitrile		BSN medical GmbH
Gloves, blue nitrile	35PLUS	BINGOLD, Hamburg
Leukosilk tape		BSN MEDICAL GmbH
Nitrocellulose blotting membrane	Amersham 0.45 µm	GE Healthcare, Germany
One way cannula		Braun, Melsungen
One way injection		Braun, Melsungen
Parafilm		Bemis, USA
Pasteur pipette		Brand, Wertheim
PCR reaction tubes	Multiply-µStrip Pro 8-Strip	Sarstedt, Nümbrecht
Pipette tips	1-10, 20-200, 100-1000 µl	SARSTEDT, Nümbrecht & EPPENDORF, Hamburg
Filter tips	1-10, 20-200, 100-1000 µl	SARSTEDT, Nümbrecht
Plastic pipettes	5 ml, 10 ml, 25 ml	SARSTEDT, Nümbrecht
Petri dishes	2 ml, 10x35 mm	THERMO SCIENTIFIC,

Petri dishes	5 ml, 15x60 mm; 10 ml, 14x90 mm	Denmark Sarstedt, Nümbrecht
reaction tubes	1.5 ml, 2 ml	SARSTEDT, Nümbrecht & EPPENDORF, Hamburg
Scalpel		BRAUN, Melsungen
Sterile filter	0.22 µm	SARSTEDT, Nümbrecht
TC-6-well plates	2-4 ml, 85.2x 127.8 mm	SARSTEDT, Nümbrecht
TC-12-well plates	2-4 ml, 85.2x 127.8 mm	SARSTEDT, Nümbrecht
Transfection cuvettes	0.2 cm	Bio-Rad, München

2.1.13 Computer Software

Program	Version	Company
ApE-A plasmid Editor	v2.0.49	Wayne Davis, Utah, USA
Axiovision 40	v 4.7.0.0	Zeiss, Jena
CorelDRAW® X6	16.0.0.707	Corel Corporation
Corel® PHOTO-PAINT™ X6	16.0.0.707	Corel Corporation
FACS DIVA	6.1.3	BECTON DICKISON
GraphPad Prism	6.0d	GraphPad Software, La Jolla, USA
ImageJ 64	1.43u	Open Source (http://rsbweb.nih.gov/ij/)
Image Lab	5.2.1	Bio-Rad Laboratories
Imaris x64	7.8	Bitplane AG, Zürich, Schweiz
Microsoft Office	2010	Microsoft Corporations, Redmond, USA

2.1.14 Databases and online sources

Program	Address (URL)	Application
BLAST	http://blast.ncbi.nlm.nih.gov	Protein alignments
ExPASy	http://myhits.isb-sib.ch	Motif scan
PlasmoDB	http://plasmodb.org	<i>Plasmodium</i> Database
ToxoDB	https://toxodb.org/	Toxoplasma Database
PubMed	http://www.ncbi.nlm.nih.gov	Literature research
Clustal Omega	https://www.ebi.ac.uk/Tools/msa/clustalo/	Multiple Sequence Alignment
InterPro	https://www.ebi.ac.uk/interpro/	Protein domain prediction
HHPred	https://toolkit.tuebingen.mpg.de/tools/hhpred	homology detection

2.2 Methods

2.2.1 Molecular biology methods

2.2.1.1 Polymerase chain reaction (PCR)

For amplification of DNA elements, polymerase chain reactions (PCR) were conducted. PCRs were carried out for specific amplification and subsequent cloning of DNA fragments (preparational PCR) or analytical purposes, such as colony PCRs (Section 2.2.1.5) for identification of positive clones after transformation and for confirmation of correct integration of plasmids into the parasite genome (Section 2.2.1.8) (analytical PCR). Genomic DNA (gDNA) of *P. falciparum* 3D7 parasites (Section 2.2.1.7) and isolated plasmids (Section 2.2.1.2; 2.2.1.3) were used as templates. Phusion high fidelity polymerase (NEB) was usually used to perform the preparative PCRs since its proof-reading activity reduces the probability of undesired mutations. For analytical PCRs, the FirePol polymerase was used. Typical reaction mixes and cycler settings for preparative and analytical PCRs are listed in Table 1. Annealing or elongation temperatures were adjusted for different PCR fragments.

Table 1 | Standard mix for preparative and analytical PCRs and thermocycling settings.

Preparative PCR		Analytical PCR	
Reagents	Volume	Reagents	Volume
5x Phusion buffer	10 μ l	10x FIREPol buffer	5 μ l
dNTP's	5 μ l	dNTP's	5 μ l
Primer fw	1 μ l	MgCl ₂	4 μ l
Primer rv	1 μ l	Primer fw	2.5 μ l
Phusion DNA polymerase	0.5 μ l	Primer rv	2.5 μ l
Template	0.5 μ l	FIREPol DNA polymerase	0.5 μ l
dH ₂ O	ad 50 μ l	Template	0.5 μ l
		dH ₂ O	ad 50 μ l

PCR program			
Phase		Temperature	Time
Initial denaturation		95 °C	4 min
25-30 cycles	Denaturation	95 °C	30 s
	Annealing	42-60 °C	30 s
	Elongation	52-72 °C	1-12 min
Final hold		4 °C	

2.2.1.2 Purification of PCR products and digested vectors

For subsequent ligation (Section 2.2.1.4) the resulting PCR products and digested vector DNA are purified from the enzymes (polymerase and digestion enzymes), residual salts, and oligonucleotides using the commercial NucleoSpinGel and PCR Clean-up kit (Macherey-Nagel) according to the manufacturer's protocol. PCR products and vector DNA were eluted with 50 μ l of elution buffer.

2.2.1.3 Digestion of PCR products and vectors

For subsequent ligation (Section 2.2.1.4) preparative digestions (Table 2) were performed for PCR products and vectors using different DNA restriction enzymes. DpnI was used to deplete methylated template DNA. Analytical digestions were performed of mini and midi DNA preparations (Section 2.2.2.3) to exclude recombination and confirm the correct insertion of PCR products into the plasmid. The incubation time for the digestions was 2.5 h at 37 °C.

Table 2 | Standard mix for preparative DNA digestion.

Preperative DNA digestion	
Reagents	Volume
10x NEB CutSmart buffer	10 μ l
Enzyme	each 1 μ l
DNA (plasmid or PCR product)	10-30 μ l
dH2O	ad 50 μ l

2.2.1.4 Gibson assembly

The Gibson DNA assembly (Gibson et al., 2009) is a method for the ligation of up to six different inserts into one vector. For ligation, the PCR products need to have an overlap of 15-35 bp with the vector sequence and do not require sticky ends. Consequently, only DpnI digestion of the insert is required for the depletion of the methylated template DNA. The ligation mix (Table 3) was incubated at 50 °C for 60 minutes and then used for the transformation of E.coli chemo-competent cells (Section 2.2.2.1).

Table 3 | Standard mix for Gibson DNA assembly.

Gibson assembly	
Reagents	Volume
Assembly master mix	7.5 μ l
Vector DNA	each 1 μ l
PCR product (Insert)	0.5 μ l
dH2O	ad 10 μ l

2.2.1.5 Colony PCR screen to detect bacterial clones

The DNA ligation can result in a mixture of plasmids containing the original and the new replacing insert. PCR screening of bacterial colonies after transformation (Section 2.2.1.5) is a rapid technique to identify positive clones containing the correct insert. To this end, an insert- and a vector-specific primer were used so that PCR products were generated only when the plasmid containing the new desired insert was present in a colony. As templates, different bacterial colonies were picked separately with sterile pipette tips and placed into PCR reaction tubes containing the mix of an analytical PCR (Table 1). The PCR reactions were analyzed by agarose gel electrophoresis (Section 2.2.1.9) to identify clones with the expected product size.

2.2.1.6 Sequencing of plasmid DNA

To exclude that the insert contains mutations it was sequenced. 200-800 ng plasmid DNA or PCR product was mixed with 3 μ l (10 mM) of a specific sequencing primer and adjusted with dH2O to a final volume of 15 μ l. The sequencing reaction was performed by Sequence Laboratories Göttingen (SeqLab).

2.2.1.7 Isolation of genomic DNA

Genomic DNA (gDNA) from transgenic and wildtype *P. falciparum* 3D7 was isolated and used for PCR analysis to confirm the correct integration of knock-in constructs into the parasite genome and as a template for preparative PCRs. 5 ml of a parasite culture was centrifuged at 1800 x g for 3 minutes. Purification of gDNA from the blood pellet was performed using the QIAamp DNA Mini Kit according to the manufacturer's protocol. The gDNA was eluted with 200 μ l dH2O and stored at -20 °C.

2.2.1.8 PCR to verify genome integration

Three different primer combinations (Appendix A.2) were used to confirm 5' and 3' integration and disruption of the endogenous locus. To verify correct integration, a forward primer that binds to the endogenous genomic locus upstream of the target sequence was used in combination with a vector-specific reverse primer. To confirm correct integration at the 3' end, a vector-specific forward primer (pArlsense55) was used along with a reverse primer that binds to the endogenous genomic locus downstream of the target gene. To ensure complete removal of the endogenous target region, PCR was performed with the forward endogenous 5' primer and the reverse endogenous 3' primer.

2.2.1.9 Agarose gel electrophoresis

Due to their phosphate backbone, DNA molecules are negatively charged and can be separated in an electric field in an agarose matrix as they move towards the anode, corresponding to their size. 1% agarose gels were prepared by dissolving agarose (Invitrogen) in 1x TAE buffer through boiling in a microwave. Ethidium bromide was added to a final concentration of 1 µg/ml and the solution was transferred to a gel tray where it cooled down until it became solid. The gel was placed in an electrophoresis chamber containing 1x TAE buffer. The DNA samples were mixed with 6x DNA loading dye and loaded into the wells next to a DNA ladder. A voltage of 150 V was applied for 30 minutes and DNA bands were analyzed under UV light in comparison to the DNA ladder to determine the size of the bands.

2.2.2 Microbiological methods

2.2.2.1 Transformation of *E.coli* chemo competent cells

To increase plasmid uptake of the *E.coli* XL10 Gold strain, bacteria were rendered chemo-competent via the rubidium chloride method, which results in a decreased stability of the bacterial cell wall (Hanahan, 1983). An aliquot of 100 µl of chemo-competent *E.coli* was slowly thawed on ice. 10 µl of a ligation mixture (Section 2.2.1.4) was added and incubated on ice for 15-30 minutes. Then the suspension was heat-shocked at 42 °C for 30 seconds and immediately placed back on ice for 5 minutes. The entire suspension was plated on a pre-warmed LB agar plate containing ampicillin

as the selection drug. The plate was incubated overnight at 37 °C and the grown bacterial colonies were screened for positive clones as described in section 2.2.1.5.

2.2.2.2 Cultivation and storage of *E. coli* transgenic cells

Positives clones (detected by colony PCR screening (Section 2.2.1.5) from an agar plate or glycerol stock were inoculated in LB-medium containing ampicillin overnight at 37 °C under constant shaking. For plasmid mini preparations 1.5 ml of LB-medium was used in a 2 ml reaction tube, and for plasmid midi preparations, 150 ml of LB-medium was used in a 1 l Erlenmeyer flask. For long-term storage, 500 μ l of overnight bacteria culture was mixed with 500 μ l of glycerol and immediately stored at -80 °C.

2.2.2.3 Purification of bacterial plasmids (Mini Prep and Midi Prep)

The bacteria overnight culture was centrifuged and the supernatant was discarded. For small-scale purification plasmids were purified with the Nucleo Spin Plasmid Kit and for medium-scale purification with the QIAfilter Plasmid Midi Kit.

2.2.3 Cell biological methods

2.2.3.1 Cell culture of *P. falciparum*

A standard procedure was used for the continuous cultivation of intraerythrocytic blood stages of *P. falciparum* (Trager and Jensen, 1976). Parasites were cultivated in Petri dishes filled with 5 or 10 ml of RPMI 1640 complete medium containing 0.5 % Albumax and erythrocytes (blood group 0+) at a hematocrit of 5 %. Culture dishes were incubated at 37 °C under a low-oxygen atmosphere in airtight boxes gassed with 1 % O₂, 5 % CO₂, and 94 % N₂ to simulate human bloodstream conditions. For the selection of transgenic parasites, different drugs were added according to the particular selection marker. The intraerythrocytic asexual life cycle of the parasite lasts about 48 h. As a result, parasitemia increases by a factor of 4-10 after about 2 days. The parasitemia (percentage infection of erythrocytes by the parasite) was determined by cell counting of Giemsa-stained blood smears. The medium was changed every other day. When parasitemia reached 5-10 %, the culture was diluted accordingly to prevent death.

2.2.3.2 Blood smears and Giemsa staining

For the determination of the parasitemia or to analyze the development of the parasite, ~0.8 μ l of cultured blood was dropped onto one slide and smeared with a second slide in a 45 ° angle to obtain a single layer of RBCs. Once air-dried, the smears were fixed in methanol (99.8 %) for 10 seconds and stained in a Giemsa solution (10 %) for ~15 minutes. The slides were rinsed with water, dried, and the parasitemia was determined by counting infected and uninfected cells using an optical light microscope (Section 2.2.5.1).

2.2.3.3 *P. falciparum* cryo-stabilates

P. falciparum parasites can be stored for several years either at -80 °C or in liquid nitrogen. For cryopreservation of the transgenic cell lines, 5-10 ml of the culture was centrifuged at 1800 x g for 3 minutes with a ring parasitemia of 5-10 %, the supernatant was discarded, and the cell pellet was resuspended in 1 ml of malaria freezing solution (MFS), and transferred to a sterile 2 ml cryotube and stored at -80 °C in a freezer or at -196 °C in liquid nitrogen. To recultivate frozen parasite strains, the cryotube was removed from the freezer and rapidly thawed in a water bath at 37 °C. The cell suspension was transferred to a 15 ml Falcon tube and centrifuged at 1800 x g for 3 minutes. The supernatant was discarded and the pellet was carefully resuspended in 1 ml of malaria thawing solution (MTS). Centrifuged again at 1800 x g for 3 minutes and the resulting pellet was resuspended in pre-warmed RPMI medium and placed in a 5 ml dish. Blood was added to obtain 5 % hematocrit. The next day, the medium was changed and the required selection drug was added.

2.2.3.4 Parasite synchronization with Sorbitol

Synchronous development of *P. falciparum* from the ring stage onwards can be achieved by lysis of mature stages with 5 % D-sorbitol (Lambros and Vanderberg, 1979). To synchronize the parasites, 5-10 ml of parasite culture was pelleted in a 15 ml falcon tube by centrifugation at 1800 x g for 3 minutes. The supernatant was discarded and the pellet was resuspended in 2 ml pre-warmed 5 % D-Sorbitol in dH₂O and incubated at 37 °C. After 10 minutes of incubation, the tube was centrifuged again at 1800 x g for 3 minutes, washed with 5 ml RPMI complete medium, and transferred into a new petri dish containing RPMI medium. A culture was obtained that contained only

parasites 0-18 hours post-invasion. To obtain a tighter time frame, the procedure can be repeated after 10 hours.

2.2.3.5 Differential purification of *P. falciparum* infected erythrocytes in a Percoll gradient

A Percoll gradient was used to separate trophozoites and schizonts from uninfected erythrocytes and ring-stage parasites. For this purpose, 400 μ l of 80 % Percoll was pipetted into a 2 ml reaction tube and carefully overlaid by 400 μ l of the 60 % and 400 μ l 40 % Percoll solution. A parasite culture was pelleted by centrifugation at 1800 x g for 3 minutes, the supernatant was discarded and the cells were slowly layered onto the top of the gradient. After centrifugation at 2000 x g for 5 minutes, the layers containing the desired parasite stages were transferred to a new tube and washed with RPMI complete medium.

2.2.3.6 Transfection of *P. falciparum*

2.2.3.6.1 Segmenter/Merozoite tranfection

Transfection of *P. falciparum* parasites was accomplished by electroporation. 50 μ g plasmid DNA was precipitated by adding 1/10 volume of 3 M sodium acetate (pH 5.2) and 3 volumes of absolute ethanol and pelleted by centrifugation at 20000 x g for 15 minutes. The DNA pellet was washed with 70 % ethanol, centrifuged, and air-dried under sterile conditions. The pellet was dissolved in 10 μ l TE-buffer and 90 μ l of Amaxa transfection solution was added. Late schizont stage parasites were harvested by carefully overlaying 4 ml of 60 % Percoll solution with 8ml of parasite suspension and subsequent centrifugation at 2500 x g for 8 minutes. The schizont layer was collected, transferred to a new 15-ml tube, and washed with total RPMI medium. 10-15 μ l of the schizont pellet was mixed with the DNA solution and transferred into an electroporation cuvette (2 mm, BioRad). The electroporation was performed using the Nucleofector II AAD-1001N (Amaxa) and program U-033. Immediately after electroporation, the parasites were transferred to a 1.5 ml reaction tube containing 300 μ l red blood cells and 500 μ l RPMI complete medium pre-warmed to 37 °C. The tube was incubated with vigorous shaking in a thermomixer at 37 °C for 30 minutes. Then, the parasites were transferred to a 15x60 mm Petri dish containing 6 ml of total RPMI medium. After 24 hours, the medium was changed and the selection drug was added. In the following 5

days, the medium was changed daily, then every other day. The parasites were detected in Giemsa smears at approximately 8-15 days post-transfection.

2.2.3.6.2 Ring-stage tranfection

For the transfection of ring-stage *P. falciparum* parasites, the BioRad transfection system was used. For this, ~10 ml of parasite culture with a ring-stage parasitemia of ~5 % was centrifuged at 2000 x g for 3 min. 100 µg of plasmid DNA was dissolved in 20 µl of TE buffer and 380 µl of Cytomix was added. Together with 200 µl of pelleted parasite culture, the mix was transferred to an electroporation cuvette (2 mm, Biorad). The electroporation was performed using a Gene Pulser Xcell (Biorad; conditions: 310 V, 950 µF, ∞ Ω). The content of the cuvette was then transferred to a Petri dish containing RPMI medium (5 % hematocrit): The Culture medium was changed daily for the next 5 days. and the transgenic parasites were selected with the respective selection drug.

2.2.3.7 Selection linked integration (SLI)

Plasmid integration into the *P. falciparum* genome is important for the localization and functional studies of endogenous proteins. The SLI method developed by Birnbaum et al. (2017) (Figure 15) is a robust and rapid method for achieving genomic integrations. To this end, the SLI plasmid (or a modified SLI variant) was transfected and parasites containing the episomal plasmid were selected by addition of the endosomal selection marker (WR99210) to the parasite culture. In addition to WR resistance, the plasmids contain a promoterless, C-terminal homologous targeting region (length: 500-1500 bp) of the gene of interest, linked to the desired protein tag and a selection marker (neomycin or DHODH resistance), separated by a skip peptide. This expression cassette is transcribed only under the endogenous promoter after single crossover integration into the target locus. Due to the skip peptide, the tagged protein of interest and the additional resistance marker are two separate translation products, and parasites carrying the integration can be selected using the additional resistance marker associated with the integration. To this end, the culture was adjusted to ~4% parasitemia, and neomycin or DSM1 was added to the parasite culture. To confirm correct integration, the gDNA (Section 2.2.1.7) of the integrands was isolated and PCR was performed for integration control (Section 2.2.1.8).

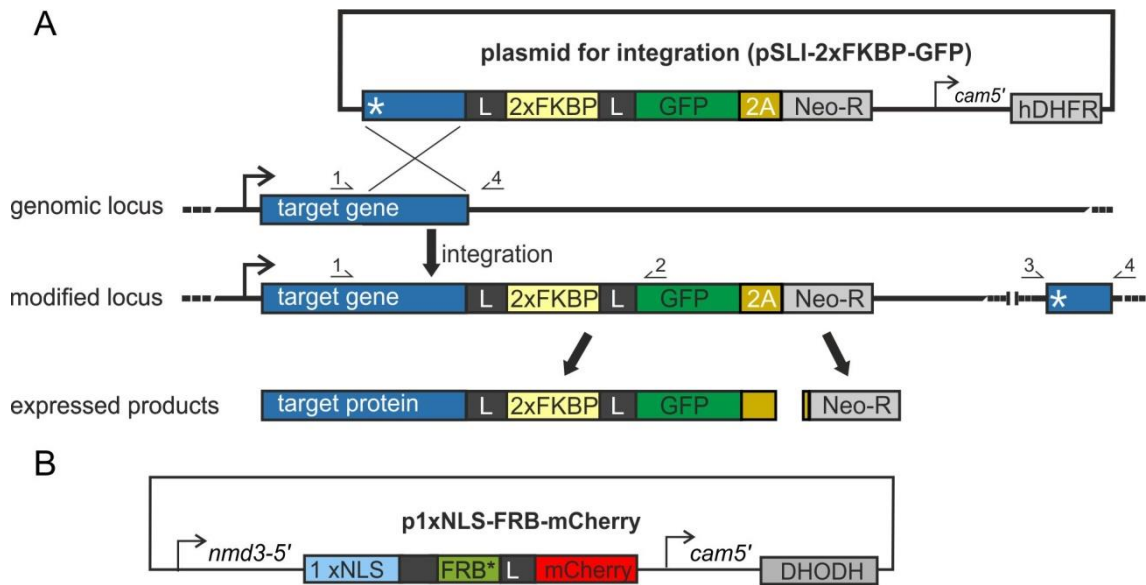


Figure 15 | Scheme of selection linked integration strategy and knock-sideway (Birnbaum et al., 2017). **A** A homology targeting region (500-1000bp) of the protein of interest is inserted into the pSLI sandwich construct. Through single crossover integration, the 2xFKBP-GFP-2xFKBP tagged protein and the resistance marker (neomycin) get expressed under the endogenous promoter. Due to the 2A skip peptide, the resistance marker is a translational independent product of the tagged protein. hDHFR: WR99210 resistance marker; L3 and L4: linker; GFP: green fluorescent protein; 2A: T2A skip peptide; Neo-R: neomycin resistance; FKBP12; asterisk: stop codon; arrows promoters; arrows with numbers 1-4: primers used for integration check PCR **B** Plasmids for mislocalization of target proteins. FKBP tagged proteins can be mislocalized by a so called mislocalizer either through the nucleus containing a nuclear localization signal (NLS). L, linker; hDHDR and DHODH, resistance marker; arrows, promoter (*nmd3-5'*; *cam5'*).

2.2.3.8 Knock-sideway of target protein using the FKBP-FRB* system

For functional analysis of the target protein, the knock-sideway method was used, which allows inducible conditional removal of the target protein from its site of action to an unrelated cell compartment e.g. the nucleus (Figure 16). It is based on heterodimerization of FKBP and FRB* induced by a ligand called rapalog. To this end, FKBP domains were fused to the endogenous protein using the SLI method (Section 2.2.3.7), and the FRB* is separately expressed fused to a protein sequence containing trafficking information for a different cellular compartment, e.g. NLS (mislocalizer) (Figure 15B). After the addition of rapalog, FRB* and FKBP dimerize, and the protein of interest gets removed from its site of action by the mislocalizer. For the knock-sideway experiment parasites expressing the endogenously FKBP-tagged protein and a mislocal-

izer (NLS) were divided into two dishes. Rapalog (AP21967, Clontech) was added to one of these dishes at a final concentration of 25 nM, while the other dish served as a control. The mislocalization was checked microscopically after different time points in comparison to the control culture.

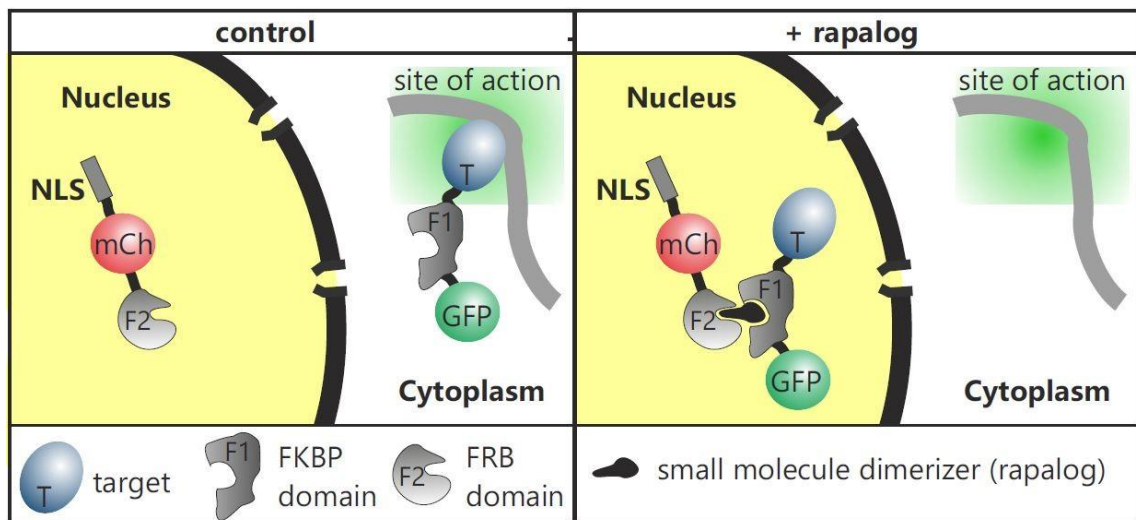


Figure 16 I Scheme of knock-sideway experiment. The endogenously expressed target protein is tagged with a FKBP domain and GFP is removed from its original sites of action through ligand (rapalog) induced dimerization with the FRB domain of an episomal expressed mislocalizer containing a localization signal and a mCherry tag. T: target protein; NLS: nuclear localization signal; F1: FKBP12 domain; F2: FRB* domain; mCh: mCherry; GFP: green fluorescent protein (Birnbbaum et al., 2017).

2.2.3.9 SLI-based conditional deletion using *diCre-mediated gene excision*

SLI-system combined with the dimerizable Cre (diCre)-system was used for generation of inducible knock-out (Birnbbaum et al., 2017, Jullien et al., 2007, Jullien et al., 2003, Andenmatten et al., 2013) (Figure 17). Target gene was disrupted using SLI-TGD. Additionally, a recodoned copy of the target gene was expressed, permitting parasite survival (Figure 17A). Plasmid (pSkip-Flox) expressing the dimerizable Cre-recombinase (diCre) (Figure 17B). The diCre is split into two fragments, respectively fused to FRB and FKBP containing nuclear localization signals (NLS). The addition of the dimerizing compound rapalog causes the two parts to dimerize, resulting in the

activation of the recombinase and thus the inducible excision of the recodonzed functional target gene flanked by loxP-sites.

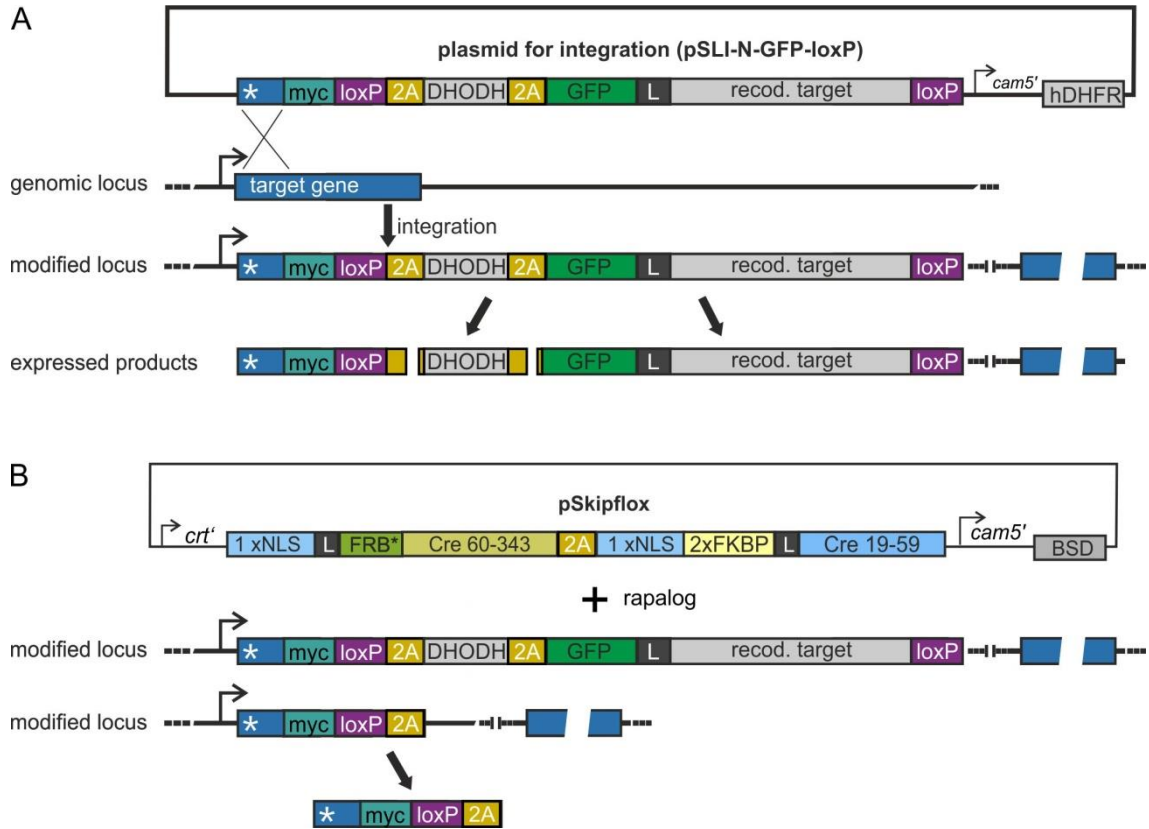


Figure 17 | Conditional deletion of a target gene using the diCre-based excision system. A Targeted gene disruption using SLI-system in combination with the insertion of a recodonzed copy of the target gene flanked by loxP sites. The hDHFR is used for episomal selection and SLI resistance (DHODH) for selection. DHODH gets expressed under the endogenous promotor of parasites that have integrated the SLI plasmid into the genome. **B** The diCre recombinase is episomally expressed and cleaved into two parts, respectively fused to FRB and FKBP containing nuclear localization signals (NLS). When rapalog is added, the two parts of diCre dimerize and the recodonzed gene copy gets excised, leaving the parasite with the truncated protein. L, linker; hDHDR, BSD and DHODH, resistance marker; arrows, promoter (*crt*; *cam5'*).

2.2.3.10 Growth assays with synchronized parasites using conditional inactivation systems

2.2.3.10.1.1 Knock-sideway of VPS45^{endo} induced in schizont stages

Parasites of the *PVPS45-2xFKBP-GFPint+1xNLS-FRB-mCh* cell line were purified using 60% Percoll to gain a narrow time window of a tightly synchronous parasites. These parasites were allowed to invade for 6 hours uRBCs under culture conditions followed by synchronization with 5% sorbitol. The freshly invaded 0 to 6-hour-old ring-stage parasites were cultured until they reached the early schizont stage (36 to 42 h. p.i.). The culture was split into two parts, and the knock-sideway of the VPS45 protein was induced by adding rapalog (Clontech) to a final concentration of 250 nM in one part while keeping the other as an untreated control. Six hours later (42 to 48 h.p.i.), both cultures were treated with the protein kinase G inhibitor compound 2 at a final concentration of 1 μ M to arrest parasite egress before exoneme/microneme secretion. This leads to the enrichment of mature schizonts of the same developmental stage and decreases potential developmental delay effects (Bisio et al., 2020b).

After 5 hours of continuous culture (47 to 53 h.p.i.), samples were taken for electron microscopy and immunofluorescence assay, and compound 2 was washed off to allow the continuation of parasite development to enable the determination of an invasion effect. Giemsa smears were prepared 0 to 6 h.p.i., 36 to 42 h.p.i., 42 to 48 h.p.i., 47 to 53 h.p.i., and 61 to 67 h.p.i. For the comparison to the endocytosis phenotype, rapalog was added already to the 0- to 6- h.p.i. rings to inactivate *PVPS45* already at the beginning of the cycle.

2.2.3.11 Flow cytometry growth assay

To determine whether mislocalization of the target protein or skipped gene (DiCre) affected on the parasite life cycle, growth assays were performed. For this purpose, a culture with an adjusted parasitemia of 0.1 % was divided into a control dish and a 2-ml dish treated with rapalog (250 nM). The medium was changed daily and the parasitemia was measured once every 24 hours for 5 consecutive days (2.5 growth cycles). To this end, the culture was homogenized and 20 μ L of each culture was added to 80 μ L medium containing 1 μ L DHE (0.5 mg/ mL) and 1 μ L Hoechst 33342 (0.45 mg/ mL). After staining in the dark for 20 min, parasites were inactivated with 400 μ l 0.000325 % glutaraldehyde in RPMI, and parasitemia was measured by flow cytometry using a

LSR-II cytometer according to a modified protocol of (Malleret et al., 2011). Results were displayed with GraphPad Prism.

2.2.3.12 Vesicle accumulation assay

For this purpose, a mixed culture containing up to 5 % ring-stage parasites was synchronized by sorbitol treatment to obtain 0 -18 hour old parasites, which were then cultured for 16 hours to reach the trophozoite stages. The culture (16-34 h.p.i.) was split into two 2-ml dishes and one dish was treated with 20 μ l rapalog. After 0-8 hours (depending on the experiment), the parasites were taken out of the incubator and imaged rapidly. The vesicles accumulating in the trophozoite-stage parasite were counted blindly in the captured DIC images.

2.2.3.13 Bloated food vacuole assay

Mixed parasite culture was treated twice with 5% sorbitol at 10 h intervals to obtain a synchronized parasite culture at the ring stage (10-18 h.p.i.). The parasites were cultivated for 8 hours (18- 26 h.p.i.) and split into two 1 ml dishes and 33 μ M E64 protease inhibitor (Sigma Aldrich) was added. One dish was additionally treated with rapalog (250 nM), while the other served as control. The parasites were cultivated for 8 hours, stained with 4.5 μ g/ ml DHE for 20 min at room temperature, washed once in RPMI, and imaged. The DIC image was used for counting the bloated and non-bloated food vacuoles and to measure the parasite diameter. Analysis of the images was blinded.

2.2.3.14 Preloading of red blood cells and infection of preloaded cells

Preloaded RBCs were prepared following the protocol of Sven Flemming (Flemming, 2015) which is based on other previously established protocols (Abu Bakar et al., 2010, Frankland et al., 2006, Murphy et al., 2007). 200 μ l of RBCs was washed in cold DPBS (2000 x g, 1.5 min) and 32 μ l of packed RBCs were added to a lysis solution consisting of 64 μ l lysis buffer, 1 μ l 30 mM DTT solution, 2 μ l 50 mM MgATP and 1 μ l fluorescently labeled dextran. The resulting mixture was placed on ice and rotated overhead at 4 °C for 10 minutes. Resealing of lysed RBCs was performed by gently adding 25 μ l of 5x resealing buffer to the mixture, followed by careful shaking (350 x g) at 37 °C for 60 minutes. The preloaded cells were washed three times with RPMI and stored in RPMI at 4 °C. For the invasion of preloaded RBCs, trophozoites were isolated from a mixed

culture using Mini-Percoll. After the harvesting and washing of the trophozoite layer, they were mixed with the preloaded cells in a 2 ml dish and cultivated for 43 hours until the parasites reinvaded the preloaded cells and developed to mid trophozoite stages. Rapalog (250 nM) was added to inactivate endocytosis-associated proteins.

2.2.3.15 IFAs with formaldehyde- and glutaraldehyde-fixed cells performed in suspension

IFAs in suspension were performed as previously described (Tonkin et al., 2004). 1 ml of parasite culture was centrifuged at 12,000 rpm for 1 minute. Following a wash step with 1x PBS, cells were fixed with 500 μ l of fixation-solution (4% formaldehyde/0.0075% glutaraldehyde in 1x PBS) for 30 min at room temperature. After fixation, cells were washed three times with 1x PBS and then permeabilized with 2-3 pellet volumes of 0.1% Triton X-100 in 1x PBS for 10 min at room temperature. After three washing steps with 1x PBS, cells were blocked with 500 μ l 3% BSA in 1x PBS for 1 h at room temperature and washed once with 1x PBS. Cells were then incubated with 100 μ l of the primary antibody diluted in 3% BSA in 1x PBS for 1 h at RT or overnight at 4°C. After three washes with 1x PBS, 100 μ l of the secondary antibody diluted in 3% BSA in 1x PBS was applied alongside DAPI (1 μ g/ml) and the cells were incubated for 1 h at room temperature protected from light. Upon completion of three final washing steps, ~6 μ l of the cell suspension was placed on a slide, covered with a glass coverslip, and imaged using a fluorescence microscope. The cell pellet was stored at 4°C in 100 μ l 1x PBS containing 0.1 mg/ml ampicillin.

2.2.3.16 Hemoglobin Immunofluorescence Assay

For immunofluorescence assays (IFAs) to detect hemoglobin-filled vesicles, 4 ml of *PFVPS45-2xFKBP-GFP*-synchronized knock-sideway parasites (16-34 h.p.i) were divided into two 2-ml dishes, one of which was grown with 250 nM rapalog (Clontech) for 6 hours, while the other dish served as a negative control. Cells were then washed with DPBS and applied on a ConA coated 10-well slide (Thermo Scientific). After 10 minutes of incubation excess cell material was washed off with DPBS. 0.03 % saponin in 1 x PBS was added for 5 minutes to enable the removal of the host cell cytosol achieved through 3 subsequent wash steps in 1 x PBS. The cells were fixed at room temperature for 30 min in 1 x PBS containing 4 % formaldehyde, washed 3 times in 1 x PBS followed by permeabilization with 0.1 % Triton X-100 in 1x PBS for 10 min at RT. After 3 wash steps, the sample was incubated in 'blocking solution' (3% BSA in 1x PBS

and 100 mg/ ml ampicillin) for one hour at RT. Thereafter the cells were incubated at 4 °C overnight in blocking-solution containing the primary antibody (Rabbit anti- hemoglobin (SIGMA) diluted 1/1000). Parasites were then washed three times for 5 minutes in 1 x PBS before the second antibody (Alexa Fluor 647-conjugated goat anti-Rabbit antibody (Life Technologies)), diluted 1:2000 in blocking solutions, was added and incubated for 1 hour at room temperature. Cells on the slide were washed three times with 1x PBS, and the slide was subsequently covered with a coverslip using Dako fluorescence mounting medium for imaging.

2.2.3.17 Isolation of parasites by saponin lysis and protein extraction

The detergent saponin was used to isolate parasites from erythrocytes. To this end, a culture with a parasitemia of 5-10 % was pelleted by centrifugation and the pellet was washed in DPBS once. Cells were resuspended in 10 pellet volumes of cold saponin at a concentration of 0,03 % in DPBS, resulting in lysis of the red blood cells and PVM but leaving the PPM intact due to the different lipid composition of these membranes. After incubation on ice for 15 min, the parasites were centrifuged at 16000 x g for 5 min at 4 °C and washed in DPBS until no hemoglobin was visible in the supernatant. 4 µl of 25x protease inhibitor was added to the pellet which was then resuspended in 96 µl of SDS lysis buffer and incubated for 5 minutes on ice. Following centrifugation at 16000 x g for 5 minutes, the supernatant was transferred to a new reaction tube. 1/ 5 volumes of 6x SDS sample buffer were added and incubated at 85 °C for 5 minutes. Protein extracts were used directly or stored at -20 °C until 10 µl of the sample was applied to SDS-PAGE. (Section 2.2.4.1).

2.2.4 Biochemical methods

2.2.4.1 Sodium dodecyl sulphate- polyacrylamide gel electrophoresis (SDS PAGE)

Proteins were separated according to their molecular weight by applying a voltage, using discontinuous SDS-PAGE (Laemmli, 1970). The influence of the intrinsic charge of the proteins is neutralized by the addition of the anionic detergent SDS, which denatures secondary and non-disulfide-bound tertiary structures so that the proteins become linear molecules and acquire a negative net charge. A polypeptide chain binds

amounts of SDS that are proportional to its relative molecular mass so that the final separation of proteins depends almost entirely on differences in the relative molecular mass of the proteins. DTT (dithiothreitol) present in the SDS sample buffer leads to the reduction of disulfide bonds, contributing to an unfolded conformation. Acrylamide gels were polymerized by the addition of ammonium persulfate (APS) in the presence of the catalyst TEMED. In this work, polyacrylamide gels with a concentration of 12% acrylamide were prepared.

Heat denaturation protein samples (Section 2.2.3.17) were loaded into the gel pockets, alongside a pre-stained protein ladder containing dye-labeled proteins of defined size. A voltage of 100-150 V was applied for 60-90 minutes and the gels containing the separated proteins were subjected to Western blot analysis (Section 2.2.4.2).

2.2.4.2 Western blot

Proteins separated by SDS-PAGE (Section 2.2.4.1) were transferred to nitrocellulose membranes by the wet transfer method to make them accessible for antibody detection (Section 2.2.4.3). To this end, the polyacrylamide gel was layered on a nitrocellulose membrane and enclosed on both sides with 3 Whatman filter papers and a metal sponge in a blotting cassette. For electroblotting, the sandwich was placed in a tank blotting chamber, with the nitrocellulose facing the anode and the polyacrylamide gel facing the cathode, so that the negatively charged proteins ran towards the membrane in the electric field. The chamber was filled with 1x transfer buffer and the transfer was performed by applying a voltage of 100 V at 4 °C for 1 hour or 15 V overnight.

2.2.4.3 Immunodetection of proteins

Subsequent to the transfer of the proteins to a nitrocellulose membrane (Section 2.2.4.2), proteins can be visualized by immunodetection. To inhibit non-specific antibody binding, the membrane was blocked for 1 hour at RT with 5 % milk powder in 1x PBS. Next, the membrane was incubated with the primary antibody diluted in 5% milk powder in 1x PBS for 2 hours at RT or overnight at 4 °C. After three 5-minute wash steps with 1x PBS, the secondary antibody conjugated to the reporter enzyme horseradish peroxidase (HRP) was diluted in 5 % milk powder in 1x PBS and applied to the membrane for one hour at RT. After three additional washing steps, the membrane was incubated for 5 minutes with a mixture of equal volumes of luminol/enhancer and per-

oxide solution from an ECL detection kit (Bio-Rad) and transferred to a transparent film. Chemiluminescence was detected using a Chem-iDoc XRS+ system (Bio-Rad).

2.2.4.4 Dimerization induced in vitro proximity biotinylation of interacting proteins (DiQ-BioID)

Small scale experiments were done with 5 ml cultures to test conditions and efficiency of biotinylation and analyzed by Western Blot probed with Streptavidin-HRP. The probes for analysis by mass spectrometry were scaled up to 150 ml of culture per condition (3x 50 ml culture bottles per condition). The mixed stage parasite cultures starting with 2 to 5 % parasitemia were grown for 24 hours in the presence of biotin and rapalog (final concentration of 250 nM) and fed every 8 hours to prevent starvation of the parasites. After 24 hours of growth the parasitemia resulted in circa 10 %. The culture was centrifuged (6000 x g, 20 min, room temperature) and the supernatant discarded. The parasites were lysed with 50 ml of 0.003 % saponin for the pellet of each condition as already described (3.3.7). The isolated parasites were transferred to a 2 ml reaction tube, washed 2 times with DPBS and lysed with 2 ml lysis buffer (lysis buffer for mass spectrometry) and sealed with parafilm. Two freeze-and-thaw cycles at -80 °C and thawing on ice were done for complete lysis of the parasite cells. The cell debris was sedimented by centrifugation at 16,000 x g for 10 min and the supernatant transferred to a 15 ml falcon and diluted in a ratio of 1:2 with 50 nM TrisHCl pH 7.5, 2x protease inhibitor cocktail, 1 mM PMSF. 50 µl of Streptavidin-Sepharose (equilibrated in 50 nM TrisHCL pH 7.5) were added and incubated overnight at 4 °C rotating head over head. The beads were sedimented by centrifugation at 1600 x g for 1 min, transferred in a 1.5 ml reaction tube and washed twice with 500 µl lysis buffer, once in 500 µl cold dH₂O (Ampuwa), two times in 500 µl cold TrisHCl pH 7.5 and three times in 500 µl cold 100 mM TEAB. Centrifugation after each step was carried out with 1600 x g for 2 min at room temperature and incubation done horizontally rolling on a roller mixer for 2 min for each washing step. After the last washing step the sepharose was re-suspended in 50 µl 100mM TEAB and shipped on ice for mass spectrometry analysis. The mass spectrometry analysis was performed by Wieteke Hoeijmakers (Radboud Institute, Nijmegen, Netherlands) using dimethyl labeling for quantification (Boersema et al., 2009). Falcons, reaction tubes and tips were exclusively used from the brands Eppendorf and Nunc for the probes for mass spectrometry to avoid contamination with polymers.

2.2.4.5 In-cell DSP cross-linking and co-immunoprecipitation (CoIP)

A target protein was purified from lysed parasite mixture by binding to agarose beads coupled to antibodies (GFP Nanobody/ V_HH). Proteins interacting with the target proteins are co-immunoprecipitated. The entire protocol was carried out on ice. Between 10 and 20 ml of the parasite culture was centrifuged (2000 x g, 3 min) and the supernatant was discarded. To obtain labile protein-protein interactions ahead of co-immunoprecipitation, the lysine-reactive crosslinker dithiobis[succinimidylpropionate] (DSP) was used. For this purpose, 20 mM DSP in DMSO was prepared and diluted further in DPBS down to 0.3 mM. Cross-linking of proximal and interacting proteins was performed in a rolling falcon tube for 30 minutes at room temperature. Following the centrifugation, the supernatant was discarded, and 10 ml of quenching buffer was applied to the pellet and incubated at room temperature for 10 min. Subsequently, parasites were isolated by using selective RBC lysis with saponin (Section 2.2.3.17). Purified parasites were washed twice with DPBS and resuspended in 250 µl RIPA buffer (+2x protease inhibitor and 10 mM PMSF). Lysates were then centrifuged at 16 000 x g at 4 °C and the supernatants were each diluted with 750 µl of dilution buffer (+2x protease inhibitor cocktail). These diluted supernatants were pooled in a 2-ml reaction tube, while 50 µl were transferred to a tube containing 17 µl of 4x SDS sample buffer serving as the input sample in the Western blot analysis. 20 µl of the GFP-agarose beads were equilibrated in dilution buffer and transferred to the diluted supernatant, followed by incubated rolling overhead for 1 to 2 hours at 4 °C. The agarose beads were pelleted (2500 x g, 3 min, 4 °C) and 50 µl of the supernatant was transferred to a tube containing 17 µl 4x SDS sample buffer serving as the supernatant sample in the Western blot analysis. The beads were washed five times with dilution buffer (centrifugation steps at 2500 x g), and 50 µl of the supernatant from the last wash step was transferred to a tube containing 17 µl of 4x SDS sample buffer serving as the final wash fraction sample in the for Western blot analysis. The agarose pellet was incubated with 30 µl of 4x SDS sample buffer at 85 °C for 10 min to elute proteins bound to the agarose beads. The beads were pelleted by centrifugation at 2500 x g for 1 minute and 50 µl of the supernatant from the last wash step was transferred to a tube containing 17 µl of 4x SDS sample buffer serving as the elution sample in the for Western blot analysis. 5-10 µl of the input, supernatant and final wash step and 10 µl of the eluate were loaded on the polyacrylamid-gel for SDS-PAGE (Section 2.2.4.1) and subsequent Western blot analysis (Section 2.2.4.2).

2.2.5 Microscopy

2.2.5.1 Optical light microscope

The Giemsa smears (Section 2.2.3.2) were analyzed using a Zeiss Axio Lab.A1 microscope. Images were acquired using the 1000x/1.4 oil immersion objective, a Zeiss Axio Cam ERC 5S C4742-95, and Zen2.3 software (blue edition). Images were processed using Corel PHOTO-PAINT X6.

2.2.5.2 Fluorescence microscope

Fluorescent-labeled parasites were analyzed using a Zeiss Axioscope M1 fluorescence microscope. For staining of cell nuclei, DAPI was added to a portion of the culture at a final concentration of 1 µg/ml and incubated for 10 minutes at RT. 6 µl was transferred to a glass slide and covered with a coverslip. Images were immediately acquired using the 1000x/1.4 oil immersion lens, an Orca C4742-95 Camera, and the Axio software. Different filter cubes corresponding to the fluorescent molecule were used for excitation and detection. Images were processed using Corel PHOTO-PAINT X6.

2.2.5.3 Transmission electron microscopy (TEM)

The desired parasite stages were enriched using Percoll and the isolated parasites were after washing steps (3x in PBS) fixed with 2.5 % glutaraldehyde in 50 mM cacodylate buffer pH 7.4 for 0.5 -1 h at room temperature. For post-fixation and staining of the cell membranes 2 % osmium tetroxide (OsO₄) in H₂O was added and incubated for 40 minutes on ice in the dark. After three washes with dH₂O, uranyl acetate was added for 30 minutes at room temperature to provide contrast enhancement. Cells were washed 2 to 3 times with dH₂O and dehydrated in an ethanol series for 5 minutes each at 50 %, 70 %, 90 % (2x), 95 % (3x), and 100 %. An epon-ethanol mixture (1:1) was added and incubated overnight at RT by shaking. The next day, cells were incubated with 100 % Epon for 6 hours and then replaced with new Epon. For polymerization, the sample was kept at 60°C for 1-3 days.

3 Results

In this work, proteins of HCCU typically associated with initiation (Section 3.1), early endosome (Section 3.2), and late endosome (Section 3.3) in the endosomal pathway were identified, characterized, and functionally analyzed.

3.1 Early- endocytosis associated proteins in HCCU

3.1.1 The heterotetrameric AP-2 complex in *P. falciparum*

The AP-2 complex is typically involved in the initiation of endocytosis (Figure 18A). In model organisms, the heterotetrameric AP-2 complex is known to consist of the trunk, flexible hinge, and appendage domains (Figure 18B), composed of the four adaptor proteins (AP-2 α , β 2, μ 2, and σ 2), whose orthologues are also present in *P. falciparum* (Figure 18C). AP-2 usually plays a role in CME (Section 1.9.1.1.1). However, localization studies with AP-2 μ showed that Clathrin seems to be absent from this compartment, but co-localizes with proteins of the K13 complex (Figure 13) (Birnbaum et al., 2020, Henrici et al., 2020). In addition, as in K13, mutations in AP-2 μ and AP-2 α were found in artemisinin-resistant parasite lines (Figure 18C) (Henriques et al., 2013, Henriques et al., 2015, Henrici et al., 2019b, Rocamora et al., 2018).

The initiation of endocytosis in malaria parasites appears to occur by an unusual endocytic mechanism. Therefore this work aimed to gain more knowledge about the poorly investigated adapter proteins, in particular AP-2 β (Section 3.1.1.1), AP-2 α (Section 3.1.1.2), and AP-2 σ (Section 3.1.1.3) of the AP-2 functional complex in *P. falciparum*.

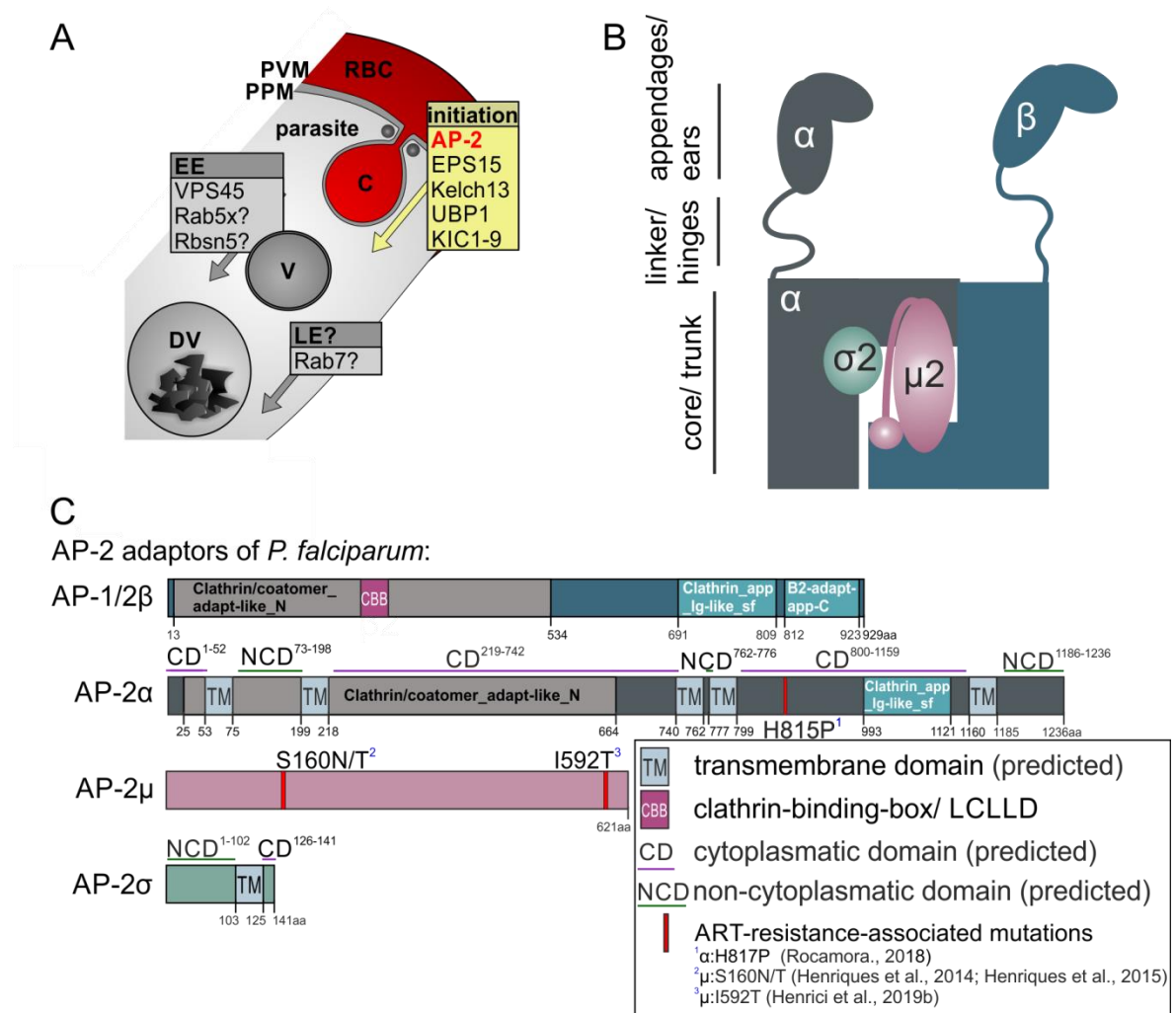


Figure 18 | AP-2 complex. **A** Schematic illustration of the HCCU process in *P. falciparum*. Known or suspected (indicated by a question mark) proteins involved in the initiation, early, or late endosomal steps of the HCCU. AP-2 complex associated with the initiation step of endocytosis is highlighted. Rab5x stands for Rab5b or Rab5c. Abbreviations: RBC: red blood cell; C: cystosome; EE: early endosome; LE: late endosome; DV: digestive vacuole; V: HCC-containing vesicle; PPM: parasite plasma membrane; PVM: parasitophorous vacuolar membrane. Modified from (Sabitzki et al., 2020). **B** Schematic illustration of the heterotetrameric AP-2 complex found in model organisms. AP-2 consists of four subunits, the two large adaptin subunits (~70 kDa) α and β , the medium-sized μ 2-subunit (~50 kDa), and a small σ 2-subunit (~17 kDa). The complex forms a large globular central core/trunk, composed of μ 2, σ 2, and the N-terminal domains of the two large adaptins, that is connected via long flexible linkers ('hinge') to folded C-terminal appendage ('ear') domains of α and β adaptin. **C** Predicted protein domain architecture of the AP-2 adaptor proteins (AP-1/2 β (929 aa); AP-2 α (1236 aa), AP-2 μ (621 aa) and AP-2 σ (141 aa) of *P. falciparum* (InterPro). Clathrin-binding box (LCLLD) was identified in AP-1/2 β using a domain motif scan (LΦXΦ[DE]). TM, predicted transmembrane domains; CBB, Clathrin-binding box; CD, predicted cytoplasmatic domains; NCD, predicted non-cytoplasmatic domains. ART-resistance-associated mutations (AP-2 α :H817P; AP-

2 μ :S160N/T; AP-2 μ :I592T) are indicated (Henrici et al., 2020, Henriques et al., 2014, Henriques et al., 2015, Henrici et al., 2019a).

3.1.1.1 AP-1/2 β of *P. falciparum*

3.1.1.1.1 Protein domain prediction of AP-1/2 β of *P. falciparum* parasites

In *P. falciparum* the 929 aa long β -adaptin (PF3D7_0528100, AP-1/2 complex subunit beta, putative) is shared by the AP-2 and AP-1 complex and consequently likely has functions in distinct vesicular trafficking processes in the parasite. While AP-2 is known to mediate early endocytosis processes from the PM to the EE, AP-1 is required for trafficking processes from the Golgi to the endosomes (reviewed in (Park and Guo, 2014)). Prediction and comparison (Figure 19) of the protein domain architecture of PfAP-1/2 β with β -adaptins of *H. sapiens* (P63010; AP2 β 1 and Q10567; AP1 β 1), *T. gondii* (TGME49_240870; beta adaptin protein, putative), and *S. cerevisiae* (P27351; AP2 β) using InterPro (Blum et al., 2021) showed that they share the general domain with an N-terminal Clathrin/coatomer_adapt-like_N domain found in the protein's trunk and two C-terminal domains (Clathrin_app_Ig-like_sf and B2-adapt-app-C) in the appendage region, the latter do not appear to be present in *S. cerevisiae*. Human HsAP-2 β and HsAP-1 β contain Clathrin-binding boxes (LLNLD) in their flexible hinge regions, where they are accessible to Clathrin by conformational changes only in the active state of the protein complex (Beacham et al., 2019). Interestingly, in AP-1/2 β of *P. falciparum*, a Clathrin-binding box could not be found in the hinge region. However, one was identified (LCLLD) using a domain motif scan (with the consensus pattern: L Φ X Φ [DE]) in the N-terminal trunk of the protein, similar to AP-2 β of *S. cerevisiae* whose trunk contains two Clathrin-binding boxes (LLDLD and LLRLD). In *T. gondii* no Clathrin-binding box could be detected.

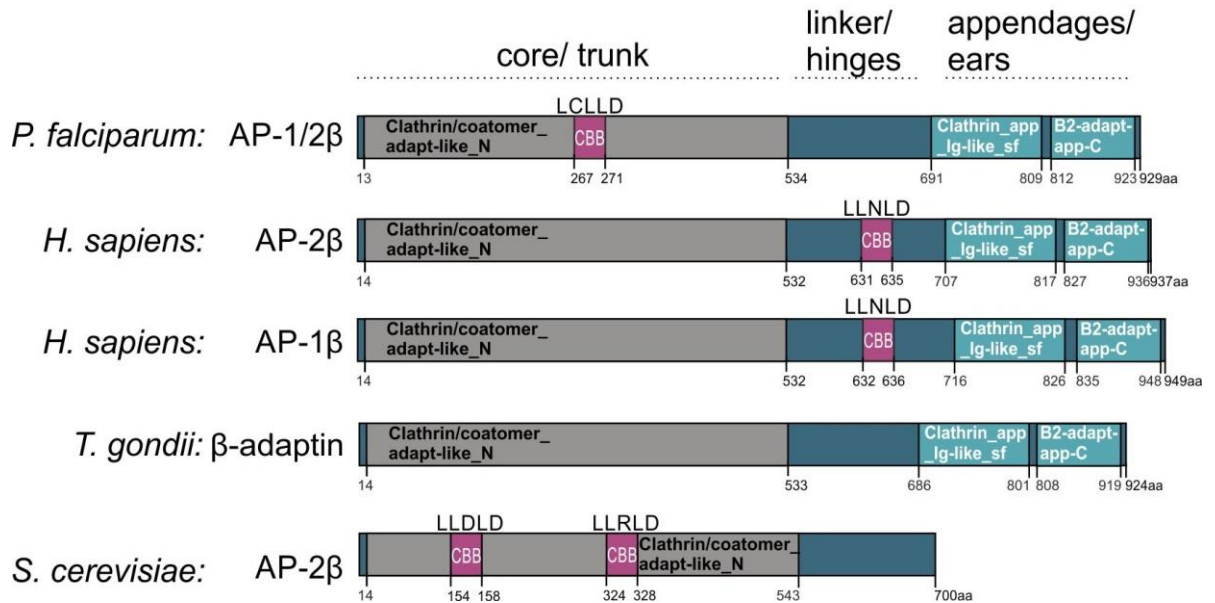


Figure 19 | Comparison of predicted protein domains and motifs of PfAP-1/2β and its orthologues. Schematic illustration of the protein domain architecture of *P. falciparum* AP-1/2β in comparison to AP-2β from *H. sapiens* (P63010), *S. cerevisiae* (P27351), β-adaptin of *T. gondii* (TGME49_240870), and to human AP-1β (Q10567). CBB, Clathrin-binding box.

3.1.1.1.2 Subcellular localization of AP-1/2β in blood stages of *P. falciparum* parasites

To investigate the localization and function, AP-1/2β was tagged by modification of the endogenous gene locus using the SLI-system (Birnbbaum et al., 2017). The resultant fusion protein was tagged at the C-terminus with 2xFKBP-GFP-2xFKBP (Figure 20A). Correct integration was confirmed by PCR of genomic DNA of the corresponding AP-1/2β-2xFKBP-GFP-2xFKBP^{endo} parasite line (Figure 20C). The AP-1/2β-2xFKBP-GFP-2xFKBP^{endo} parasites showed AP-1/2β^{endo} expression through the entire blood cycle (Figure 20B), with usually one or two foci in ring stages. In trophozoite stages, the number of foci increased. Most trophozoites showed at least one signal at the PPM in close proximity to the DV and frequently in proximity to the nucleus. Occasionally AP-1/2β^{endo} was observed surrounding structures visible in differential interference contrast (DIC) images (Figure 20D). In schizonts was visible in several foci that suggest distribution to each newly formed merozoite (Figure 20B).

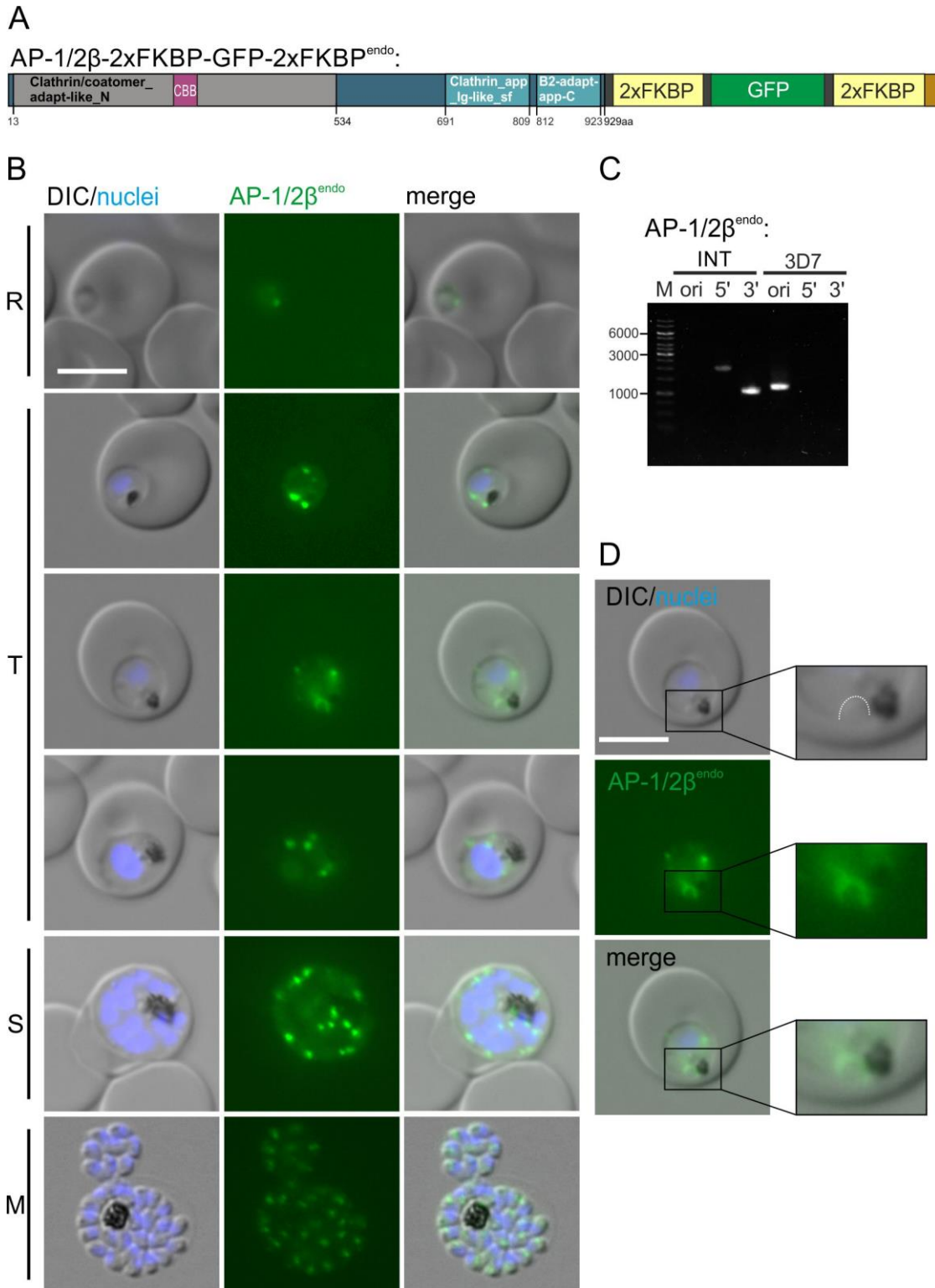


Figure 20 | Subcellular localization of AP-1/2 β -2xFKBP-GFP-2xFKBP^{endo}. **A** Schematic illustration of the AP-1/2 β protein C-terminally tagged with 2xFKBP-GFP-2xFKBP. **B** Live-cell microscopy images of the indicated stages of AP-1/2 β -2xFKBP-GFP-2xFKBP^{endo} parasites. Nuclei were stained with DAPI. R; ring, T; trophozoite, and S; schizont stages. DIC, differential interference contrast. The scale bar represents 5 μ m. **C** Agarose gel showing PCR-products to assess correct integration of the SLI-plasmid into the ge-

nome of *P. falciparum* (3D7) parasites to obtain the indicated cell line (5' integration junction: 5'INT: 2105 bp (AP-1/2 β int fw+ GFP85 rv); 3' integration junction: 3'INT: 1112 bp (pARLsense55+ AP-1/2 β int rv) and ori (indicating presence or absence of original unmodified locus): 1262 bp (AP-1/2 β int fw+ AP-1/2 β int rv)). **D** Higher magnifications of the boxed areas show AP-1/2 β signal surrounding structures visible in the DIC image (indicated by a dashed white line) at the plasma membrane close to the DV. The scale bar represents 5 μ m.

3.1.1.1.3 AP-1/2 β has dual localization to the Golgi apparatus and the K13-positive compartment

For further localization studies, GRASP-mCh^{epi} (Figure 21A), Clathrin-LC-mCh^{epi} (Figure 21B), and K13-mCh^{epi} (Figure 21C) were episomally co-expressed in AP-1/2 β -2xFKBP-GFP-2xFKBP^{endo} parasites.

Co-expression of a fluorescently tagged GRASP showed that some AP-1/2 β ^{endo} foci overlapped with the Golgi-apparatus (Figure 21A; blue arrows), while other foci, mainly found in close proximity to the DV at the plasma membrane, showed no overlapping signals (Figure 21A; white arrows). Consistent with this, some of the AP-1/2 β ^{endo} foci were overlapping with Clathrin (Figure 21B; blue arrows), which was reported to interact with typical proteins of the Golgi apparatus (Birnbaum et al., 2020). Some additional AP-1/2 β ^{endo} foci in close proximity to the DV showed no overlapping Clathrin signals (Figure 21B; white arrows). However, AP-1/2 β ^{endo} signals were found at the DV overlapping with K13^{epi}, which is known to co-localize with AP-2 μ at the plasma membrane but not with Clathrin (Figure 21C; blue arrows) (Birnbaum et al., 2020). Not all of the AP-1/2 β ^{endo} signals overlapped with K13^{epi} foci (Figure 21C; white arrow) and not all signals overlapped with AP-1/2 β ^{endo} (Figure 21C; purple arrow). Overall this permits the conclusion that AP-1/2 β ^{endo} is found in foci at the Golgi as well as at the Kelch13 compartment, congruent with a dual role of this subunit in both AP-1 and AP-2.

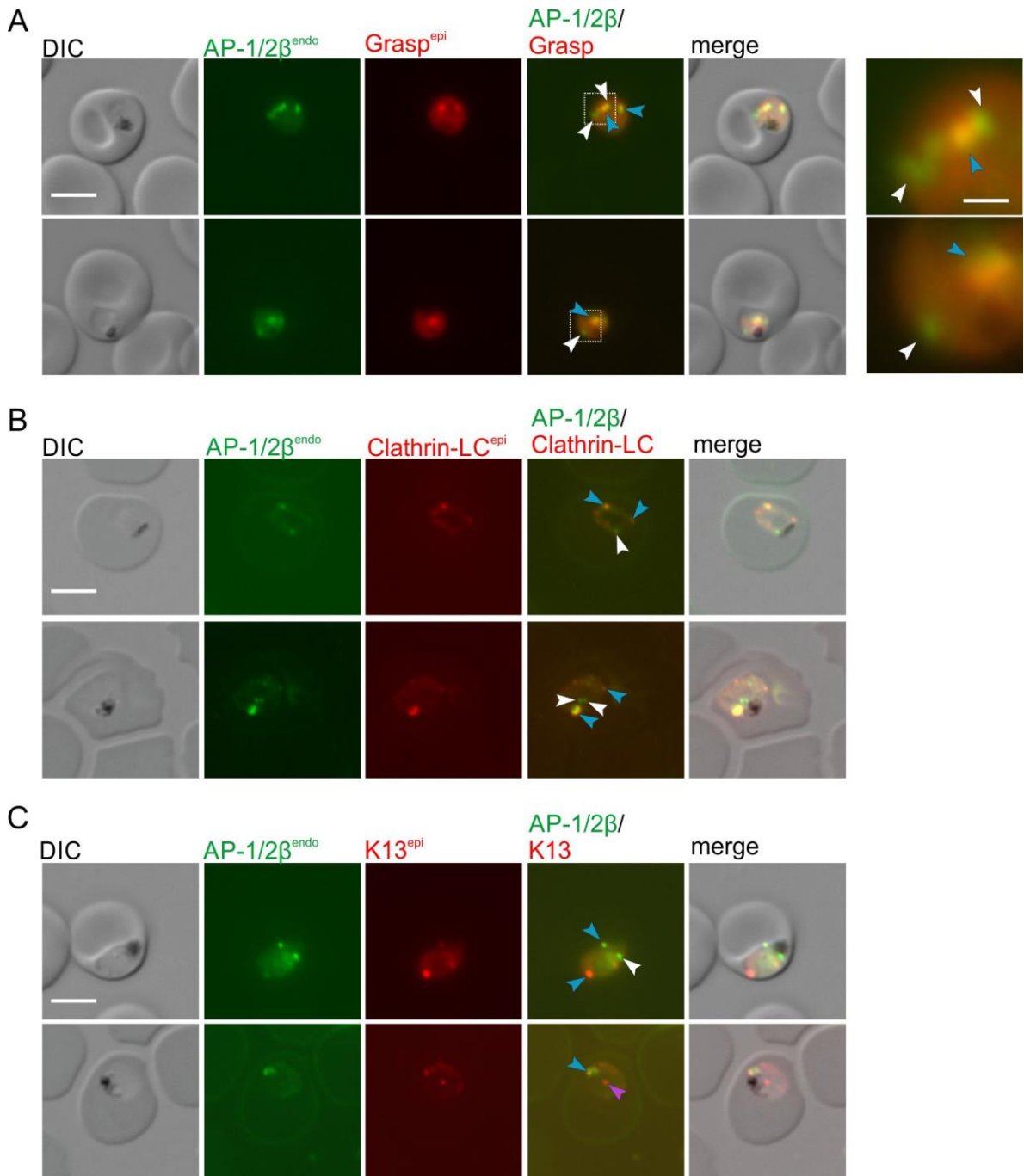


Figure 21 | AP-1/2 β ^{endo} foci of *P. falciparum* co-localize with K13^{epi}, Grasp^{epi}, and Clathrin-LC^{epi} foci.

A Live-cell microscopy images of AP-1/2 β -2xFKBP-GFP-2xFKBP^{endo} parasites, co-expressing GRASP-mCh^{epi}. Blue arrows: AP-1/2 β ^{endo} foci overlapping with GRASP^{epi} signal. White arrows: AP-1/2 β ^{endo} foci without overlapping GRASP^{epi} signal. **B** Microscopy images of dried smears of AP-1/2 β -2xFKBP-GFP-2xFKBP^{endo} parasites, co-expressing Clathrin-LC-mCh^{epi}. Blue arrows: AP-1/2 β ^{endo} foci overlapping with Clathrin-LC^{epi}. White arrows: AP-1/2 β ^{endo} foci without overlapping Clathrin-LC^{epi} signal. **C** Live-cell microscopy images of AP-1/2 β -2xFKBP-GFP-2xFKBP^{endo} parasites, co-expressing K13-mCh^{epi}. Blue arrows: AP-

$1/2\beta^{\text{endo}}$ foci overlapping with $K13^{\text{epi}}$. White arrow: $AP-1/2\beta^{\text{endo}}$ foci without overlapping $K13^{\text{epi}}$ signal. Purple arrow: $K13^{\text{epi}}$ foci without overlapping $AP-1/2\beta^{\text{endo}}$ signal. The scale bar represents 5 μm . DIC, differential interference contrast; endo, endogenous; epi, episomal.

3.1.1.1.4 AP-1/2 β is important for the development of parasite blood stages

To investigate its function, AP-1/2 β was conditionally inactivated using knock-sidaway (Figure 22) (Birnbbaum et al., 2017, Robinson et al., 2010, Haruki et al., 2008). For this purpose, the AP-1/2 β -2xFKBP-GFP-2xFKBP $^{\text{endo}}$ parasite cell line was co-transfected with the *nmd3*¹xNLS-FRB-mCherry mislocalizer plasmid. Cultivation of parasites in the presence of rapalog for 8 h led to a partial mislocalization of AP-1/2 β^{endo} to the nucleus (100% of the parasites had some AP-1/2 β^{endo} signal remaining outside of the nucleus at the PPM) (Figure 22A, white arrows) with reverse localization of the mislocalizer to the AP-1/2 β^{endo} remaining at its original site (Figure 22A, blue arrows). To determine the effect of this partial mislocalization and the relevance of AP-1/2 β for the parasite blood cycle, we monitored the parasitemia after conditional inactivation of AP-1/2 β^{endo} by knock-sidaway (+ rapalog) compared to the control over 5 days (2.5 growth cycles). Despite the incomplete mislocalization of AP-1/2 β^{endo} , the knock-sidaway led to a drastic growth defect in comparison to the control parasites (Figure 22B), indicating its essentiality for the parasite blood stages. Due to the likely dual role of AP-1/2 β^{endo} in both AP1 and AP-2, this important role can not be specifically assigned to one of these two adaptor complexes.

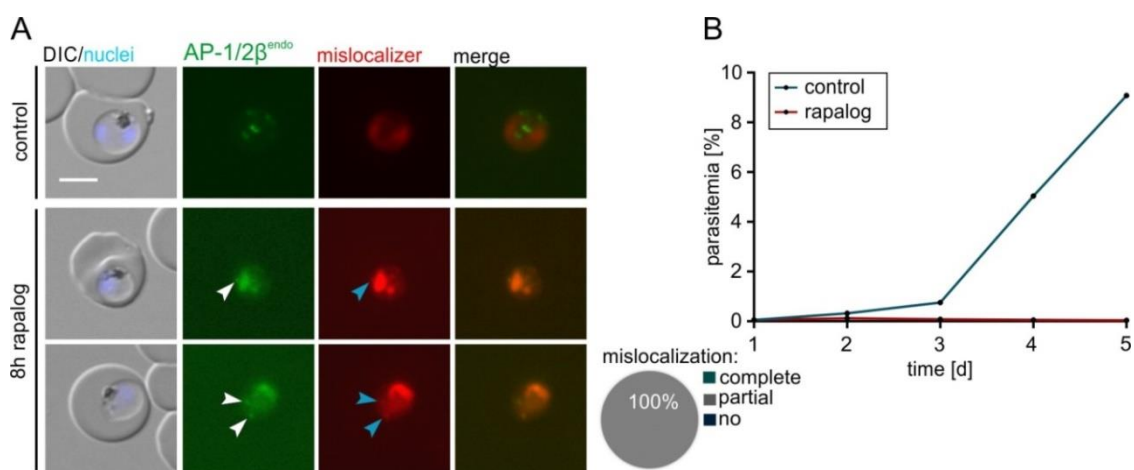


Figure 22 | AP-1/2 β is important for the survival of *P. falciparum* blood-stage parasites. **A** Knock-sidaway of AP-1/2 β -2xFKBP-GFP-2xFKBP $^{\text{endo}}$ parasites expressing a nuclear mislocalizer (*nmd3*¹NLS-FRB-mCh) (Birnbbaum et al., 2017). Images were taken 8 h after induction of knock-sidaway of parasites

cultivated in the presence of rapalog compared to the control. Knock-sideway was classified in complete, partial, or absent (no) mislocalization in 12 parasites. White arrows: AP-1/2 β^{endo} signal remaining outside of the nucleus at the PPM. Blue arrows: reverse localization of the mislocalizer. Nuclei were stained with DAPI. DIC, differential interference contrast. The scale bar indicates 5 μm . **B** Flow cytometry growth curve over 2.5 growth cycles of the AP-1/2 β -2xFKBP-GFP-2xFKBP $^{\text{endo}}$ +*nmd3*NLS-FRB-mCh knock-sideway parasites grown with rapalog and without rapalog (control). One representative of $n = 3$ independent experiments, all replicas are shown in the supplements (Appendix B).

3.1.1.2 AP-2 α of *P. falciparum*

3.1.1.2.1 AP-2 α of *P. falciparum* contains unusual predicted transmembrane domains

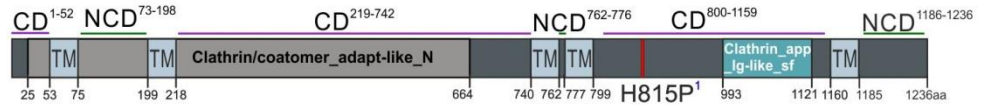
Besides AP-2 β , AP-2 α is the other of the two large adaptin subunits of the AP-2 complex. Prediction (Figure 23A) of the protein domains of *PfAP-2 α* (1236 aa) (PF3D7_0617100; AP-2 complex subunit alpha, putative) and comparison with the α -adaptins of *H. sapiens* (O95782), *P. berghei* (PBANKA_1116700), and *S. cerevisiae* (P38065) using InterPro (Blum et al., 2021) showed that all proteins contain the N-terminal Clathrin/coatomer_adapt-like_N domain in the protein trunk and the Clathrin_app_Ig-like_sf domain in the C-terminal part (domains also present in β -adaptin (Figure 19) (Section 3.1.1.1.1). However, AP-2 α of *P. falciparum* and *P. berghei* lacks the α -adaptin_app_sub_C domain present in the C-terminal end of human and yeast AP-2 α . In AP-2 α (adaptin n-terminal region domain-containing protein) of *T. gondii* (TGME49_221940) none of the two C-terminal domains could be detected. Interestingly, in AP-2 α of *P. falciparum* and *P. berghei* transmembrane domains (TM) were predicted (TMHMM/ Phobius). This is unusual since the AP-2 complex of *H. sapiens* is found to be cytosolic in an assembled but closed/inactive state and only once recruited to the PM it can undergo conformational changes leading to transitions into an open/activated state (Partlow et al., 2019, Beacham et al., 2019, Jackson et al., 2010b, Kadlecova et al., 2017). If these TM predictions are accurate, and not falsely caused by hydrophobic patches of a different function, the AP-2 α protein would be inserted into the PPM and subdivided into cytosolic and non-cytosolic domains (Figure 23B). This would result in different accessibility (from the cytosol or the PV) for the accessory proteins. Consequently, the conformational assembly of the AP-2 complex would differ and thus the mechanism mediating the functionality of AP-2 in *P. falciparum* would

have to be distinctly different from AP-2 of *H. sapiens*. However, experiments are required to verify the existence of the TMs in AP-2 α of *P. falciparum*.

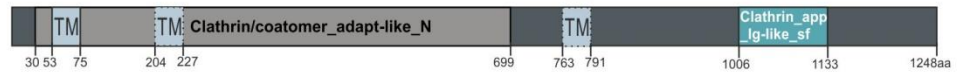
A

AP-2 α :

P. falciparum



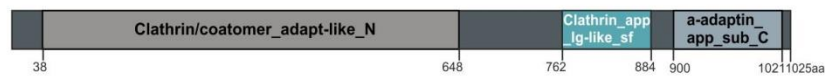
P. berghei



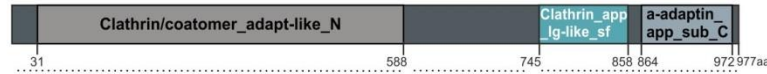
T. gondii



S. cerevisiae



H. sapiens



core/ trunk

linker/
hinges

appendages/
ears

B

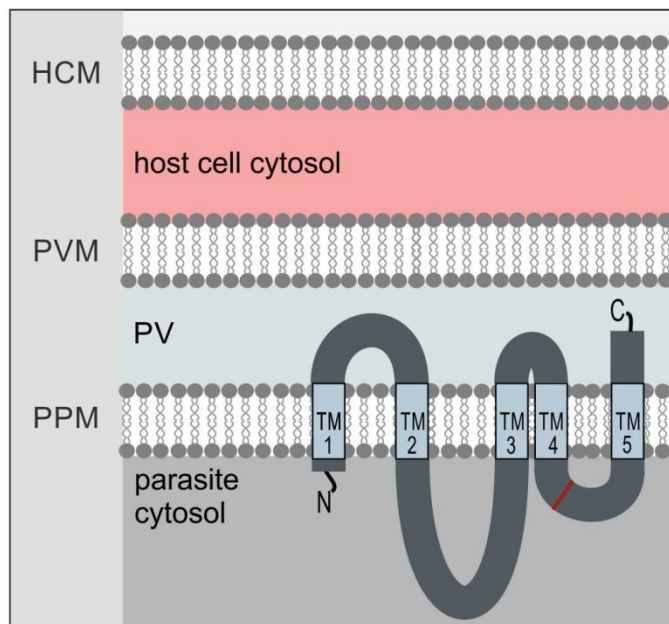


Figure 23 | AP-2 α of *P. falciparum* contains unusual predicted transmembrane domains. **A** Schematic illustration of the AP-2 α protein domain architecture of *P. falciparum* (PF3D7_0617100) in comparison to AP-2 α from *H. sapiens* (O95782), *S. cerevisiae* (P38065), *T. gondii* (TGME49_221940 (adaptin n-terminal region domain-containing protein)), and *P. berghei* (PBANKA_1116700). TM, predicted transmembrane domains (solid box: TMHMM and Phobius predicted; dashed boxes: only predicted by Phobius); CD, predicted cytoplasmic domains; NCD, predicted non-cytoplasmic domains. ART-resistance-associated mutation (AP-2 α :H817P (Henrici et al., 2020)) is indicated. **B** Schematic illustration of the predicted AP-2 α protein membrane topology assuming all predicted TM domains are correct. HCM, host cell membrane; PVM, parasitophorous vacuole membrane; PV, parasitophorous vacuole; PPM, parasite plasma membrane.

3.1.1.2.2 Subcellular localization of AP-2 α in blood stages of *P. falciparum* parasites

To investigate the localization and function, AP-2 α was endogenously tagged by modification of the *ap-2 α* gene locus using the SLI-system (Birnbaum et al., 2017), resulting in two different cell lines (Figure 24 and Figure 25). In the resulting two cell lines AP-2 α was either tagged with 3xHA at the C-terminus (Figure 24A) or at the N-terminus with GFP (Figure 25A). Correct integration of the modifying plasmid was confirmed by PCR of genomic DNA of the corresponding AP-2 α -3xHA^{endo} (Figure 24B) and the N-GFP-AP-2 α ^{endo}(loxP) parasite line (Figure 25B).

An α -HA-IFA of AP-2 α -3xHA^{endo} parasites showed several foci in trophozoites which increased in number in schizont stages. In trophozoites, at least one signal at the PPM in close proximity to the DV was visible (Figure 24C).

This observation was consistent with the AP-2 α ^{endo} foci present in live-cell images of the N-GFP-AP-2 α ^{endo}(loxP) cell line (Figure 25C). This cell line showed endogenous AP-2 α with a singular focus in ring stages and most trophozoites showed at least one signal at the PPM in close proximity to the DV. In schizonts, several foci of AP-2 α ^{endo} were visible (Figure 25C).

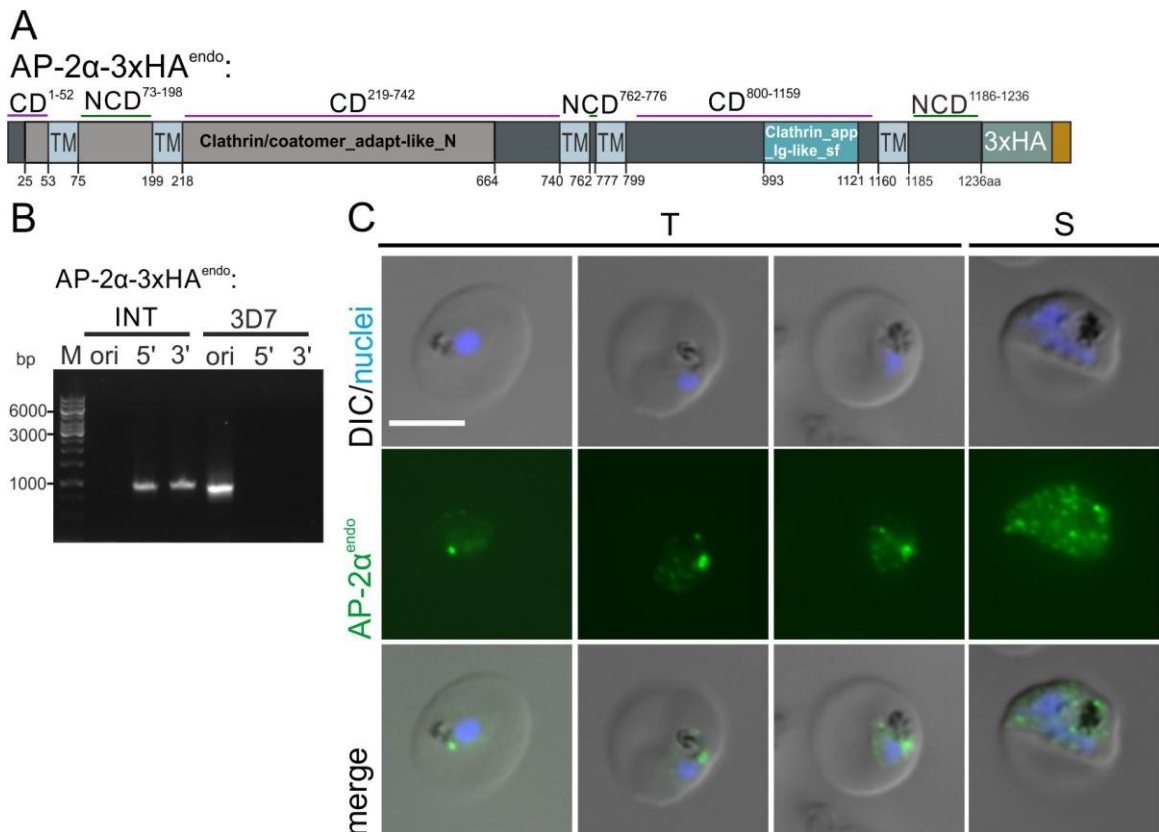


Figure 24 | Subcellular localization of AP-2 α -3xHA^{endo}. **A** Schematic illustration of the AP-2 α protein C-terminally tagged with 3xHA. **B** Agarose gel showing PCR-products to assess correct integration of the SLI-plasmid into the genome of *P. falciparum* (3D7) parasites to obtain the indicated cell line (5' integration junction: 5'INT: 963 bp (AP-2 α -3xHAint(1) fw+ Neo40 rv); 3' integration junction: 3'INT: 858 bp (pARLsense55+ AP-2 α -3xHAint rv) and ori (indicating presence or absence of original unmodified locus): 801 bp (AP-2 α -3xHAint(1) fw+ AP-2 α -3xHAint rv)). **C** Microscopy images of the indicated stages of an IFA of formaldehyde and glutaraldehyde fixed AP-2 α -3xHA^{endo} parasites. α -HA (rat) was used to detect HA. Nuclei were stained with DAPI. T; trophozoite and S; schizont stages. HA, 3x hemagglutinin; DIC, differential interference contrast. The scale bar represents 5 μ m.

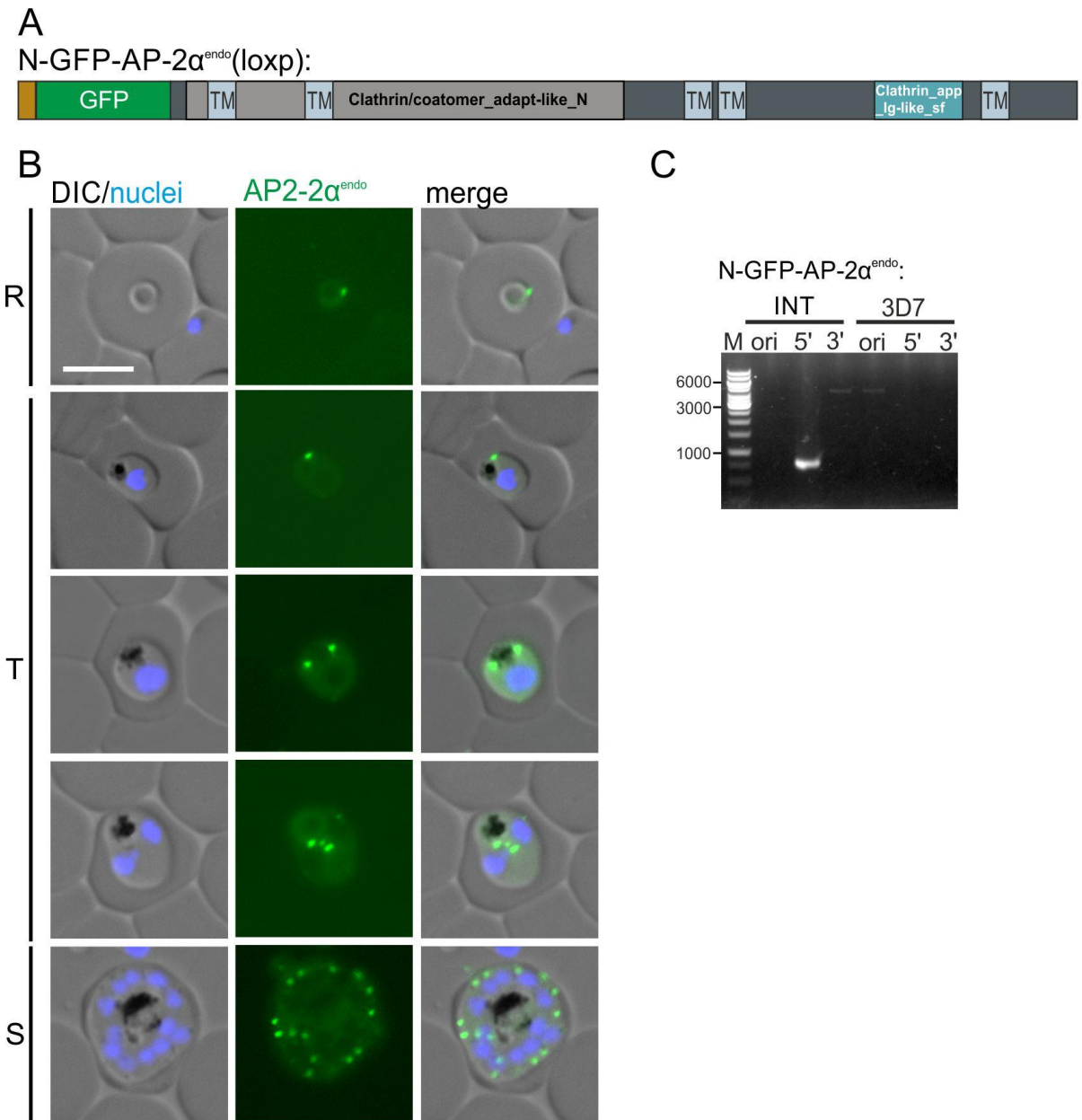


Figure 25 | Subcellular localization of N-GFP-AP-2 α^{endo} (loxP). **A** Schematic illustration of the AP-2 α protein N-terminally tagged with GFP. **B** Live-cell microscopy images of the indicated stages of N-GFP-AP-2 α^{endo} (loxP) parasites. Nuclei were stained with DAPI. R; ring, T; trophozoite, and S; schizont stages. DIC, differential interference contrast. The scale bar represents 5 μ m. **C** Agarose gel showing PCR-products to assess correct integration of the SLI-plasmid into the genome of *P. falciparum* (3D7) parasites to obtain the indicated cell line (5' integration junction: 5'INT: 795 bp (AP-2aint(2) fw+ DHODH42 rv); 3' integration junction: 3'INT: 4664bp (pARLsense55+ AP-2aint rv) and ori (indicating presence or absence of original unmodified locus): 4630 bp (AP-2aint(2) fw+ AP-2aint rv)).

3.1.1.2.3 AP-2 α is important for the development of parasite blood stages

To functionally investigate AP-2 α , the N-GFP-AP-2 α^{endo} (loxP) cell line was co-transfected with an episomal plasmid (pSkip-Flox) expressing the dimerizable Cre-recombinase (diCre). The diCre is split into two fragments, respectively fused to FRB and FKBP containing nuclear localization signals (NLS). The addition of the dimerizing compound rapalog causes the two parts to dimerize, resulting in the activation of the recombinase and thus the inducible excision of the recodonized functional *ap-2 α* flanked by loxP-sites (Birnbaum et al., 2017, Jullien et al., 2007, Jullien et al., 2003, Andenmatten et al., 2013).

Cultivation of synchronous N-GFP-AP-2 α^{endo} (loxP)+ pSkip-Flox parasites in the presence of rapalog for 48 h led to the excision of recodonized functional *ap-2 α* (Figure 26A). Flow cytometry-based monitoring of parasite growth of synchronous N-GFP-AP-2 α^{endo} (loxP)+ pSkip-Flox parasites starting with rings of the first cycle showed a drastic growth defect in the rapalog-treated parasites in comparison to the control parasites and revealed that the parasites failed to progress to the next cycle (Figure 26B). It can be concluded that AP-2 α is important for parasite blood stage growth.

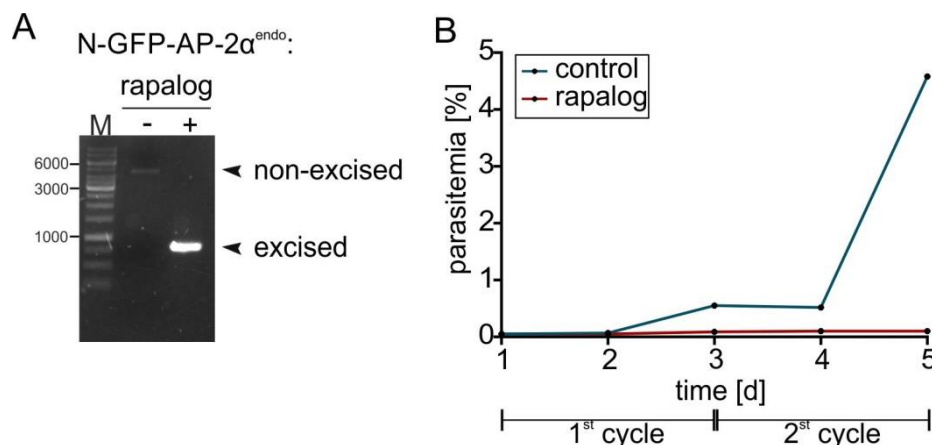


Figure 26 | AP-2 α is important for the survival of *P. falciparum* blood-stage parasites. **A** Agarose gel showing PCR-products to test for excision of the floxed functional *ap-2 α* in synchronous control (-) and rapalog-cultured (+) N-GFP-AP-2 α^{endo} (loxP)+ pSkip-Flox parasites. Non-excised *ap-2 α* : 5345 bp and excised *ap-2 α* : 750 bp (AP-2 α int(2) fw+ pARLminus rv). **B** Flow cytometry growth curves of synchronous control and rapalog-cultured N-GFP-AP-2 α^{endo} (loxP)+ pSkip-Flox parasites over 2 growth cycles, starting with rings in the 1st cycle (n = 1 experiment).

3.1.1.2.4 AP-2 α loss leads to a growth defect in trophozoite-staged parasites

Due to the slow kinetics of the conditional gene excision method, different induction times (0 h, 12 h, and 24 h after the first sorbitol synchronization of the parasites) were used to observe the effect of the loss of AP-2 α^{endo} at different stages in the N-GFP-AP-2 α^{endo} (loxP)+ pSkip-Flox cell line (Figure 27A). Giemsa smears were prepared at 72 h and 96 h after the first sorbitol synchronization (Figure 27B) and live-cell images were taken at 72 h (induction 12 h after 1st sorbitol treatment) (Figure 27C). The Giemsa smears revealed that the parasites did not develop beyond the young trophozoite stage (induction 0 h after 1st sorbitol treatment) (Figure 27B; i) or mid trophozoite stages (induction 24 h after 1st sorbitol treatment) (Figure 27B; iii), although some remaining AP-2 α^{endo} signal was detectable in these parasites (Figure 27C; blue arrows). This already indicated that a reduced amount of AP-2 α^{endo} is sufficient to exert a severe effect on trophozoite growth. In addition, some of the parasites appeared to possess little hemozoin in relation to their size (Figure 27B and C; blue frames). A striking phenotype after AP-2 α^{endo} loss was parasite-formed membranous loops that extended into the host cell cytosol (Figure 27B; white arrows) and which were visible in live-cell microscopy images upon membrane staining using the lipid probe Nile red (Figure 27D; white arrows).

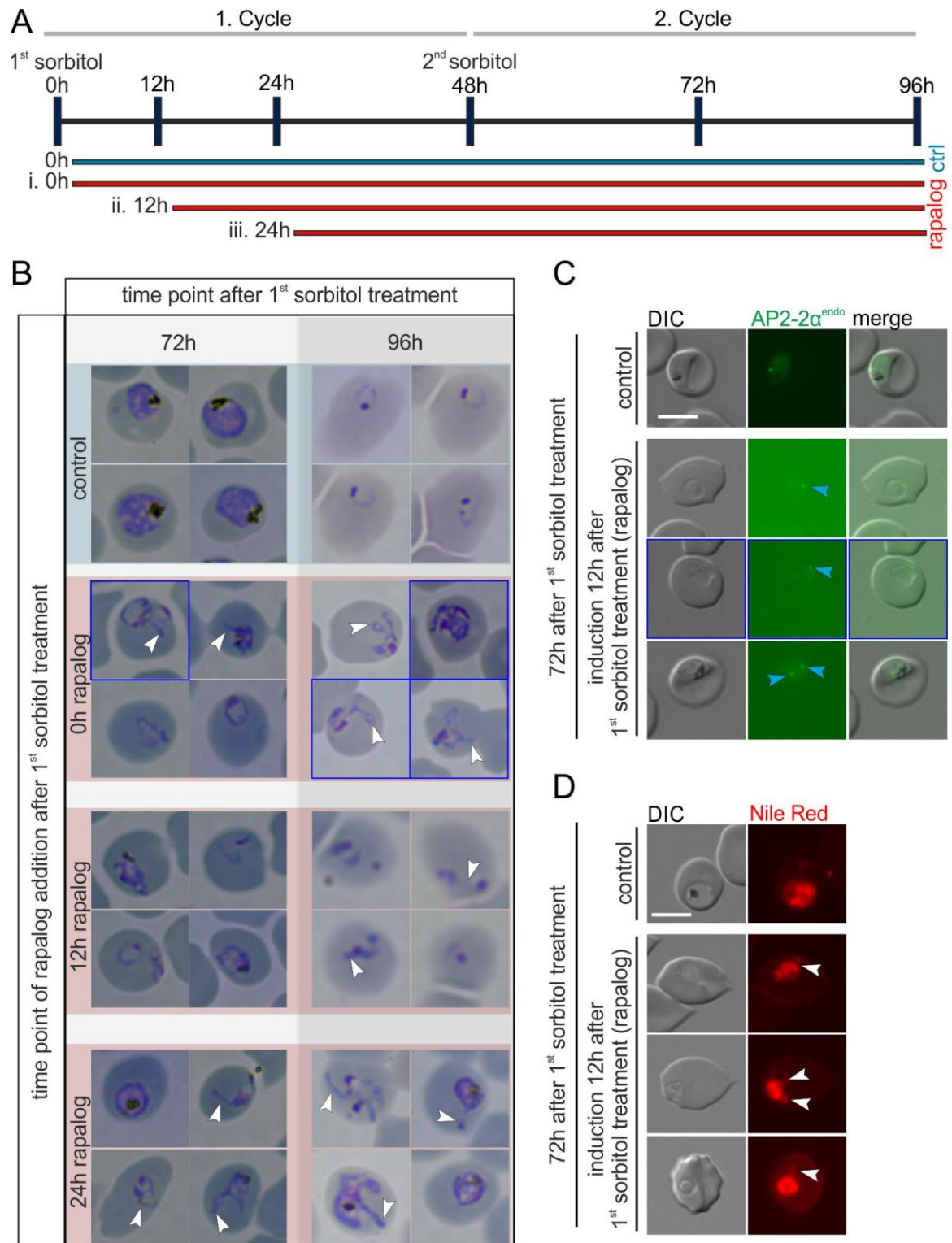


Figure 27 | AP-2 α loss leads to a growth defect in trophozoite-staged parasites. **A** Schematic illustration of the experimental procedure: Parasites of the N-GFP-AP-2 α^{endo} (loxP)+ pSkip-Flox cell line were synchronized twice with sorbitol within 48 h and cultivated for 96 h in the presence or absence (control) of rapalog. The excision of recodonized functional *ap-2 α* was induced at different time points ((i.) 0 h, (ii.) 12 h, and (iii.) 24 h) after the 1st sorbitol treatment. **B** Light-microscopy images of Giemsa-stained blood

smears obtained from the experiment described in (A). White arrows: membranous loops formed by the parasite upon AP-2 α^{endo} loss. Blue frames: parasites with little hemozoin relative to the control. **C** Live-cell microscopy images of N-GFP-AP-2 α^{endo} (loxP)+ pSkip-Flox. Images were taken 72 h after induction of 1st Sorbitol treatment of parasites cultivated in the presence of rapalog (excision induction 24 h after 1st sorbitol treatment) compared to the control. Blue arrows: remaining AP-2 α^{endo} signal. **D** Live-cell microscopy images of Nile red stained parasites described in (C). White arrows: membranous loops formed by the parasite upon AP-2 α^{endo} loss. DIC, differential interference contrast. The scale bar represents 5 μm .

3.1.1.3 AP-2 σ of *P. falciparum*

3.1.1.3.1 AP-2 σ of *P. falciparum* parasites contains an unusual predicted transmembrane domain

With only 141 aa in *P. falciparum* (PF3D7_0217300; AP-2 complex subunit sigma, putative) σ -adaptin is the smallest adaptin of the AP-2 complex. Prediction and comparison of the protein domains of PfAP-2 σ (Figure 28A) with the σ -adaptins of *H. sapiens* (P53680), *P. berghei* (PBANKA_0314000), *T. gondii* (TGME49_313450), and *S. cerevisiae* (Q00381), using InterPro (Blum et al., 2021) showed that in PfAP-2 σ , like in the AP-2 α of *P. falciparum*, an unusual TM was predicted (TMHMM/ Phobius), which is absent in AP-2 σ of *H. sapiens*, *T. gondii*, and *S. cerevisiae* but was predicted, together with one additional TM, in AP-2 σ of *P. berghei*. If this TM prediction is accurate and not due to a random hydrophobic patch, the protein would be inserted into the PPM with a cytosolic C-terminal and a non-cytosolic C-terminal domain, the latter extending into the PV of the parasite (Figure 28B). These unusual predicted TMs in AP-2 σ and AP-2 α of *P. falciparum* indicate an altered mechanism of the AP-2 complex compared to *H. sapiens* AP-2. Experiments are needed to confirm the presence of the TM in AP-2 σ of *P. falciparum*.

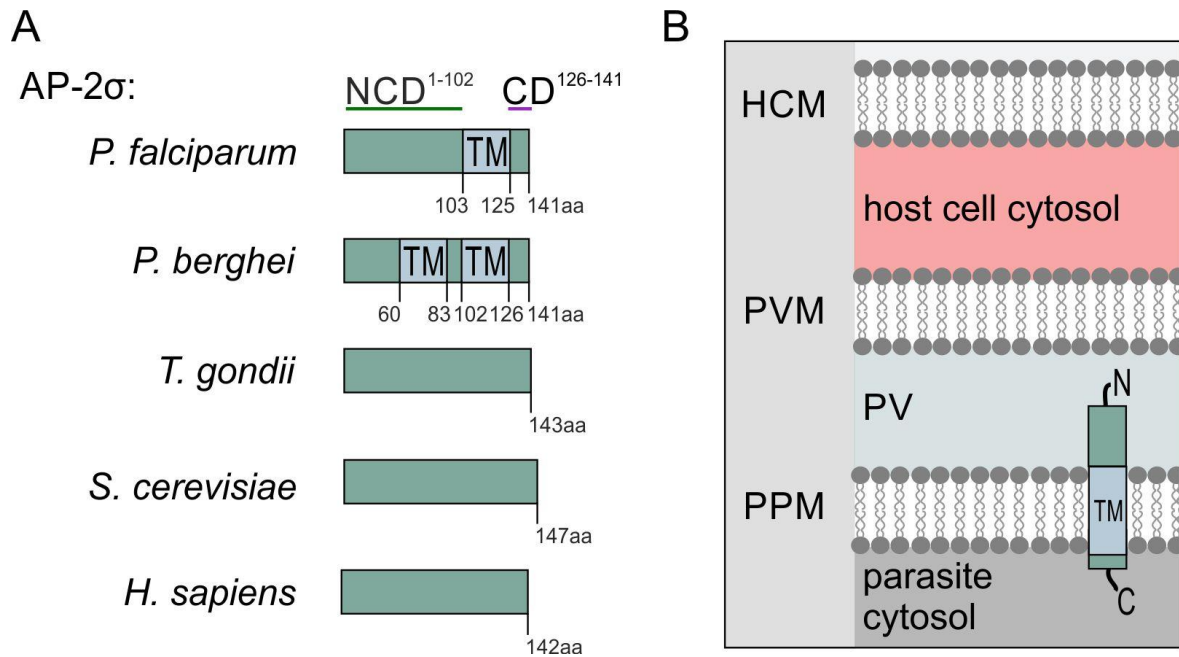


Figure 28 | AP-2 σ of *P. falciparum* contains an unusual predicted transmembrane domain. **A** Schematic illustration of the AP-2 σ (PF3D7_0217300) protein domain architecture of *P. falciparum* in comparison to AP-2 σ from *H. sapiens* (P53680), *S. cerevisiae* (Q00381), *T. gondii* (TGME49_313450), and *P. berghei* (PBANKA_0314000). TM, predicted transmembrane domains; CD, predicted cytoplasmic domains; NCD, predicted non-cytoplasmic domains. **B** Schematic illustration of the predicted AP-2 σ protein membrane topology. HCM, host cell membrane; PVM, parasitophorous vacuole membrane; PV, parasitophorous vacuole; PPM, parasite plasma membrane.

3.1.1.3.2 Subcellular localization of AP-2 σ in blood stages of *P. falciparum* parasites

To examine the localization and function, AP-2 σ was endogenously tagged by modification of the *ap-2 σ* gene locus using the SLI-system (Birnbbaum et al., 2017), resulting in two different cell lines (Figure 29 and Figure 30). In the resulting two cell lines AP-2 σ was either tagged with 3xHA (Figure 29A) or 2xFKBP-GFP (Figure 30A) at the C-terminus. Correct integration of the modifying plasmid was confirmed by PCR of genomic DNA of the corresponding AP-2 σ -3xHA^{endo} (Figure 29B) and the AP-2 σ -2xFKBP-GFP^{endo} parasite line (Figure 30B).

An α -HA-IFA of AP-2 σ -3xHA^{endo} parasites showed several foci in trophozoites which increased in number in schizont stages. In trophozoites, at least one signal at the PPM was visible (Figure 29C).

This observation was consistent with the AP-2 σ^{endo} foci present in live-cell images of the AP-2 σ -2xFKBP-GFP endo cell line (Figure 30C). This cell line showed endogenous AP-2 σ with a singular focus in ring stages and most trophozoites showed at least one signal at the PPM in close proximity to the DV. In schizonts, several foci of AP-2 σ^{endo} were visible (Figure 30C).

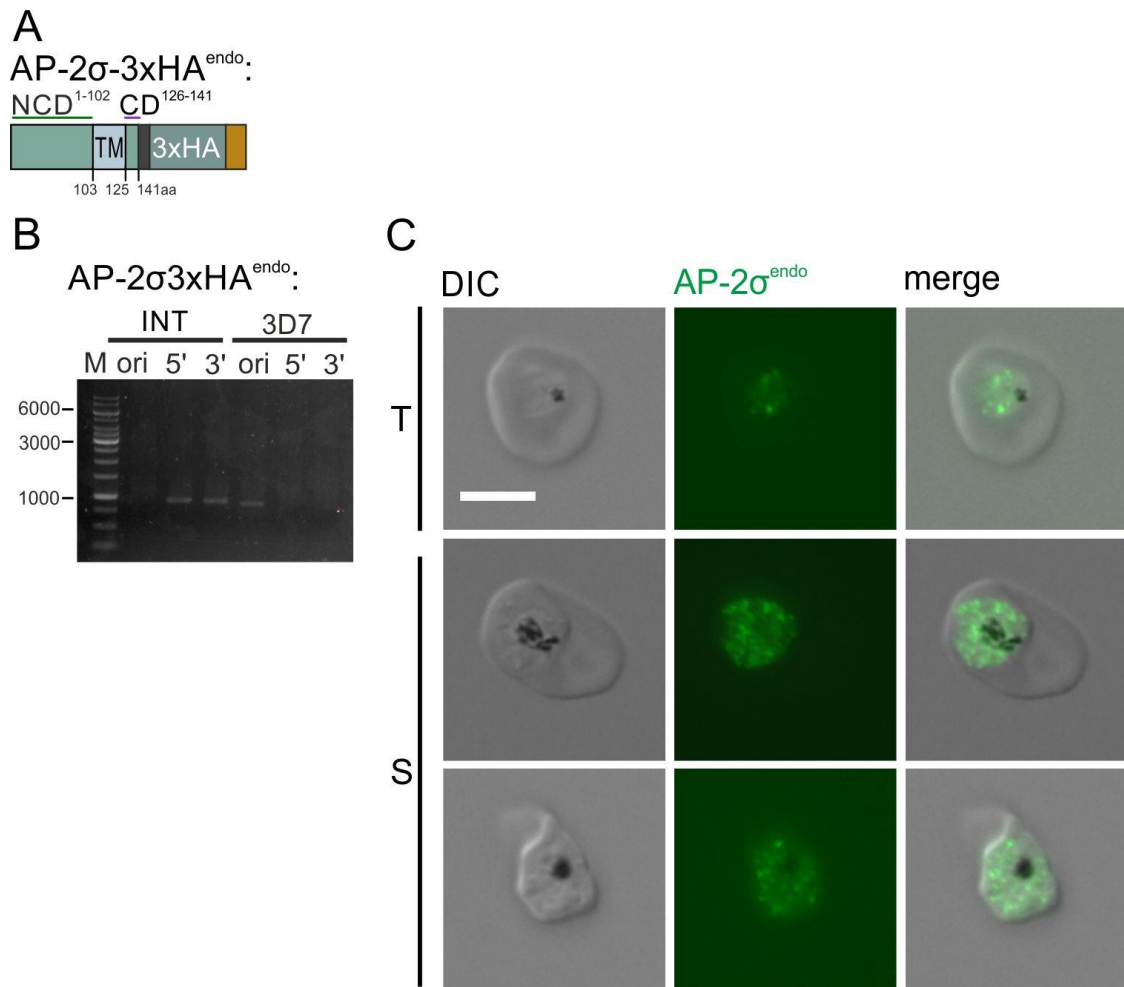


Figure 29 | Subcellular localization of AP-2 σ -3xHA endo . **A** Schematic illustration of the AP-2 σ protein C-terminally tagged with 3xHA. HA, 3x hemagglutinin; TM, predicted transmembrane domain; CD, predicted cytoplasmic domains; NCD, predicted non-cytoplasmic domains. **B** Microscopy images of indicated stages of an IFA of formaldehyde and glutaraldehyde fixed AP-2 σ -3xHA endo parasites. α -HA (rat) was used to detect HA. T; trophozoite and S; schizont stages. DIC, differential interference contrast. The scale bar represents 5 μ m. **C** Agarose gel showing PCR-products to assess correct integration of the SLI-plasmid into the genome of *P. falciparum* (3D7) to obtain the indicated cell line (5' integration junction: 5'INT: 997

bp (AP-2 σ int fw+ Neo40 rv); 3' integration junction: 3'INT: 958 bp (pARLsense55+ AP-2 σ int rv) and ori (indicating presence or absence of original unmodified locus): 901 bp (AP-2 σ int fw+ AP-2 σ int rv).

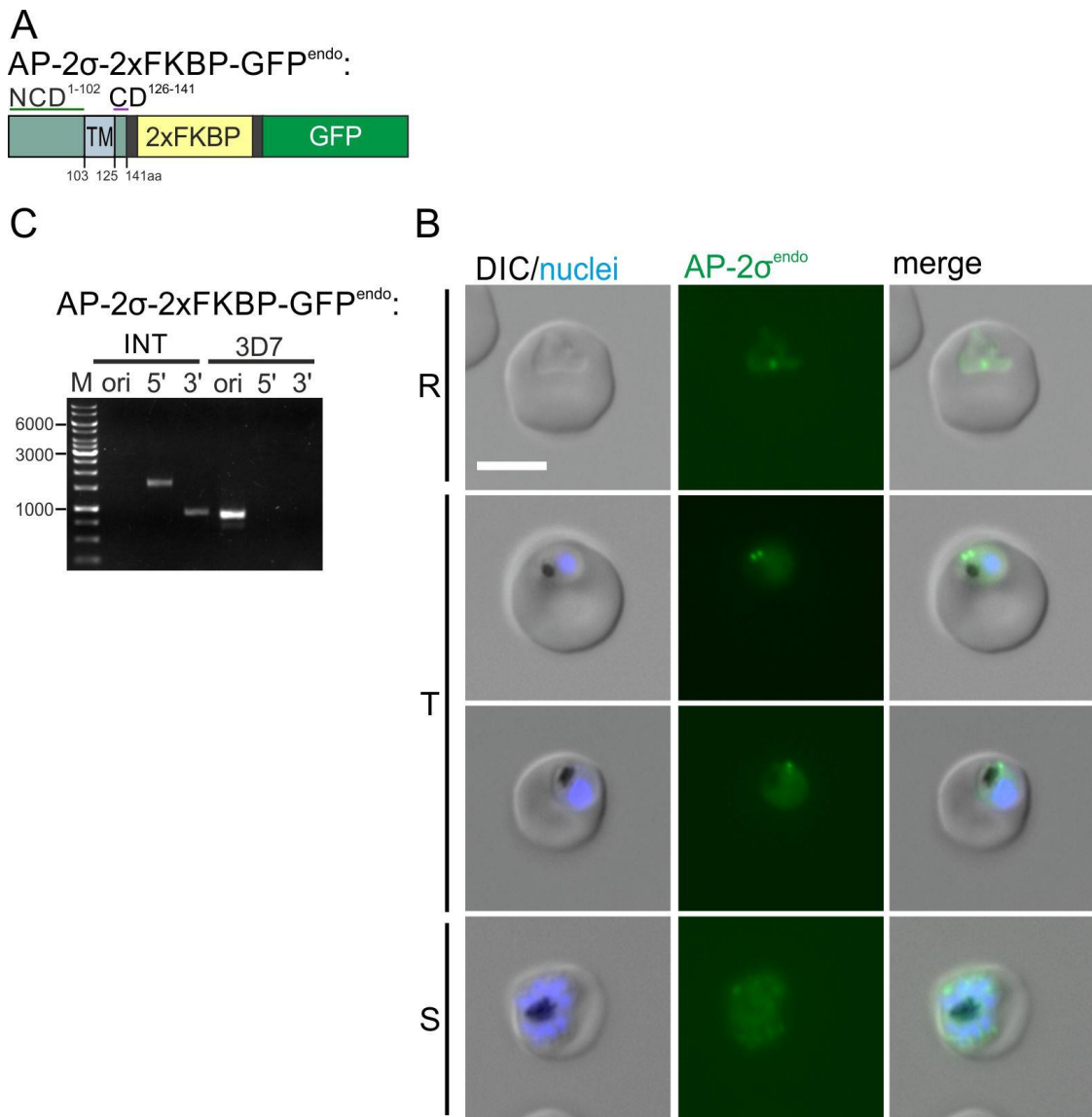


Figure 30 | Subcellular localization of AP-2 σ -2xFKBP-GFP^{endo}. **A** Schematic illustration of the AP-2 σ protein C-terminally tagged with 2xFKBP-GFP. **B** Live-cell microscopy images of the indicated stages of AP-2 σ -2xFKBP-GFP^{endo} parasites. Nuclei were stained with DAPI. R; ring, T; trophozoite, and S; schizont stages. DIC, differential interference contrast. The scale bar represents 5 μ m. **C** Agarose gel showing PCR-products to assess correct integration of the SLI-plasmid into the genome of *P. falciparum* (3D7) to obtain the indicated cell line (5' integration junction: 5'INT: 1648 bp (AP-2 σ int fw+ GFP85 rv); 3' integration junction: 3'INT: 958 bp (pARLsense55+ AP-2 σ int rv) and ori (indicating presence or absence of original unmodified locus): 901 bp (AP-2 σ int fw+ AP-2 σ int rv)).

3.1.1.3.3 AP-2 σ is important for the development of parasite blood stages

To investigate its function, AP-2 σ was conditionally inactivated using knock-sideway (Figure 31) (Birnbaum et al., 2017, Robinson et al., 2010, Haruki et al., 2008). For this purpose, the AP-2 σ -2xFKBP-GFP^{endo} parasite cell line was co-transfected with the *nmd3*'1xNLS-FRB-mCherry mislocalizer plasmid. Cultivation of parasites in the presence of rapalog for 12 h led to a partial mislocalization of AP-2 σ to the nucleus (100% of the parasites had a mixed phenotype with a clear transfer of AP-2 σ to the nucleus but also signal remaining outside of the nucleus at the PPM) (Figure 31A, white arrows) with reverse localization of the mislocalizer (Figure 31A, blue arrows). To determine the effect of this partial mislocalization and the relevance of AP-2 σ for the parasite blood cycle, we monitored the parasitemia after conditional inactivation of AP-2 σ by knock-sideway (+ rapalog) compared to the control over 5 days (2.5 growth cycles). Despite the incomplete mislocalization of AP-2 σ , the knock-sideway led to a drastic growth defect in comparison to the control parasites (Figure 31B), indicating its essentiality for the growth of parasite blood stages.

To determine whether reverse mislocalization of the mislocalizer to the AP-2 σ signal affects AP-2 σ functionality, a FRB-mCh plasmid was transfected into the AP-2 σ -2xFKBP-GFP^{endo} cell line. The addition of rapalog led to the localization of FRB-mCh to the AP-2 σ signal (Figure 31C, white arrow). Monitoring the parasitemia after induction of dimerization of AP-2 σ with FRB-mCh (+ rapalog) compared to the control over 5 days (2.5 growth cycles), showed a substantial growth defect (Figure 31D), almost comparable to the knock-sideway (Figure 31B), indicating that reverse localization of mCherry fused FRB already severely interferes with the function of AP-2 σ .

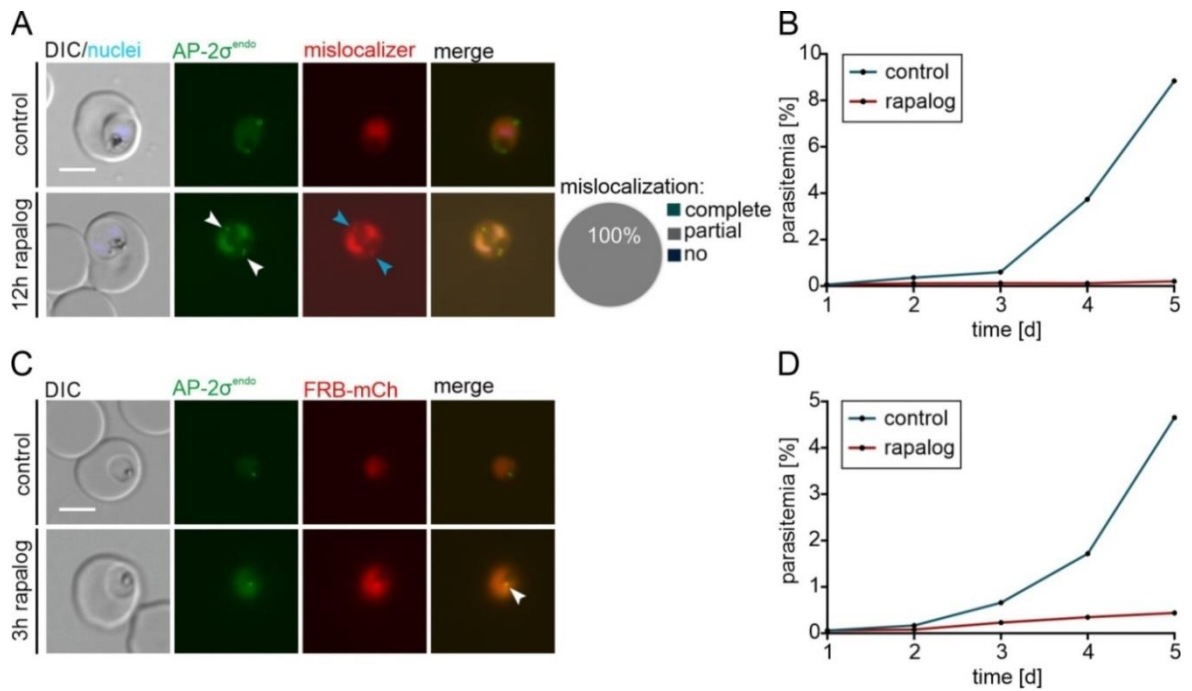


Figure 31 | AP-2 σ is important for the survival of *P. falciparum* blood-stage parasites. **A** Knock-sideway of AP-2 σ -2xFKBP-GFP^{endo} parasites expressing a nuclear mislocalizer (*nmd3*^{NLS}-FRB-mCh) (Birbaum et al., 2017). Images were taken 12 h after induction of knock-sideway of parasites cultivated in the presence of rapalog compared to the control. Knock-sideway was classified in complete, partial, or absent (no) mislocalization in 32 parasites. Nuclei were stained with DAPI. DIC, differential interference contrast. The scale bar indicates 5 μ m. White arrows: AP-2 σ^{endo} signal remaining outside of the nucleus at the PPM. Blue arrows: reverse localization of the mislocalizer. **B** Flow cytometry growth curve over 2.5 growth cycles of the AP-2 σ -2xFKBP-GFP^{endo} + *nmd3*^{NLS}-FRB-mCh^{epi} cell line shown in A. Parasites cultivated in the presence of rapalog compared to the control. One representative of n = 3 independent experiments, all replicas are shown in the supplements (Appendix B). **C** AP-2 σ -2xFKBP-GFP^{endo} parasites expressing *nmd3*^{FRB}-mCh. Images were taken 3 h after induction of FRB FKBP dimerization through cultivation of the parasites in the presence of rapalog compared to the control. White arrows: localization of FRB-mCh to the AP-2 σ signal. Nuclei were stained with DAPI. DIC, differential interference contrast. The scale bar indicates 5 μ m. DIC, differential interference contrast. **D** Flow cytometry growth curve over 2.5 growth cycles of the AP-2 σ -2xFKBP-GFP^{endo} + *nmd3*^{FRB}-mCh^{epi} cell line shown in C. Parasites cultivated in the presence of rapalog compared to the control. One representative of n = 3 independent experiments, all replicas are shown in the supplements (Appendix B).

3.1.1.3.4 AP-2 σ inactivation affects HCCU

To investigate the role of AP-2 σ in HCCU, bloated food vacuole assays were performed (Figure 32) (Jonscher et al., 2019, Birnbaum et al., 2020). For this purpose, synchronized parasites were treated with the protease inhibitor E64 to inhibit the digestion of hemoglobin in the DV (Sijwali and Rosenthal, 2004). As a result, newly internalized hemoglobin reaching the DV accumulates, resulting in a bloated food vacuole phenotype in parasites with an intact HCCU process. Upon AP-2 σ^{endo} inactivation (AP-2 σ -2xFKBP-GFP $^{\text{endo}}$ + NLS-mislocalizer) the parasites showed a mixed phenotype of ~70.81 % bloated (Figure 32A; white arrow) and ~29.19% non-bloated DV's (Figure 32A; blue arrow), while in the control parasites DV bloating was unaffected (Figure 32A; upper panel). Since the diameter of the parasites showed no significant difference to the control (Figure 32B), the parasites were still viable over the assay time, excluding pre-mature parasite death as a reason for this outcome. The significant but moderate effect on HCCU could be explained by the absence of a complete mislocalization of AP-2 σ^{endo} to the nucleus (Figure 31A) which may result in slower kinetics of inactivation and therefore the relevance in HCCU may not be fully captured using this assay.

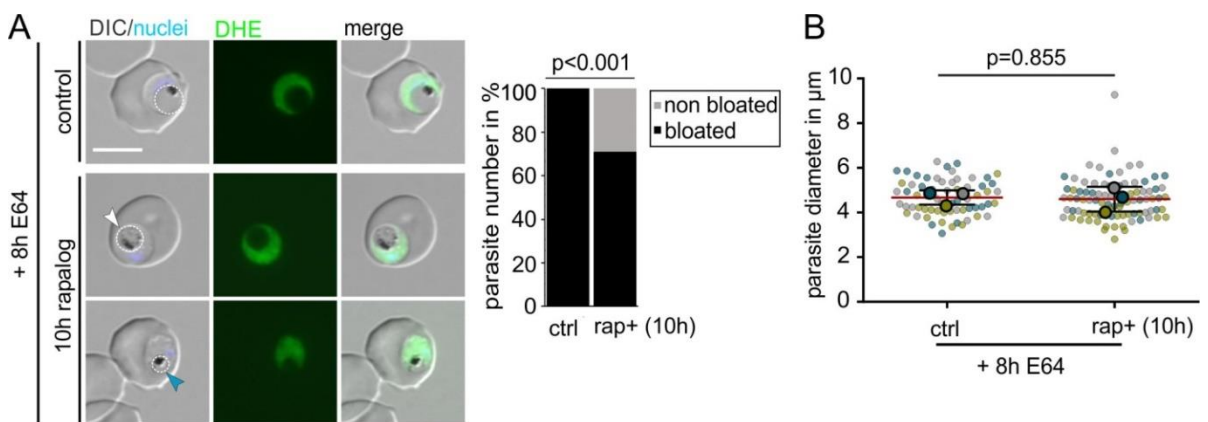


Figure 32 | AP-2 σ is involved in the HCCU of *P. falciparum* blood stages. **A** AP-2 σ -2xFKBP-GFP $^{\text{endo}}$ + *nmd3*NLS-FRB-mCh (mislocalizer) synchronous parasites treated 8 h with E64 in the presence or absence (control) of rapalog (10 h (parasites were incubated for 2 h with rapalog prior E64 addition)). Left: Live-cell images of the parasites stained with DHE (cytosol). Nuclei were stained with DAPI. DIC, differential interference contrast. Right: Quantification of the number of cells with bloated FVs. Fisher's exact test. Pooled from $n = 3$ independent experiments with 21, 21 and 22 cells (control) and 25, 33 and 32 cells (rapalog), respectively. P-value indicated. **B** Superplot showing the diameter of parasites analyzed in the bloated FV assay seen in (A) (cells from the 3 experiments are distinguished by blue, yellow, grey dots); two-tailed unpaired t-test of the means, p-values indicated; mean (red); error bars (black) show S.D..

3.2 Early endosome associated structures and proteins in HCCU

The first essential protein identified in the HCCU of *P. falciparum*, termed *PNVPS45* (Jonscher et al., 2019), is the orthologue of VPS45 in other eukaryotic organisms and is associated with intermediate steps of endocytosis (Section 1.10.1.2) (Figure 33A). VPS45 is typically a part of a fusion-machinery located at the EE in mammals (Section 1.9.1.2), where it is linked to Rab5 via Rbsn5 (Figure 33B) (Collins and Zimmerberg, 2009). Inactivation of Rab5b (Flemming, 2015, Schmitt, 2020) results in a similar phenotype as inactivation of VPS45, indicating that Rab5b plays a role in the same step of HCCU. We therefore hypothesized that Rab5b might be a component of the EE fusion complex. If VPS45-dependent endosomal transport is evolutionarily conserved, it can be expected to also depend on an equivalent of the Rab5 effector protein Rbsn5 which up to now had been elusive in malaria parasites.

3.2.1 Identification of the putative *P. falciparum* Rbns5

To identify potential Rbns5 candidates, *in silico* searches were performed. BLAST searches using human Rbns5 (Q9H1K0) identified the FYVE-containing protein (FCP, PF3D7_1460100) as the top hit. However, with low amino acid sequence identities of 46% (score 51.2; E value 4e-07) over the entire region, mostly restricted to the FYVE domain, it was uncertain if FCP corresponds to Rbns5 in other organisms or to a different FYVE-domain-containing protein such as e.g., the early endosomal antigen 1 (EEA1).

For clarification HHPred (Zimmermann et al., 2018, Gabler et al., 2020) was used, a method that is more sensitive to detect remote homology as it also considers predicted secondary structure similarities. It identified PF3D7_1310300 as the top hit for *HsRbns5*, detecting similarity over 212 amino acids (E value 5e-12), including also regions outside of the FYVE domain. FCP was the second-best hit of this HHPred search but the similarity covered a shorter sequence region and showed only a low level of conservation (E value 3,3e-10). Therefore, we concluded that PF3D7_1310300 was the most likely candidate for *PfRbns5*.

PF3D7_1310300 (annotated as a putative zinc finger protein) is a protein of 247 aa containing a FYVE zinc finger in its N-terminal half (Plasmodb.org) (Figure 33C). Comparison of the protein domain architecture using the prediction tool InterPro (Blum et

al., 2021) of PF3D7_1310300 with *HsRbns5* and its yeast (*S. cerevisiae*) homolog Vac1/PEP7 (P32609) showed that the *P. falciparum* protein misses the NPF repeat region found in the C-terminal half of human Rbns5 and the region containing the N-terminal C2H2 zinc finger in *HsRbns5* and Vac1/PEP7. Also, a Rab binding domain was not predicted by this method. However, a multiple sequence alignment (Figure 33D) (ClustalOmega (Sievers et al., 2011, Goujon et al., 2010)) of the Rab5 binding domain of *HsRbns5* (627-784 aa [PMID:16034420]) with the entire sequences of the putative Rbns5's of *P. falciparum*, *P. berghei*, *P. malariae*, *P. knowlesi* and *P. vivax* identified a putative Rab5 binding domain downstream of the FYVE domain of *PfRbns5*.

Based on this analysis and the functional data in the following sections we named PF3D7_1310300 *P. falciparum* Rabenosyn 5 (*PfRbns5*).

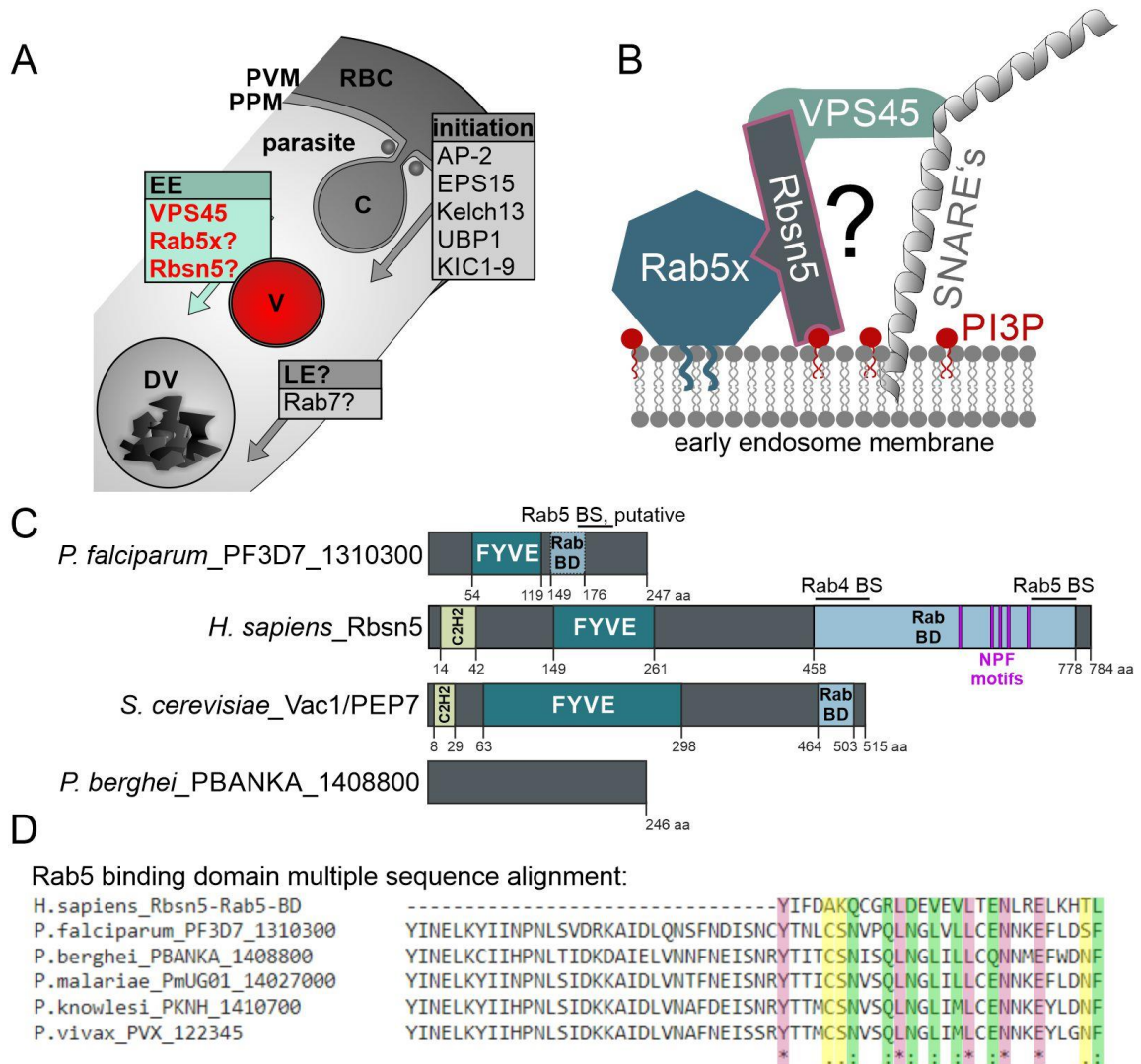


Figure 33 | Identification of a putative *P. falciparum* Rbsn5 protein and comparison to its homologs.

A Schematic illustration of the HCCU process in *P. falciparum*. Known or suspected (indicated by a question mark) proteins involved in the initiation, early, or late endosomal steps of the HCCU. Putative proteins (Rab5x, Rbsn5, and VPS45) involved at an early endosomal step are highlighted. Rab5x stands for Rab5b or Rab5c. Abbreviations: RBC: red blood cell; C: cytosome; EE: early endosome; LE: late endosome; DV: digestive vacuole; V: HCC-containing vesicle; PPM: parasite plasma membrane; PVM: parasitophorous vacuolar membrane. Modified from (Sabitzki et al., 2020). **B** Schematic illustration of the Rab5-Rbsn5-VPS45 fusion complex found in model organisms at early endosomal membranes and interacting with SNARE proteins and PI3P. **C** Comparison of the domain architecture (InterPro (Blum et al., 2021)) of the putative Rbsn5 protein (PF3D7_1310300) of *P. falciparum* (247 aa), *H. sapiens* Rbsn5 (784 aa), and the VAC1/PEP7 protein of *S. cerevisiae* (515 aa). BD, binding domain; BS, binding site. **D** Part of multiple sequence alignment (ClustalOmega) of the Rab5 binding domain of *HsRbsn5* with the entire aa sequence of putative Rbsn5s of *P. falciparum*, *P. berghei*, *P. malariae*, *P. knowlesi*, and *P. vivax*. Complete alignment in the supplements (Appendix C).

3.2.2 Subcellular localization of *PfRbsn5*

To investigate its localization and function, *PfRbsn5* was endogenously tagged by modification of the *Rbsn5* gene locus with the sequence encoding 2xFKBP-GFP-2xFKBP using the SLI-system (Birnbaum et al., 2017) (Figure 34A). Correct integration was confirmed by PCR on genomic DNA of the corresponding *Rbsn5*-2xFKBP-GFP-2xFKBP^{endo} parasite line (Figure 34C). The cell line (*Rbsn5*-2xFKBP-GFP-2xFKBP^{endo}) showed *Rbsn5*^{endo} in foci that were frequently proximal to the nucleus (Figure 34B, white arrow). In addition, a population of *Rbsn5*^{endo} was found dispersed in the cytosol with fainter accumulations and in some cells a faint dispersed signal in the nucleus (Figure 34B, light blue arrow) or at the DV (Figure 34B, dark blue arrow). The nucleus-proximal foci increased in number and intensity with the age of the parasite in the blood cycle and a more intense focus was observed at the DV in schizont stage parasites (Figure 34B, purple arrow). Co-expression of a fluorescently tagged Grasp showed that these *Rbsn5*^{endo} foci were in close proximity or overlapped with the Golgi-apparatus (Figure 34D). The localization of *Rbsn5*^{endo} was similar to the previously observed localization of *VPS45*^{endo} (Jonscher et al., 2019).

3.2.3 *Rbsn5* co-localizes with *VPS45* to *Rab5b* positive membranes

For further localization studies, *sf3a2*^{VPS45-mCh^{epi} and *sf3a2*^{Rab5b-mCh^{epi} plasmids were generated. Episomal co-expression of *VPS45*-mCh^{epi} in *Rbsn*-2xFKBP-GFP-2xFKBP^{endo} parasites showed overlapping signals of both proteins (Figure 35 A; white arrows) and co-expression of *Rab5b*-mCh^{epi} in *Rbsn*-2xFKBP-GFP-2xFKBP^{endo} (Figure 35 B; white arrows) and in *VPS45*-2xFKBP-GFP^{endo} (Figure 35 C; white arrows) parasite lines indicated localization of *Rbsn5* and *VPS45* to *Rab5b* positive membranes.}}

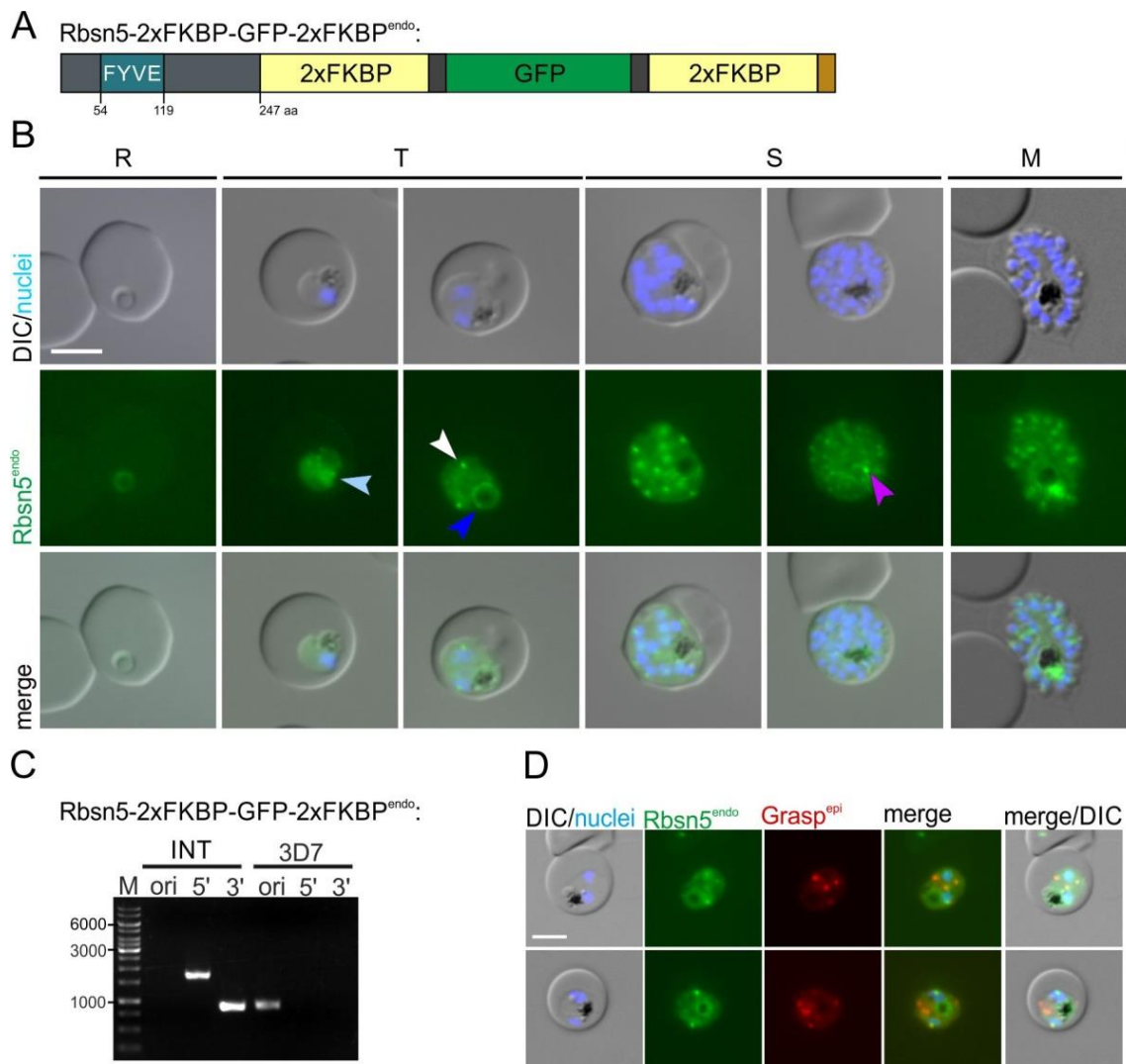


Figure 34 | Subcellular localization of *Pf*Rbsn5. **A** Schematic illustration of the *Pf*Rbsn5 protein tagged at the C-terminus with 2xFKBP-GFP-2xFKBP. **B** Live-cell microscopy images of the indicated stages of Rbsn5-2xFKBP-GFP-2xFKBP^{endo} parasites. The white arrow indicates nucleus-proximal foci, the light blue arrow indicates a faint dispersed Rbsn5^{endo} signal in the nucleus and a dark blue arrow indicates Rbsn5^{endo} signal at the food vacuole. Nuclei were stained with DAPI. R, ring; T, trophozoite; S, schizont and M, merozoite stages. The scale bar represents 5 μ m. **C** Agarose gel showing PCR-products to assess correct integration of the SLI-plasmid into the genome of *P. falciparum* (3D7) to obtain the indicated cell line (5'INT: 1760 bp (Rbsn5int fw+ GFP85 rv); 3'INT: 890 bp (pARL55sense+Rbsn5int rv) and ori (indicating presence or absence of original unmodified locus): 935 bp (Rbsn5int fw+ Rbsn5int rv)). **D** Live-cell microscopy images of Rbsn5-2xFKBP-GFP-2xFKBP^{endo} parasites, co-expressing Grasp^{epi}. The scale bar represents 5 μ m. DIC, differential interference contrast; endo, endogenous; epi, episomal.

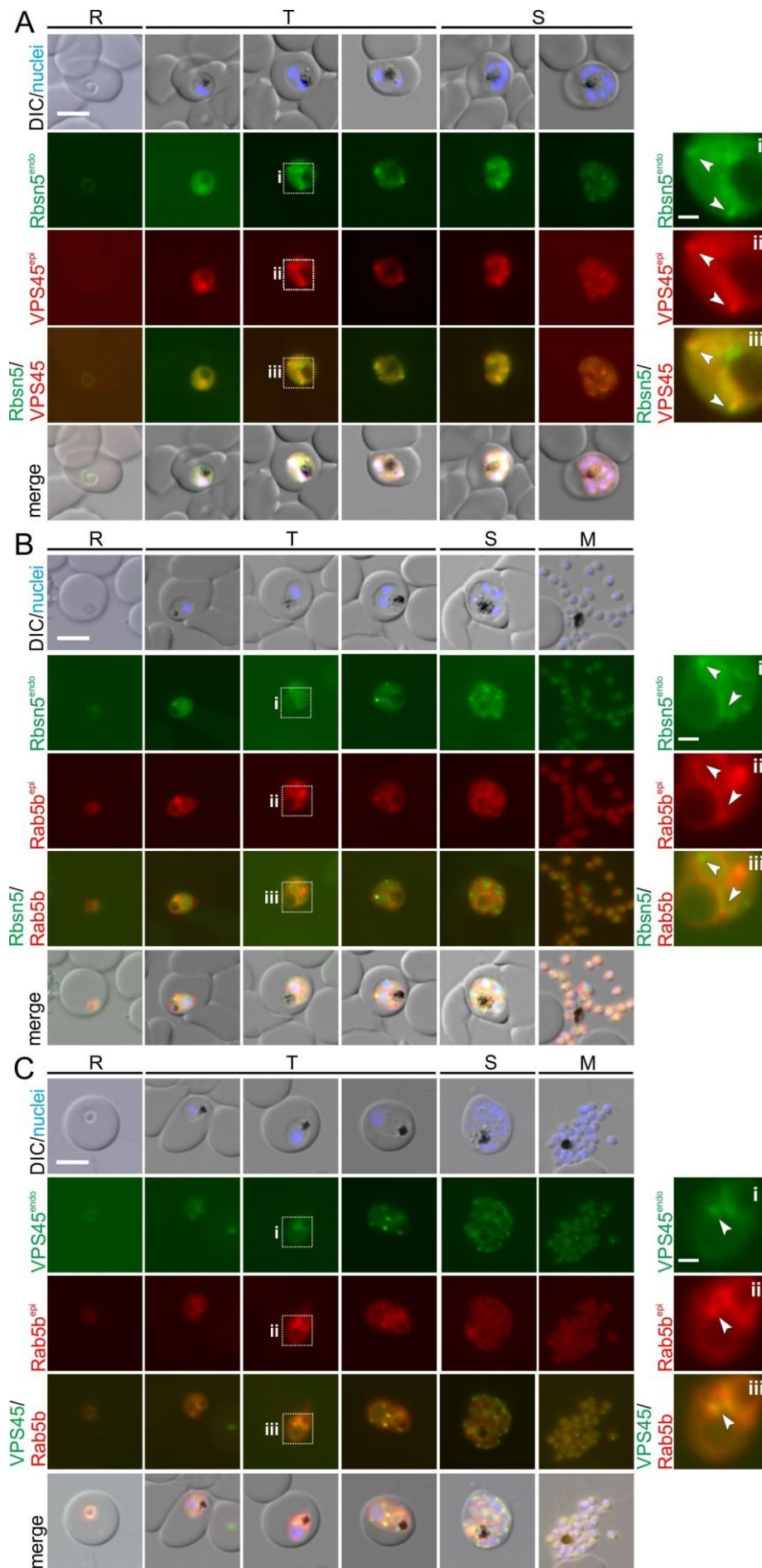


Figure 35 | Rbsn5 co-localizes with VPS45 to Rab5b positive membranes. **A** Live-cell microscopy images of the indicated stages of Rbsn5-2xFKBP-GFP-2xFKBP^{endo} parasites, co-expressing the sf3a2'VPS45-mCh^{epi} plasmid. White arrows indicate overlapping of Rbsn5^{endo} and VPS45^{epi} signal. **B** Live-cell microscopy images of the indicated stages of Rbsn5-2xFKBP-GFP-2xFKBP^{endo} parasites, co-expressing Rab5b-mCh^{epi}. White arrows indicate localization of Rbsn5^{endo} to Rab5b^{epi} positive signals. **C** Live-cell microscopy images of the indicated stages of VPS45-2xFKBP-GFP-2xFKBP^{endo} parasites, co-expressing Rab5b-mCh^{epi}. White arrows indicate localization of VPS45^{endo} to Rab5b^{epi} positive signals. Dashed boxes (i-iii) in the images outline the areas of magnification seen on the right. DIC, differential interference contrast; endo, endogenous; epi, episomal; R, ring; T, trophozoite; S, schizont and M, merozoite stages. The scale bars in the left images represent 5 μ m and The scale bars in the magnification images on the right site represent 1 μ m. Nuclei were stained with DAPI.

3.2.4 Conditional inactivation of Rbsn5 leads to an accumulation of vesicular structures and parasite death

To investigate its function, Rbsn5 was conditionally inactivated via knock-sideway (Birnbaum et al., 2017, Haruki et al., 2008, Robinson et al., 2010) by expressing the 1xNLS-FRB-mCh^{epi} mislocalizer plasmid in the Rbsn5-2xFKBP-GFP-2xFKBP^{endo} cell line. The addition of rapalog efficiently removed Rbsn5^{endo} into the nucleus within 1 h (Figure 36A). To determine the relevance of Rbsn5^{endo} for the parasite blood cycle, the parasitemia was monitored after conditional inactivation of Rbsn5^{endo} by knock-sideway (+ rapalog) compared to the control over 5 days (2.5 growth cycles). Rbsn5^{endo} inactivation led to a substantial growth defect in comparison to the control parasites (Figure 36B), suggesting that Rbsn5 function is important for the growth of *P. falciparum* asexual blood stages. Monitoring the parasites in a narrower time frame by DIC microscopy showed that the inactivation of Rbsn5^{endo} led to an accumulation of vesicular structures in the parasite cell (Figure 36C, blue arrows; D), a prominent phenotype previously observed upon PVPS45 inactivation (Jonscher et al., 2019). The number of these vesicular structures per parasite increased over time from an average of 1.060 ± 0.2534 at induction of the knock-sideway to an average of 5.618 ± 2.035 two hours and 12.59 ± 0.6516 eight hours after Rbsn5 inactivation, while the number of vesicles stayed low in control parasites (1.259 ± 0.2062) (Figure 36C, white arrows; D).

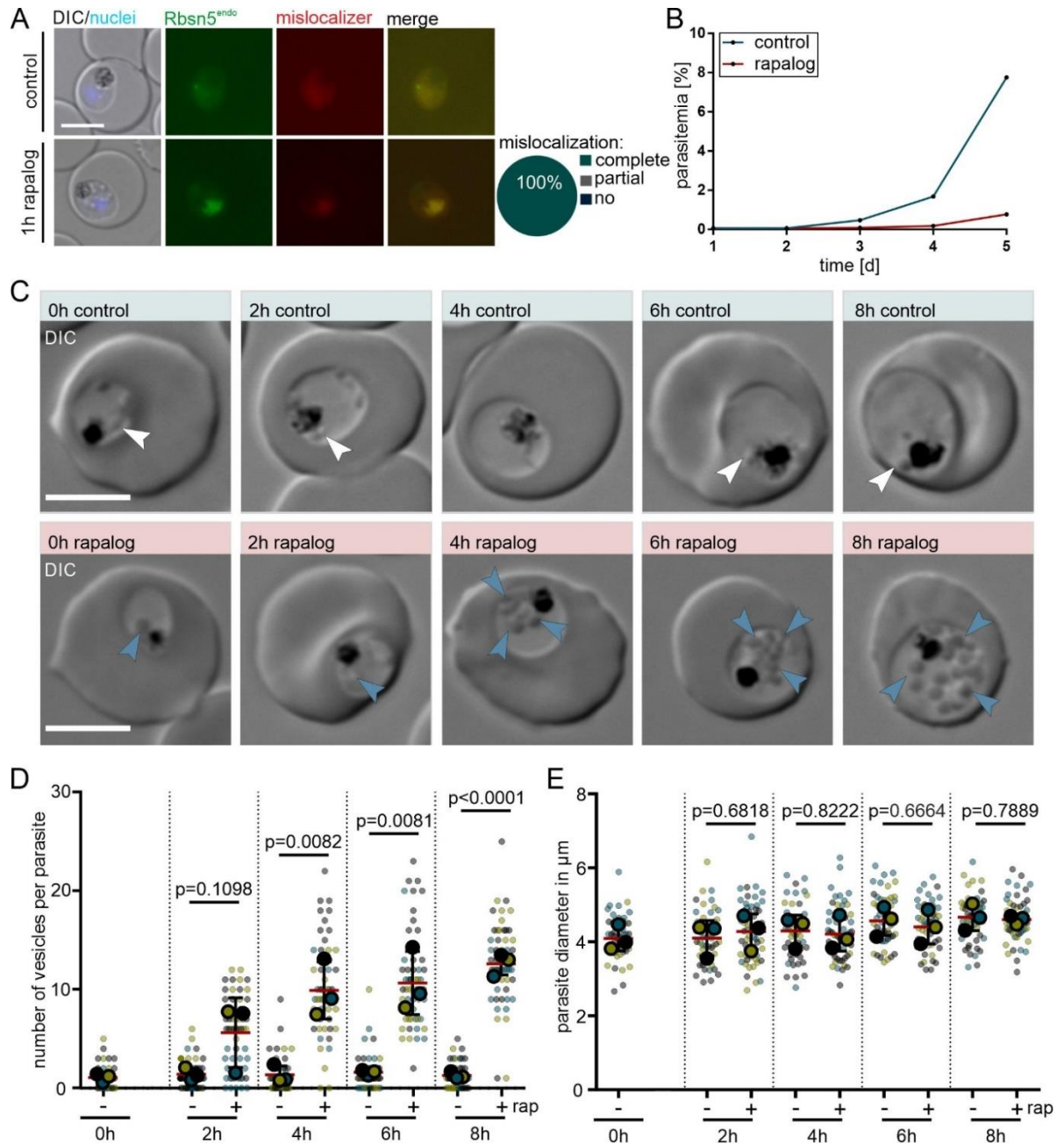


Figure 36 | Inactivation of *PfRbsn5* leads to accumulation of vesicular structures in the parasite cell and subsequent parasite death.

A Knock-sideway of *PfRbsn5*-2xFKBP-GFP-FKBP^{endo} parasites expressing a nuclear mislocalizer from an episomal plasmid (*nmd3*NLS-FRB-mCh^{epi}) (Birnbaum et al., 2017). Images were taken 1 h after induction of knock-sideway of parasites cultivated in the presence of rapalog compared to the control. Knock-sideway was classified in complete, partial, or absent (no) mislocalization in 30 parasites (n = 2). Nuclei were stained with DAPI. The scale bar represents 5 μm. DIC, differential interference contrast. **B** Flow cytometry growth curve over 2.5 growth cycles of the *PfRbsn5*-2xFKBP-GFP-2xFKBP^{endo} + *nmd3*NLS-FRB-mCh^{epi} cell line. Parasites cultivated in the presence of rapalog compared to the control. One representative of n = 3 independent experiments, all replicas are shown in the supplements (Appendix B). **C** Representative DIC live-cell images of parasites 0 h, 2 h, 6 h, and 8 h after induction of knock-sideway in *PfRbsn5*-2xFKBP-GFP-2xFKBP^{endo} + *nmd3*NLS-FRB-mCh^{epi} parasites.

Accumulation of vesicular structures (blue arrows) in the knock-sideway parasites (rapalog) is visible in comparison to the control (white arrows). DIC, differential interference contrast. The scale bar represents 5 μm . **D** Trophozoites of *PfRbsn5-2xFKBP-GFP-2xFKBP^{endo}+ nmd3'NLS-FRB-mCh^{epi}* synchronous parasites were cultivated in the presence (+) or absence (-) of rapalog and the number of vesicles per parasite quantified at 0 h, 2 h, 6 h, and 8 h after induction of the knock-sideway. **E** Diameter in μm of parasites analyzed in D. Data in D and E show superplots (Lord et al., 2020) from $n = 3$ independent experiments (data of the individual experiments are in blue ($n = 147$ parasites), yellow ($n = 176$ parasites), and black ($n = 144$ parasites) dots, respectively); two-tailed unpaired t-test of the means, p-values indicated; mean (red); error bars (black) show S.D.).

3.2.5 *PfRbsn5* is involved in HCCU

To more closely examine the phenotype in the parasites with inactivated Rbns5, they were analyzed by electron microscopy. This approach revealed multiple vesicular structures per parasite section that contained material with an electron density similar to that of the host cell cytosol (Figure 37A). In the control parasites, vesicular structures were observed only occasionally. Some of the vesicular structures induced upon Rbns5^{endo} inactivation contained vesicles of smaller dimensions (Figure 37A, white arrows), an observation previously made in vesicles induced upon VPS45^{endo} inactivation (Jonscher et al., 2019) and that might correspond to intraluminal bodies found in endosomes of model organisms. A similar observation of an accumulation of vesicular structures with occasional intraluminal vesicles was made in electron microscopy images of Rab5b-2xFKBP-GFP-2xFKBP^{endo}+ NLS-mislocalizer parasites upon Rab5b^{endo} inactivation (Figure 37B).

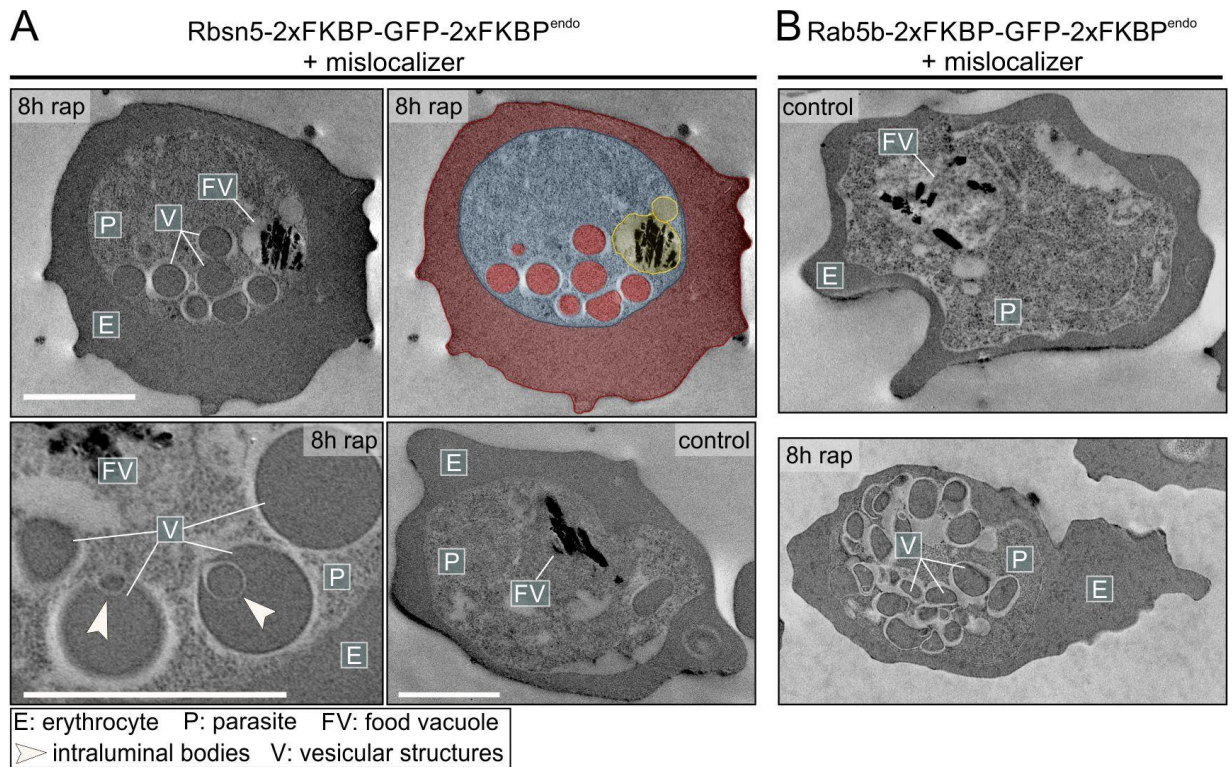


Figure 37 | Vesicular structures after Rbsn5 or Rab5b inactivation contain material with an electron density resembling that of the host cell cytosol. Electron microscopy images of **A** *Pf*Rbsn5-2xFKBP-GFP-2xFKBP^{endo} and **B** Rab5b-2xFKBP-GFP-2xFKBP^{endo} parasites co-expressing a nuclear mislocalizer from an episomal plasmid (*nmd3*^{NLS-FRB-mCh^{epi}). Synchronous parasites were cultivated for 8 h in the presence or absence of rapalog. Rbsn5^{endo}: representative of n = 42 (rapalog) and 32 (control) cells is shown. The top left image in A is also shown with false coloring. E, erythrocyte (red); P, parasite (blue); FV; food vacuole (yellow); V; vesicular structure (red). White arrows indicate vesicles within vesicles that may correspond to intraluminal bodies. The scale bars represent 2 μ m.}

To show that the observed vesicular structures indeed contain host cell cytosol, we let the parasites invade and grow in erythrocytes preloaded with fluorescent dextran prior to the inactivation of Rbsn5 (Figure 38A). The resulting vesicles in the Rbsn5 inactivated parasite were positive for the dextran and therefore filled with host cell cytosol (Figure 38B).

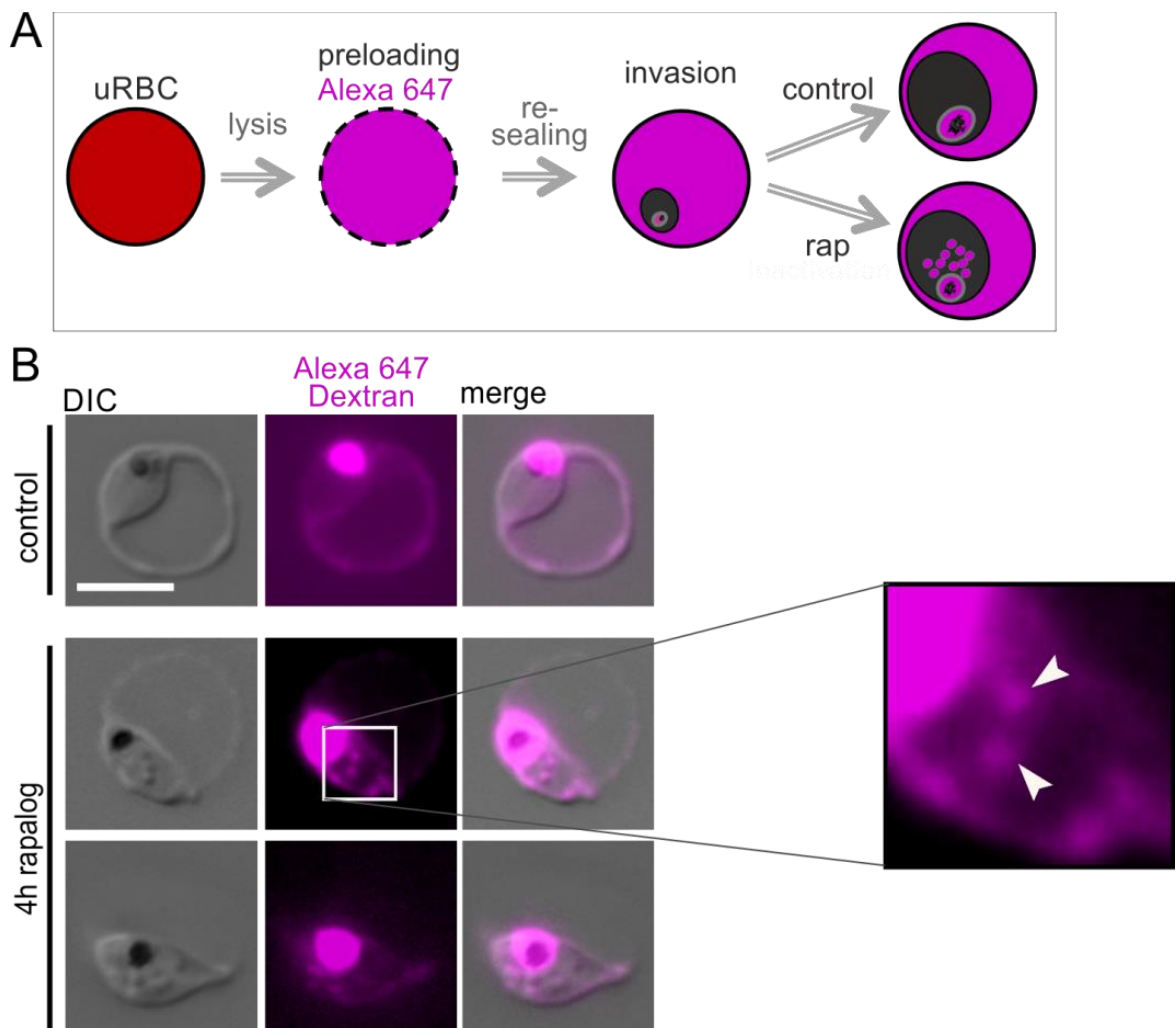


Figure 38 | Vesicular structures induced by inactivation of Rbsn5 contain host cell cytosol.

A Schematic illustration of the experimental procedure: RBCs are preloaded with fluorescent dextran (Alexa647); Parasites invade and develop within preloaded RBCs cultivated in the presence or absence of rapalog. **B** Live-cell images of preloaded iRBCs with *PfRbsn5-2xFKBP-GFP-2xFKBP^{endo} + nmd3^{NLS}-FRB-mCh* parasites cultivated 4 h in the presence or absence (control) of rapalog. DIC, differential interference contrast. White arrows indicate vesicular structures positive for Alexa647 dextran. The scale bar represents 5 μ m.

3.2.6 Accumulating vesicular structures upon Rbsn5 inactivation are positive for the early endosomal marker PI3P

Vesicles induced upon *VPS45^{endo}* inactivation were previously observed to be positive for the early endosomal marker PI3P (Jonscher, 2018). To test if vesicles induced upon *Rbsn5^{endo}* inactivation also share this endosomal characteristic, the *PfRbsn5-2xFKBP-GFP-2xFKBP^{endo}* parasite line was transfected with a newly generated plasmid

(*crt*P40-mSca_ *nmd3*'NLS-FRB-T2A-DHODH^{epi}), that expressed P40 as a marker for PI3P while simultaneously permitting mislocalization of Rbsn5^{endo} to the nucleus upon the addition of rapalog (Figure 39A). In contrast to the previous plasmid (Jonscher et al., 2019) the marker was not T2A connected to the mislocalizer, avoiding potential skipping issues that could lead to a remaining non-skipped protein. In untreated parasites, PI3P was mainly found at the DV's membrane, but sporadically one or two small circular PI3P positive structures were observed adjacent to the DV (Figure 39B, white arrows)), in agreement with previous reports (Flemming, 2015, Jonscher, 2018, Tawk et al., 2010a). Upon inactivation of Rbsn5^{endo}, increasing accumulations of PI3P near the DV were seen over time (Figure 39B, blue arrows). The location of this signal overlapped with the vesicle-like structures visible in the DIC images (Figure 39B, purple arrows) that corresponded to the vesicular structures observed after Rbns5 inactivation in Figure 36. Of the accumulating vesicles, approximately ~71% were PI3P positive 2 h upon inducing inactivation of Rbsn5, a ratio that remained stable with increasing numbers of accumulating vesicles at 3 h and 6 h post induction (Figure 39C).

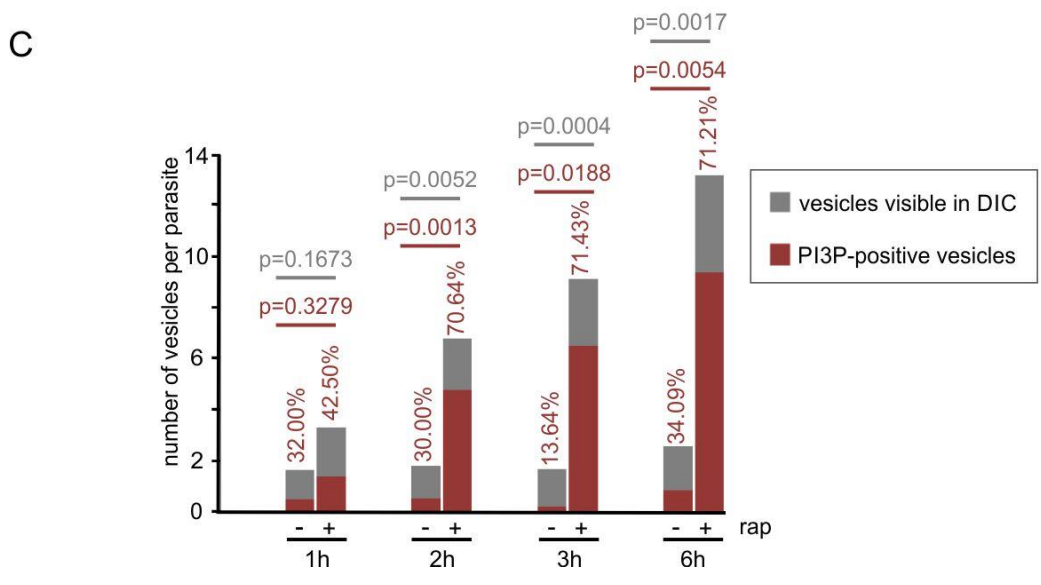
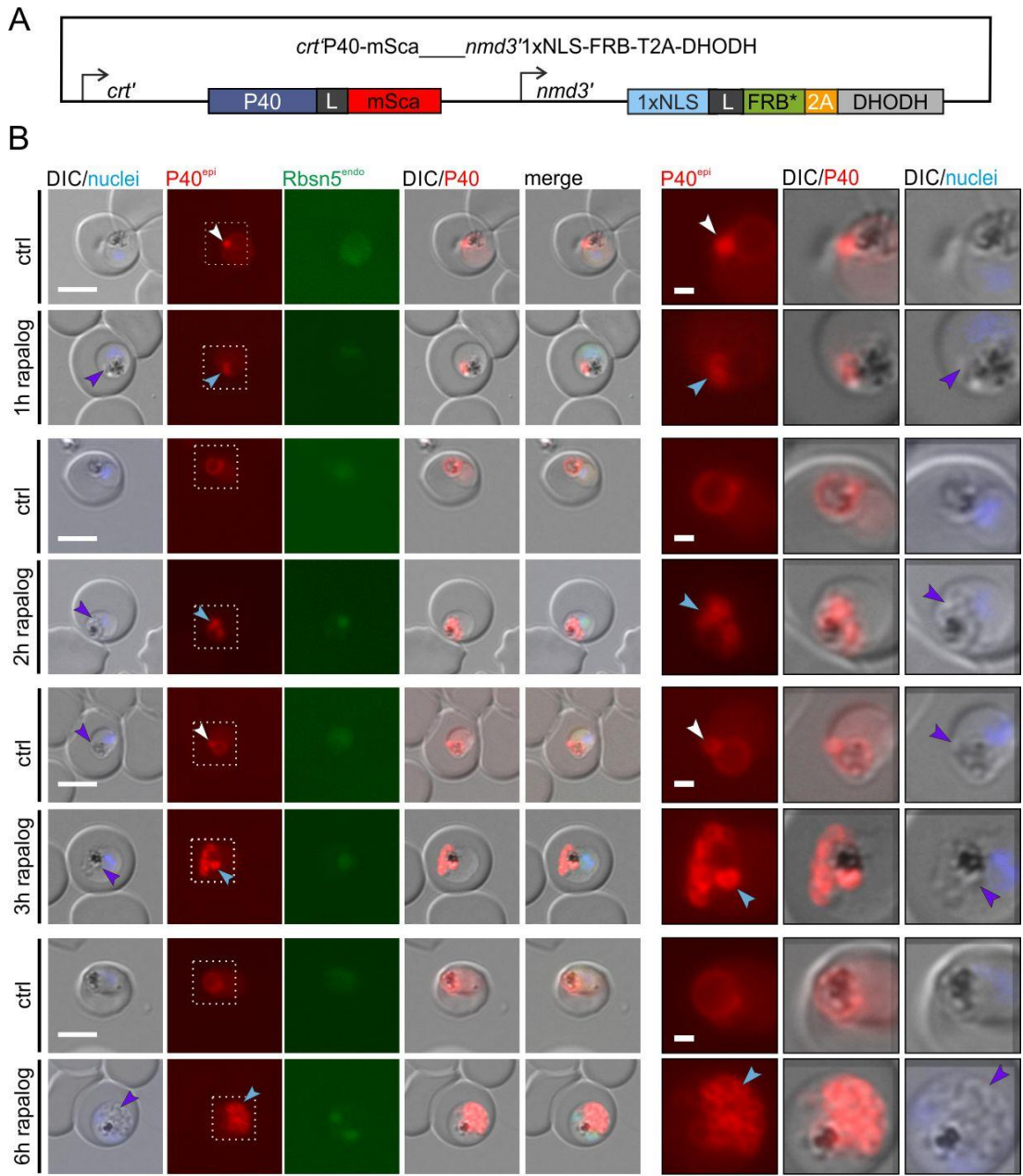


Figure 39 | Accumulating vesicular structures upon Rbsn5 inactivation are positive for the early endosomal marker PI3P. **A** Schematic of the *crt*P40_*nmd3*NLS-FRB-T2A-DHODH plasmid, that combines the PI3P marker P40 with a mislocalization cassette on the same plasmid. **B** Synchronous parasites of *Pf*Rbsn5-2xFKBP-GFP-2xFKBP^{endo} containing the *crt*P40-mSca_*nmd3*NLS-FRB-T2A-DHODH plasmid were cultivated in the presence or absence of rapalog. Live-cell images of trophozoites were taken 1 h, 2 h, 3 h, and 6 h after induction of the knock-sideway. White arrows: PI3P positive structures adjacent to the DV. Blue arrows: increasing accumulations of PI3P near the DV over time. Purple arrows: overlap of PI3P signal with the vesicle-like structures visible in the DIC images. The scale bar represents 5 μ m. Dashed boxed areas are magnified on the right. The scale bar represents in the magnification images 1 μ m. Nuclei were stained with DAPI. DIC, differential interference contrast. **C** Quantification of the vesicle number in DIC (grey) and the number of PI3P positive vesicles (red) of cells imaged in (B). Pooled from n = 2 independent experiments with 15 (1 h), 11 (2 h), 13 (3 h) and 17 (6 h) (control) and 12 (1 h), 16 (2 h), 13 (3 h) and 15 (6 h) cells (rapalog), respectively. Two-tailed unpaired t-test; p-values indicated.

3.2.7 Rbsn5 is essential for the delivery of internalized HCC to the DV

The results so far suggested that the observed vesicular structures could be HCCU intermediates. To test whether this is the case, bloated food vacuole assays were performed (Figure 40) (Jonscher et al., 2019, Birnbaum et al., 2020), as in section 3.1.1.3.4. Consequently, newly internalized hemoglobin reaching the DV accumulates due to E64 treatment, resulting in a bloated food vacuole phenotype in parasites with an intact HCCU process. This was observed in two control cell lines permitting the conditional inactivation of essential vesicle trafficking proteins that are likely not involved in endocytosis: upon Sand1 (Figure 40A) (*Sand1*-2xFKBP-GFP^{endo}+ NLS-mislocalizer) and Rab5a inactivation (Figure 40B) (*Rab5b*-2xFKBP-GFP^{endo}+ NLS-mislocalizer), DVs showed a bloated phenotype, comparable to controls without rapalog. Upon Rbsn5 inactivation, the DV did not bloat, while the diameter of the parasites showed no significant difference to the control (Figure 40C), indicating that parasites were still viable over the assay time and excluding pre-mature parasite death as a reason for the severely diminished HCCU. These findings were confirmed by electron microscopy inspection of the cells analyzed after a bloated food vacuole assay: after inactivation of Rbsn5 the parasites showed vesicular structures in the cytoplasm but small and DVs that were much less electron-dense than the host cell whereas controls showed an enlarged DV filled with electron-dense material (Figure 40D). These data indicate that Rbsn5 has an essential function in the transport of internalized host cell cytosol to the DV and additionally confirms that Rab5a is not involved in HCCU.

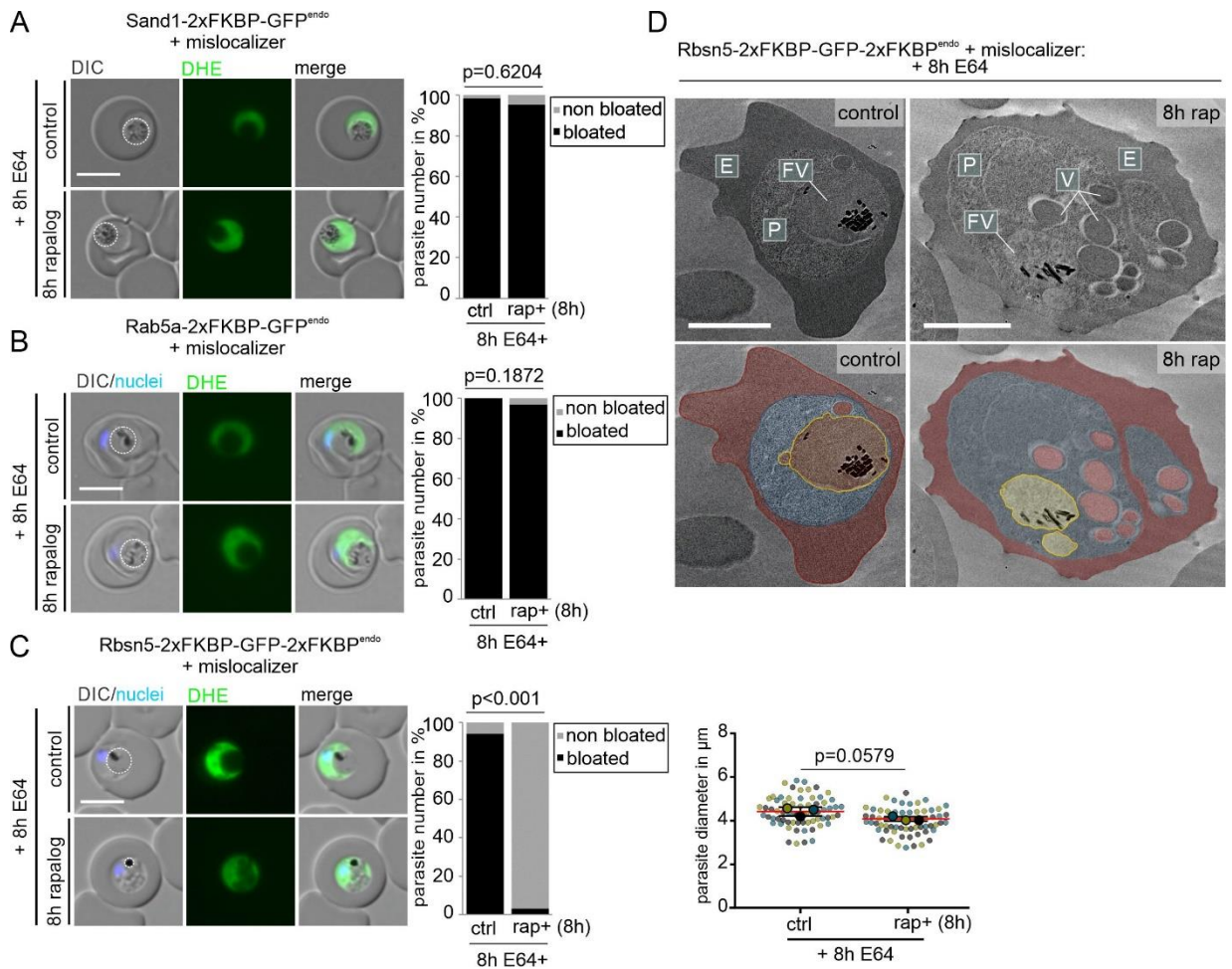


Figure 40 | Rbsn5, but not Sand1 and Rab5a are involved in the HCCU of *P. falciparum* blood stages. **A** Sand1-2xFKBP-GFP^{endo} + *nmd3*NLS-FRB-mCh (mislocalizer) synchronous parasites treated 8 h with E64 in the presence or absence (control) of rapalog (8 h). Left: Live-cell images of the parasites stained with DHE (cytosol). Right: Quantification of the number of cells with bloated FVs. Fisher's exact test. Pooled from $n = 3$ independent experiments with 22, 21 and 21 cells (control) and 29, 18 and 23 cells (rapalog), respectively. P-values indicated. **B** Rab5a-2xFKBP-GFP^{endo} + *nmd3*NLS-FRB-mCh (mislocalizer) synchronous parasites treated 8 h with E64 in the presence or absence (control) of rapalog (8 h). Quantification of the number of cells with bloated FVs. Fisher's exact test. Pooled from $n = 3$ independent experiments with 23, 22 and 33 cells (control) and 21, 26 and 13 cells (rapalog), respectively. P-values indicated. DIC, differential interference contrast. **C** *Pf*Rbsn5-2xFKBP-GFP-2xFKBP^{endo} + *nmd3*NLS-FRB-mCh (mislocalizer) synchronous parasites treated 8 h with E64 in the presence or absence (control) of rapalog (8 h). Left: Live-cell images of the parasites stained with DHE (cytosol). Mid: Quantification of the number of cells with bloated FVs. Fisher's exact test. Pooled from $n = 3$ independent experiments with 20, 26 and 22 cells (control) and 22, 20 and 20 cells (rapalog), respectively. P-values indicated. Right: Superplot showing diameter of parasites analyzed in the bloated FV assay (cells from the 3 experiments are distinguished by blue, yellow, and black dots); two-tailed unpaired t-test of the means, p-values indicated; mean (red); error bars (black) show S.D.. **D** Electron microscopy images of *Pf*Rbsn5-2xFKBP-GFP-2xFKBP^{endo} + *nmd3*NLS-FRB-mCh (mislocalizer) synchronous parasites treated 8 h with E64 in the presence or absence (control) of rapalog (8 h). The Bottom shows images from the top with false coloring. E,

erythrocyte (red); P, parasite (blue); FV; food vacuole (yellow); V; vesicular structure (red); The scale bars represent 2 μm .

3.2.8 *PfRbsn5*, *PfRab5b*, and *PfVPS45* inactivation leads to the accumulation of hemoglobin filled vesicles that possess no continuous connection to the host cell

To evaluate whether the observed vesicular structures after inactivation of VPS45, Rbsn5, and Rab5b are indeed vesicles and are not still connected to the host cell cytosol - e.g. like cytostomes -, synchronous *PfVPS45-2xFKBP-GFP^{endo}*, *PfRbsn5-2xFKBP-GFP-FKBP^{endo}*, and *PfRab5b-2xFKBP-GFP-FKBP^{endo}* parasites expressing a nuclear mislocalizer (from plasmid *nmd3*NLS-FRB-mCh^{epi}) were treated with saponin to remove the host cell cytosol content prior to carrying out an anti-hemoglobin IFA (Figure 41A). We observed an average number of 9.440 ± 0.07615 , 8.227 ± 0.5365 , and 4.482 ± 0.4717 of spherical shaped anti-hemoglobin positive individual areas after 6 h of VPS45, Rbsn5, and Rab5b inactivation, respectively (Figure 41B; white arrows; C). In contrast, the control showed, significantly less (0.6071 ± 0.1417 , 0.2551 ± 0.03573 and 0.3250 ± 0.06143) individual anti-hemoglobin positive areas (Figure 41B, C). However, the control parasites showed a notably larger hemoglobin positive area corresponding to the DV (Figure 41B; blue arrows), indicating a larger size of the DV and the presence of non-degraded hemoglobin. This independently supports the previous result of the bloated FV assays that less HCC reaches the DV upon VPS45, Rbsn5, and Rab5b inactivation. These findings demonstrate that although the structures appearing after inactivation of these proteins contain HCC, they do not possess a connection to the host cell and consequently they can be designated as vesicles. This experiment was confirmed by electron microscopy with saponin lysed parasites after Rbsn5 and Rab5b inactivation which revealed that the vesicles induced in the parasite were filled with electron-dense material while the host cell was translucent which is indicative of successful release of host cell cytosol (Figure 41D).

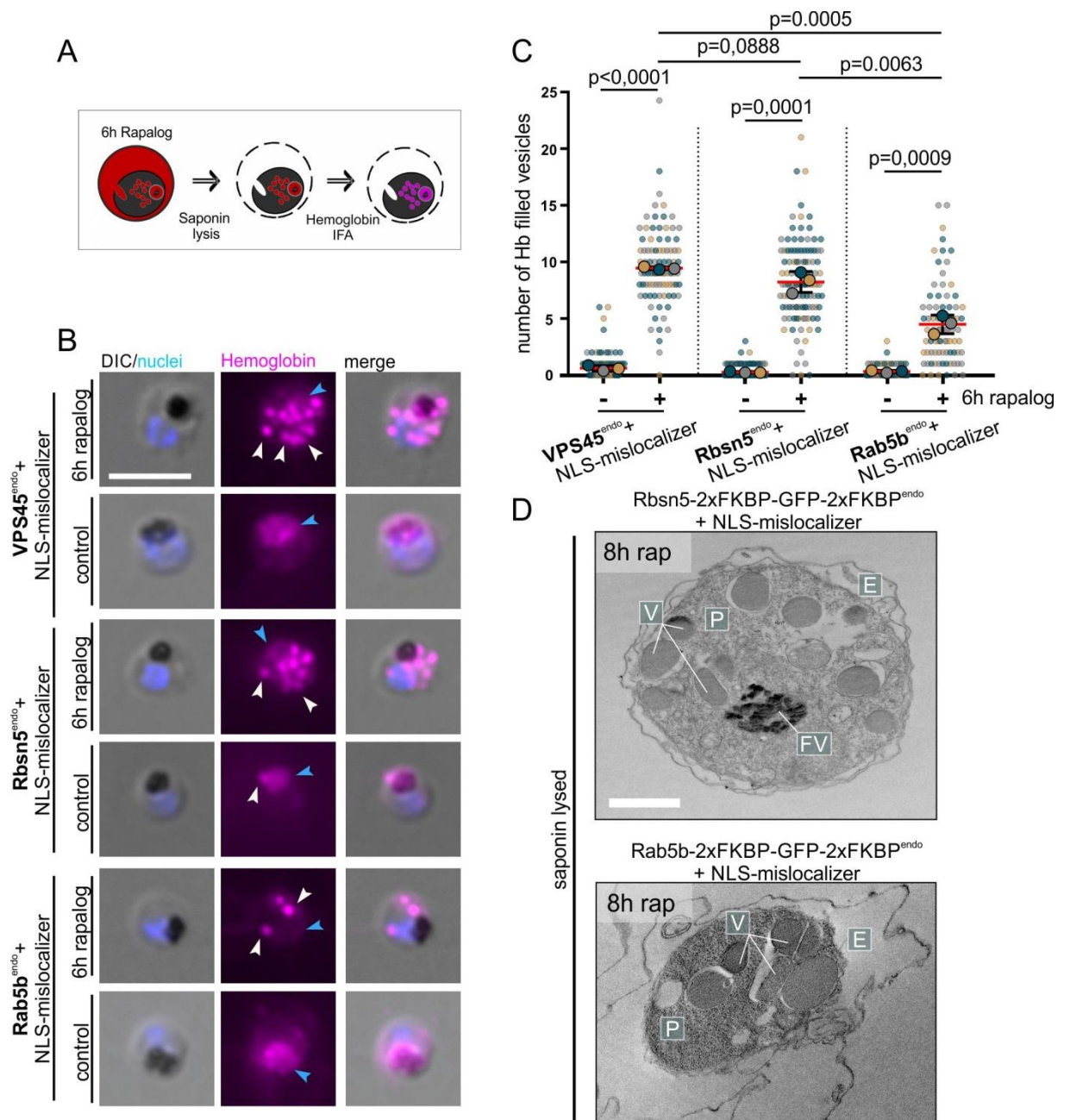


Figure 41 | Rbsn5, VPS45, and Rab5b inactivation induced vesicular structures are filled with hemoglobin and are not connected to the host cell cytosol. **A** Schematic illustration of saponin treatment and hemoglobin IFA of iRBCs 6 h after VPS45, Rbsn5, or Rab5b conditional inactivation in the corresponding knock-out cell lines. **B** Microscopy images of IFAs of formaldehyde-fixed, synchronous *PfVPS45-2xFKBP-GFP^{endo}*, *PfRbsn5-2xFKBP-GFP-FKBP^{endo}* and *PfRab5b-2xFKBP-GFP-FKBP^{endo}* parasites co-expressing a nuclear mislocalizer from an episomal plasmid (*nmd3*^{NLS-FRB-mCh^{epi}). Parasites were cultivated for 6 h in the presence or absence (control) of rapalog. White arrows indicate spherical-shaped anti-hemoglobin positive signals, blue arrows indicate DV. α -hemoglobin (from Rabbit) was used to detect hemoglobin. Nuclei were stained with DAPI. DIC, differential interference contrast. The scale bar represents 5 μ m. **C** Quantification of spherical shaped anti-hemoglobin positive signals 6 h after induction}

of the knock-sideway per parasite shown in B. Superplot from $n = 3$ independent experiments with VPS45^{endo}+ NLS-mislocalizer: 32, 31 and 39 cells (control) and 24, 29 and 34 cells (rapalog), Rbsn5^{endo}+ NLS-mislocalizer: 27, 60 and 49 cells (control) and 23, 44 and 47 cells (rapalog) and Rab5b^{endo}+ NLS-mislocalizer: 24, 24 and 20 cells (control) and 26, 32 and 21 cells (rapalog), respectively; two-tailed unpaired t-test of the means, p-values indicated; mean (red); error bars (black) show S.D. **D** Electron microscopy images of saponin treated *Pf*Rbsn5-2xFKBP-GFP-2xFKBP^{endo}+ NLS-mislocalizer (*nmd3*'NLS-FRB-mCh^{epi}) and Rab5b-2xFKBP-GFP-2xFKBP^{endo}+ NLS-mislocalizer parasites 8 h after rapalog (rap)- induced Rbsn5^{endo} or Rab5b^{endo} conditional inactivation. Representatives of Rbsn5^{endo}: $n = 12$ and Rab5b^{endo}: 50 cells are shown. E, erythrocyte; P, parasite; FV; food vacuole; V; vesicular structure. The scale bars represent 2 μ m.

3.2.9 A modification of the SLI plasmid enables endogenous tagging and inactivation of Rbsn5 by a single plasmid

Due to the restricted number of selection markers available for *P. falciparum*, the number of integrated plasmids, as well as the simultaneous episomal expression of plasmids, is limited. Previous plasmid combinations to simultaneously mislocalize a target and observe a marker contained a non-fluorescently tagged mislocalizer on the episomal plasmid using a T2A skip peptide to cope with the limited number of expression sites on the plasmid (Jonscher et al., 2019). To improve this system and increase the variation possibilities, the SLI-sandwich plasmid was modified to introduce a non-fluorescently labeled mislocalizer sequence into the genome along with selection-linked integration at the genomic target site. While the tagged GOI is expressed under its endogenous promoter, the mislocalizer is expressed under a distinct promoter (*nmd3*') together with the hDHFR selection cassette from which it is separated by a skip peptide (Figure 42A). To test this approach, Rbsn5 was used as the POI. Correct integration was confirmed by PCR on genomic DNA of the corresponding Rbsn5-2xFKBP-GFP-2xFKBP^{endo}_ndm3'NLS-FRB-T2A-hDHFR parasite line (Figure 41B). Upon addition of rapalog, Rbsn5-2xFKBP-GFP-2xFKBP^{endo} was successfully mislocalized to the nucleus (Figure 41C), vesicular structures accumulated as evident in the DIC images (Figure 41, white arrow) and monitoring after conditional inactivation over 5 days (2.5 growth cycles) showed a drastic growth defect in comparison to the control parasites (Figure 41C; D). Hence, results comparable to those using an episomally expressed mislocalizer (Figure 36; Figure 39) were obtained with this single plasmid system, validating this approach.

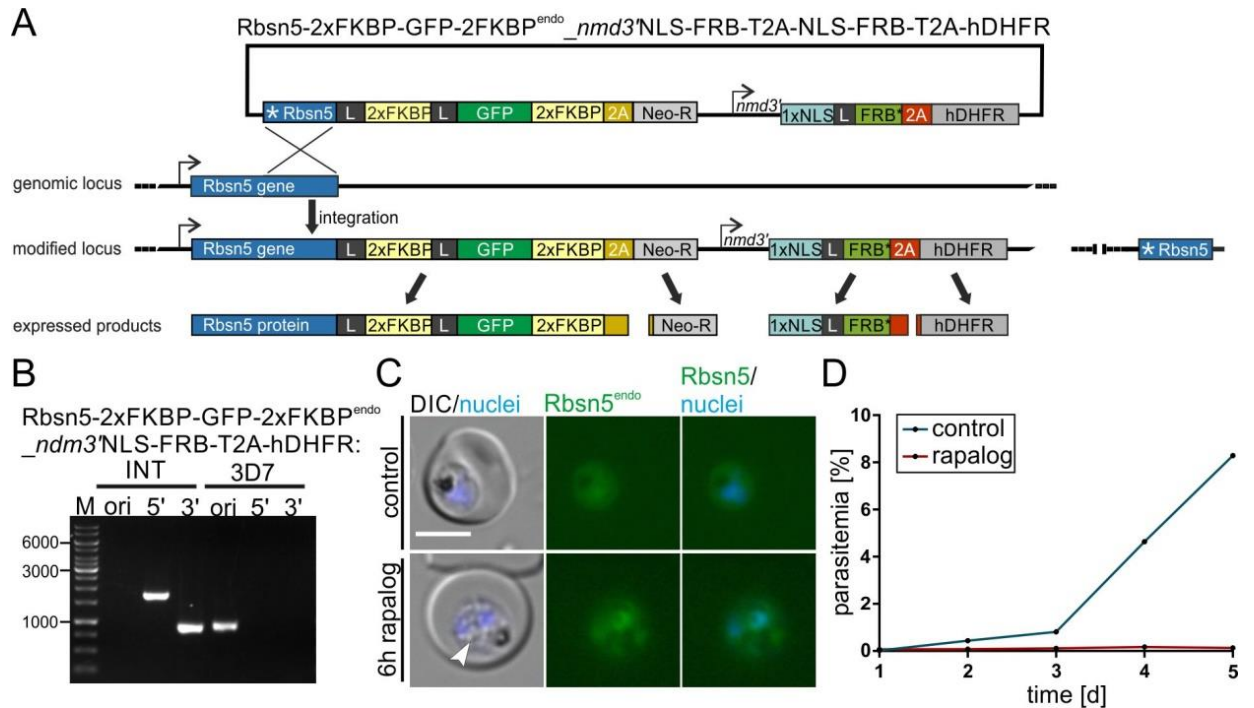


Figure 42 | Modified SLI-sandwich plasmid enables endogenous tagging and mislocalization of POI. **A** Schematic of selection linked integration strategy combined with a mislocalization cassette on the same plasmid. **B** Agarose gel showing PCR-products to assess correct integration of the SLI-plasmid into the genome of *P. falciparum* (3D7) parasites to obtain the indicated cell line. (5'INT: 1760 bp (Rbsn5int fw+ GFP85 rv); 3'INT: 890 bp (pARL55sense+Rbsn5int rv) and ori (indicating presence or absence of original unmodified locus): 935 bp (Rbsn5int fw+ Rbsn5int rv)). **C** Knock-sidaway with *Pf*Rbsn5-2xFKBP-GFP-FKBP^{endo}_nmd3'NLS-FRB-T2A-hDHFR parasites. Images were taken 6 h after induction of knock-sidaway of parasites cultivated in the presence of rapalog compared to the control. Nuclei were stained with DAPI. DIC, differential interference contrast. The scale bar represents 5 μ m. **D** Flow cytometry growth curve over 2.5 growth cycles of the *Pf*Rbsn5-2xFKBP-GFP-2xFKBP^{endo}_ndm3'NLS-FRB-T2A-hDHFR cell line. Parasites cultivated in the presence of rapalog compared to the control. One representative of $n = 3$ independent experiments, all replicas are shown in the supplements (Appendix B).

3.2.10 Inactivation of Rbsn5^{endo} affects VPS45^{epi} and Rab5b^{epi} localization

If Rbsn5 acts together in a functional complex with VPS45 and Rab5b, it is likely that inactivation by mislocalization of Rbsn5^{endo} to the nucleus exerts an effect on these proteins. The system introduced in 3.2.9 permitted the assessment of such effects. In order to do this, the Rbsn5-2xFKBP-GFP-2xFKBP^{endo}_ndm3^{NLS}-FRB-T2A-hDHFR parasite line was transfected either with the *sf3a2*∖VPS45-mCh^{epi} or *sf3a2*∖Rab5b-mCh^{epi} plasmids, respectively, and the localization of these proteins after Rbsn5^{endo} inactivation was assessed (Figure 43). Due to the mislocalization of Rbsn5^{endo} into the nucleus, VPS45^{epi} also showed an increasing nuclear localization (Figure 43A). Therefore, it can be assumed that VPS45^{epi} is indirectly pulled into the nucleus by direct or indirect interaction with Rbsn5^{endo}. Rab5b^{epi}, however, showed no nuclear localization upon Rbsn5^{endo} inactivation (Figure 43B). This does not necessarily exclude an interaction, as it can also be explained by its membrane anchoring property, which might represent a stronger association than a potential interaction with Rbsn5 that may also be transient. However, inactivation of Rbsn5^{endo} showed an effect on Rab5b^{epi} localization (Figure 43B). Accumulations of Rab5b^{epi} signal that were absent in the control were observed (Figure 43B; blue arrows) and the emerging vesicles (evident in the DIC images) also appeared to be surrounded by a faint Rab5b^{epi} signal (Figure 43B; white arrows), similar to that observed for PI3P (compare Figure 39, and (Jonscher et al., 2019)). These results suggested localization of Rab5b on the HCC-filled vesicles, further underlining the endosomal character of these vesicles and a function of Rab5b in the endosomal pathway of *P. falciparum* parasites.

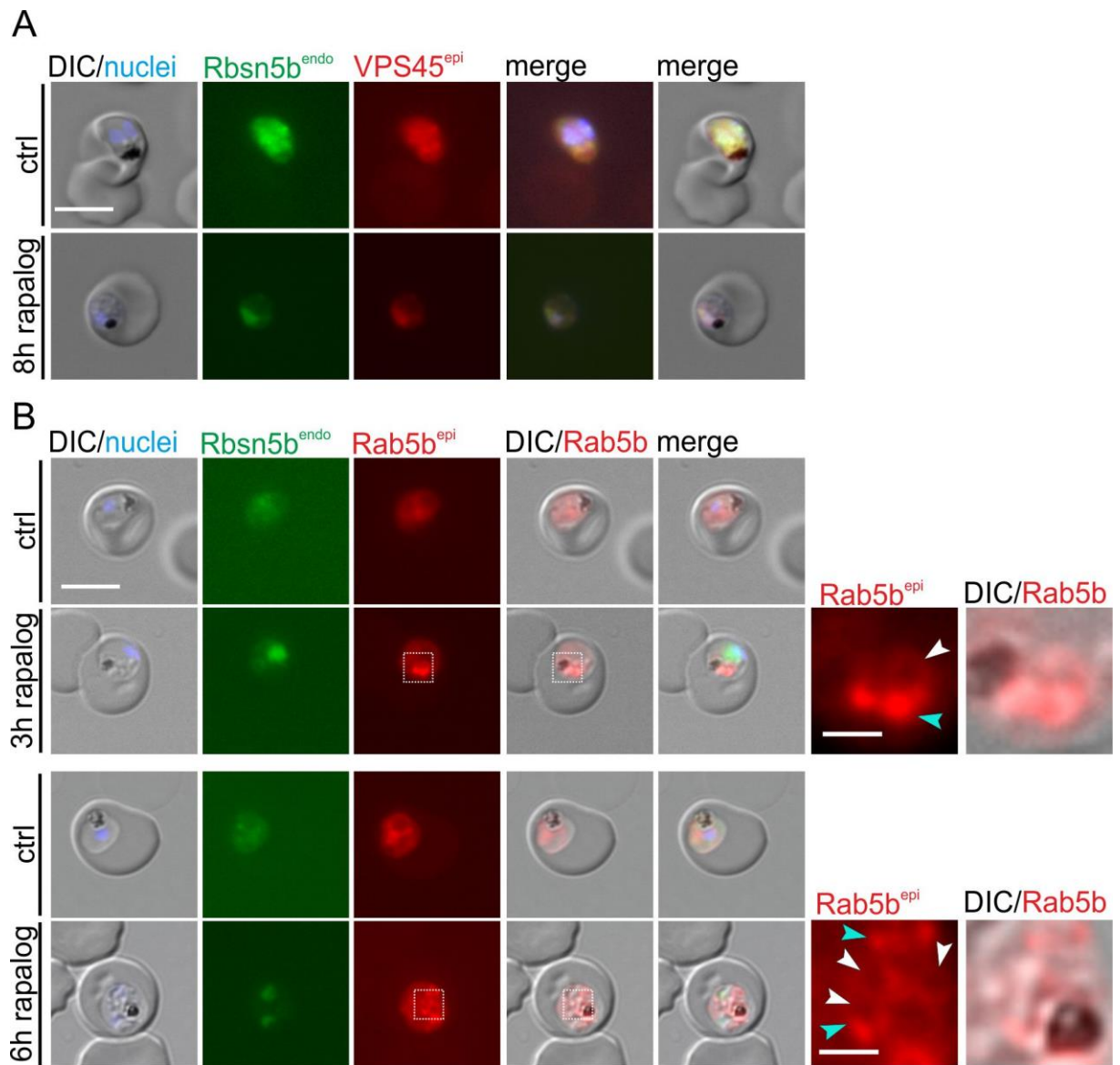


Figure 43 | Inactivation of Rbsn5^{endo} affects VPS45^{epi} and Rab5b^{epi} localization. **A** Live-cell microscopy images of Rbsn5-2xFKBP-GFP-2xFKBP^{endo}_ndm3NLS-FRB-T2A-hDHFR parasites, co-expressing VPS45 from the *sf3a2*VPS45-mCh^{epi} plasmid. Parasites were cultivated for 8 h in the presence or absence (control) of rapalog. Representative images of n = 10 (control) and n=15 (rapalog) cells. **B** Live-cell microscopy images of Rbsn5-2xFKBP-GFP-2xFKBP^{endo}_ndm3NLS-FRB-T2A-hDHFR parasites, co-expressing Rab5b from the *sf3a2*Rab5b-mCh^{epi} plasmid. Parasites were cultivated for 3 h and 6 h in the presence or absence (control) of rapalog. Dashed boxes in the images outline the areas of magnification seen on the right. White arrows indicate Rab5b^{epi} signal surrounding vesicles observed by DIC. Blue arrows indicate Rab5b accumulations. Representative images of n = 2 independent experiments with 6, 7 (3 h) and 11, 5 (6 h) (control) and 11, 9 (3 h) and 19, 11 (6 h) cells (rapalog). Nuclei were stained with DAPI. DIC, differential interference contrast. The scale bar represents 5 μ m in the left panels and 1 μ m in the magnifications on the right.

3.2.11 Rab5b and VPS45 are interaction partners of Rbsn5

To further determine if Rbsn5 interacts with VPS45 and Rab5b, co-immunoprecipitations (CoIPs) were performed (Figure 44) (CoIP experiments were kindly performed by Ulrike Fröhlke). Using anti-GFP beads, the endogenously GFP-tagged Rbsn5 was immunoprecipitated and it was determined whether Rab5b-mCh^{epi} (Figure 44A) and VPS45-mCh^{epi} (Figure 44B) were co-precipitated using the Rbsn5-2xFKBP-GFP-2xFKBP^{endo} cell lines expressing the respective protein from the episomal plasmid. Using anti-mCherry antibodies, bands corresponding to Rab5b-mCh^{epi} (Figure 44A) and VPS45-mCh^{epi} (Figure 44B) were found in the GFP bead eluates, while the control protein BIP was not enriched. These data show that Rbsn5 interacts with Rab5b and VPS45 in *P. falciparum* parasites and therefore support the hypothesis of their function in a conserved complex in *P. falciparum* parasites.

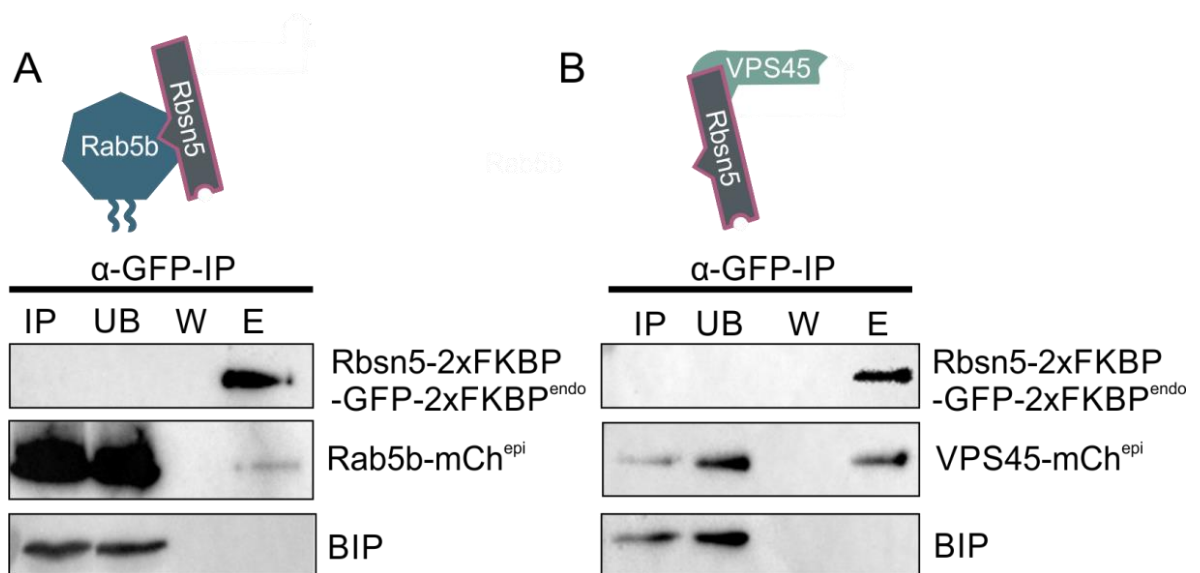


Figure 44 | Rab5b and VPS45 are interacting partners of Rbsn5. Immunoprecipitation (IP) of Rbsn5-2xFKBP-GFP-2xFKBP^{endo}_{ndm3}NLS-FRB-T2A-hDHFR parasite line episomally expressing Rab5b-mCh^{epi} (**A**) or VPS45-mCh^{epi} (**B**). IP, input extract; UB, unbound (total extract after IP); W, last wash; E, eluate. One representative of n = 3 independent experiments, all replicas, and complete blots are shown in the supplements (Appendix E).

3.2.12 Conditional double inactivation of Rbsn5 and KIC7 leads to less vesicle accumulation

The presence of vesicles resulting from the inactivation of proteins associated with EE in model organisms leads to the question of the site of their origin in the parasite cell. Previously, we found that a Kelch13-defined compartment was relevant for HCCU (Birnbaum et al., 2020). Kelch13 and its interactors (KICs), such as KIC7, alongside other proteins, are needed for an early step of endocytosis that differs in the composition of proteins and structures involved from those known from model organisms.

We previously showed that the inactivation of essential K13 compartment proteins results in a reduction of the amount of hemoglobin reaching the DV (Birnbaum et al., 2020). However, whether the vesicles accumulating after Rbsn5 inactivation that may represent EE structures are affected by this and, consequently, the Kelch13 compartment is positioned upstream of the Rbsn5 compartment in the HCCU pathway, has not formally been demonstrated. Conditional inactivation of an essential EE protein such as Rbsn5 together with an early endocytosis protein, such as KIC7, would be required to show this. If part of a serially connected pathway, abrogating endocytosis initiation using KIC7 inactivation should lead to a decreased accumulation of the vesicles induced upon Rbsn5 inactivation (Figure 45A). However, simultaneous inactivation of two proteins by mislocalization was so far restricted by the limitation of selection markers. Taking advantage of the redesigned SLI constructs permitting mislocalization directly with the integration of a single plasmid that also results in an endogenous Rbsn5-2xFKBP-GFP fusion protein (Section 3.2.9), a second target was endogenously tagged with the sequence encoding 2xFKBP-mScarlet, based on a modification of the SLI2a plasmid (Naranjo Prado, 2020, Stäcker, 2021) (Figure 45B). This enabled us for the first time to simultaneously inactivate two different proteins by conditional inactivation in one cell line (Figure 46).

Figure 45 | Conditional double inactivation strategy. **A** Schematic illustration of simultaneous double mislocalization of the early endocytosis protein KIC7 and the early endosome-associated protein Rbsn5, showing the expected reduction in vesicle accumulation compared to Rbsn5 inactivation alone. **B** Scheme of a selection linked integration strategy enabling endogenously tagging and simultaneous mislocalization of two POI's.

Using this approach first the parasites with the integrated Rbsn5-2xFKBP-GFP^{endo}_ndm3NLS-FRB-T2A-hDHFR plasmid were used to either integrate the KIC7-2xFKBP-mSca^{endo} or the Sand1-2xFKBP-mSca^{endo} (control) plasmids, respectively. The correct integration of these plasmids was confirmed by PCR on the genomic DNA (Figure 46A) and the maintenance of the integration of the original Rbsn5-2xFKBP-GFP^{endo}_ndm3NLS-FRB-T2A-hDHFR plasmid was also confirmed in these parasites. The corresponding parasite lines showed nuclear localization of both of the endogenously tagged proteins upon induction of knock-sideway with rapalog which resulted in an accumulation of vesicles in the parasite (Figure 46B). Simultaneous inactivation of KIC7^{endo} and Rbsn5^{endo} led to an accumulation of 3.793 ± 0.2643 vesicles per parasite. This was significantly less than in the control cell lines in which Rbsn5^{endo} alongside Sand1^{endo}, an essential protein not involved in endocytosis (Birnbbaum et al., 2017), were inactivated and resulted in 6.694 ± 0.3331 vesicles per parasite. If Rbsn5^{endo} was inactivated alone this resulted in 8.810 ± 1.075 vesicles per parasite (Figure 46C). The diameter of the parasites in all of these experiments did not differ significantly, indicating that these effects were not due to differences in viability of the parasites over the course of the assay (Figure 46D).

These results indicate that KIC7 is necessary for processes upstream of those resulting in the vesicles accumulating upon Rbsn5 inactivation. Therefore, these experiments provide evidence that the content of these vesicles originates from the Kelch13-defined compartment that feeds into a more conserved endosomal delivery process to the DV.

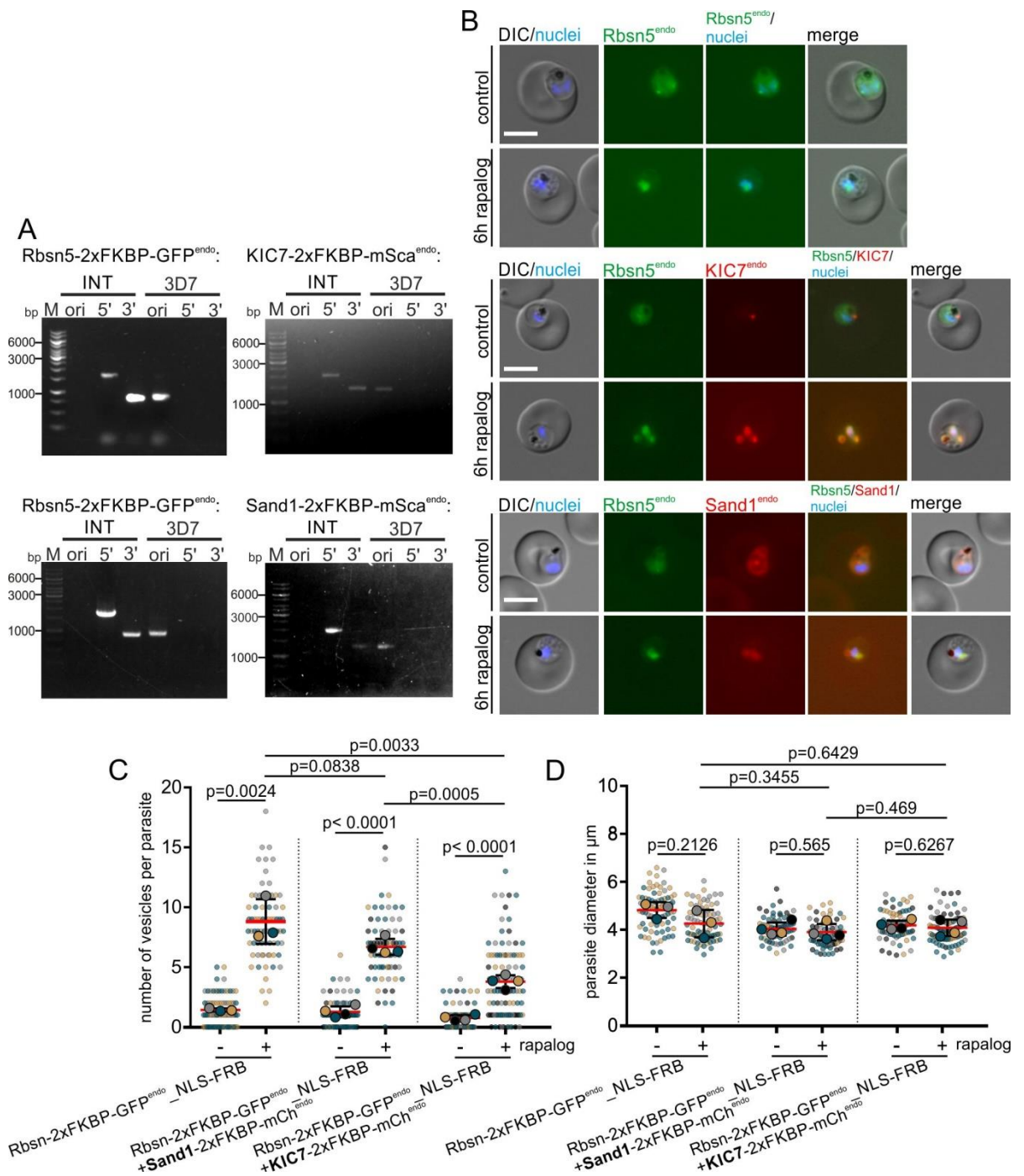


Figure 46 | Conditional double inactivation of Rbsn5 and KIC7 leads to less vesicle accumulation.

A Agarose gel showing PCR-products to assess correct double integration of the SLI-plasmids into the genome of *P. falciparum* (3D7) parasites to obtain the indicated cell lines. Rbsn5-2xFKBP-GFP^{endo}_ndm3NLS-FRB-T2A-hDHFR (5'INT: 1760 bp (Rbsn5int fw+ GFP85 rv); 3'INT: 890 bp (pARL55sense+Rbsn5int rv) and ori (indicating presence or absence of original unmodified locus): 935 bp (Rbsn5int fw+ Rbsn5int rv)). KIC7-2xFKBP-mCh^{endo}: (5'INT: 2129 bp (KIC7int fw+ mSca38rv); 3'INT: 1517 bp (pARL55sense+KIC7int rv) and ori (indicating presence or absence of original unmodified locus): 1479

bp (KIC7int fw+ KIC7int rv). Sand1-2xFKBP-mSca^{endo}: (5'INT: 2004 bp (Sand1int fw+ mSca38rv); 3'INT: 1310 bp (pARL55sense+ Sand1int rv) and ori (indicating presence or absence of original unmodified locus): 1290 bp (Sand1int fw+ Sand1int rv)). **B** Knock-sideway of *PfRbsn5-2xFKBP-GFP^{endo}_nmd3NLS-FRB-T2A-hDHFR* (control); *PfRbsn5-2xFKBP-GFP^{endo}_nmd3NLS-FRB-T2A-hDHFR+ KIC7-2xFKBP-mSca^{endo}* and *PfRbsn5-2xFKBP-GFP^{endo}_nmd3NLS-FRB-T2A-hDHFR+ Sand1-2xFKBP-mSca^{endo}* parasites. Representative images were taken 6 h after induction of knock-sideway of parasites cultivated in the presence of rapalog compared to the control. Nuclei were stained with DAPI. DIC, differential interference contrast. The scale bar represents 5 μ m. **C** Trophozoites of highly synchronous parasites (30-33 h.p.i.) were cultivated in the presence (+) or absence (-) of rapalog and the number of vesicles per parasite quantified 6 h after induction of the knock-sideway. **D** Diameter in μ m of parasites analyzed in C. Data in (C) and (D) are shown in superplots and were pooled from n = 3 (*PfRbsn5-2xFKBP-GFP^{endo}_nmd3NLS-FRB-T2A-hDHFR*) or n = 4 (*PfRbsn5-2xFKBP-GFP^{endo}_nmd3NLS-FRB-T2A-hDHFR+ KIC7-2xFKBP-mSca^{endo}* and *PfRbsn5-2xFKBP-GFP^{endo}_nmd3NLS-FRB-T2A-hDHFR+ Sand1-2xFKBP-mSca^{endo}*) independent experiments with *PfRbsn5-2xFKBP-GFP^{endo}_nmd3NLS-FRB-T2A-hDHFR*: 21 (grey dots), 31 (yellow dots) and 30 (blue dots) cells (control) and 23, 30 and 24 cells (rapalog), *PfRbsn5-2xFKBP-GFP^{endo}_nmd3NLS-FRB-T2A-hDHFR+ KIC7-2xFKBP-mCh^{endo}*: 15 (black dots), 19 (grey dots), 18 (yellow dots) and 19 (blue dots) cells (control) and 21, 20, 22 and 35 cells (rapalog), and *PfRbsn5-2xFKBP-GFP^{endo}_nmd3NLS-FRB-T2A-hDHFR+ Sand1-2xFKBP-mSca^{endo}*: 14 (black dots), 16 (grey dots), 13 (yellow dots) and 9 (blue dots) cells (control) and 20, 12, 9 and 26 cells (rapalog), respectively; two-tailed unpaired t-test of the means, p-values indicated; mean (red); error bars (black) show S.D.).

3.2.13 Localization of the early endocytosis associated proteins K13 and AP-2 σ is not affected upon Rbsn5 inactivation

To investigate the effect of Rbsn5 inactivation on early endocytosis-associated proteins, the *Rbsn5-2xFKBP-GFP-2xFKBP^{endo}_nmd3NLS-FRB-T2A-hDHFR* parasite line was co-transfected with the *nmd3K13-mCh^{epi}* plasmid (Figure 47A) as was the *Rbsn5-2xFKBP-GFP-2xFKBP^{endo}* parasite line with the newly generated *sf3a2'AP-2 σ -mCh^{epi}_nmd3NLS-FRB-T2A-DHODH^{epi}* plasmid (Figure 47B). In the control cells, K13^{epi} (Birnbbaum et al., 2020) and AP-2 σ ^{epi} (Section 3.1.1.3.2) showed their characteristic localization with foci found close to the DV at the PPM (Figure 47A, B). Upon inactivation of Rbsn5^{endo} there was no obvious change in this localization. Neither K13^{epi} nor AP-2 σ ^{epi} appeared to co-localize with the accumulating vesicles and their function in the HCCU is therefore probably limited to the early phase of endocytosis. In 4 out of 7 (K13) and 4 of a total of 6 (AP-2 σ) cells one hour after Rbsn5 inactivation, it was observed that the vesicles induced after Rbsn5-inactivation seemed to initiate at the site of the early endocytosis associated proteins (Figure 47A, B; white arrows), consistent with the results from the previous section 3.2.12. However, whether these structures

are indeed corresponding to the Rbsn5-inactivation induced vesicles or not needs to be verified by time-lapse microscopy.

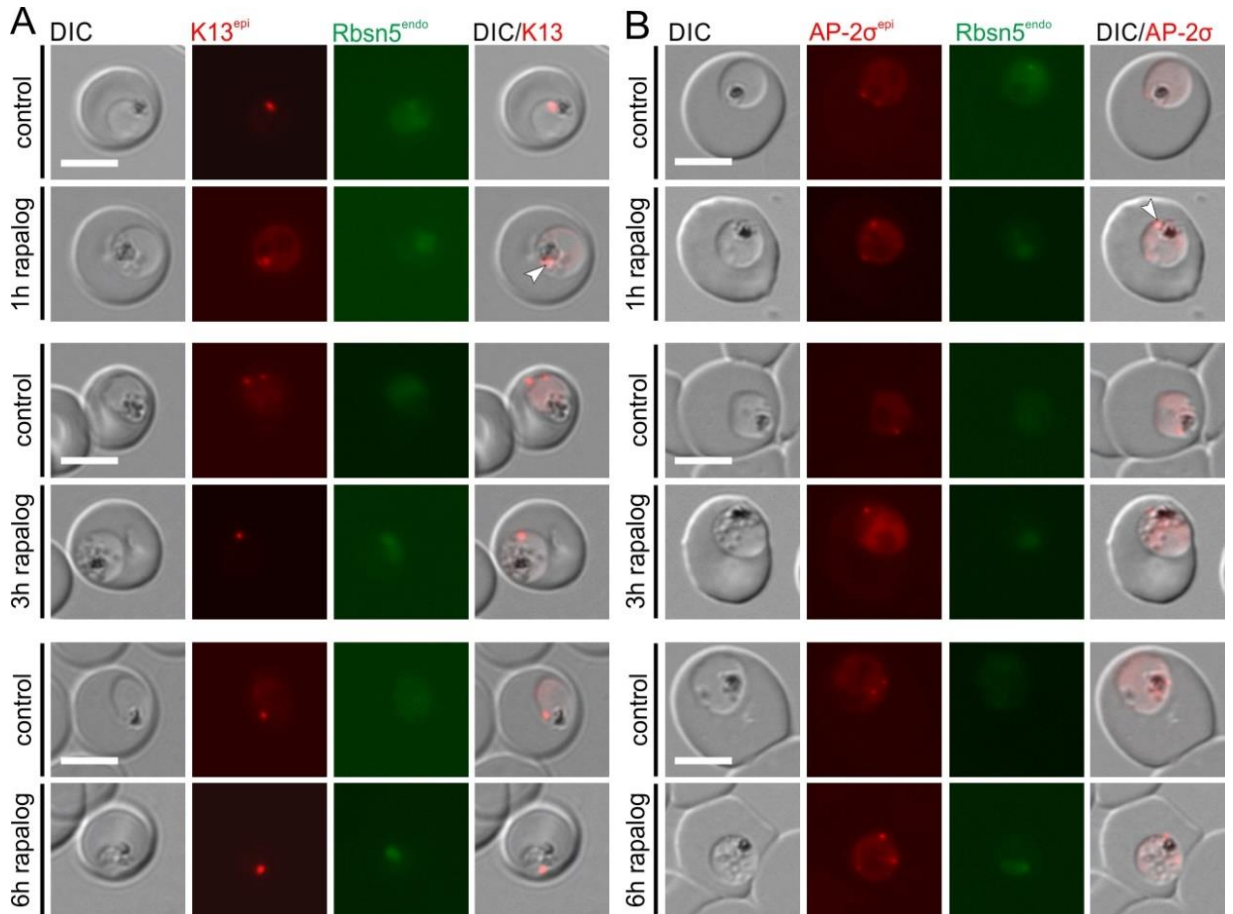


Figure 47 | Inactivation of Rbsn5 does not affect the localization of early endocytosis proteins K13 and AP-2σ. **A** Rbsn5-2xFKBP-GFP-2xFKBP^{endo}_{ndm3}NLS-FRB-T2A-hDHFR parasite line co-transfected with *ndm3*K13-mCh^{epi} plasmid. Live-cell images were taken 1 h, 3 h, and 6 h after induction of the knock-sideway with 7 (1 h), 8 (3 h) and 7 (6 h) (control), and 7 (1 h), 12 (3 h) and 14 (6 h) cells (rapalog), respectively. **B** Rbsn-2xFKBP-GFP-2xFKBP^{endo} parasite line with the *sf3a2*'AP-2σ-mCh_{ndm3}'NLS-FRB-T2A-DHODH^{epi} plasmid. Parasites were cultivated in the presence or absence (control) of rapalog. Live-cell images were taken 1 h, 3 h, and 6 h after induction of the knock-sideway with 6 (1 h), 14 (3 h) and 22 (6 h) (control) and 6 (1 h), 26 (3 h) and 18 (6 h) cells (rapalog), respectively. DIC, differential interference contrast. The scale bar represents 5 μm.

3.2.14 Plasmepsin II accumulates within or at forming vesicles induced upon Rbsn5 inactivation

Plasmepsin II (PMII) is an aspartic protease known to be involved in the proteolytic hemoglobin degradation in the DV (Section 1.8.6). PMII is expressed as an unglycosylated type II integral membrane proenzyme (proPMII) containing a transmembrane domain followed by a cleavage site in its N-terminal region (Figure 48A) and is assumed to be proteolytically processed to mature and soluble PMII in the acidic environment of the DV (Francis et al., 1997a, Klemba et al., 2004a). A previous publication (Klemba et al., 2004a) proposed that proPMII is trafficked through the secretory pathway to the cytostome from where it is delivered alongside hemoglobin to the DV. To investigate PMII localization and trafficking, a *sf3a2*PMII-mCh_ *nmd3*NLS-FRB-T2A-DHODH^{epi} plasmid was generated and co-transfected into a variety of cell lines of endogenously tagged endocytosis proteins associated with endosomal steps (Figure 48 and Figure 49) or the initiation of HCCU (Figure 50) that also permitted the conditional inactivation of these proteins and monitoring the fate of PMII. Expression of PMII^{epi} from the *sf3a2*PMII-mCh_ *nmd3*NLS-FRB-T2A-DHODH^{epi} plasmid in the VPS45-2xFKBP-GFP^{endo} parasite line showed localization of PMII^{epi} within the DV (Figure 48B; light blue arrow) and very faintly at the ER (Figure 48B; dark blue arrow), as previously reported (Klemba et al., 2004a). VPS45^{endo} foci were observed in proximity to the PMII signal that likely corresponds to the ER (Figure 48B; white arrow), coherent with its observed localization near the Golgi apparatus (Jonscher et al., 2019).

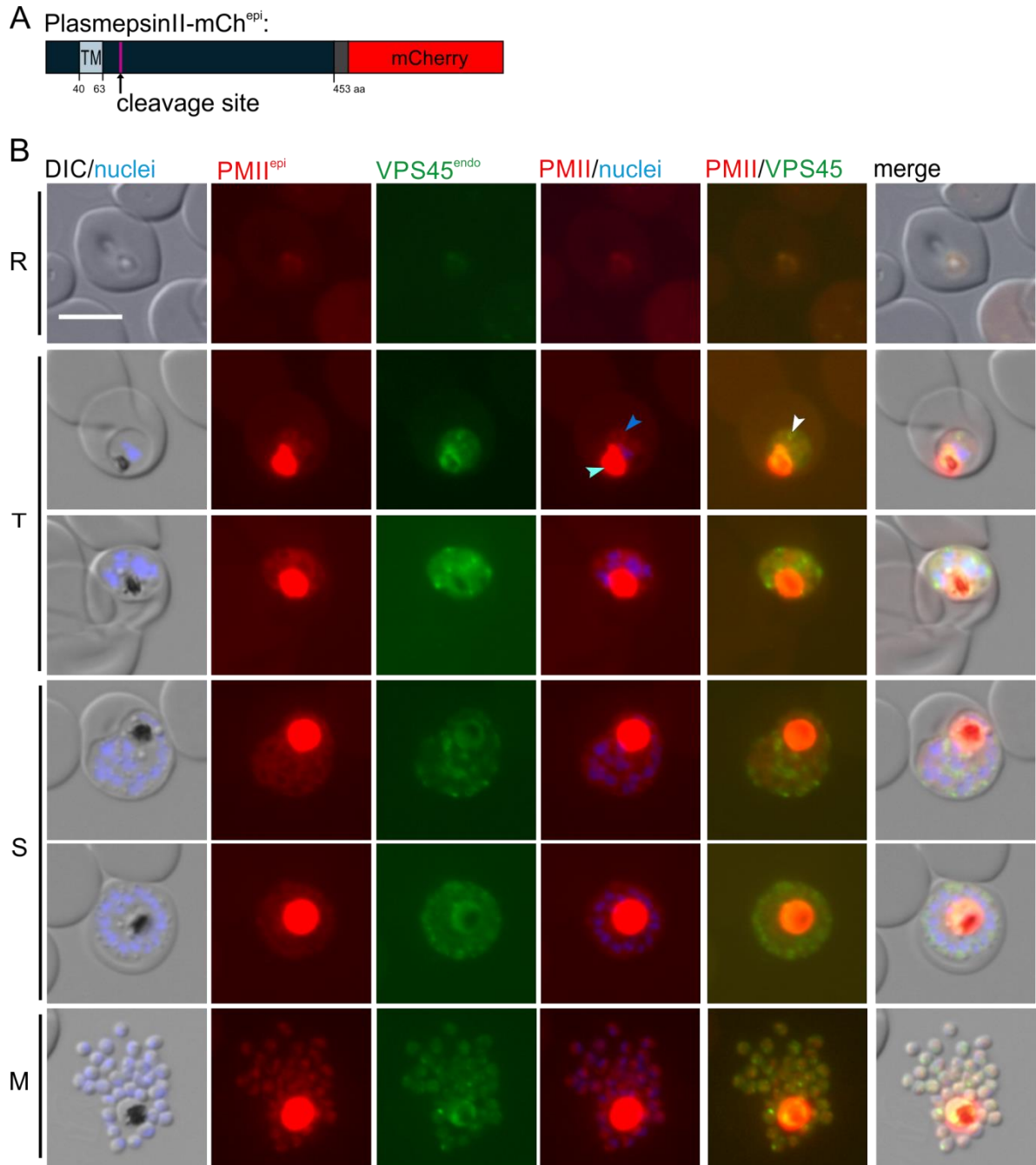


Figure 48 | PMII localizes to the DV and the ER. **A** Schematic illustration of the proPMII protein (453 aa) tagged at the C-terminus with mCherry. ProPMII contains a transmembrane domain (TM) and a cleavage site in its N-terminal region. **B** Live-cell microscopy images of the indicated stages of VPS45-2xFKBP-GFP^{endo} parasites containing the *sf3a2*PMII-mCh_{*nmd3*}NLS-FRB^{epi} plasmid. The light blue arrow indicates the localization of PMII^{epi} within the DV. The dark blue arrow indicates the localization of PMII^{epi} to the ER. The white arrow indicates localization of VPS45^{endo} foci at the PMII^{epi} positive ER. R, ring; T, trophozoite; S, schizont and M, merozoite stages. The scale bar represents 5 μ m. Nuclei were stained with DAPI. PMII, Plasmeprin II; DIC, differential interference contrast.

Inactivation of the early endosome associated proteins VPS45^{endo} (Figure 49A) and Rbsn5^{endo} (Figure 49B) (Rbsn5-2xFKBP-GFP-2xFKBP^{endo} parasite line) in synchronous trophozoite stages led to an accumulation of PMIIepi signal in the same region the induced accumulating vesicles were visible in the DIC images (Figure 49A, B), suggesting a localization in or at these endosome-like structures. Inactivation of Rbsn5^{endo} led to a shift in the PMepi fluorescence ratio. The DV fluorescence fraction relative to the total fluorescence of the parasites was reduced by about ~23 % compared to the control and therefore shifted in favor of the fluorescence outside of the DV in the parasite cell (Figure 49C); while the overall fluorescence per parasite area in μm^2 was unaffected (Figure 49D). In addition, the area of the DV relative to the total area of the parasite was ~14.5 % smaller in Rbsn5 inactivated parasites compared to the control (Figure 49E), while the total area of the parasites did not significantly differ (Figure 49F). The smaller DVs, likely resulted from reduced amounts of HCC reaching the DV, due to an impaired HCCU in support of the data obtained with the bloated FV assays (Figure 40C). The reduced size and PMIIepi fluorescence of the DV together with an increase of fluorescence outside of the DV in the parasite cell as well as the PMIIepi signal accumulations found at the location of the vesicles occurring upon Rbsn5^{endo} inactivation indicate and involvement of endosomal steps of HCCU in the transport of PMII to the DV.

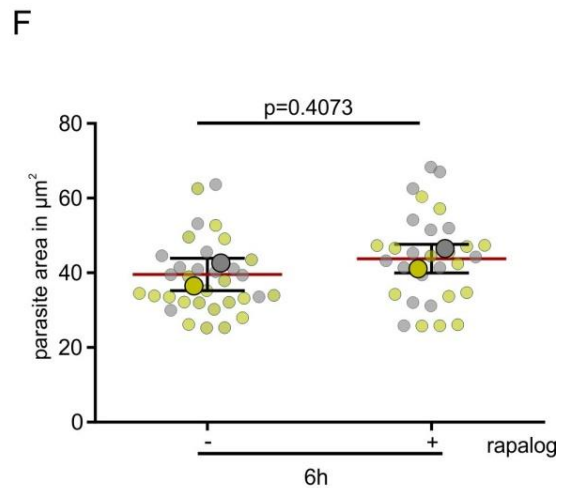
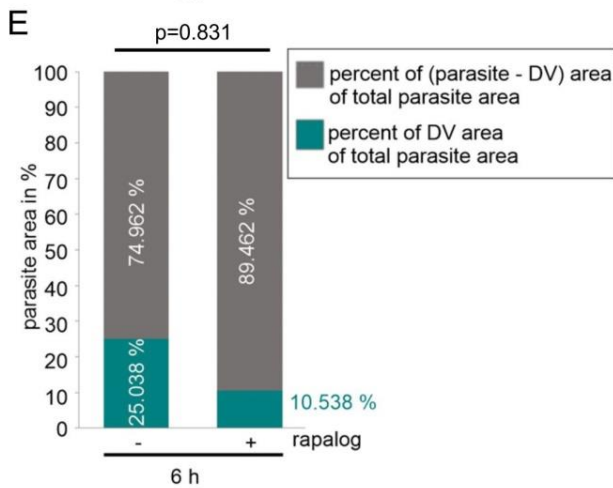
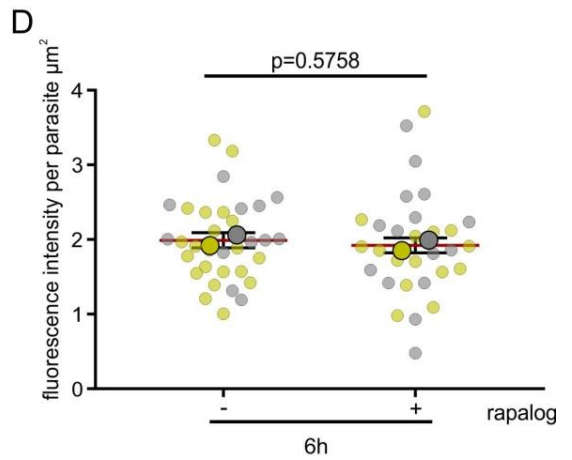
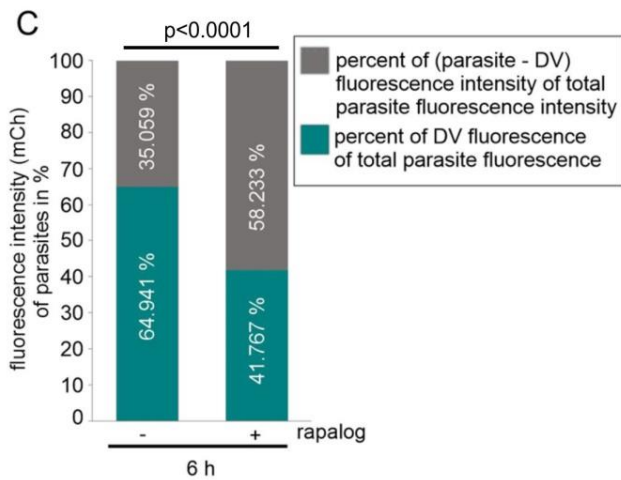
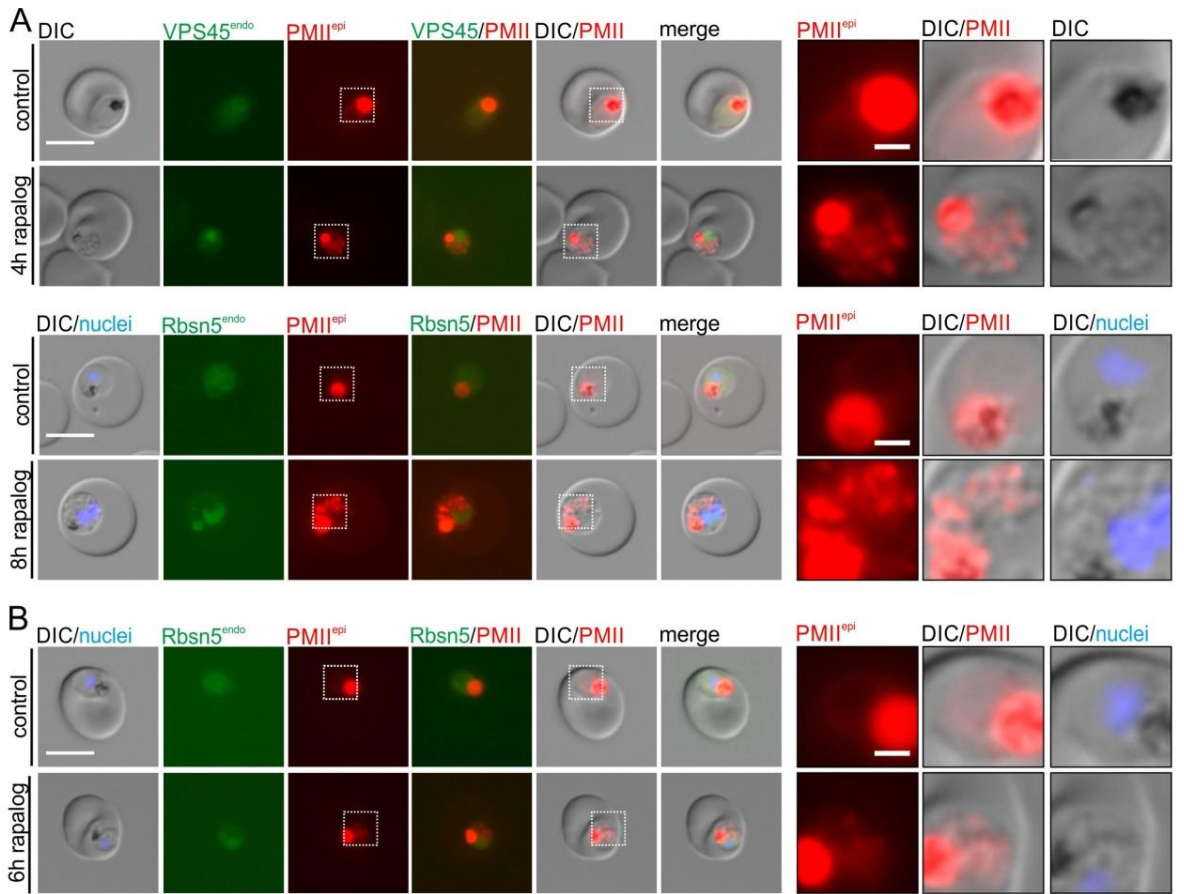


Figure 49 | PMII is enriched upon conditional inactivation of VPS45 and Rbsn5 in the region of accumulating vesicles. **A** Live-cell images of VPS45-2xFKBP-GFP^{endo} parasites and **B** Rbsn5-2xFKBP-GFP-2xFKBP^{endo} parasites episomally co-expressing PMII^{epi} and a nuclear mislocalizer from the *sf3a2*PMII-mCh_ *nmd3*NLS-FRB^{epi} plasmid. Parasites were cultivated in the presence or absence (control) of rapalog. Live-cell images were taken 4 h, 8 h in (A), and 6 h in (B) after induction of the knock-sideway. The scale bar represents 5 μm . Dashed boxed areas are magnified on the right. The scale bar in the magnified images represents 1 μm . Nuclei were stained with DAPI. PMII, Plasmepsin II; DIC, differential interference contrast. **C** Fluorescence intensity in % of total fluorescence intensity (mCh) of synchronous Rbsn5-2xFKBP-GFP-2xFKBP^{endo} trophozoites co-expressing PMII^{epi} and a nuclear mislocalizer (see B) cultivated in the presence (+) or absence (-) of rapalog quantified 6 h after induction of the knock-sideway. Blue: percent of DV fluorescence of total parasite fluorescence. Grey: percent of the fluorescence integrated intensity of the parasite without the DV versus total parasite fluorescence integrated intensity. **D** Superplot of integrated fluorescence density per μm^2 of parasites analyzed in (C). **E** Area percentages of total parasite area of trophozoites analyzed in (C). Blue: percentage of DV area of total parasite area. Grey: percent of (parasite - DV) area of total parasite area. **F** Superplot of parasite areas in μm^2 of parasites analyzed in (C). Data of the individual experiments are in yellow (n = 21 and 14 cells (control)) and grey (n = 15 and 16 cells (rapalog)), dots, respectively); two-tailed unpaired t-test of the means, p-values indicated; mean (red); error bars (black) show S.D.).

3.2.15 Evidence for the transport route of PMII to the DV

Expression of mCherry tagged PMII from the *sf3a2*PMII-mCh_ *nmd3*NLS-FRB-T2A-DHODH^{epi} plasmid in the AP-2 σ -2xFKBP-GFP^{endo} parasite line showed no overlapping signal of AP-2 σ ^{epi} and PMII^{epi} (Figure 50A). Furthermore, localization of PMII^{epi} to the PPM was not observed, indicating that transport to cytosomal structures might not occur or that the amount of PMII in the PPM did not exceed the detection limit. Conditional inactivation of AP-2 σ ^{endo} by its typical partial mislocalization to the nucleus (described in Section 3.1.1.3.3) also showed no evidence for visible accumulation of PMII^{epi} at the plasma membrane (Figure 50B) or the site of the remaining AP-2 σ foci (Figure 50B; white arrow). Suggesting either that PMII^{epi} is never transported to the plasma membrane or cytosome, or that the reduced endocytosis did not sufficiently reduce PMII internalization, or that the transport is regulated by a negative feedback loop responding to an impaired endocytosis. However, since the attempts of conditional inactivation of AP-2 σ showed only a slow effect on HCCU (3.1.1.3.4), these experiments should be repeated with an early endocytosis protein with more rapid inactivation kinetics, such as KIC7, to clarify this tentative conclusion.

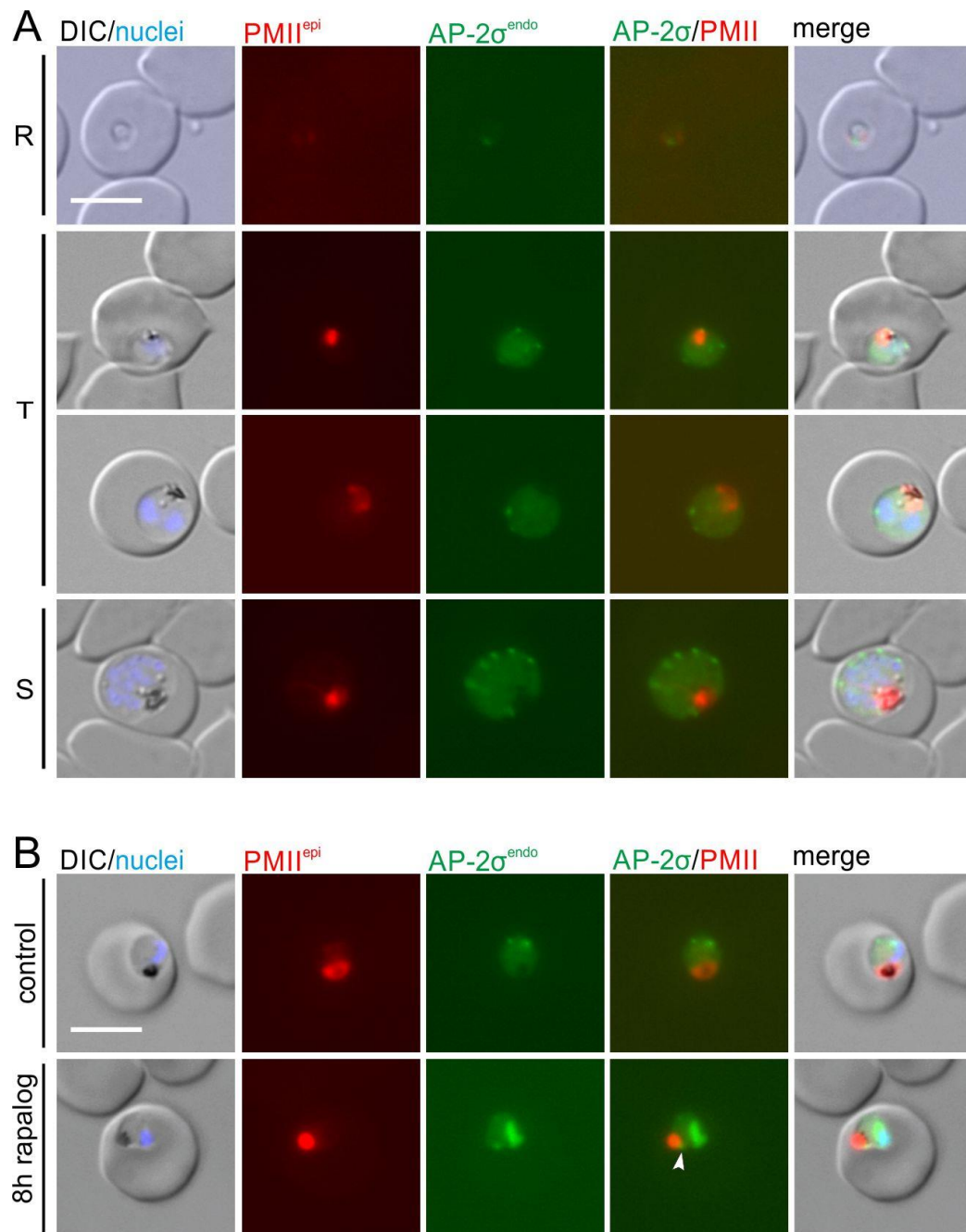


Figure 50 | Plasmepsin II does not co-localize with the early endocytosis-associated protein AP-2σ. **A** Live-cell microscopy images of the indicated stages of AP-2σ-2xFKBP-GFP^{endo} parasites containing the *sf3a2*PMII-mCh_{*nmd3*}NLS-FRB^{epi} plasmid. R, ring; T, trophozoite, and S, schizont-stages. **B** Live-cell images of AP-2σ-2xFKBP-GFP^{endo} parasites co-expressing *sf3a2*PMII-mCh_{*nmd3*}NLS-FRB^{epi}. Parasites were cultivated for 8 h in the presence or absence (control) of rapalog. Representative images from n = 2 independent experiments with 23 and 29 cells (rapalog) and 29 and 17 cells (control). The scale bar represents 5 μm. Nuclei were stained with DAPI. PMII, Plasmepsin II; DIC, differential interference contrast.

3.2.16 Biotinylation of proteins within vesicles induced upon Rbsn5 inactivation

To generate the possibility to investigate which proteins are present besides the ingested hemoglobin inside the accumulating vesicles upon Rbsn5 inactivation, two constructs expressing two different promiscuous biotin ligases (BirA* and miniTurbo) were cloned. Both plasmids contain the GBP¹⁻¹⁰⁸ sequence as an export signal (Schulze et al., 2015). This way, the expressed fusion proteins are exported to the host cell where they can be assumed to be partly re-internalized via the HCCU process and transported along the endosomal pathway to its terminal destination in the parasite's DV (Figure 51A; control). We hypothesized that the biotin ligase-containing GBP¹⁻¹⁰⁸ fusion proteins would consequently be present in the accumulating vesicles upon inactivation of Rbsn5 and therefore might allow biotinylation and identification of vesicle internal proteins by comparing it to the control using quantitative mass spectrometry (Figure 51A; rapalog). First, the Rbsn5-2xFKBP-GFP^{endo}_ndm3^{NLS}-FRB-T2A-hDHFR cell line was transfected with the *crt*GBP¹⁻¹⁰⁸-BirA*-mSca plasmid (Figure 51B). The control parasite showed the GBP¹⁻¹⁰⁸-BirA*-mSca fusion protein distributed in the host cell (Figure 51B; purple arrows) and the parasite DV (Figure 51B; white arrows). Upon inactivation of Rbsn5 for 8 h, vesicles positive for GBP¹⁻¹⁰⁸-BirA*-mSca had accumulated in the parasite (Figure 51B; blue arrows). Biotinylation experiments in which the parasite grew for 8 h in the presence of biotin (50 μM) either with or without rapalog (Figure 51C; i.) showed biotinylation of GBP¹⁻¹⁰⁸-BirA*-mSca itself with a band at ~79 kDa (Figure 51C, i., blue arrow) and other proteins in both, the control and the rapalog-treated sample. Apart from hemoglobin and GBP¹⁻¹⁰⁸-BirA*-mSca itself, there were comparably few clearly detectable bands and the streptavidin labeling appeared modest. Indirect detection of hemoglobin monomers, present only in the rapalog-treated parasite sample, demonstrated the presence of the accumulating hemoglobin-filled vesicles (Figure 51C, i., red arrow). To exclude that the detected biotinylation is not exclusively caused by the biotinylation of proteins in the host cell and thus the result of biotinylation of proteins of the PVM, Maurer's clefts or erythrocyte membrane, iRBC treated with rapalog for 8 h were lysed with saponin to remove the HCC and then incubated with biotin for 8 h (Figure 51C; ii.). This showed a similar banding pattern as in the experiment without saponin (Figure 51C; i.), demonstrating that biotinylation does not take place exclusively by BirA in the host cell. BirA* possesses slow kinetics and biotin is intended to be added for 18-24 h for efficient biotinylation (Roux et al., 2012). However, the time reduction to 8 h in this cell line is necessary because prolonged inactivation of Rbsn5

induced by rapalog addition would result in parasite death. Furthermore, as the accumulating of vesicles requires several hours, sufficient material for biotinylation would likely only be present towards the end of the assay time, resulting in an even lower yield of biotinylated proteins in the intended compartment.

To circumvent these problems, the miniTurbo biotin ligase was used, which allows biotin labeling within minutes (Branon et al., 2018). For this purpose, the Rbsn5-2xFKBP-GFP^{endo} cell line was transfected with the *crt*'GBP¹⁻¹⁰⁸-mSca-miniTurbo_*ndm3*NLS-FRB-T2A-DHODH^{epi} plasmid. The resulting parasites showed analogous fluorescence signals to the Rbsn5-2xFKBP-GFP^{endo}_ndm3NLS-FRB-T2A-hDHFR+ *crt*'GBP¹⁻¹⁰⁸-BirA*-mSca cell line (Appendix D). Induced inactivation by rapalog followed by biotin addition for 30 min (prior saponin lysis: (Figure 51D; i.) or after saponin lysis: (Figure 51D; ii.)) showed significant biotinylation in both, the rapalog treated parasites as well as in the control parasites, although the intensities and number of clearly distinguishable bands were still somewhat modest. Taken together, these results indicate that the chosen approach indeed can biotinylate the content of the endosomal vesicles accumulating after Rbsn5 inactivation but only a full mass spectrometry analysis can reveal if the approach indeed reveals endosomal proteins of the parasite.

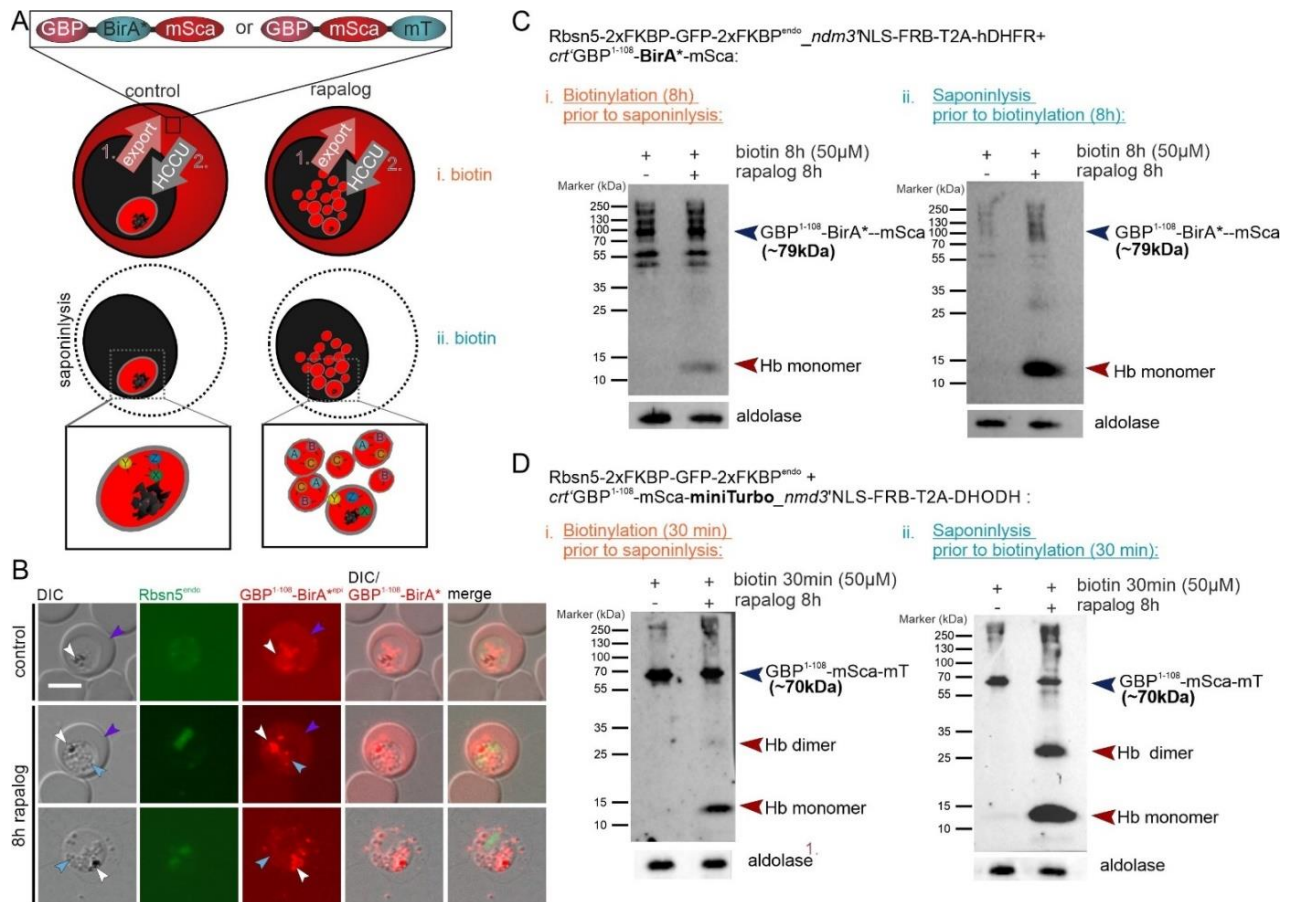


Figure 51 | Biotinylation of proteins within vesicles induced upon Rbsn5 inactivation. **A** Schematic illustration of the experimental procedure: Parasites exporting and subsequently taking up the biotinylerizer GBP¹⁻¹⁰⁸-BirA*-mSca or GBP¹⁻¹⁰⁸-mT are cultivated in the presence (for inactivation of Rbsn5) or absence (control) of rapalog. Inactivation of Rbsn5 leads to the accumulation of vesicles positive for the biotinylerizer. Biotin addition leads to biotinylation of proteins in close proximity to the biotinylerizer. Biotin was added either to intact parasites (i. biotin) or saponin-lysed parasites (ii. biotin). **B** Live-cell microscopy images of Rbsn5-2xFKBP-GFP^{endo}_ndm3NLS-FRB-T2A-hDHFR parasites, co-expressing GBP¹⁻¹⁰⁸-BirA*-mSca. Parasites were cultivated for 8 h in the presence or absence (control) of rapalog. Purple arrows: GBP¹⁻¹⁰⁸-BirA*-mSca fusion protein distributed in the HCC. White arrows: GBP¹⁻¹⁰⁸-BirA*-mSca fusion protein located in the DV. Blue arrows: GBP¹⁻¹⁰⁸-BirA*-mSca fusion protein located in accumulating vesicles upon Rbsn5 inactivation. The scale bar represents 5 μ m. DIC, differential interference contrast. **C** Western blots of biotinylation experiment of Rbsn5-2xFKBP-GFP^{endo}+ GBP¹⁻¹⁰⁸-BirA*-mSca cultivated 8 h in the presence (+) or absence (-) (control) of rapalog. Parasites were treated for 8 h with 50 μ M biotin either prior to saponin lysis (i.) or after saponin lysis (ii.). Western blots were probed with Streptavidin-HRP to detect biotinylated proteins. **D** Western blots of biotinylation experiment of Rbsn5-2xFKBP-GFP^{endo}_ndm3NLS-FRB-T2A-hDHFR+ GBP¹⁻¹⁰⁸-BirA*-mSca cultivated for 8 h in the presence (+) or absence (-) (control) of rapalog. Parasites were treated for 30 min with 50 μ M biotin either prior to saponin lysis (i.) or after saponin lysis (ii.). Western blots were probed with Streptavidin-HRP to detect biotinylated proteins. Blue arrows, biotinylerizer; red arrows, Hb (hemoglobin) monomer or Hb dimer. α - aldolase served as a loading control.

3.2.17 Conditional inactivation of VPS45 in schizonts affects IMC biogenesis and indicates the presence of HCCU in the late stages of *P. falciparum*.

Parts of the endosomal system in Apicomplexa are known to be repurposed for the formation of the secretory organelles required for host cell invasion (Breinich et al., 2009, Krai et al., 2014, Kremer et al., 2013, Tomavo et al., 2013a). Therefore, we investigated the role of the early endosomal protein VPS45 in schizonts of *P. falciparum* parasites (results published in (Bisio et al., 2020a)).

Since conditional inactivation of VPS45^{endo} (cell line: VPS45-2xFKBP-GFP+ NLS-FRB-mCh) (Jonscher et al., 2019) in early trophozoites results in parasites filled with vesicle and prevents the progressing of the parasites to the schizonts stage (Appendix F), VPS45^{endo} was specifically inactivated in highly synchronized schizonts and the effects on their development were examined (Figure 52A). Induction of VPS45^{endo} knock-sideway (using rapalog) in 36- to 42 h.p.i schizonts severely impaired schizogony (Figure 52A; B) and led to an arrest of the parasites in the schizont stage with the consequence of failed egress, invasion, and ring-formation (Figure 52C).

These parasites showed a defect in IMC formation (Figure 52D) and failed to invaginate the PPM, a central process for the formation of the daughter merozoites (Figure 52E). The formation of rhoptries and micronemes appeared to be unaffected by VPS45 inactivation in late stages (Appendix F).

Ultrastructural analysis by electron microscopy (performed by Bohumil Maco, (University of Geneva) showed that upon VPS45^{endo} inactivation, the parasites possessed a partially formed IMC but failed to engulf cytoplasmic content to form merozoites (Figure 52F;+Rapalog [36 to 42 h.p.i.]). This cytokinesis phenotype is different from the vesicle accumulation phenotype observed upon VPS45^{endo} inactivation early in the cycle (Figure 52F;+Rapalog [0 to 6 h.p.i.]). However, not all parasites showed a cytokinesis defect, and some merozoites were formed (Figure 52G). These merozoites were significantly smaller in comparison to the wild-type merozoites (Figure 52H), resembling defects typical for proteins needed for correct IMC formation. Additionally, it was observed that the residual body of the schizonts was increased in size upon conditional VPS45^{endo} inactivation (Figure 52G). The presence of accumulated host cell cytosol-

filled endocytic vesicles detected in these schizonts indicates that HCCU is still active in a very late stage of development.

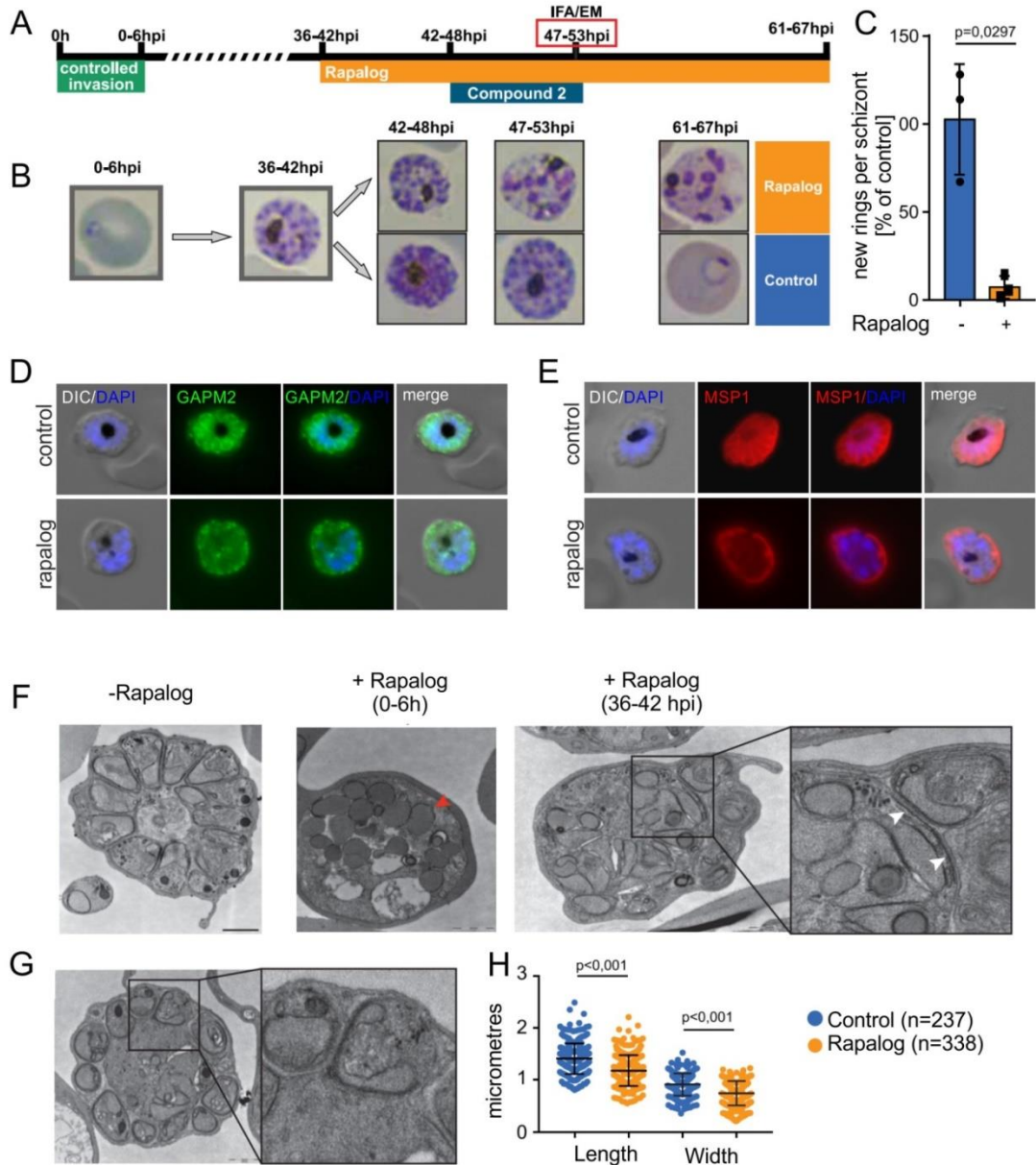


Figure 52 | VPS45 plays a role in IMC biogenesis. **A** Schematic illustration of the experimental procedure to conditionally inactivate VPS45^{endo} in schizonts using an established knock-sideway line (Jonscher et al 2019) and controlled invasion to obtain parasites of the indicated stage window. **B** Giemsa smears show that parasites with inactivated VPS45^{endo} (rapalog) at 36 to 42 h.p.i. are arrested at the schizont stage. **C** Quantification of newly formed rings per schizont after compound 2 removal. Parasites ± rapalog (25 hours). Bars show the SD for three independent experiments. **D** IFA of VPS45^{endo} KS parasites ± rapalog (11 hours) demonstrates that IMC biogenesis is impaired in VPS45^{endo} inactivated parasites. GAPM2, parasite IMC; DAPI, nuclei. The scale bar represents 5 μm. **E** IFA of VPS45^{endo} KS parasites ± rapalog (11 hours). PPM of schizont fails to engulf cytoplasmic content and form merozoites when VPS45^{endo} is

inactivated. MSP1, PPM; DAPI, nuclei. The scale bar represents 5 μm . **F** Electron micrographs of \pm rapalog-treated VPS45^{endo} knock-sideway parasites (47 to 53 h.p.i.). Early ring stage treatment (0 to 6 h.p.i.) with rapalog leads to the arrest of the parasites in the trophozoite stage. Later treatment at the early schizont stage (36 to 42 h.p.i.) leads to a partial IMC formation. IMC biogenesis initiates but fails to elongate (right inset). White arrowheads show IMC. Red arrowhead shows endocytic vesicles. The scale bars represent 1 μm . **G** Schizonts possess an enlarged residual body in the presence of rapalog and smaller merozoites (right inset). The scale bar represents 1 μm . **H** Quantification of the size (length and width) of merozoites formed in the presence or absence of rapalog. Bars show SD. P-value is indicated. Published in (Bisio et al., 2020a))

3.3 Late endosome associated structures and proteins in HCCU

3.3.1 Rab7 of *P. falciparum* shares high similarity to its orthologue in *H. sapiens*.

In model organisms, Rab7 is located and functions in the endosomal pathway at a late endosomal structure (Rink et al., 2005, Kuchitsu and Fukuda, 2018, Fujiwara et al., 2016) and in malaria parasites has been found near the DV although its role in the parasite is so far unclear (Siddiqui et al., 2020, Krai et al., 2014). It is therefore, possible that the *P. falciparum* orthologue of Rab7 (*PfRab7*; PF3D7_0903200) may have a localization and function in the HCCU of parasite blood stages (Figure 53A). *PfRab7* is a protein of 206 amino acids that contains a small GTP-binding domain and a C-terminal lipid modification motif (CC), as a site for prenylation. Its domain architecture and protein length show a high resemblance to human Rab7a and an alignment identified 80% similarity to *HsRab7a* across its entire sequence (Figure 53B; C), which might indicate a conserved function of Rab7 in the malaria parasite.

3.3.2 Subcellular localization of Rab7 in blood stages of *P. falciparum*

To investigate the localization and function, Rab7 was endogenously tagged at the *Rab7* gene locus using the SLI-system (Birnbaum et al., 2017). The resultant fusion protein was tagged at the N-terminus with 2xFKBP-GFP-2xFKBP (Figure 54A). Correct integration was confirmed by PCR of genomic DNA of the corresponding N-2xFKBP-GFP-2xFKBP-Rab7^{endo}(loxP) parasite line (Figure 54D) and the Rab7 fusion protein of the expected size (~105kDa) was detected on an anti-GFP-probed western blot (Figure 54E). The cell line (N-2xFKBP-GFP-2xFKBP-Rab7^{endo}) showed endogenous Rab7 expression through the entire blood cycle (Figure 54B), with a diffuse cytoplasmic signal in ring stages. In trophozoite stages, Rab7 was detected in circles that were adjacent to the DV (Figure 54B; C), overall resembling the pattern observed previously in a non-SLI generated endogenous GFP-Rab7 parasite line (Flemming, 2015). The circular label surrounded structures, visible in the DIC images (Figure 54C; white dashed lines), and frequently contained an area with higher fluorescent intensity (Figure 54C; white arrows). While in young trophozoites, one circular structure was observed, in older trophozoites, the number increased to two or three foci per DV. However, in schizont-stages only one or none of these structures adjacent to the DV were visible. In addition to the circular structures at the DV, small Rab7 foci were observed in the parasite cell, which increased in number with the age of the parasite in the blood cycle and might represent circular structures with smaller diameters (Figure 54C; blue arrow). In schizonts, Rab7 was visible in many foci that may again represent small circles.

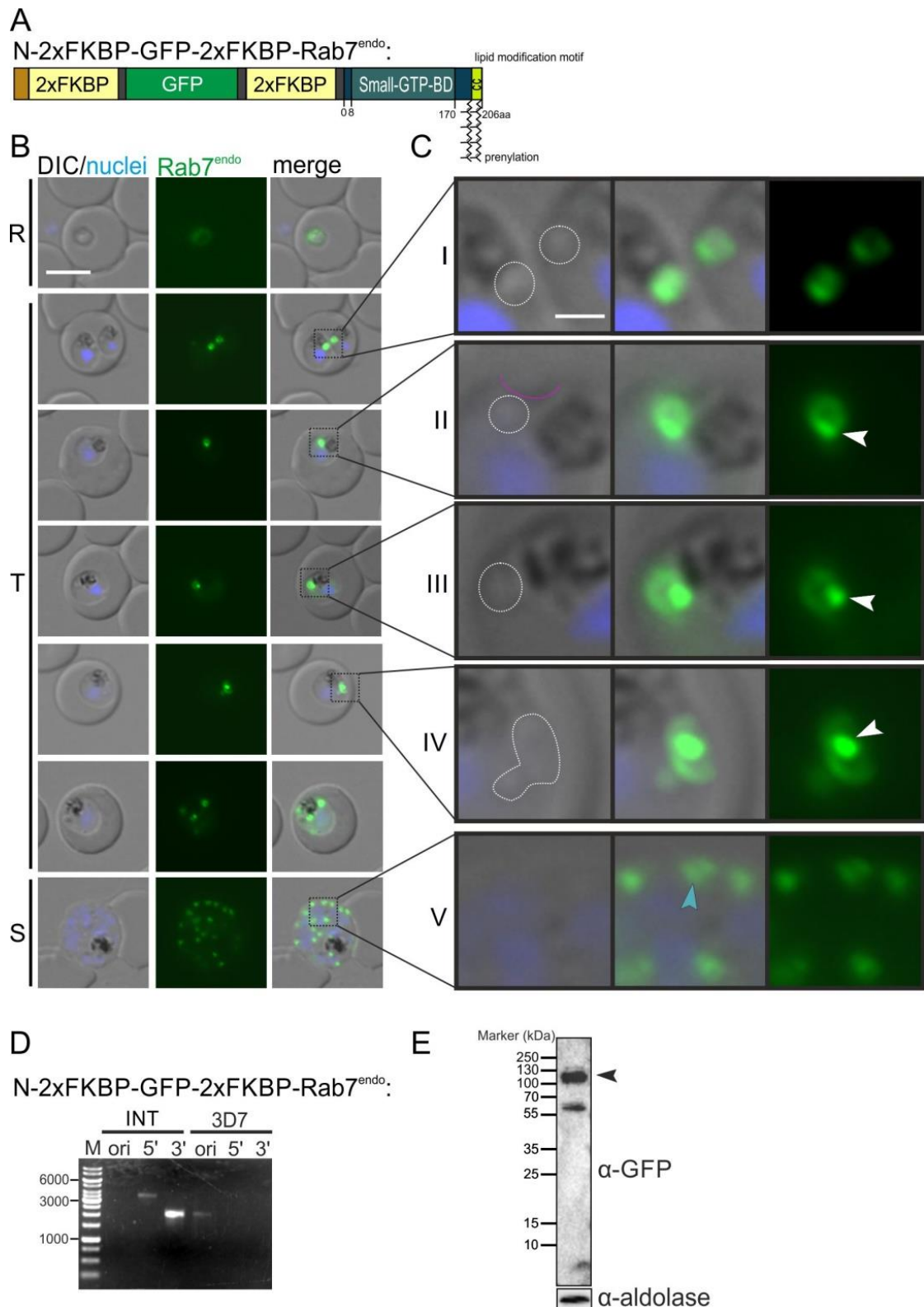


Figure 54 | Analysis and subcellular localization of N-2xFKBP-GFP-2xFKBP-Rab7^{endo}. **A** Schematic illustration of the Rab7 protein N-terminally tagged with 2xFKBP-GFP-2xFKBP. **B** Live-cell microscopy images of the indicated stages of N-2xFKBP-GFP-2xFKBP-Rab7^{endo} parasites. Dashed boxes in the merged images outline the areas of magnification seen in **C**. R; ring, T; trophozoite, and S; schizont stages. Nuclei were stained with DAPI. The scale bar represents 5 μ m. DIC, differential interference contrast.

C Magnifications of boxed areas (I-V) seen in B show circular Rab7 signals localizing around structures visible in the DIC images (indicated by dashed white lines) close to the DV. White arrows indicate foci of brighter fluorescence intensity within the circular Rab7 signals. The blue arrow indicates a smaller circular Rab7 signal in schizont stages. The scale bar represents 1 μ m. **D** Agarose gel showing PCR-products to assess correct integration of the SLI-plasmid into the genome of *P. falciparum* (3D7) to obtain the indicated cell line (5' integration junction: 5'INT: 3532 bp (Rab7int fw+ GFP85 rv); 3' integration junction: 3'INT: 2059 bp (pARLsense55+ Rab7int rv) and ori (indicating presence or absence of original unmodified locus): 2099 bp (Rab7int fw+ Rab7int rv)). **E** Western blot analysis of protein extracts obtained from saponin-lysed N-2xFKBP-GFP-2xFKBP-Rab7^{endo} parasites using an α -GFP antibody (1: 1000; mouse). The black arrow indicates Rab7 fusion protein of the expected size (~105 kDa). α -aldolase served as a loading control).

3.3.3 Rab7 is important for the development of parasite blood stages

To investigate its function, Rab7 was conditionally inactivated using knock-sideway (Figure 55) (Birnbbaum et al., 2017, Robinson et al., 2010, Haruki et al., 2008). To this end, the N-2xFKBP-GFP-2xFKBP-Rab7^{endo}(loxP) parasite cell line was co-transfected with the *nmd3*'1xNLS-FRB-mCherry mislocalizer plasmid. Cultivation of parasites in the presence of rapalog for 12 h led to an incomplete mislocalization of Rab7 to the nucleus (75% of the parasites had some Rab7 signal remaining at the DV; 25% of cells showed a complete mislocalization without detectable signal remaining outside of the nucleus) (Figure 55A). To determine the effect of this partial mislocalization and the relevance of Rab7 for the parasite blood cycle, we monitored the parasitemia after conditional inactivation of Rab7 by knock-sideway (+ rapalog) compared to the control over 5 days (2.5 growth cycles). Despite the incomplete mislocalization of Rab7, the knock-sideway led to a profound growth defect in comparison to the control parasites (Figure 55B), indicating its essentiality for the parasite blood stages.

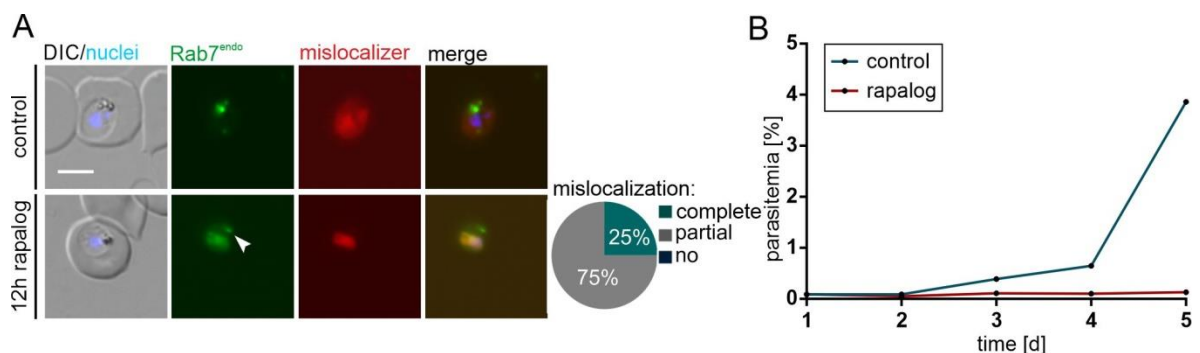


Figure 55 | Rab7 is important for the survival of *P. falciparum* blood-stage parasites. **A** Knock-sideway of N-2xFKBP-GFP-2xFKBP-Rab7^{endo} using a nuclear mislocalizer (*nmd3*'NLS-FRB-mCh) (Birnbbaum et al., 2017). Images were taken 12 h after induction of knock-sideway of parasites cultivated in the presence of rapalog compared to the control. Knock-sideway was classified in complete, partial, or

absent (no) mislocalization in 12 parasites. Nuclei were stained with DAPI. DIC, differential interference contrast. The scale bar indicates 5 μ m. **B** Flow cytometry growth curve over 2.5 growth cycles of the N-2xFKBP-GFP-2xFKBP-Rab7^{endo}+ *nmd3*¹NLS-FRB-mCh cell line. Parasites were cultivated in the presence of rapalog compared to the control without rapalog. One representative of n = 3 independent experiments, all replicas are shown in the supplements (Appendix B).

3.3.4 Inactivation of Rab7 affects schizont formation.

Initiation of knock-sideway in synchronous ring-stages of N-2xFKBP-GFP-2xFKBP-Rab7^{endo}(loxP)+ *nmd3*¹NLS-FRB-mCherry cell line parasites (Figure 56 A) showed that parasites can develop to trophozoite-stages (Figure 56 B, C i.), but mature to malformed schizont-stages (Figure 56 B, C ii.), that fail to enter the next cycle (Figure 56 B, C iii.). These preliminary data suggest that Rab7 plays an important role in the later blood stages. However, due to the incomplete mislocalization (Figure 56 C; white arrows) with some Rab7 remaining at the DV, it cannot be excluded that the function of Rab7 is partly preserved and further experiments are necessary to determine or exclude its relevance in the early stages of parasite development.

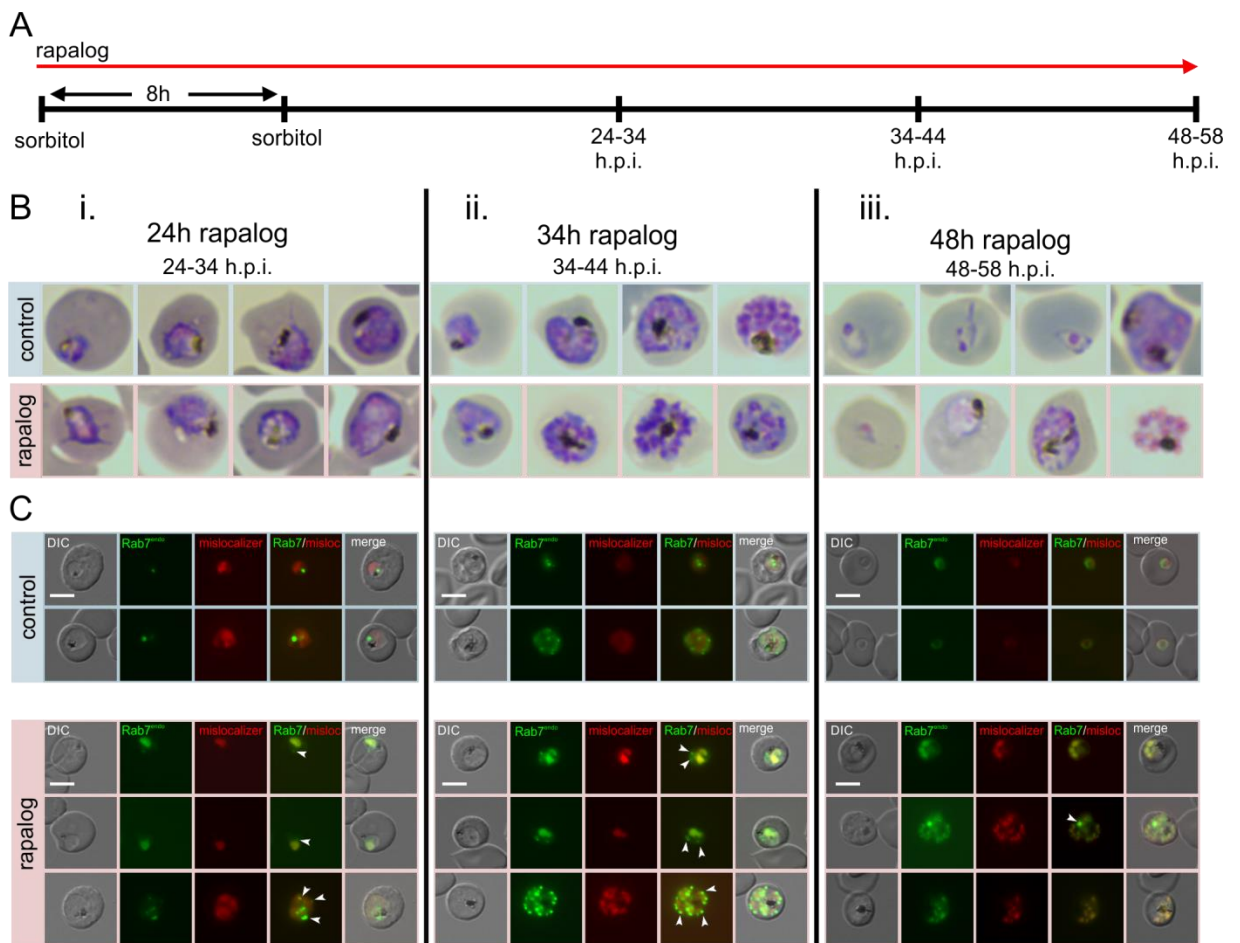


Figure 56 | Synchronous parasites with partially mislocalized Rab7 develop to malformed schizont-stages and fail to enter the next cycle. **A** Schematic illustration of the experimental procedure: Parasites of the N-2xFKBP-GFP-2xFKBP-Rab7^{endo}(loxP)+ *nmd3*¹xNLS-FRB-mCherry were synchronized twice with sorbitol within 8 h and cultivated for 48 h in the presence or absence (control) of rapalog. **B** Light-microscopy images of Giemsa-stained blood smears and **C** Live-cell microscopy images of parasites obtained from the experiment described in (A). n=1 experiment. Smears were prepared and images were taken i.: 24 h, ii.: 34 h, and iii.: 48 h upon induction of knock-sidaway with rapalog. White arrows: incomplete mislocalization of Rab7^{endo} to the nucleus. DIC, differential interference contrast. The scale bar represents 5 μ m.

3.3.5 K13 is localizing close to Rab7 positive circular structures adjacent to the DV.

Live-cell microscopy imaging of the N-2xFKBP-GFP-2xFKBP-Rab7^{endo}(loxP) cell line episomally co-expressing mCh-K13^{epi} (Figure 57 A) showed only poorly overlapping signal (15% overlap; 20% partial overlap; 65% no overlap) of the Rab7 circular structures at the DV and K13 in trophozoites (Figure 57 B). However, in 85% of these parasites, at least one K13 focus was located in close proximity to the Rab7 positive circular structures adjacent to the DV (Figure 57 C).

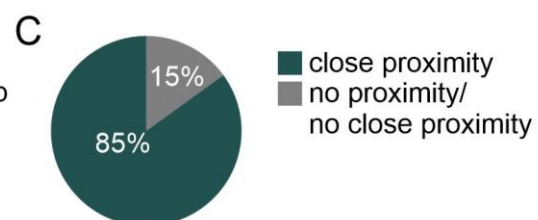
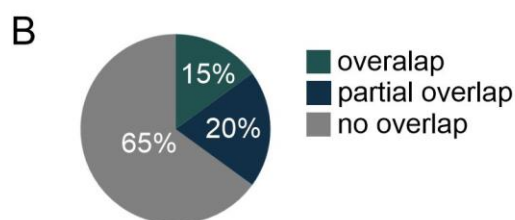
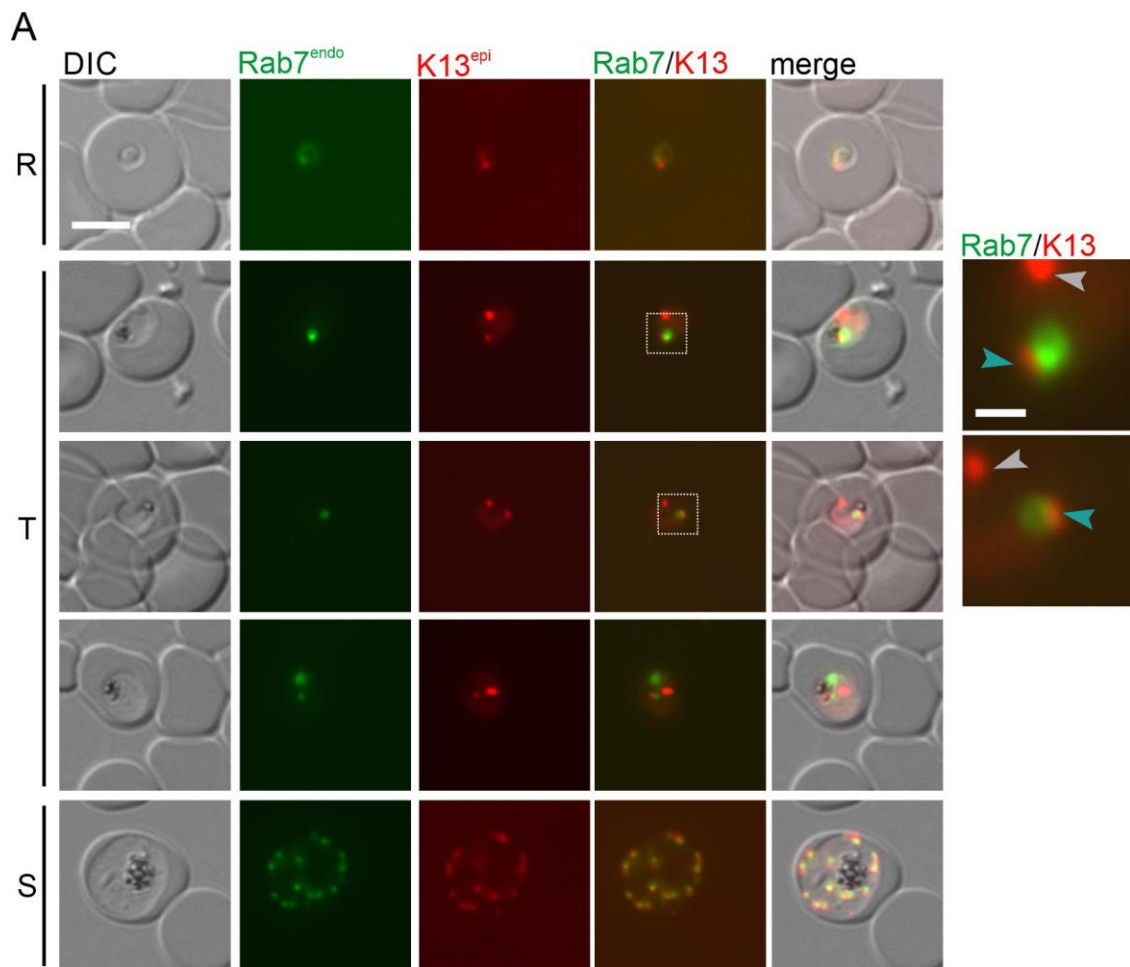


Figure 57 | K13 localizes in close proximity to Rab7 positive circular structures at the DV. **A** Live-cell microscopy images of the indicated stages of N-2xFKBP-GFP-2xFKBP-Rab7^{endo}(loxP) parasites, co-expressing *nmd3*mCh-K13. Dashed boxes in the merged images outline the areas of magnification. Blue arrows: K13 signal with close proximity to Rab7 positive circular structure at the DV. Grey arrows: K13 signal without overlap with Rab7 signal. R; ring, T; trophozoite, and S; schizont stages. DIC, differential interference contrast. The scale bar represents 5 μ m. **B** K13^{epi} signals were classified in overlap, partial overlap, or no overlap with Rab7^{endo} Rab7 positive circular structures at the DV in 19, 17, and 24 parasites (n = 3). **C** K13^{epi} signals were classified in close and no or no close proximity to Rab7 positive circular structures at the DV.

3.3.6 Rab7 positive circular structures adjacent to the DV do not overlap with hemoglobin signal.

To determine whether the Rab7 circular structures adjacent to the DV are filled with hemoglobin, an anti-hemoglobin IFA was performed with synchronous, saponin-treated, and formaldehyde-fixed N-2xFKBP-GFP-2xFKBP-Rab7^{endo}(loxP) parasites (Figure 58). No overlap of Rab7 and hemoglobin signal was found, indicating that the Rab7 circular structure is either not filled with hemoglobin or that the hemoglobin signal is too faint for detection. However, these results are preliminary and further experiments have to be conducted to rule out with certainty that the Rab7 delineated region indeed lacks HCC.

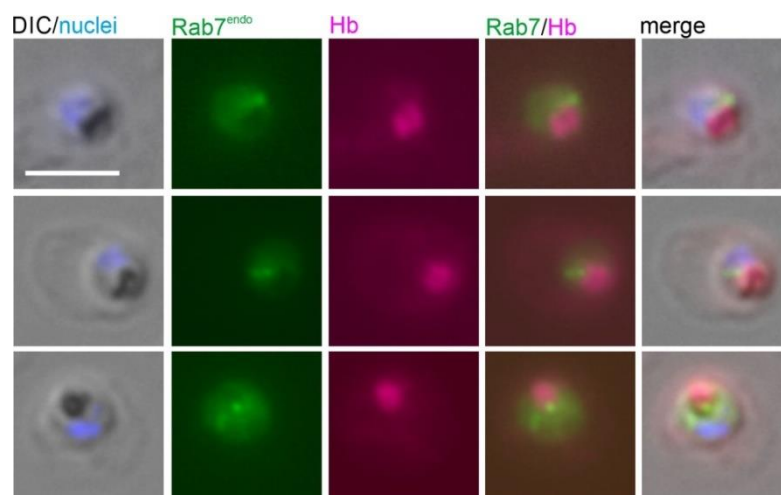


Figure 58 | Rab7 positive circular structures adjacent to the DV do not overlap with hemoglobin signal. Microscopy images of a hemoglobin -IFA of saponin-treated, formaldehyde-fixed, synchronous N-2xFKBP-GFP-2xFKBP-Rab7^{endo}(loxP) parasites. Representative images of 31 parasites of n = 1 experiment. The scale bars represent 5 μ m. Nuclei were stained with DAPI. DIC, differential interference contrast.

4 Discussion

4.1 New improved tools to investigate endocytosis

Due to the restricted number of selection markers available for *P. falciparum* parasites, the integration, as well as the simultaneous episomal expression of plasmids, is limited. In this work, new improved tools were established to mitigate this issue. Firstly, constructs were designed that allowed simultaneous conditional inactivation of one endogenously tagged protein along with colocalization of an independent episomally expressed marker. While this was already achieved in a previously established approach expressing p40 and an NLS mislocalizer under one promoter separated by a T2A skip peptide (Jonscher et al., 2019), this system had a drawback: since the cleavage of the two proteins by the T2A skip peptide was not always successful or complete, it could not be excluded that the observed localization of the marker was not caused by the localization of the remaining unskipped marker-T2A-mislocalizer and consequently could lead to false conclusions. For instance, when attempting to use this system for this work, reverse localization of the mislocalizer was observed, e.g. especially targeting early endocytosis proteins that are relatively difficult to mislocalize from their site of action and reverse mislocalization of unskipped construct led to false positive marker signals at the early endocytosis compartment. In addition, the observed nuclear signal of VPS45^{epi} upon mislocalization of Rbsn5^{endo}, caused by the interaction of both proteins which led to indirect mislocalization of VPS45^{epi}, could in principle also have been explained by incorrect skipping if this system were used. A further drawback of the previous system lies in the fact that the skip peptide is cleaved prior to its last proline, which causes the proline to remain N-terminal to the second protein and can cause incorrect localization, e.g. lyn with its N-terminal myristoylation site could no longer bind to the plasma membrane.). To circumvent these problems, a construct was made which enables the expression of the non-fluorescently labeled mislocalizer and the fluorescently labeled marker under two different promoters. The mislocalizer was expressed from the resistance cassette by fusing it with the resistance marker via a T2A

skip peptide. In this case, defective skipping does not affect the localization of the marker protein. In addition, the standard minimal *cam5'* promoter typically used to express the resistance marker was replaced with the stronger *nmd3'* promoter and thus provides reliable mislocalization while the promoter of the marker can still be adapted. One potential drawback of using this stronger promoter is that the parasites will likely carry fewer plasmids, as more resistance marker is produced, potentially reducing the amount of marker protein made per parasite.

The restriction to four selection markers has the consequence that currently only two proteins can be endogenously tagged using SLI, which so far made the mislocalization of either one or both proteins in the case of double integration unfeasible. To improve this system and increase the variation possibilities, the SLI-sandwich plasmid was modified to introduce a non-fluorescently labeled mislocalizer sequence into the genome along with selection-linked integration at the genomic target site. While the tagged GOI is expressed under its endogenous promoter, the mislocalizer is expressed under a distinct promoter (*nmd3'*) together with the hDHFR selection cassette from which it is separated by a skip peptide. The mislocalization of Rbsn5^{endo} using this approach was successful. However, it should be noted that this method of genomic plasmid integration results in a less expressed mislocalizer than the episomal approach using the same promoter since only one copy is present, and thus adequate promoter choice is more critical. Attempts to use the weak minimal *cam5'* promoter (Crabb and Cowman, 1996) were unsuccessful, suggesting that the resulted mislocalizer expression was too low.

Furthermore, to enable simultaneous inactivation of two proteins by mislocalization, a second target was endogenously tagged with the sequence encoding 2xFKBP-mScarlet, based on a modification of the SLI2a plasmid (Naranjo Prado, 2020, Stäcker, 2021). This enabled, for the first time simultaneous inactivation of two different proteins by conditional inactivation in one cell line. However, using this approach different inactivation kinetics of the two proteins cannot be compensated by different inactivation times, which would be possible by setting up two independent inactivation systems and would also permit higher flexibility. Such an orthogonal system would be highly desirable for the future.

Other work in our laboratory created the capacity to disrupt a target gene in a line with an already endogenously tagged protein of interest (Stäcker, 2021) or to conditionally

excise a gene using diCre in a line where a second protein was endogenously tagged (Stäcker, 2021). This latter system is similar to what was created here using knocksideway of one target while observing a marker. Overall, the system generated here and by others results in versatile options for conditionally inactivating or deleting other targets while observing a marker of interest. While this is very well suited to study proteins for which some information is already known, they are less suited for initial experiments or screens, as the location of the target and appropriate markers need first to be established. Hence, it is recommended to use standard SLI approaches (Birnbaum et al 2017) to localize the protein and assess mislocalization with an episomal standard mislocalizer before using the more sophisticated system introduced here to obtain deeper functional data about a target of interest.

4.2 Initiation of endocytosis in *P. falciparum* parasites

The initiation of endocytosis in blood stages of *P. falciparum* parasites has several uncommon characteristics that indicate that it has evolutionarily adapted to the particular circumstances faced by the parasites, such as being surrounded by a double membrane (PPM and PVM) and the requirement to take up large volumes of protein-dense material at high rates from its host cell. An unusual structure called the cytostome, an invagination of both membranes with an electron-dense collar at its neck and filled with host cell cytosol, is believed to be involved in the initiation of endocytosis in *P. falciparum* parasites (Sabitcki et al., 2020). Recent work suggests that the K13 structures observed in the cell may represent cytosomal collars (Yang et al., 2019) which would also agree with CLEM data that the K13 compartment protein Eps15 is found at host cell cytosol filled vesicular structures in the parasite of which some were clearly identified as cytostomes (Birnbaum et al., 2020). The fact that K13 colocalizes with proteins typical for the initiation of endocytosis such as AP-2 μ (Birnbaum et al., 2020) supports the assumption that it is the site of endocytosis initiation. It is possible that endocytic material gets taken up by a non-discriminatory bulk process (Sabitcki et al., 2020). This hypothesis might explain/account for the differences in the protein domains identified in the adaptors of the AP-2 complex in *P. falciparum* compared to model organisms but to date, only little experimental data exists on the AP-2 complex. Hence, experimental work is needed to lend credibility to this idea.

4.2.1 Components of the AP-2 adaptor complex in *P. falciparum* parasites display unique features

4.2.1.1 AP-2 α and AP-2 σ of *P. falciparum* parasites possess unusual hydrophobic regions predicted to be transmembrane domains

AP-2 is a typical complex involved in the initiation of CME at the plasma membrane. In model organisms, such as *H. sapiens*, the AP-2 complex is found to be cytosolic in an assembled but closed/inactive state and only gets recruited to the plasma membrane when it - due to conformational changes - transits into an open/activated state (Partlow et al., 2019, Beacham et al., 2019, Jackson et al., 2010a, Kadlecova et al., 2017). In its active form, the complex binds to the cytosolic part of an integral membrane protein, such as a cargo receptor to which an extracellular ligand has bound. This enables specific and regulated endocytosis of certain substances relevant to the cell at a certain point in time. This specificity is potentially not necessary in the case of the blood-stage malaria parasite, which must ingest and digest large amounts of host cell material at high rates to not only meet its amino acid requirements but also generate the space necessary for its growth. A continuous uptake of HCC into the parasite - and thus the absence of a need for different specific cargo receptors - would also make regulation by attachment and deactivation by the detachment of the AP-2 complex from the plasma membrane potentially redundant. In addition, receptor-associated endocytosis would have to be more complex due to the presence of an additional membrane, the PVM, which is also invaginated with the plasma membrane. These assumptions would suit the fact that in the *P. falciparum* AP-2 α and AP-2 σ adaptor components unusual transmembrane domains are predicted (five and one respectively). These predictions may represent bona fide transmembrane domains or hydrophobic patches mediating membrane association or partial insertion independent of the canonical ER-based insertion mechanisms. Both possibilities indicate a more permanent localization of at least part of the AP-2 complex at the PPM than in model organisms, such as *H. sapiens* and *S. cerevisiae* in which none of the AP-2 adaptors possesses similar hydrophobic regions.

In this work, the α -, σ -, and some of the β - adaptin of the PfAP-2 complex were found to be in foci at PPM in close proximity to the DV. The co-localization of these foci with Kelch13 suggests their localization at the cytostome. The assumption of a stable interaction with the PPM is supported by the observation that a complete mislocalization of

AP-2 σ away from the initiation site to the nucleus was not possible. The fact that a partial mislocalization was possible however indicates that this subunit is either not inserted into the PPM like a bona fide transmembrane domain protein or that not all of the protein molecules reached that state. In some parasites, a semicircular AP-2 signal surrounding a semicircular DIC structure at the PPM was observed, suggesting that AP-2 may at least in some instances be localized around the corpus of the cytostome.

In model organisms, the binding to the membrane-spanning cargo-loaded receptor is thought to stabilize the AP-2 complex in its active form (Kovtun et al., 2020) and link the membrane to other necessary accessory proteins involved in vesicle maturation. This cargo-adaptor interaction could potentially be mimicked by the transmembrane domains/ hydrophobic patches predicted in AP-2 α and AP-2 σ of *P. falciparum* parasites, thus representing a combination of AP-2 complex and cargo receptor-like elements necessary for endocytosis and by that allowing receptor-independent endocytosis. Another option is that the hydrophobic patches themselves have the purpose to promote vesicle formation since the partial insertion of a hydrophobic protein motif between lipid head groups can induce local membrane curvature (McMahon and Boucrot, 2015). This would be plausible since the absence of Clathrin at the initiation site of endocytosis in *P. falciparum* parasites (Birnbaum et al., 2020, Henrici et al., 2020) necessitates a different bending mechanism. No BAR domain proteins have so far been identified in malaria parasites that could fulfill such a function. Further evidence that AP-2 α plays a unique role in *P. falciparum* parasite's endocytosis is the fact that, with 259 additional aa, it is significantly larger (by about one-fifth) than its human homolog. While small and large insertions are a common phenomenon in *P. falciparum* proteins (e.g. (Quevillon et al., 2003, Voss et al., 2002)) in the case of AP-2 α they suggest that together with the distribution of the TMs/ hydrophobic patches, the hinge and ear regions might not possess the same flexibility than in human AP-2 α . This also indicates a different spatial configuration of the components in the AP-2 adapter complex compared to AP-2 in *H. sapiens*.

In the case that the hydrophobic regions represent bona fide transmembrane domains, the different intracellular and extracellular protein segments of AP-2 α and AP-2 σ would have different accessibility for accessory proteins. Interactions with factors on the non-cytosolic side of the membrane might be relevant to support the bending of both membranes or indeed enable a more complex receptor interaction in the PV or connection to the PVM to contribute to the invagination of both membranes.

This work shows that AP-2 α is essential for blood-stage parasites. Inactivation of AP-2 α resulted in a growth arrest in trophozoites and these parasites appeared to have less hemozoin and exhibited membrane deformations that extended as loops into the host cell. This might be due to the role of AP-2 α in endocytosis, as most host cell cytosol uptake and digestion occur in the trophozoite stages (Goldberg and Slater, 1992), and thus the disruption of this process has the greatest effect on these stages. The membrane loops might suggest that secretion (adding membrane to the PPM) is proceeding while no membranes are being taken up by the endocytosis process. However, it should also be noted that similar loops have been observed previously in parasites lacking proteins not involved in endocytosis (Garten et al., 2018, Mesén-Ramírez et al., 2019). It is therefore unclear if this phenotype is specific or simply indicative of reduced parasite viability. The fact that a residual amount of AP-2 α^{endo} was still detectable at its original site in the parasite after induction of the knock-sideway indicates that even an incomplete reduction of the amount of AP-2 α suffices to severely impair trophozoite growth.

Conditional inactivation of AP-2 σ led to parasite death indicating its essentiality for parasite blood stages. However, incomplete mislocalization and reverse-localization of the mislocalizer were observed. Reverse localization has also been previously observed for certain knock-sideway targets (Jonscher, 2018) and it is unclear what effect it has on the target. To better explore the impact of the reverse mislocalization, I generated a construct for conditional dimerization of FRB-mCh with AP-2 σ^{endo} . This showed that recruiting FRB-mCh to AP-2 σ was sufficient to interfere with its function and resulted in parasite death. This, together with the fact that attempts to tag AP-2 σ with 2xFKBP-GFP-2xFKBP failed, may suggest that additional C-terminal tags or proteins added by dimerization lead to steric hindrance effects that either reduce directly AP-2 σ functionality or its ability to interact with other proteins important for initiation of endocytosis. Even though the reverse localization of the mislocalizer was sufficient for the inactivation of AP-2 σ , it might result in slower inactivation kinetics. This could potentially explain the moderate effect on the HCCU observed in the bloated food vacuole assays.

Based on the results with the FRB-mCh construct recruited to AP-2 σ , recruitment of FRB-mCh might represent an attractive method to inactivate specific proteins if they cannot be mislocalized. The disadvantage of this approach is that it might only work for a subset of proteins. As an advantage, this method likely will have faster inactivation

kinetics than for instance diCre based gene excision which is an alternative that is independent of mislocalization and can be used for any type of target protein.

4.2.1.2 AP-2 β shows a translocated Clathrin binding box

Another peculiarity of the endocytosis of malaria parasites is the absence of Clathrin at the localization of the AP-2 complex (Birnbaum et al., 2020, Henrici et al., 2020) and thus at the site of initiation. This also seems to be the case for *Toxoplasma gondii* (Pieperhoff et al., 2013), raising the possibility that this is a feature common to all Apicomplexans. In the human AP-2 complex, a predicted Clathrin binding site is located in the flexible hinge region of the β -adaptin and only becomes accessible to Clathrin after conformational changes due to activation of the adaptor complex (Beacham et al., 2019, Kelly et al., 2014). The β -adaptin of *P. falciparum* lacks a Clathrin-binding box in the hinge region but such a sequence was detected by motif scans in the N-terminal trunk domain.

In *P. falciparum* parasites, it had been suspected that the β -adaptin is shared between AP-2 and AP-1 as in various other organisms (Nevin and Dacks, 2009). This work provides direct evidence for this. Fluorescence images of trophozoite stage parasites showed that AP-1/2 β has two distinct localizations. Firstly, it localized with K13 at the plasma membrane close to the DV, which is probably the initiation site of endocytosis, and secondly with the Golgi marker GRASP. Thus, it can be assumed that Clathrin is only required for the AP-1 complex dependent processes of the parasite, but not for AP-2. These different demands on a single adaptin could be an explanation for the different positions of the Clathrin-binding box. Thus, different conformations could allow access to the Clathrin binding site only in the AP-1 complex, while this region in the AP-2 complex remains hidden, yet the hinge regions in AP-2 and AP-1 remain accessible as a binding site for other crucial accessory proteins.

In this work, it was shown that AP-2 β is essential for the progression of *P. falciparum* parasites through the blood stage. However, due to the double localization of AP-2 β , it is not known whether the essential role can be attributed to functions at the Golgi or the Kelch13 compartment or both localizations.

4.3 Early endosome associated structures and proteins in HCCU of *P. falciparum*

4.3.1 *P. falciparum* parasites possess an evolutionarily conserved Rbsn5-VPS45-SNARE fusion complex

In mammals, a fusion complex is located at early endosomes involving Rab5 linked to VPS45 via the Rab5 effector protein Rbsn5 (Collins and Zimmerberg, 2009). In this work, a putative plasmodial Rbsn5 was identified, which hitherto had been elusive (using computational methods). Conditional inactivation of *PfRbsn5* in trophozoite-stage parasites resulted in the accumulation of hemoglobin-filled vesicular structures that had no continuous connection to the host cell, prevented transport of internalized HCC to the DV, and led to parasite death. These findings indicated its essential involvement in the HCCU process of *P. falciparum* parasites. Inactivation of *PfRbsn5* and simultaneous localization of the early endosomal marker PI3P showed that ~71% of these vesicular structures were positive for PI3P, indicating an endosomal character. This assumption was further supported by vesicles of smaller dimensions visible within the vesicular structures in the electron microscopy images. These intraluminal vesicles are a typical component of endosomes in model organisms and their presence would indicate the involvement of proteins of the ESCRT-III complex at this structure. However, not all ESCRT components have been detected in malaria parasites (Leung et al., 2008) and the role of this complex in the formation of intraluminal vesicles in the parasite remains to be determined.

Overall, a similar phenotype to the one with the *PfRbsn5* knock-sideway was previously observed upon inactivation of *PfVPS45* (Jonscher et al., 2019) and *PfRab5b* (Flemming, 2015, Schmitt, 2020). Localization studies in this work here revealed that *PfVPS45* localizes along with Rbsn5 to *PfRab5b*-positive membranes in close proximity to the Golgi-apparatus within the parasite and that the localization of these proteins is affected by the inactivation of *PfRbsn5*. The increasing nuclear localization of VPS45^{epi} upon Rbsn5^{endo} mislocalization suggested that it is indirectly pulled into the nucleus by an interaction of both proteins. In contrast, Rab5b^{epi} did not show nuclear localization upon Rbsn5^{endo} inactivation. This may be explained by its property of membrane anchoring via N-terminal myristoylation, which may represent a stronger association than an interaction with Rbsn5 or a more transitory interaction to Rbsn5-VPS45.

However, a functional interaction was also supported by the finding that inactivation of Rbsn5^{endo} resulted in accumulations of Rab5b^{epi}. A proportion of the emerging vesicles also appeared to be surrounded by a weak Rab5b^{epi} signal similar to what was found for PI3P. These results suggest the localization of Rab5b to the vesicle membrane, further emphasizing the endosomal nature of these vesicles and the function of Rab5b in the endosomal pathway of *P. falciparum* parasites. Co-immunoprecipitation experiments confirmed that PfRab5b and PfVPS45 are direct interaction partners of PfRbsn5. These data provide strong evidence that the Rab5-Rbsn5-VPS45-SNARE fusion complex in *P. falciparum* and thus this step of the canonical endosomal pathway is evolutionarily conserved. The inactivation of one of the components of the fusion complex therefore presumably leads to disturbed fusion processes of the intermediate endosomal structure with either other endosomes or the DV, resulting in the observed vesicle accumulation phenotype. However, it should be noted that the location of these proteins proximal to the Golgi as detected here and for VPS45 also previously (Jonscher et al., 2019) may also indicate less straightforward explanations of these findings. Either this location represents an equivalent of the early endosomal compartment described in *T. gondii* (Harper et al., 2006, Parussini et al., 2010, Sangare et al., 2016), which would indicate that endosomal transport intersects at this site (or is at least in close proximity) with secretory compartments or that the observed effect on HCCU is more indirect, e.g. due to defective recycling via the trans Golgi that results in slowed or inactivated endosomal maturation.

Of the 3 Rab5 isoforms in malaria parasites, these findings link Rab5b to endosomal processes and confirmed the previous interpretation of the growth phenotype that Rab5a is not involved in host cell cytosol uptake (Birnbaum et al., 2017) in a more direct way using the bloated food vacuole assay. The third Rab5 orthologue of malaria parasites, Rab5c, remains to be analyzed but overall resembles more Rab5a, as it has the typical C-terminal prenylation motifs (Quevillon et al., 2003).

4.3.2 KIC7 is necessary for processes upstream of those resulting in the vesicles accumulating upon Rbsn5 inactivation

Simultaneous conditional inactivation of the endosomal protein Rbsn5 together with the early endocytosis protein KIC7 led to a significant reduction in vesicle accumulation, compared to the controls (inactivation of Rbsn5 or Rbsn5 together with Sand1). This indicated that KIC7 is necessary for processes upstream of those resulting in the vesi-

cles accumulating upon Rbsn5 inactivation and these experiments provide evidence that the content of these vesicles originates from the Kelch13-defined compartment that feeds into a more conserved endosomal delivery process to the DV. However, the interpretation of these experiments is complicated by the different inactivation kinetics of KIC7 and Rbsn5. Since KIC7 needs significantly longer (~3 h) than Rbsn5 (<1 h) to be mislocalized to the nucleus, vesicles accumulate until the inactivation of KIC7 is sufficient to inhibit vesicle formation, preventing a more absolute phenotype of loss of vesicle accumulation. The establishment of an independent instead of a simultaneous inactivation system might provide a better approach in the future and is expected to result in a clearer difference and hence a more unequivocal conclusion.

Although endosomal vesicle formation seems to depend on the compartment of early endocytosis defined by Kelch13, neither AP-2 σ nor Kelch13 could be found at the accumulating endosomal vesicles, indicating that they have no further function at this step of endocytosis. Further, this suggests that these proteins dissociate, remain at the cytotomal neck, or are sorted away from the pinched-off vesicles, rather than staying on the endosomal vesicles and being recycled back to the plasma membrane. Interestingly, it was observed that the induced vesicles close to the early endocytosis site, may indicate that they are formed by pinching off the entire cytostome. Alternatively, they could be the result of smaller vesicles that pinched off from the cytostome and fused or collected in nearby pre-existing endosomes that inflated to the observed size. Resolving these different options is at present difficult, firstly due to limits of resolution for imaging and secondly, because no markers of the cytotomal bulb membrane and the potentially forming vesicle are known that could be used to better track the formation of the HCC filled vesicles.

4.3.3 Plasmeprin II is transported to the DV via endosomal structures

In a previous publication (Klemba et al., 2004a), it was proposed that proPMII gets transported via the secretory pathway as an integral transmembrane protein to the PPM and to the cytostome, from where it is trafficked along with hemoglobin to the DV, where it is presumed to be proteolytically processed in the acidic environment of the DV to mature and soluble PMII. In this work, the episomally expressed PMII showed ER and DV localization as previously described (Francis et al., 1997a, Klemba et al., 2004a). Inactivation of Rbsn5 and VPS45 showed that PMII seemed to be present in or at the accumulating endosomal structures and also led to a reduction of PMII reaching

the DV, indicating that PMII gets transported to the DV via the observed endosomal vesicles. There was no evidence of hemoglobin degradation in the vesicles induced upon Rbsn5 inactivation as the electron density of their content did not appear to differ from the host cell cytosol in the electron microscopy images. This suggests that the condition in these vesicles did not promote cleavage of proPMII to active PMII. However, the dot-shaped appearance of the PMII signal in these endosomal vesicles was different from the circular enclosing signals observed for PI3P or Rab5b, suggesting that at least no exclusive localization in the outer endosomal vesicle membrane was present. Thus, it cannot be excluded that proPMII had already been cleaved to PMII and released into the vesicle lumen, but this would raise the question of how both observed endosomal vesicle membranes (Jonscher et al., 2019) could be crossed. Western blots analysis of parasites at different time points after Rbsn5 inactivation could provide information about the site of cleavage by assessing the ratio of proPMII to PMII at different time points after inactivation of Rbsn5 or VPS45. Moreover, it was difficult to determine from the microscopic images whether the PMII signal was indeed inside and not on the outside of the endosomal vesicles. Therefore, it is also possible that the observed PMII signals were external to the endosomal structure and were e.g. accumulating proPMII-loaded transport vesicles derived from the ER or Golgi apparatus that failed to fuse with the membrane of the endosomal vesicle due to the inactivation of one of the proteins in the Rab5-Rbsn5-VPS45-SNARE fusion complex. Alternatively, it constitutes PMII accumulating in the intermembrane space of double membraned endosomal vesicles, although this would mean that cleavage of proPMII would already have taken place which would require an acidic milieu which seems unlikely for this site. Colocalization of Clathrin and PMII after inactivation of RBSN5 could provide information, since vesicles originating at the TGN in mammals are Clathrin-coated (Hanners and Tooze, 2003), and the presence of Clathrin at the rudimentary Golgi apparatus of *P. falciparum* (Jonscher, 2018, Henrici et al., 2020) suggests that this might be conserved. In addition, a proPMII construct with a defective cleavage site could yield information about the localization and appearance without cleavage and thus serve as a comparison.

Neither in the control nor by inactivation of Rbsn5 could any signal or accumulation of PMII at the plasma membrane be observed. This indicates that there may be no transport to the DV via the plasma membrane and cytostome as previously postulated (Klemba et al., 2004a), but rather transport could occur directly to the endosomal structure from where trafficking onwards to the DV takes place. However, further experi-

ments should exclude that a potential PMII signal at the plasma membrane was not simply too weak for detection. This may be possible considering that the PPM is a much larger structure that may result in a dilution of the PMII signal beyond detection.

The observed localization of proteins at the induced endosomal vesicle and the presence of intraluminal vesicles raise the question of the exact composition of the endosomal vesicles. One possibility to investigate the content of the vesicles might be the GBP-biotinylizer constructs, which get endocytosed by the parasites after their previous export and are found to be located in the accumulating endosomal vesicles after Rbsn5 inactivation. The use of the fast miniTurboID in particular might allow the identification of the vesicle content by mass spectrometry of biotinylated purified proteins. However, the significant excess of hemoglobin and the solubility of the constructs might make the identification of the protein content of these vesicles more difficult. Another possibility to reveal the proteome of the endosomal vesicle would be the extraction of the entire vesicle and biotinylizer constructs targeting the outer and inner membranes. With these approaches, it would be possible to determine not only the composition but also the spatial localization of various proteins in these endosomal vesicles. Finally, it might also be possible to purify the vesicles using density gradients or using magnetic beads after pre-loading of the host cell with magnetic content.

4.3.4 VPS45 is relevant for IMC biogenesis in schizonts and HCCU is present in the late stages of *P. falciparum* parasites

It is known that parts of the endosomal system in Apicomplexa are repurposed for the formation of the secretory organelles required for host cell invasion (Breinich et al., 2009, Krai et al., 2014, Kremer et al., 2013, Tomavo et al., 2013a). The IMC of *P. falciparum* parasites is presumably assembled from Clathrin-coated vesicles derived from the ER-Golgi secretory pathway (Bannister et al., 2000b). Since SEC/Munc18 proteins, such as VPS45, are critical for vesicle fusion events in model organisms (Südhof and Rothman, 2009), VPS45's role in the formation of secretory organelles was investigated (Bisio et al., 2020b).

The conditional inactivation of VPS45^{endo} impaired schizogony led to the arrest of the parasites in the schizont stage with the consequence of failed egress, invasion, and generation of novel ring-stages. Electron microscopy images revealed that the parasites possessed a defect in IMC formation, while the formation of micronemes and

rhoptries seemed to be unaffected. This indicates a role of VPS45 in the process of IMC formation and thus suggests a role for VPS45 in addition to endocytosis. Therefore, VPS45 and other typical endocytosis proteins could be conserved to some extent but might also have a dual and specific function adapted to the unique demands of the parasite. However, it may also be that these defects in schizonts are secondary to the endocytosis defect. It is possible that the accumulating vesicles reduce the total membrane material available for the formation of merozoites and that this results in an impairment of merozoite generation. An argument against this interpretation is that we also observed parasites that had a defect in merozoites but no accumulated vesicles.

Most of the uptake and digestion of host cell cytosol is known to occur in the trophozoite stages (Goldberg and Slater, 1992), however, endocytosis is already active in ring stages (Birnbaum et al., 2020, Lazarus et al., 2008, Bannister et al., 2004). The presence of accumulated endocytic vesicles filled with host cell cytosol after inactivation of VPS45 in schizonts revealed that HCCU also still takes place at very late developmental stages and shows that VPS45 can also be relevant for different processes at the same stage. However, it cannot be excluded that the observed defects are not a secondary consequence of the accumulating vesicles

4.4 Late endosome associated structures and proteins in HCCU

The maturation model states that early endosomes mature into late endosomes and a key step in endosome maturation is the conversion from Rab5 to Rab7 at the endosomal compartment (Rink et al., 2005). The domain architecture and protein length of Rab7 of *P. falciparum* and *H. sapiens* show a high resemblance and an alignment identified 80% similarity across its entire sequence, supporting a conserved function of Rab7 in the malaria parasite. Attempts of conditional inactivation of Rab7^{endo} showed incomplete mislocalization which however led to a severe growth defect, indicating an important function of Rab7 for the parasite blood stages. DiCre-based gene excision or a combination of diCre and knock-sideway as previously tested for the inactivation of Kelch13 (Birnbaum et al., 2017) might offer an improvement for the inactivation of Rab7 in the future. Rab7^{endo} showed one to three circular structures at the DV in trophozoites and its signal surrounded structures visible in the DIC images. However, these

structures were not observed to the same extent in the DIC images of wild-type 3D7 parasites and are probably the result of impaired Rab7-dependent processes caused by the protein tag that also could explain the observed slowed growth of the N-2xFKBP-GFP-2xFKBP-Rab7^{endo} cell line. EM or introduction of markers into this line might provide insight into the nature of this compartment that may in wt cells go unnoticed. As such, this cell line might also provide an opportunity to understand the role of the Rab in the parasite.

The circular structure could indicate a vesicular character. Preliminary data from a hemoglobin-IFA have not detected hemoglobin in these structures, implying that if they represent late endosomes, they get only transiently filled. Rab7 inactivation did not reveal any striking phenotype that indicates a role in the HCCU process, such as vesicle accumulation, decreased amounts of hemozoin, or an altered DV. Giemsa smears of synchronous parasites showed that Rab7 inactivation leads to malformed schizont stages that fail to enter the next cycle, indicating that Rab7 is crucial for schizont formation. This finding fits with the fact that previous work inactivating its GEF, Sand1 showed a similar phenotype, supporting a role of these two proteins in schizont formation but not an essential function in endocytosis (Birnbaum et al., 2017). Schizonts showed multiple small Rab7 signals that seemed to represent circular structures with smaller diameters. It could be speculated that Rab7 is also repurposed in schizonts for the secretory pathway and the effect of Rab7 inactivation on secretory organelles should be examined. However, due to the incomplete mislocalization of Rab7 from the circular structure at the DV in trophozoites, it cannot be excluded that the function is not yet significantly impaired at this stage and therefore a possible function in the HCCU process cannot be fully excluded.

Besides the Rab GTPase switch with maturation to the late endosome, the phosphoinositol of the endosomal membrane is converted from PI3P to PI(3,5)P2 (Marat and Haucke, 2016). However, a switch of phosphoinositides in later HCCU steps of the malaria parasite seems not to occur since the lysosome-like digestive vacuole is positive for PI3P, while PI(3,5)P2 has not been detected in *Plasmodium* parasites (Tawk et al., 2010b). This could be an indication that late endosomes are not present in *P. falciparum* or at least have a composition that differs from that of model organisms. Co-localization studies of Rab7 and PI3P might provide further insights.

However, Rab7 is not exclusive to the endocytic pathway. Rab7 is also located at autophagosomes in model organisms and is assumed to regulate the autophagosome-lysosome fusion step during autophagy (Kuchitsu and Fukuda, 2018). Co-localization studies of Rab7 in *P. falciparum* with autophagy-related-protein-8 (ATG8)-positive acidic structures induced under starvation conditions may indicate a function of Rab7 in autophagy (Tomlins et al., 2013). Autophagy and endocytosis are both intersecting pathways for the degradation and recycling of intracellular and extracellular components that share a common endpoint at the lysosome, where their cargo gets degraded (Birgisdottir Å and Johansen, 2020). Interestingly, Kelch13 was observed at the Rab7 circular structure, indicating a potential function of Kelch13 at the Rab7-positive compartment or the result of the spatial proximity of two independent processes and compartments.

Assuming that this Kelch13 signal proximal to the Rab7 signal is not spatial proximity of unrelated compartments would raise several possibilities. It would mean that Kelch13 is present both, at late endosomal or autophagy-related structures as well as in early endocytosis while absent at intermediate endocytic structures. Autophagy and endocytosis pathways share a number of the components of the molecular machinery involved (Birgisdottir Å and Johansen, 2020), thus, Kelch13 localization could indicate an additional Kelch13 function in autophagy independent of early endocytosis. Furthermore, Kelch13 localization could indicate a regulation mechanism between early endocytosis and late endocytosis or autophagy. Some publications from other organisms provide evidence that early endocytosis factors interact with ATG8s. Adaptor-associated kinase 1 (AAK1), involved in the phosphorylation of AP-2 (Conner 2002, Henderson and Conner, 2007), interacts with ATG8s and LC3 and contains LIR (LC3-interacting region) motifs (Loi et al., 2016, Birgisdottir Å and Johansen, 2020), which ensures the targeting of autophagy receptors to LC3 or other ATG8 family proteins. The alpha-adaptin of the AP-2 complex has also been found to contain a putative LIR motif and was proposed to function as an LC3 receptor (Tian et al., 2013).

Endosomes and autophagosomes are also involved in retromer-associated recycling and sorting processes of transmembrane proteins (Cullen and Steinberg, 2018). Rab7 of *P. falciparum* was found to co-localize with a possible retromer complex near the DV in close proximity to the Golgi-apparatus and therefore its role in recycling processes from a putative late endosome to the Golgi apparatus has been proposed (Siddiqui et al., 2020, Krai et al., 2014). However, this could also indicate a recycling process to the

plasma membrane. Identifying the role of the Rab7-positive compartment and its relationship to Kelch13 could potentially contribute to understand why Kelch13 is essential and mediates resistance at the ring- but not at later stages. To determine the relationship between early endocytosis and Rab7, colocalization studies with simultaneous inactivation of early endocytosis proteins could provide further insight.

4.5 Proposed working model of HCCU in *P. falciparum* parasites

The conclusions and hypotheses that emerged from the results of this thesis, together with previous findings (Sabitcki et al., 2020) are summarized in the following working model of HCCU (Figure 59).

The initiation of endocytosis occurs in a clathrin-independent but AP-2-dependent process at the PIP2-positive plasma membrane, involving the cytosome, an invagination of the PPM and PVM with an electron-dense ring at its neck at which Kelch13 seems to be present. Observed semicircular signals of AP-2 adaptins at DIC structures at the PPM indicate that AP-2 might in some instances be present at the corpus of the forming cytostome. The alpha and the beta adaptin of the heterotetrameric AP-2 complex possess unusual hydrophobic patches that might participate in the curvature of the membrane and thus might be involved in cytostome formation or formation of smaller vesicles from the cytostome. The more permanent attachment of AP-2 at the PPM could also compensate for the cooperative and cargo-dependent binding to cargo receptors as this may not be needed for the suspected receptor-independent bulk-uptake process. It can be speculated that cytostome fission from the plasma membrane results in a vesicle that matures to an early endosomal structure. Alternatively, it is equally possible that smaller vesicles pinch off the cytostome, which fuse to form a larger early endosome. However, this fusion event would then likely be independent of the Rab5-Rbsn5-VPS45-SNARE fusion complex, since inactivation still leads to the formation of endosomal structures. These double-membranous and host cell cytosol filled endosomal structures accumulate after Rab5/Rbsn5/VPS45 inactivation and possess early endosomal properties. They are PI3P and Rab5b positive and contain smaller vesicles that may represent intraluminal vesicles. Furthermore, Golgi/or ER-derived proPMII that is destined for the DV appears to be transported directly to and via these endoso-

mal structures. The observation that Rbsn5 and VPS45 are found in close proximity, but not consistently overlapping, with GRASP might indicate a Golgi-proximal compartment that could resemble the endosome-like compartment (ELC), observed in *T. gondii* that represents an intersection between secretory and endocytic traffic (McGovern et al., 2018). The accumulation upon inhibition of the Rab5-Rbsn5-VPS45-SNARE fusion complex suggests that either (i) these early endosomal structures fail to fuse directly with the DV or a potential late endosome or (ii) the Golgi-derived vesicles that are required for maturation of the early endosome into a potential late endosome are inhibited from fusing with the early endosome. A Rab7-positive circular structure at the DV could represent a late endosome or autophagosome at which, for example, sorting recycling processes take place or represent a station for parasite proteins destined for degradation in the DV. Localization of Kelch13 at this compartment could indicate an interception of early endocytosis and late endocytosis or autophagy or simply close proximity of parallel pathways to the DV. Fusion of the outer membrane of the double-membranous EE or LE with the single-membranous DV would likely release the inner vesicle part into the DV, followed by the degradation of this now single-membranous vesicle, and the contained hemoglobin. Fusion might also lead to the contact of proPMII with the acidic environment of the DV resulting in cleavage and activation of the enzyme to soluble PMII, which is important for the hemoglobin degradation cascade.

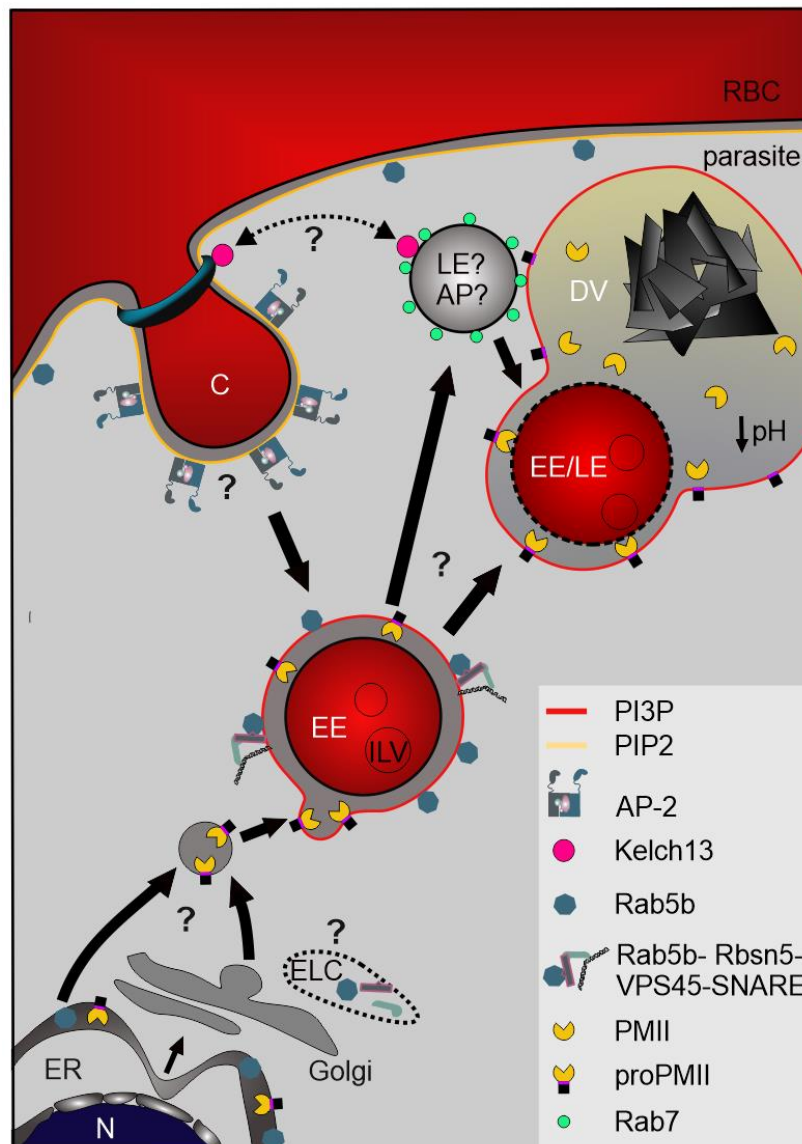


Figure 59 | Proposed working model of HCCU in *P. falciparum*. Initiation of endocytosis occurs in a clathrin-independent but AP-2-dependent process at the PIP2-positive plasma membrane involving the cytosome an invagination of the PPM and PVM with an electron-dense ring at its neck at which Kelch13 is present, while the AP-2 complex surrounds the cytosome corpus and might promote membrane curvature. Host cell material reaches PI3P-positive EEs, which accumulate upon inactivation of proteins of the Rab5-Rbsn5-VPS45-SNARE fusion complex and contain ILV. Rbsn5 and VPS45 might be present in a Golgi-proximal compartment that could resemble an endosome-like compartment (ELC), observed in *T. gondii*, an intersection between secretory and endocytic pathway. EE fuse either directly with DV or prior mature/fuse with LE. A Rab7 circular compartment at the DV might be LE or AP. The presence of Kelch13 at this structure indicates interception of early endocytosis and LE/autophagy. ProPMII gets transported through ER/Golgi to EE and via endosomes to DV where it gets cleaved to active soluble PMII. C, cytosome; EE, early endosome; ILV, intraluminal vesicle; ELC, endosome-like compartment; LE, late endosome; AP, autophagosome; DV, digestive vacuole; N, nucleus; ER, endoplasmic reticulum; RBC, red blood cell.

References

- ABDULRAHEEM, M. A., ERNEST, M., UGWUANYI, I., ABKALLO, H. M., NISHIKAWA, S., ADELEKE, M., ORIMADEGUN, A. E. & CULLETON, R. 2021. High prevalence of *Plasmodium malariae* and *Plasmodium ovale* in co-infections with *Plasmodium falciparum* in asymptomatic malaria parasite carriers in Southwest Nigeria. *medRxiv*, 2021.01.14.21249635.
- ABU BAKAR, N., KLONIS, N., HANSEN, E., CHAN, C. & TILLEY, L. 2010. Digestive-vacuole genesis and endocytic processes in the early intraerythrocytic stages of *Plasmodium falciparum*. *J Cell Sci*, 123, 441-50.
- AIKAWA, M., HEPLER, P. K., HUFF, C. G. & SPRINZ, H. 1966. The feeding mechanism of avian malarial parasites. *J Cell Biol*, 28, 355-73.
- AMINO, R., GIOVANNINI, D., THIBERGE, S., GUEIRARD, P., BOISSON, B., DUBREMETZ, J. F., PRÉVOST, M. C., ISHINO, T., YUDA, M. & MÉNARD, R. 2008. Host cell traversal is important for progression of the malaria parasite through the dermis to the liver. *Cell Host Microbe*, 3, 88-96.
- ANDENMATTEN, N., EGARTER, S., JACKSON, A. J., JULLIEN, N., HERMAN, J. P. & MEISSNER, M. 2013. Conditional genome engineering in *Toxoplasma gondii* uncovers alternative invasion mechanisms. *Nat Methods*, 10, 125-7.
- ARAMA, C. & TROYE-BLOMBERG, M. 2014. The path of malaria vaccine development: challenges and perspectives. *Journal of Internal Medicine*, 275, 456-466.
- ARIEY, F., WITKOWSKI, B., AMARATUNGA, C., BEGHAIN, J., LANGLOIS, A. C., KHIM, N., KIM, S., DURU, V., BOUCHIER, C., MA, L., LIM, P., LEANG, R., DUONG, S., SRENG, S., SUON, S., CHUOR, C. M., BOUT, D. M., MÉNARD, S., ROGERS, W. O., GENTON, B., FANDEUR, T., MIOTTO, O., RINGWALD, P., LE BRAS, J., BERRY, A., BARALE, J. C., FAIRHURST, R. M., BENOIT-VICAL, F., MERCEREAU-PUIJALON, O. & MÉNARD, D. 2014. A molecular marker of artemisinin-resistant *Plasmodium falciparum* malaria. *Nature*, 505, 50-5.
- ARMISTEAD, J. S., MORLAIS, I., MATHIAS, D. K., JARDIM, J. G., JOY, J., FRIDMAN, A., FINNEFROCK, A. C., BAGCHI, A., PLEBANSKI, M., SCORPIO, D. G., CHURCHER, T. S., BORG, N. A., SATTABONGKOT, J. & DINGLASAN, R. R. 2014. Antibodies to a single, conserved epitope in Anopheles APN1 inhibit universal transmission of *Plasmodium falciparum* and *Plasmodium vivax* malaria. *Infect Immun*, 82, 818-29.
- ATKINSON, S. C., ARMISTEAD, J. S., MATHIAS, D. K., SANDEU, M. M., TAO, D., BORHANI-DIZAJI, N., TARIMO, B. B., MORLAIS, I., DINGLASAN, R. R. & BORG, N. A. 2015. The Anopheles-midgut APN1 structure reveals a new malaria transmission-blocking vaccine epitope. *Nat Struct Mol Biol*, 22, 532-9.

- AZARNIA TEHRAN, D., LÓPEZ-HERNÁNDEZ, T. & MARITZEN, T. 2019. Endocytic Adaptor Proteins in Health and Disease: Lessons from Model Organisms and Human Mutations. *Cells*, 8, 1345.
- BAER, K., KLOTZ, C., KAPPE, S. H., SCHNIEDER, T. & FREVERT, U. 2007. Release of hepatic *Plasmodium yoelii* merozoites into the pulmonary microvasculature. *PLoS Pathog*, 3, e171.
- BAKER, D. A. 2010. Malaria gametocytogenesis. *Molecular and biochemical parasitology*, 172, 57-65.
- BANNISTER, L. H., HOPKINS, J. M., FOWLER, R. E., KRISHNA, S. & MITCHELL, G. H. 2000a. A brief illustrated guide to the ultrastructure of *Plasmodium falciparum* asexual blood stages. *Parasitol Today*, 16, 427-33.
- BANNISTER, L. H., HOPKINS, J. M., FOWLER, R. E., KRISHNA, S. & MITCHELL, G. H. 2000b. Ultrastructure of rhoptry development in *Plasmodium falciparum* erythrocytic schizonts. *Parasitology*, 121 (Pt 3), 273-87.
- BANNISTER, L. H., HOPKINS, J. M., MARGOS, G., DLUZEWSKI, A. R. & MITCHELL, G. H. 2004. Three-Dimensional Ultrastructure of the Ring Stage of *Plasmodium falciparum*: Evidence for Export Pathways. *Microscopy and Microanalysis*, 10, 551-562.
- BARTOLONI, A. & ZAMMARCHI, L. 2012. Clinical aspects of uncomplicated and severe malaria. *Mediterranean journal of hematology and infectious diseases*, 4, e2012026-e2012026.
- BASTUREA, G. 2019. Endocytosis. *Materials and Methods*, 9.
- BEACHAM, G. M., PARTLOW, E. A. & HOLLOPETER, G. 2019. Conformational regulation of AP1 and AP2 clathrin adaptor complexes. *Traffic*, 20, 741-751.
- BEACHAM, G. M., PARTLOW, E. A., LANGE, J. J. & HOLLOPETER, G. 2018. NECAPs are negative regulators of the AP2 clathrin adaptor complex. *eLife*, 7, e32242.
- BENNINK, S., KIESOW, M. J. & PRADEL, G. 2016. The development of malaria parasites in the mosquito midgut. *Cellular microbiology*, 18, 905-918.
- BERNABEU, M. & SMITH, J. D. 2017. EPCR and Malaria Severity: The Center of a Perfect Storm. *Trends Parasitol*, 33, 295-308.
- BIRGISDOTTIR, Á, B. & JOHANSEN, T. 2020. Autophagy and endocytosis - interconnections and interdependencies. *J Cell Sci*, 133.
- BIRNBAUM, J., FLEMMING, S., REICHARD, N., SOARES, A. B., MESEN-RAMIREZ, P., JONSCHER, E., BERGMANN, B. & SPIELMANN, T. 2017. A genetic system to study *Plasmodium falciparum* protein function. *Nat Methods*, 14, 450-456.
- BIRNBAUM, J., SCHARF, S., SCHMIDT, S., JONSCHER, E., HOEIJMAKERS, W. A. M., FLEMMING, S., TOENHAKKE, C. G., SCHMITT, M., SABITZKI, R.,

- BERGMANN, B., FROHLKE, U., MESEN-RAMIREZ, P., BLANCKE SOARES, A., HERRMANN, H., BARTFAI, R. & SPIELMANN, T. 2020. A Kelch13-defined endocytosis pathway mediates artemisinin resistance in malaria parasites. *Science*, 367, 51-59.
- BISIO, H., CHAABENE, R. B., SABITZKI, R., MACO, B., MARQ, J. B., GILBERGER, T.-W., SPIELMANN, T. & SOLDATI-FAVRE, D. 2020a. The ZIP Code of Vesicle Trafficking in Apicomplexa: SEC1/Munc18 and SNARE Proteins. *mBio*, 11, e02092-20.
- BLACKMAN, M. J. & BANNISTER, L. H. 2001. Apical organelles of Apicomplexa: biology and isolation by subcellular fractionation. *Mol Biochem Parasitol*, 117, 11-25.
- BLUM, M., CHANG, H.-Y., CHUGURANSKY, S., GREGO, T., KANDASAAMY, S., MITCHELL, A., NUKA, G., PAYSAN-LAFOSSE, T., QURESHI, M., RAJ, S., RICHARDSON, L., SALAZAR, G. A., WILLIAMS, L., BORK, P., BRIDGE, A., GOUGH, J., HAFT, D. H., LETUNIC, I., MARCHLER-BAUER, A., MI, H., NATALE, D. A., NECCI, M., ORENGO, C. A., PANDURANGAN, A. P., RIVOIRE, C., SIGRIST, C. J. A., SILLITOE, I., THANKI, N., THOMAS, P. D., TOSATTO, S. C. E., WU, C. H., BATEMAN, A. & FINN, R. D. 2021. The InterPro protein families and domains database: 20 years on. *Nucleic Acids Research*, 49, D344-D354.
- BOS, J. L., REHMANN, H. & WITTINGHOFER, A. 2007. GEFs and GAPs: Critical Elements in the Control of Small G Proteins. *Cell*, 129, 865-877.
- BRANON, T. C., BOSCH, J. A., SANCHEZ, A. D., UDESHI, N. D., SVINKINA, T., CARR, S. A., FELDMAN, J. L., PERRIMON, N. & TING, A. Y. 2018. Efficient proximity labeling in living cells and organisms with TurboID. *Nat Biotechnol*, 36, 880-887.
- BRAY, P. G., MUNGTHIN, M., RIDLEY, R. G. & WARD, S. A. 1998. Access to hemozoin: the basis of chloroquine resistance. *Mol Pharmacol*, 54, 170-9.
- BREINICH, M. S., FERGUSON, D. J. P., FOTH, B. J., VAN DOOREN, G. G., LEBRUN, M., QUON, D. V., STRIEPEN, B., BRADLEY, P. J., FRISCHKNECHT, F., CARRUTHERS, V. B. & MEISSNER, M. 2009. A Dynamin Is Required for the Biogenesis of Secretory Organelles in *Toxoplasma gondii*. *Current Biology*, 19, 277-286.
- BUCŞAN, A. N. & WILLIAMSON, K. C. 2020. Setting the stage: The initial immune response to blood-stage parasites. *Virulence*, 11, 88-103.
- BULL, P. C. & ABDI, A. I. 2016. The role of PfEMP1 as targets of naturally acquired immunity to childhood malaria: prospects for a vaccine. *Parasitology*, 143, 171-186.
- CAI, J., CHEN, S., ZHU, F., LU, X., LIU, T. & XU, W. 2021. Whole-Killed Blood-Stage Vaccine: Is It Worthwhile to Further Develop It to Control Malaria? *Frontiers in Microbiology*, 12.

- CAMPO, B., VANDAL, O., WESCHE, D. L. & BURROWS, J. N. 2015. Killing the hypnozoite--drug discovery approaches to prevent relapse in *Plasmodium vivax*. *Pathogens and global health*, 109, 107-122.
- CASARES, S., BRUMEANU, T.-D. & RICHIE, T. L. 2010. The RTS,S malaria vaccine. *Vaccine*, 28, 4880-4894.
- CDC 2021. Malaria's Impact Worldwide.
- CHEN, Z. & SCHMID, S. L. 2020. Evolving models for assembling and shaping clathrin-coated pits. *Journal of Cell Biology*, 219.
- CHRISTOFORIDIS, S., MIACZYNSKA, M., ASHMAN, K., WILM, M., ZHAO, L., YIP, S. C., WATERFIELD, M. D., BACKER, J. M. & ZERIAL, M. 1999. Phosphatidylinositol-3-OH kinases are Rab5 effectors. *Nat Cell Biol*, 1, 249-52.
- COLLINS, K. A., BROD, F., SNAITH, R., ULASZEWSKA, M., LONGLEY, R. J., SALMAN, A. M., GILBERT, S. C., SPENCER, A. J., FRANCO, D., BALLOU, W. R. & HILL, A. V. S. 2021. Ultra-low dose immunization and multi-component vaccination strategies enhance protection against malaria in mice. *Sci Rep*, 11, 10792.
- COLLINS, K. A., SNAITH, R., COTTINGHAM, M. G., GILBERT, S. C. & HILL, A. V. S. 2017. Enhancing protective immunity to malaria with a highly immunogenic virus-like particle vaccine. *Sci Rep*, 7, 46621.
- COLLINS, R. N. & ZIMMERBERG, J. 2009. A score for membrane fusion. *Nature*, 459, 1065-1066.
- COLLINS, W. E. & JEFFERY, G. M. 2005. *Plasmodium ovale*: parasite and disease. *Clin Microbiol Rev*, 18, 570-81.
- CONNER, S. D. S., SANDRA L. 2002. Identification of an adaptor-associated kinase, AAK1, as a regulator of clathrin-mediated endocytosis. *Journal of Cell Biology*, 156, 921-929.
- COWLES, C. R., EMR, S. D. & HORAZDOVSKY, B. F. 1994. Mutations in the VPS45 gene, a SEC1 homologue, result in vacuolar protein sorting defects and accumulation of membrane vesicles. *J Cell Sci*, 107 (Pt 12), 3449-59.
- COWMAN, A. F., GALATIS, D. & THOMPSON, J. K. 1994. Selection for mefloquine resistance in *Plasmodium falciparum* is linked to amplification of the pfmdr1 gene and cross-resistance to halofantrine and quinine. *Proc Natl Acad Sci U S A*, 91, 1143-7.
- COX-SINGH, J., DAVIS, T. M. E., LEE, K.-S., SHAMSUL, S. S. G., MATUSOP, A., RATNAM, S., RAHMAN, H. A., CONWAY, D. J. & SINGH, B. 2008. *Plasmodium knowlesi* Malaria in Humans Is Widely Distributed and Potentially Life Threatening. *Clinical Infectious Diseases*, 46, 165-171.
- CRABB, B. S. & COWMAN, A. F. 1996. Characterization of promoters and stable transfection by homologous and nonhomologous recombination in *Plasmodium*

- falciparum*. *Proceedings of the National Academy of Sciences of the United States of America*, 93, 7289-7294.
- CULLEN, P. J. & STEINBERG, F. 2018. To degrade or not to degrade: mechanisms and significance of endocytic recycling. *Nature Reviews Molecular Cell Biology*, 19, 679-696.
- CUNNINGHAM, J., JONES, S., GATTON, M. L., BARNWELL, J. W., CHENG, Q., CHIODINI, P. L., GLENN, J., INCARDONA, S., KOSACK, C., LUCHAVEZ, J., MENARD, D., NHEM, S., OYIBO, W., REES-CHANNER, R. R., GONZALEZ, I. & BELL, D. 2019. A review of the WHO malaria rapid diagnostic test product testing programme (2008–2018): performance, procurement and policy. *Malaria Journal*, 18, 387.
- DALAL, S. & KLEMBA, M. 2015. Amino acid efflux by asexual blood-stage *Plasmodium falciparum* and its utility in interrogating the kinetics of hemoglobin endocytosis and catabolism in vivo. *Mol Biochem Parasitol*, 201, 116-22.
- DATOO, M. S., NATAMA, M. H., SOMÉ, A., TRAORÉ, O., ROUAMBA, T., BELLAMY, D., YAMEOGO, P., VALIA, D., TEGNERI, M., OUEDRAOGO, F., SOMA, R., SAWADOGO, S., SORGHO, F., DERRA, K., ROUAMBA, E., ORINDI, B., RAMOS LOPEZ, F., FLAXMAN, A., CAPPUCCINI, F., KAILATH, R., ELIAS, S., MUKHOPADHYAY, E., NOE, A., CAIRNS, M., LAWRIE, A., ROBERTS, R., VALÉA, I., SORGHO, H., WILLIAMS, N., GLENN, G., FRIES, L., REIMER, J., EWER, K. J., SHALIGRAM, U., HILL, A. V. S. & TINTO, H. 2021. Efficacy of a low-dose candidate malaria vaccine, R21 in adjuvant Matrix-M, with seasonal administration to children in Burkina Faso: a randomised controlled trial. *The Lancet*, 397, 1809-1818.
- DAVID, P. H., HOMMEL, M., MILLER, L. H., UDEINYA, I. J. & OLIGINO, L. D. 1983. Parasite sequestration in *Plasmodium falciparum* malaria: spleen and antibody modulation of cytoadherence of infected erythrocytes. *Proceedings of the National Academy of Sciences*, 80, 5075.
- DAVIDSON, G., CHUA, T. H., COOK, A., SPELDEWINDE, P. & WEINSTEIN, P. 2019. Defining the ecological and evolutionary drivers of *Plasmodium knowlesi* transmission within a multi-scale framework. *Malaria Journal*, 18, 66.
- DAVIS, T. M., KARUNAJEEWA, H. A. & ILETT, K. F. 2005. Artemisinin-based combination therapies for uncomplicated malaria. *Med J Aust*, 182, 181-5.
- DE LEON, J. C., SCHEUMANN, N., BEATTY, W., BECK, J. R., TRAN, J. Q., YAU, C., BRADLEY, P. J., GULL, K., WICKSTEAD, B. & MORRISSETTE, N. S. 2013. A SAS-6-like protein suggests that the Toxoplasma conoid complex evolved from flagellar components. *Eukaryotic cell*, 12, 1009-1019.
- DE NIZ, M., BURDA, P. C., KAISER, G., DEL PORTILLO, H. A., SPIELMANN, T., FRISCHKNECHT, F. & HEUSSLER, V. T. 2017. Progress in imaging methods: insights gained into *Plasmodium* biology. *Nat Rev Microbiol*, 15, 37-54.
- DEMAS, A. R., SHARMA, A. I., WONG, W., EARLY, A. M., REDMOND, S., BOPP, S., NEAFSEY, D. E., VOLKMAN, S. K., HARTL, D. L. & WIRTH, D. F. 2018. Mutations in *Plasmodium falciparum* actin-binding protein coronin confer

- reduced artemisinin susceptibility. *Proc Natl Acad Sci U S A*, 115, 12799-12804.
- DETTMER, J., HONG-HERMESDORF, A., STIERHOF, Y.-D. & SCHUMACHER, K. 2006. Vacuolar H⁺-ATPase activity is required for endocytic and secretory trafficking in Arabidopsis. *The Plant cell*, 18, 715-730.
- DIXON, M. W. A., DEARNLEY, M. K., HANSEN, E., GILBERGER, T. & TILLEY, L. 2012. Shape-shifting gametocytes: how and why does *P. falciparum* go banana-shaped? *Trends in Parasitology*, 28, 471-478.
- DOBBS, K. R. & DENT, A. E. 2016. *Plasmodium* malaria and antimalarial antibodies in the first year of life. *Parasitology*, 143, 129-138.
- DOOLAN, D. L., DOBAÑO, C. & BAIRD, J. K. 2009. Acquired immunity to malaria. *Clinical microbiology reviews*, 22, 13-36.
- DOU, Z., MCGOVERN, O. L., DI CRISTINA, M. & CARRUTHERS, V. B. 2014. Toxoplasma gondii ingests and digests host cytosolic proteins. *MBio*, 5, e01188-14.
- DUFFY, P. E. & PATRICK GORRES, J. 2020. Malaria vaccines since 2000: progress, priorities, products. *NPJ Vaccines*, 5, 48.
- EBINE, K., HIRAI, M., SAKAGUCHI, M., YAHATA, K., KANEKO, O. & SAITONAKANO, Y. 2016. *Plasmodium* Rab5b is secreted to the cytoplasmic face of the tubovesicular network in infected red blood cells together with N-acylated adenylate kinase 2. *Malar J*, 15, 323.
- EGAN, T. J. 2008. Haemozoin formation. *Molecular and Biochemical Parasitology*, 157, 127-136.
- EHLGEN, F., PHAM, J. S., DE KONING-WARD, T., COWMAN, A. F. & RALPH, S. A. 2012. Investigation of the *Plasmodium falciparum* food vacuole through inducible expression of the chloroquine resistance transporter (PfCRT). *PLoS one*, 7, e38781-e38781.
- ELKIN, S. R., LAKODUK, A. M. & SCHMID, S. L. 2016. Endocytic pathways and endosomal trafficking: a primer. *Wiener medizinische Wochenschrift (1946)*, 166, 196-204.
- ELLIOTT, D. A., MCINTOSH, M. T., HOSGOOD, H. D., 3RD, CHEN, S., ZHANG, G., BAEVOVA, P. & JOINER, K. A. 2008. Four distinct pathways of hemoglobin uptake in the malaria parasite *Plasmodium falciparum*. *Proc Natl Acad Sci U S A*, 105, 2463-8.
- EZOUGOU, C. N., BEN-RACHED, F., MOSS, D. K., LIN, J. W., BLACK, S., KNUEPFER, E., GREEN, J. L., KHAN, S. M., MUKHOPADHYAY, A., JANSE, C. J., COPPENS, I., YERA, H., HOLDER, A. A. & LANGSLEY, G. 2014. *Plasmodium falciparum* Rab5b is an N-terminally myristoylated Rab GTPase that is targeted to the parasite's plasma and food vacuole membranes. *PLoS One*, 9, e87695.

- FALADE, C. O., AJAYI, I. O., NSUNGWA-SABIITI, J., SIRIBIÉ, M., DIARRA, A., SERMÉ, L., AFONNE, C., YUSUF, O. B., GANSANE, Z., JEGEDE, A. S., SINGLOVIC, J. & GOMES, M. 2016. Malaria Rapid Diagnostic Tests and Malaria Microscopy for Guiding Malaria Treatment of Uncomplicated Fevers in Nigeria and Prereferral Cases in 3 African Countries. *Clinical Infectious Diseases*, 63, S290-S297.
- FIDOCK, D. A., NOMURA, T., TALLEY, A. K., COOPER, R. A., DZEKUNOV, S. M., FERDIG, M. T., URSOS, L. M., SIDHU, A. B., NAUDÉ, B., DEITSCH, K. W., SU, X. Z., WOOTTON, J. C., ROEPE, P. D. & WELLEMS, T. E. 2000. Mutations in the *P. falciparum* digestive vacuole transmembrane protein PfCRT and evidence for their role in chloroquine resistance. *Mol Cell*, 6, 861-71.
- FITCH, C. D. 1970. *Plasmodium falciparum* in owl monkeys: drug resistance and chloroquine binding capacity. *Science*, 169, 289-90.
- FITCH, C. D. 1986. Antimalarial schizontocides: ferriprotoporphyrin IX interaction hypothesis. *Parasitol Today*, 2, 330-1.
- FLAMMERSFELD, A., LANG, C., FLIEGER, A. & PRADEL, G. 2018. Phospholipases during membrane dynamics in malaria parasites. *Int J Med Microbiol*, 308, 129-141.
- FLEMMING, S. 2015. *Visualization and characterization of endocytic processes in the human Malaria parasite P. falciparum (Welch, 1897)*. Dissertation, University of Hamburg.
- FOTH, B. J. & MCFADDEN, G. I. 2003. The apicoplast: a plastid in *Plasmodium falciparum* and other Apicomplexan parasites. *Int Rev Cytol*, 224, 57-110.
- FRANCIS, S. E., BANERJEE, R. & GOLDBERG, D. E. 1997a. Biosynthesis and maturation of the malaria aspartic hemoglobinases plasmepsins I and II. *J Biol Chem*, 272, 14961-8.
- FRANCIS, S. E., SULLIVAN, D. J., JR. & GOLDBERG, D. E. 1997b. Hemoglobin metabolism in the malaria parasite *Plasmodium falciparum*. *Annu Rev Microbiol*, 51, 97-123.
- FRANKLAND, S., ADISA, A., HORROCKS, P., TARASCHI, T. F., SCHNEIDER, T., ELLIOTT, S. R., ROGERSON, S. J., KNUEPFER, E., COWMAN, A. F., NEWBOLD, C. I. & TILLEY, L. 2006. Delivery of the Malaria Virulence Protein PfEMP1 to the Erythrocyte Surface Requires Cholesterol-Rich Domains. *Eukaryotic Cell*, 5, 849-860.
- FRISCHKNECHT, F. & MATUSCHEWSKI, K. 2017. *Plasmodium* Sporozoite Biology. *Cold Spring Harbor perspectives in medicine*, 7, a025478.
- FUJIWARA, T., YE, S., CASTRO-GOMES, T., WINCHELL, C. G., ANDREWS, N. W., VOTH, D. E., VARUGHESE, K. I., MACKINTOSH, S. G., FENG, Y., PAVLOS, N., NAKAMURA, T., MANOLAGAS, S. C. & ZHAO, H. 2016. PLEKHM1/DEF8/RAB7 complex regulates lysosome positioning and bone homeostasis. *JCI insight*, 1, e86330-e86330.

- GABLER, F., NAM, S.-Z., TILL, S., MIRDITA, M., STEINEGGER, M., SÖDING, J., LUPAS, A. N. & ALVA, V. 2020. Protein Sequence Analysis Using the MPI Bioinformatics Toolkit. *Current Protocols in Bioinformatics*, 72, e108.
- GAMAIN, B., CHÊNE, A., VIEBIG, N. K., TUIKUE NDAM, N. & NIELSEN, M. A. 2021. Progress and Insights Toward an Effective Placental Malaria Vaccine. *Frontiers in Immunology*, 12.
- GARTEN, M., NASAMU, A. S., NILES, J. C., ZIMMERBERG, J., GOLDBERG, D. E. & BECK, J. R. 2018. EXP2 is a nutrient-permeable channel in the vacuolar membrane of *Plasmodium* and is essential for protein export via PTEX. *Nat Microbiol*, 3, 1090-1098.
- GATTON, M. L., CHAUDHRY, A., GLENN, J., WILSON, S., AH, Y., KONG, A., ORD, R. L., REES-CHANNER, R. R., CHIODINI, P., INCARDONA, S., CHENG, Q., AIDOO, M. & CUNNINGHAM, J. 2020. Impact of *Plasmodium falciparum* gene deletions on malaria rapid diagnostic test performance. *Malaria Journal*, 19, 392.
- GENGYO-ANDO, K., KUROYANAGI, H., KOBAYASHI, T., MURATE, M., FUJIMOTO, K., OKABE, S. & MITANI, S. 2007. The SM protein VPS-45 is required for RAB-5-dependent endocytic transport in *Caenorhabditis elegans*. *EMBO Rep*, 8, 152-7.
- GEOGHEGAN, N. D., EVELYN, C., WHITEHEAD, L. W., PASTERNAK, M., MCDONALD, P., TRIGLIA, T., MARAPANA, D. S., KEMPE, D., THOMPSON, J. K., MLODZIANOSKI, M. J., HEALER, J., BIRO, M., COWMAN, A. F. & ROGERS, K. L. 2021. 4D analysis of malaria parasite invasion offers insights into erythrocyte membrane remodeling and parasitophorous vacuole formation. *Nature Communications*, 12, 3620.
- GETHING, P. W., VAN BOECKEL, T. P., SMITH, D. L., GUERRA, C. A., PATIL, A. P., SNOW, R. W. & HAY, S. I. 2011. Modelling the global constraints of temperature on transmission of *Plasmodium falciparum* and *P. vivax*. *Parasit Vectors*, 4, 92.
- GIBSON, D. G., YOUNG, L., CHUANG, R.-Y., VENTER, J. C., HUTCHISON, C. A. & SMITH, H. O. 2009. Enzymatic assembly of DNA molecules up to several hundred kilobases. *Nature Methods*, 6, 343-345.
- GOH, Y. S., MCGUIRE, D. & RÉNIA, L. 2019. Vaccination With Sporozoites: Models and Correlates of Protection. *Front Immunol*, 10, 1227.
- GOLDBERG, D. E. & SLATER, A. F. 1992. The pathway of hemoglobin degradation in malaria parasites. *Parasitol Today*, 8, 280-3.
- GOLDBERG, D. E., SLATER, A. F., BEAVIS, R., CHAIT, B., CERAMI, A. & HENDERSON, G. B. 1991. Hemoglobin degradation in the human malaria pathogen *Plasmodium falciparum*: a catabolic pathway initiated by a specific aspartic protease. *J Exp Med*, 173, 961-9.

- GOLDBERG, D. E., SLATER, A. F., CERAMI, A. & HENDERSON, G. B. 1990. Hemoglobin degradation in the malaria parasite *Plasmodium falciparum*: an ordered process in a unique organelle. *Proc Natl Acad Sci U S A*, 87, 2931-5.
- GOODMAN, C. D., SIREGAR, J. E., MOLLARD, V., VEGA-RODRÍGUEZ, J., SYAFRUDDIN, D., MATSUOKA, H., MATSUZAKI, M., TOYAMA, T., STURM, A., COZIJNSEN, A., JACOBS-LORENA, M., KITA, K., MARZUKI, S. & MCFADDEN, G. I. 2016. Parasites resistant to the antimalarial atovaquone fail to transmit by mosquitoes. *Science*, 352, 349-53.
- GORDON, D. M., MCGOVERN, T. W., KRZYCH, U., COHEN, J. C., SCHNEIDER, I., LACHANCE, R., HEPPNER, D. G., YUAN, G., HOLLINGDALE, M., SLAOU, M. & ET AL. 1995. Safety, immunogenicity, and efficacy of a recombinantly produced *Plasmodium falciparum* circumsporozoite protein-hepatitis B surface antigen subunit vaccine. *J Infect Dis*, 171, 1576-85.
- GOUJON, M., MCWILLIAM, H., LI, W., VALENTIN, F., SQUIZZATO, S., PAERN, J. & LOPEZ, R. 2010. A new bioinformatics analysis tools framework at EMBL–EBI. *Nucleic Acids Research*, 38, W695-W699.
- GRANDE, R., ANTINORI, S., MERONI, L., MENEGON, M. & SEVERINI, C. 2019. A case of *Plasmodium malariae* recurrence: recrudescence or reinfection? *Malaria Journal*, 18, 169.
- GREENWOOD, B. M., FIDOCK, D. A., KYLE, D. E., KAPPE, S. H., ALONSO, P. L., COLLINS, F. H. & DUFFY, P. E. 2008. Malaria: progress, perils, and prospects for eradication. *J Clin Invest*, 118, 1266-76.
- GREGSON, A. & PLOWE, C. V. 2005. Mechanisms of resistance of malaria parasites to antifolates. *Pharmacol Rev*, 57, 117-45.
- GRURING, C., HEIBER, A., KRUSE, F., UNGEFEHR, J., GILBERGER, T. W. & SPIELMANN, T. 2011. Development and host cell modifications of *Plasmodium falciparum* blood stages in four dimensions. *Nat Commun*, 2, 165.
- GULBRANSON, D. R., CRISMAN, L., LEE, M., OUYANG, Y., MENASCHE, B. L., DEMMITT, B. A., WAN, C., NOMURA, T., YE, Y., YU, H. & SHEN, J. 2019. AAGAB Controls AP2 Adaptor Assembly in Clathrin-Mediated Endocytosis. *Developmental Cell*, 50, 436-446.e5.
- HANAHAH, D. 1983. Studies on transformation of *Escherichia coli* with plasmids. *Journal of Molecular Biology*, 166, 557-580.
- HARDING, C. R. & MEISSNER, M. 2014. The inner membrane complex through development of *Toxoplasma gondii* and *Plasmodium*. *Cell Microbiol*, 16, 632-41.
- HARPER, J. M., HUYNH, M. H., COPPENS, I., PARUSSINI, F., MORENO, S. & CARRUTHERS, V. B. 2006. A cleavable propeptide influences *Toxoplasma* infection by facilitating the trafficking and secretion of the TgMIC2-M2AP invasion complex. *Mol Biol Cell*, 17, 4551-63.

- HARUKI, H., NISHIKAWA, J. & LAEMMLI, U. K. 2008. The anchor-away technique: rapid, conditional establishment of yeast mutant phenotypes. *Mol Cell*, 31, 925-32.
- HENDERSON, D. M. & CONNER, S. D. 2007. A Novel AAK1 Splice Variant Functions at Multiple Steps of the Endocytic Pathway. *Molecular Biology of the Cell*, 18, 2698-2706.
- HENRICI, R. C., EDWARDS, R. L., ZOLTNER, M., SCHALKWYK, D. A. V., HART, M. N., MOHRING, F., MOON, R. W., NOFAL, S. D., PATEL, A., FLUECK, C., BAKER, D. A., JOHN, A. R. O., FIELD, M. C., SUTHERLAND, C. J., TILLEY, L. & WELLEMS, T. E. 2020. The *Plasmodium falciparum* Artemisinin Susceptibility-Associated AP-2 Adaptor μ -Subunit is Clathrin Independent and Essential for Schizont Maturation. *mBio*, 11, e02918-19.
- HENRICI, R. C., VAN SCHALKWYK, D. A. & SUTHERLAND, C. J. 2019a. Modification of pfap2mu and pfubp1 Markedly Reduces Ring-Stage Susceptibility of *Plasmodium falciparum* to Artemisinin In Vitro. *Antimicrob Agents Chemother*, 64.
- HENRIQUES, G., HALLETT, R. L., BESHIR, K. B., GADALLA, N. B., JOHNSON, R. E., BURROW, R., VAN SCHALKWYK, D. A., SAWA, P., OMAR, S. A., CLARK, T. G., BOUSEMA, T. & SUTHERLAND, C. J. 2014. Directional Selection at the pfmdr1, pfcr1, pfubp1, and pfap2mu Loci of *Plasmodium falciparum* in Kenyan Children Treated With ACT. *The Journal of Infectious Diseases*, 210, 2001-2008.
- HENRIQUES, G., MARTINELLI, A., RODRIGUES, L., MODRZYNSKA, K., FAWCETT, R., HOUSTON, D. R., BORGES, S. T., D'ALESSANDRO, U., TINTO, H., KAREMA, C., HUNT, P. & CRAVO, P. 2013. Artemisinin resistance in rodent malaria - mutation in the AP2 adaptor μ -chain suggests involvement of endocytosis and membrane protein trafficking. *Malaria Journal*, 12, 118.
- HENRIQUES, G., VAN SCHALKWYK, D. A., BURROW, R., WARHURST, D. C., THOMPSON, E., BAKER, D. A., FIDOCK, D. A., HALLETT, R., FLUECK, C. & SUTHERLAND, C. J. 2015. The μ subunit of *Plasmodium falciparum* clathrin-associated adaptor protein 2 modulates in vitro parasite response to artemisinin and quinine. *Antimicrob Agents Chemother*, 59, 2540-7.
- HINNERS, I. & TOOZE, S. A. 2003. Changing directions: clathrin-mediated transport between the Golgi and endosomes. *Journal of Cell Science*, 116, 763-771.
- HOPP, C. S., KANATANI, S., ARCHER, N. K., MILLER, R. J., LIU, H., CHIOU, K., MILLER, L. S. & SINNIS, P. 2019. Quantitative intravital imaging of *Plasmodium falciparum* sporozoites: A novel platform to test malaria intervention strategies. *bioRxiv*, 716878.
- HORIUCHI, H., LIPPÉ, R., MCBRIDE, H. M., RUBINO, M., WOODMAN, P., STENMARK, H., RYBIN, V., WILM, M., ASHMAN, K., MANN, M. & ZERIAL, M. 1997. A Novel Rab5 GDP/GTP Exchange Factor Complexed to Rabaptin-5 Links Nucleotide Exchange to Effector Recruitment and Function. *Cell*, 90, 1149-1159.

- HOWES, R. E., BATTLE, K. E., MENDIS, K. N., SMITH, D. L., CIBULSKIS, R. E., BAIRD, J. K. & HAY, S. I. 2016. Global Epidemiology of *Plasmodium vivax*. *Am J Trop Med Hyg*, 95, 15-34.
- HOWES, R. E., PATIL, A. P., PIEL, F. B., NYANGIRI, O. A., KABARIA, C. W., GETHING, P. W., ZIMMERMAN, P. A., BARNADAS, C., BEALL, C. M., GEBREMEDHIN, A., MÉNARD, D., WILLIAMS, T. N., WEATHERALL, D. J. & HAY, S. I. 2011. The global distribution of the Duffy blood group. *Nature Communications*, 2, 266.
- HU, Y.-B., DAMMER, E. B., REN, R.-J. & WANG, G. 2015. The endosomal-lysosomal system: from acidification and cargo sorting to neurodegeneration. *Translational Neurodegeneration*, 4, 18.
- HUOTARI, J. & HELENIUS, A. 2011. Endosome maturation. *The EMBO journal*, 30, 3481-3500.
- ILLINGWORTH, J. J., ALANINE, D. G., BROWN, R., MARSHALL, J. M., BARTLETT, H. E., SILK, S. E., LABBÉ, G. M., QUINKERT, D., CHO, J. S., WENDLER, J. P., PATTINSON, D. J., BARFOD, L., DOUGLAS, A. D., SHEA, M. W., WRIGHT, K. E., DE CASSAN, S. C., HIGGINS, M. K. & DRAPER, S. J. 2019. Functional Comparison of Blood-Stage *Plasmodium falciparum* Malaria Vaccine Candidate Antigens. *Frontiers in Immunology*, 10.
- ITSARA, L. S., ZHOU, Y., DO, J., GRIESER, A. M., VAUGHAN, A. M. & GHOSH, A. K. 2018. The Development of Whole Sporozoite Vaccines for *Plasmodium falciparum* Malaria. *Front Immunol*, 9, 2748.
- JACKSON, L. P., KELLY, B. T., MCCOY, A. J., GAFFRY, T., JAMES, L. C., COLLINS, B. M., HÖNING, S., EVANS, P. R. & OWEN, D. J. 2010a. A large-scale conformational change couples membrane recruitment to cargo binding in the AP2 clathrin adaptor complex. *Cell*, 141, 1220-9.
- JACKSON, L. P., KELLY, B. T., MCCOY, A. J., GAFFRY, T., JAMES, L. C., COLLINS, B. M., HÖNING, S., EVANS, P. R. & OWEN, D. J. 2010b. A large-scale conformational change couples membrane recruitment to cargo binding in the AP2 clathrin adaptor complex. *Cell*, 141, 1220-1229.
- JAMIESON, D. J., THEILER, R. N. & RASMUSSEN, S. A. 2006. Emerging infections and pregnancy. *Emerging infectious diseases*, 12, 1638-1643.
- JANOUSKOVEC, J., HORÁK, A., OBORNÍK, M., LUKES, J. & KEELING, P. J. 2010. A common red algal origin of the apicomplexan, dinoflagellate, and heterokont plastids. *Proceedings of the National Academy of Sciences of the United States of America*, 107, 10949-10954.
- JANSE, C. J., VAN DER KLOOSTER, P. F., VAN DER KAAY, H. J., VAN DER PLOEG, M. & OVERDULVE, J. P. 1986. DNA synthesis in *Plasmodium berghei* during asexual and sexual development. *Mol Biochem Parasitol*, 20, 173-82.
- JEGER, J. L. 2020. Endosomes, lysosomes, and the role of endosomal and lysosomal biogenesis in cancer development. *Molecular Biology Reports*, 47, 9801-9810.

- JIN, Y., KEBAIER, C. & VANDERBERG, J. 2007. Direct microscopic quantification of dynamics of *Plasmodium berghei* sporozoite transmission from mosquitoes to mice. *Infection and immunity*, 75, 5532-5539.
- JONSCHER, E. 2018. *Identification of proteins involved in host cell cytosol uptake in the human Malaria parasite Plasmodium falciparum*. Dissertation, University Hamburg.
- JONSCHER, E., FLEMMING, S., SCHMITT, M., SABITZKI, R., REICHARD, N., BIRNBAUM, J., BERGMANN, B., HOHN, K. & SPIELMANN, T. 2019. PfVPS45 Is Required for Host Cell Cytosol Uptake by Malaria Blood Stage Parasites. *Cell Host Microbe*, 25, 166-173.e5.
- JOSEPH, B. B., WANG, Y., EDEEN, P., LAŽETIĆ, V., GRANT, B. D. & FAY, D. S. 2020. Control of clathrin-mediated endocytosis by NIMA family kinases. *PLOS Genetics*, 16, e1008633.
- JOVIC, M., SHARMA, M., RAHAJENG, J. & CAPLAN, S. 2010. The early endosome: a busy sorting station for proteins at the crossroads. *Histology and histopathology*, 25, 99-112.
- JULLIEN, N., GODDARD, I., SELMI-RUBY, S., FINA, J. L., CREMER, H. & HERMAN, J. P. 2007. Conditional transgenesis using Dimerizable Cre (DiCre). *PLoS One*, 2, e1355.
- JULLIEN, N., SAMPIERI, F., ENJALBERT, A. & HERMAN, J. P. 2003. Regulation of Cre recombinase by ligand-induced complementation of inactive fragments. *Nucleic Acids Res*, 31, e131.
- KADLECOVA, Z., SPIELMAN, S. J., LOERKE, D., MOHANAKRISHNAN, A., REED, D. K. & SCHMID, S. L. 2017. Regulation of clathrin-mediated endocytosis by hierarchical allosteric activation of AP2. *J Cell Biol*, 216, 167-179.
- KAMALIDDIN, C., ROMBAUT, D., GUILLOCHON, E., ROYO, J., EZINMEGNON, S., AGBOTA, G., HUGUET, S., GUEMOURI, S., PEIRERA, C., COPPÉE, R., BROUSSARD, C., ALAO, J. M., AUBOUY, A., GUILLONNEAU, F., DELORON, P. & BERTIN, G. I. 2019. From genomic to LC-MS/MS evidence: Analysis of PfEMP1 in Benin malaria cases. *PLoS One*, 14, e0218012.
- KATRIS, N. J., VAN DOOREN, G. G., MCMILLAN, P. J., HANSSSEN, E., TILLEY, L. & WALLER, R. F. 2014. The apical complex provides a regulated gateway for secretion of invasion factors in Toxoplasma. *PLoS pathogens*, 10, e1004074-e1004074.
- KELLY, B. T., GRAHAM, S. C., LISKA, N., DANNHAUSER, P. N., HÖNING, S., UNGEWICKELL, E. J. & OWEN, D. J. 2014. Clathrin adaptors. AP2 controls clathrin polymerization with a membrane-activated switch. *Science (New York, N.Y.)*, 345, 459-463.
- KLAYMAN, D. L., LIN, A. J., ACTON, N., SCOVILL, J. P., HOCH, J. M., MILHOUS, W. K., THEOHARIDES, A. D. & DOBEK, A. S. 1984. Isolation of artemisinin (qinghaosu) from *Artemisia annua* growing in the United States. *J Nat Prod*, 47, 715-7.

- KLEMBA, M., BEATTY, W., GLUZMAN, I. & GOLDBERG, D. E. 2004a. Trafficking of plasmepsin II to the food vacuole of the malaria parasite *Plasmodium falciparum*. *J Cell Biol*, 164, 47-56.
- KLEMBA, M., GLUZMAN, I. & GOLDBERG, D. E. 2004b. A *Plasmodium falciparum* dipeptidyl aminopeptidase I participates in vacuolar hemoglobin degradation. *J Biol Chem*, 279, 43000-7.
- KLONIS, N., CREEK, D. J. & TILLEY, L. 2013. Iron and heme metabolism in *Plasmodium falciparum* and the mechanism of action of artemisinin. *Curr Opin Microbiol*, 16, 722-7.
- KOEPFLI, C., RODRIGUES, P. T., ANTAO, T., ORJUELA-SÁNCHEZ, P., VAN DEN EEDE, P., GAMBOA, D., VAN HONG, N., BENDEZU, J., ERHART, A., BARNADAS, C., RATSIMBASOA, A., MENARD, D., SEVERINI, C., MENEGON, M., NOUR, B. Y. M., KARUNAWEEERA, N., MUELLER, I., FERREIRA, M. U. & FELGER, I. 2015. *Plasmodium vivax* Diversity and Population Structure across Four Continents. *PLOS Neglected Tropical Diseases*, 9, e0003872.
- KOJIN, B. B. & ADELMAN, Z. N. 2019. The Sporozoite's Journey Through the Mosquito: A Critical Examination of Host and Parasite Factors Required for Salivary Gland Invasion. *Frontiers in Ecology and Evolution*, 7.
- KORAM, K. A., ADU, B., OCRAN, J., KARIKARI, Y. S., ADU-AMANKWAH, S., NTIRI, M., ABUAKU, B., DODOO, D., GYAN, B., KRONMANN, K. C. & NKURUMAH, F. 2016. Safety and Immunogenicity of EBA-175 RII-NG Malaria Vaccine Administered Intramuscularly in Semi-Immune Adults: A Phase 1, Double-Blinded Placebo Controlled Dosage Escalation Study. *PLOS ONE*, 11, e0163066.
- KOVTUN, O., DICKSON, V. K., KELLY, B. T., OWEN, D. J. & BRIGGS, J. A. G. 2020. Architecture of the AP2/clathrin coat on the membranes of clathrin-coated vesicles. *Science Advances*, 6, eaba8381.
- KRAI, P., DALAL, S. & KLEMBA, M. 2014. Evidence for a Golgi-to-Endosome Protein Sorting Pathway in *Plasmodium falciparum*. *PLOS ONE*, 9, e89771.
- KREMER, K., KAMIN, D., RITTWEGER, E., WILKES, J., FLAMMER, H., MAHLER, S., HENG, J., TONKIN, C. J., LANGSLEY, G., HELL, S. W., CARRUTHERS, V. B., FERGUSON, D. J. P. & MEISSNER, M. 2013. An Overexpression Screen of *Toxoplasma gondii* Rab-GTPases Reveals Distinct Transport Routes to the Micronemes. *PLOS Pathogens*, 9, e1003213.
- KRUGLIAK, M., ZHANG, J. & GINSBURG, H. 2002. Intraerythrocytic *Plasmodium falciparum* utilizes only a fraction of the amino acids derived from the digestion of host cell cytosol for the biosynthesis of its proteins. *Mol Biochem Parasitol*, 119, 249-56.
- KUCHITSU, Y. & FUKUDA, M. 2018. Revisiting Rab7 Functions in Mammalian Autophagy: Rab7 Knockout Studies. *Cells*, 7, 215.

- KUHN, S. M. & MCCARTHY, A. E. 2006. Paediatric malaria: What do paediatricians need to know? *Paediatrics & child health*, 11, 349-354.
- KURTOVIC, L., ATRE, T., FENG, G., WINES, B. D., CHAN, J.-A., BOYLE, M. J., DREW, D. R., HOGARTH, P. M., FOWKES, F. J. I., BERGMANN-LEITNER, E. S. & BEESON, J. G. 2020. Multifunctional Antibodies Are Induced by the RTS,S Malaria Vaccine and Associated With Protection in a Phase 1/2a Trial. *The Journal of Infectious Diseases*.
- LAEMMLI, U. K. 1970. Cleavage of Structural Proteins during the Assembly of the Head of Bacteriophage T4. *Nature*, 227, 680-685.
- LAISHRAM, D. D., SUTTON, P. L., NANDA, N., SHARMA, V. L., SOBTI, R. C., CARLTON, J. M. & JOSHI, H. 2012. The complexities of malaria disease manifestations with a focus on asymptomatic malaria. *Malaria journal*, 11, 29-29.
- LAMBROS, C. & VANDERBERG, J. P. 1979. Synchronization of *Plasmodium falciparum* Erythrocytic Stages in Culture. *The Journal of Parasitology*, 65, 418-420.
- LAMIKANRA, A. A., BROWN, D., POTOČNIK, A., CASALS-PASCUAL, C., LANGHORNE, J. & ROBERTS, D. J. 2007. Malarial anemia: of mice and men. *Blood*, 110, 18-28.
- LANGEMEYER, L., BORCHERS, A.-C., HERRMANN, E., FÜLLBRUNN, N., HAN, Y., PERZ, A., AUFFARTH, K., KÜMMEL, D. & UNGERMANN, C. 2020. A conserved and regulated mechanism drives endosomal Rab transition. *eLife*, 9, e56090.
- LANGFITT, J. T., MCDERMOTT, M. P., BRIM, R., MBOMA, S., POTCHEN, M. J., KAMPONDENI, S. D., SEYDEL, K. B., SEMRUD-CLIKEMAN, M. & TAYLOR, T. E. 2019. Neurodevelopmental Impairments 1 Year After Cerebral Malaria. *Pediatrics*, 143, e20181026.
- LAURENS, M. B. 2020. RTS,S/AS01 vaccine (Mosquirix™): an overview. *Human vaccines & immunotherapeutics*, 16, 480-489.
- LAZARUS, M. D., SCHNEIDER, T. G. & TARASCHI, T. F. 2008. A new model for hemoglobin ingestion and transport by the human malaria parasite *Plasmodium falciparum*. *J Cell Sci*, 121, 1937-49.
- LEE, W.-C., RUSSELL, B. & RÉNIA, L. 2019. Sticking for a Cause: The *Falciparum* Malaria Parasites Cytoadherence Paradigm. *Frontiers in Immunology*, 10.
- LESKI, T. A., TAITT, C. R., SWARAY, A. G., BANGURA, U., REYNOLDS, N. D., HOLTZ, A., YASUDA, C., LAHAI, J., LAMIN, J. M., BAIO, V., JACOBSEN, K. H., ANSUMANA, R. & STENGER, D. A. 2020. Use of real-time multiplex PCR, malaria rapid diagnostic test and microscopy to investigate the prevalence of *Plasmodium* species among febrile hospital patients in Sierra Leone. *Malaria journal*, 19, 84-84.

- LEUNG, K. F., DACKS, J. B. & FIELD, M. C. 2008. Evolution of the multivesicular body ESCRT machinery; retention across the eukaryotic lineage. *Traffic*, 9, 1698-716.
- LEW, V. L., TIFFERT, T. & GINSBURG, H. 2003. Excess hemoglobin digestion and the osmotic stability of *Plasmodium falciparum*-infected red blood cells. *Blood*, 101, 4189-4194.
- LINGELBACH, K. & JOINER, K. A. 1998. The parasitophorous vacuole membrane surrounding *Plasmodium* and *Toxoplasma*: an unusual compartment in infected cells. *J Cell Sci*, 111 (Pt 11), 1467-75.
- LIU, B., BLANCH, A. J., NAMVAR, A., CARMO, O., TIASH, S., ANDREW, D., HANSEN, E., RAJAGOPAL, V., DIXON, M. W. A. & TILLEY, L. 2019. Multimodal analysis of *Plasmodium knowlesi*-infected erythrocytes reveals large invaginations, swelling of the host cell, and rheological defects. *Cell Microbiol*, 21, e13005.
- LO, E., NGUYEN, K., NGUYEN, J., HEMMING-SCHROEDER, E., XU, J., ETEMESI, H., GITHEKO, A. & YAN, G. 2017. *Plasmodium malariae* Prevalence and csp Gene Diversity, Kenya, 2014 and 2015. *Emerging infectious diseases*, 23, 601-610.
- LOERKE, D., METTLER, M., YARAR, D., JAQAMAN, K., JAQAMAN, H., DANUSER, G. & SCHMID, S. L. 2009. Cargo and dynamin regulate clathrin-coated pit maturation. *PLoS Biol*, 7, e57.
- LOI, M., MÜLLER, A., STEINBACH, K., NIVEN, J., BARREIRA DA SILVA, R., PAUL, P., LIGEON, L.-A., CARUSO, A., ALBRECHT, R. A., BECKER, A. C., ANNAHEIM, N., NOWAG, H., DENGJEL, J., GARCÍA-SASTRE, A., MERKLER, D., MÜNZ, C. & GANNAGÉ, M. 2016. Macroautophagy Proteins Control MHC Class I Levels on Dendritic Cells and Shape Anti-viral CD8⁺ T_H1 Cell Responses. *Cell Reports*, 15, 1076-1087.
- LORD, S. J., VELLE, K. B., MULLINS, R. D. & FRITZ-LAYLIN, L. K. 2020. SuperPlots: Communicating reproducibility and variability in cell biology. *Journal of Cell Biology*, 219.
- MAITLAND, K. 2015. Management of severe paediatric malaria in resource-limited settings. *BMC Medicine*, 13, 42.
- MALLERET, B., CLASER, C., ONG, A. S. M., SUWANARUSK, R., SRIPRAWAT, K., HOWLAND, S. W., RUSSELL, B., NOSTEN, F. & RÉNIA, L. 2011. A rapid and robust tri-color flow cytometry assay for monitoring malaria parasite development. *Scientific Reports*, 1, 118.
- MARAT, A. L. & HAUCKE, V. 2016. Phosphatidylinositol 3-phosphates-at the interface between cell signalling and membrane traffic. *The EMBO journal*, 35, 561-579.
- MARIN-MOGOLLON, C., VAN DE VEGTE-BOLMER, M., VAN GEMERT, G. J., VAN PUL, F. J. A., RAMESAR, J., OTHMAN, A. S., KROEZE, H., MIAO, J., CUI, L., WILLIAMSON, K. C., SAUERWEIN, R. W., JANSE, C. J. & KHAN, S. M. 2018. The *Plasmodium falciparum* male gametocyte protein P230p, a paralog of

- P230, is vital for ookinete formation and mosquito transmission. *Sci Rep*, 8, 14902.
- MARTZOUKOU, O., AMILLIS, S., ZERVAKOU, A., CHRISTOFORIDIS, S. & DIALLINAS, G. 2017. The AP-2 complex has a specialized clathrin-independent role in apical endocytosis and polar growth in fungi. *Elife*, 6.
- MATTE, U. & PASQUALIM, G. 2016. Lysosome: The Story Beyond the Storage. *Journal of Inborn Errors of Metabolism and Screening*, 4, 2326409816679431.
- MATZ, J. M., BECK, J. R. & BLACKMAN, M. J. 2020. The parasitophorous vacuole of the blood-stage malaria parasite. *Nature Reviews Microbiology*, 18, 379-391.
- MAYOR, S. & PAGANO, R. E. 2007. Pathways of clathrin-independent endocytosis. *Nature Reviews Molecular Cell Biology*, 8, 603-612.
- MBANEFO, A. & KUMAR, N. 2020. Evaluation of Malaria Diagnostic Methods as a Key for Successful Control and Elimination Programs. *Tropical medicine and infectious disease*, 5, 102.
- MCCOY, K. D., WELDON, C. T., ANSUMANA, R., LAMIN, J. M., STENGER, D. A., RYAN, S. J., BARDOSH, K., JACOBSEN, K. H. & DINGLASAN, R. R. 2021. Are malaria transmission-blocking vaccines acceptable to high burden communities? Results from a mixed methods study in Bo, Sierra Leone. *Malaria Journal*, 20, 183.
- MCFADDEN, G. I. & YEY, E. 2017. The apicoplast: now you see it, now you don't. *Int J Parasitol*, 47, 137-144.
- MCGOVERN, O. L., RIVERA-CUEVAS, Y. & CARRUTHERS, V. B. 2021. Emerging Mechanisms of Endocytosis in *Toxoplasma gondii*. *Life*, 11, 84.
- MCGOVERN, O. L., RIVERA-CUEVAS, Y., KANNAN, G., NARWOLD, A. J., JR. & CARRUTHERS, V. B. 2018. Intersection of endocytic and exocytic systems in *Toxoplasma gondii*. *Traffic*, 19, 336-353.
- MCLEAN, A. R. D., ATAIDE, R., SIMPSON, J. A., BEESON, J. G. & FOWKES, F. J. I. 2015. Malaria and immunity during pregnancy and postpartum: a tale of two species. *Parasitology*, 142, 999-1015.
- MCMAHON, H. T. & BOUCROT, E. 2015. Membrane curvature at a glance. *Journal of Cell Science*, 128, 1065-1070.
- MENDONÇA, V. R. D. & BARRAL-NETTO, M. 2015. Immunoregulation in human malaria: the challenge of understanding asymptomatic infection. *Memorias do Instituto Oswaldo Cruz*, 110, 945-955.
- MESÉN-RAMÍREZ, P., BERGMANN, B., TRAN, T. T., GARTEN, M., STÄCKER, J., NARANJO-PRADO, I., HÖHN, K., ZIMMERBERG, J. & SPIELMANN, T. 2019. EXP1 is critical for nutrient uptake across the parasitophorous vacuole membrane of malaria parasites. *PLOS Biology*, 17, e3000473.

- METTLEN, M., CHEN, P.-H., SRINIVASAN, S., DANUSER, G. & SCHMID, S. L. 2018. Regulation of Clathrin-Mediated Endocytosis. *Annual Review of Biochemistry*, 87, 871-896.
- MILANI, K. J., SCHNEIDER, T. G. & TARASCHI, T. F. 2015. Defining the morphology and mechanism of the hemoglobin transport pathway in *Plasmodium falciparum*-infected erythrocytes. *Eukaryot Cell*, 14, 415-26.
- MILLS, I. G., JONES, A. T. & CLAGUE, M. J. 1998. Involvement of the endosomal autoantigen EEA1 in homotypic fusion of early endosomes. *Curr Biol*, 8, 881-4.
- MILNER, D. A., JR. 2018. Malaria Pathogenesis. *Cold Spring Harbor perspectives in medicine*, 8, a025569.
- MISHRA, A., EATHIRAJ, S., CORVERA, S. & LAMBRIGHT, D. G. 2010. Structural basis for Rab GTPase recognition and endosome tethering by the C₂H₂ zinc finger of Early Endosomal Autoantigen 1 (EEA1). *Proceedings of the National Academy of Sciences*, 107, 10866-10871.
- MOHAMMADKHANI, M., KHANJANI, N., BAKHTIARI, B. & SHEIKHZADEH, K. 2016. The relation between climatic factors and malaria incidence in Kerman, South East of Iran. *Parasite Epidemiology and Control*, 1, 205-210.
- MOORE, R. B., OBORNÍK, M., JANOUSKOVEC, J., CHRUDIMSKÝ, T., VANCOVÁ, M., GREEN, D. H., WRIGHT, S. W., DAVIES, N. W., BOLCH, C. J., HEIMANN, K., SLAPETA, J., HOEGH-GULDBERG, O., LOGSDON, J. M. & CARTER, D. A. 2008. A photosynthetic alveolate closely related to apicomplexan parasites. *Nature*, 451, 959-63.
- MOTA, M. M., PRADEL, G., VANDERBERG, J. P., HAFALLA, J. C., FREVERT, U., NUSSENZWEIG, R. S., NUSSENZWEIG, V. & RODRÍGUEZ, A. 2001. Migration of *Plasmodium* sporozoites through cells before infection. *Science*, 291, 141-4.
- MOUSA, A., AL-TAIAR, A., ANSTEY, N. M., BADAUT, C., BARBER, B. E., BASSAT, Q., CHALLENGER, J. D., CUNNINGTON, A. J., DATTA, D., DRAKELEY, C., GHANI, A. C., GORDEUK, V. R., GRIGG, M. J., HUGO, P., JOHN, C. C., MAYOR, A., MIGOT-NABIAS, F., OPOKA, R. O., PASVOL, G., REES, C., REYBURN, H., RILEY, E. M., SHAH, B. N., SITEO, A., SUTHERLAND, C. J., THUMA, P. E., UNGER, S. A., VIWAMI, F., WALTHER, M., WHITTY, C. J. M., WILLIAM, T. & OKELL, L. C. 2020. The impact of delayed treatment of uncomplicated *P. falciparum* malaria on progression to severe malaria: A systematic review and a pooled multicentre individual-patient meta-analysis. *PLoS Med*, 17, e1003359.
- MUELLER, I., GALINSKI, M. R., BAIRD, J. K., CARLTON, J. M., KOCHAR, D. K., ALONSO, P. L. & DEL PORTILLO, H. A. 2009. Key gaps in the knowledge of *Plasmodium vivax*, a neglected human malaria parasite. *Lancet Infect Dis*, 9, 555-66.
- MULLARD, A. 2015. EMA approves first ever malaria vaccine. *Nature Reviews Drug Discovery*, 14, 593-593.

- MURPHY, S. C., FERNANDEZ-POL, S., CHUNG, P. H., PRASANNA MURTHY, S. N., MILNE, S. B., SALOMAO, M., BROWN, H. A., LOMASNEY, J. W., MOHANDAS, N. & HALDAR, K. 2007. Cytoplasmic remodeling of erythrocyte raft lipids during infection by the human malaria parasite *Plasmodium falciparum*. *Blood*, 110, 2132-2139.
- MURRAY, J. T., PANARETOU, C., STENMARK, H., MIACZYNSKA, M. & BACKER, J. M. 2002. Role of Rab5 in the recruitment of hVps34/p150 to the early endosome. *Traffic*, 3, 416-27.
- MWAKINGWE-OMARI, A., HEALY, S. A., LANE, J., COOK, D. M., KALHORI, S., WYATT, C., KOLLURI, A., MARTE-SALCEDO, O., IMERU, A., NASON, M., DING, L. K., DECEDERFELT, H., DUAN, J., NEAL, J., RAITEN, J., LEE, G., HUME, J. C. C., JEON, J. E., IKPEAMA, I., KC, N., CHAKRAVARTY, S., MURSHEDKAR, T., CHURCH, L. W. P., MANOJ, A., GUNASEKERA, A., ANDERSON, C., MURPHY, S. C., MARCH, S., BHATIA, S. N., JAMES, E. R., BILLINGSLEY, P. F., SIM, B. K. L., RICHIE, T. L., ZAIDI, I., HOFFMAN, S. L. & DUFFY, P. E. 2021. Two chemoattenuated PfSPZ malaria vaccines induce sterile hepatic immunity. *Nature*, 595, 289-294.
- NARANJO PRADO, I. 2020. *Quest for factors involved in the extraction of transmembrane proteins from the PPM to the PVM and the effect of jamming PTEX on PfEMP1 export in Plasmodium falciparum*. University of Hamburg.
- NDWIGA, L., OSOTI, V., OCHWEDO, K. O., WAMAE, K., BEJON, P., RAYNER, J. C., GITHINJI, G. & OCHOLA-OYIER, L. I. 2021. The *Plasmodium falciparum* Rh5 invasion protein complex reveals an excess of rare variant mutations. *Malaria Journal*, 20, 278.
- NEILL, U. S. 2011. From branch to bedside: Youyou Tu is awarded the 2011 Lasker-DeBakey Clinical Medical Research Award for discovering artemisinin as a treatment for malaria. *J Clin Invest*, 121, 3768-73.
- NEVIN, W. D. & DACKS, J. B. 2009. Repeated secondary loss of adaptin complex genes in the Apicomplexa. *Parasitol Int*, 58, 86-94.
- NIELSEN, E., CHRISTOFORIDIS, S., UTTENWEILER-JOSEPH, S., MIACZYNSKA, M., DEWITTE, F., WILM, M., HOFACK, B. & ZERIAL, M. 2000. Rabenosyn-5, a novel Rab5 effector, is complexed with hVPS45 and recruited to endosomes through a FYVE finger domain. *J Cell Biol*, 151, 601-12.
- OFORI, M. F., LAMPTEY, H., DICKSON, E. K., KYEI-BAAFOUR, E. & HVIID, L. 2018. Etiology of Placental *Plasmodium falciparum* Malaria in African Women. *The Journal of Infectious Diseases*, 218, 277-281.
- OLERIBE, O. O., OSITA-OLERIBE, P., EKOM, E., OFEM, O., IGWESI, C., CHIGOZIE, O. G., EKWEGHARIRI, M., IYALLA, G. & TAYLOR-ROBINSON, S. D. 2017. Is malaria over-diagnosed? A world malaria day 2017 experience by Excellence and Friends Management Care Centre (EFMC) and partners, Abuja Nigeria. *Pan Afr Med J*, 28, 273.

- ORESEGUN, D. R., DANESHVAR, C. & COX-SINGH, J. 2021. *Plasmodium knowlesi* – Clinical Isolate Genome Sequencing to Inform Translational Same-Species Model System for Severe Malaria. *Frontiers in Cellular and Infection Microbiology*, 11.
- OWEN, D. J., VALLIS, Y., PEARSE, B. M., MCMAHON, H. T. & EVANS, P. R. 2000. The structure and function of the beta 2-adaptin appendage domain. *The EMBO journal*, 19, 4216-4227.
- PAIN, A., FERGUSON, D. J. P., KAI, O., URBAN, B. C., LOWE, B., MARSH, K. & ROBERTS, D. J. 2001. Platelet-mediated clumping of *Plasmodium falciparum*-infected erythrocytes is a common adhesive phenotype and is associated with severe malaria. *Proceedings of the National Academy of Sciences*, 98, 1805.
- PARK, S. Y. & GUO, X. 2014. Adaptor protein complexes and intracellular transport. *Bioscience reports*, 34, e00123.
- PARTLOW, E. A., BAKER, R. W., BEACHAM, G. M., CHAPPIE, J. S., LESCHZINER, A. E. & HOLLOPETER, G. 2019. A structural mechanism for phosphorylation-dependent inactivation of the AP2 complex. *eLife*, 8, e50003.
- PARUSSINI, F., COPPENS, I., SHAH, P. P., DIAMOND, S. L. & CARRUTHERS, V. B. 2010. Cathepsin L occupies a vacuolar compartment and is a protein maturase within the endo/exocytic system of *Toxoplasma gondii*. *Mol Microbiol*, 76, 1340-57.
- PAYNE, D. 1987. Spread of chloroquine resistance in *Plasmodium falciparum*. *Parasitol Today*, 3, 241-6.
- PAYNE, R. O., MILNE, K. H., ELIAS, S. C., EDWARDS, N. J., DOUGLAS, A. D., BROWN, R. E., SILK, S. E., BISWAS, S., MIURA, K., ROBERTS, R., RAMPLING, T. W., VENKATRAMAN, N., HODGSON, S. H., LABBÉ, G. M., HALSTEAD, F. D., POULTON, I. D., NUGENT, F. L., DE GRAAF, H., SUKHTANKAR, P., WILLIAMS, N. C., OCKENHOUSE, C. F., KATHCART, A. K., QABAR, A. N., WATERS, N. C., SOISSON, L. A., BIRKETT, A. J., COOKE, G. S., FAUST, S. N., WOODS, C., IVINSON, K., MCCARTHY, J. S., DIGGS, C. L., VEKEMANS, J., LONG, C. A., HILL, A. V. S., LAWRIE, A. M., DUTTA, S. & DRAPER, S. J. 2016. Demonstration of the Blood-Stage *Plasmodium falciparum* Controlled Human Malaria Infection Model to Assess Efficacy of the *P. falciparum* Apical Membrane Antigen 1 Vaccine, FMP2.1/AS01. *The Journal of Infectious Diseases*, 213, 1743-1751.
- PAYNE, R. O., SILK, S. E., ELIAS, S. C., MIURA, K., DIOUF, A., GALAWAY, F., DE GRAAF, H., BRENDISH, N. J., POULTON, I. D., GRIFFITHS, O. J., EDWARDS, N. J., JIN, J., LABBÉ, G. M., ALANINE, D. G., SIANI, L., DI MARCO, S., ROBERTS, R., GREEN, N., BERRIE, E., ISHIZUKA, A. S., NIELSEN, C. M., BARDELLI, M., PARTEY, F. D., OFORI, M. F., BARFOD, L., WAMBUA, J., MURUNGI, L. M., OSIER, F. H., BISWAS, S., MCCARTHY, J. S., MINASSIAN, A. M., ASHFIELD, R., VIEBIG, N. K., NUGENT, F. L., DOUGLAS, A. D., VEKEMANS, J., WRIGHT, G. J., FAUST, S. N., HILL, A. V., LONG, C. A., LAWRIE, A. M. & DRAPER, S. J. 2017. Human vaccination against RH5

- induces neutralizing antimalarial antibodies that inhibit RH5 invasion complex interactions. *JCI insight*, 2, e96381.
- PERKINS, D. J., WERE, T., DAVENPORT, G. C., KEMPAIAH, P., HITTNER, J. B. & ONG'ECHA, J. M. 2011. Severe malarial anemia: innate immunity and pathogenesis. *International journal of biological sciences*, 7, 1427-1442.
- PFEFFER, S. R. 2013. Rab GTPase regulation of membrane identity. *Current opinion in cell biology*, 25, 414-419.
- PHILLIPS, M. A., BURROWS, J. N., MANYANDO, C., VAN HUIJSDUIJNEN, R. H., VAN VOORHIS, W. C. & WELLS, T. N. C. 2017. Malaria. *Nature Reviews Disease Primers*, 3, 17050.
- PIEPERHOFF, M. S., SCHMITT, M., FERGUSON, D. J. & MEISSNER, M. 2013. The role of clathrin in post-Golgi trafficking in *Toxoplasma gondii*. *PLoS One*, 8, e77620.
- PORTMAN, N., FOSTER, C., WALKER, G. & ŠLAPETA, J. 2014. Evidence of intraflagellar transport and apical complex formation in a free-living relative of the apicomplexa. *Eukaryotic cell*, 13, 10-20.
- PRUDÊNCIO, M. & MOTA, M. M. 2007. To migrate or to invade: those are the options. *Cell Host Microbe*, 2, 286-8.
- QUEVILLON, E., SPIELMANN, T., BRAHIMI, K., CHATTOPADHYAY, D., YERAMIAN, E. & LANGSLEY, G. 2003. The *Plasmodium falciparum* family of Rab GTPases. *Gene*, 306, 13-25.
- RAIBORG, C., BREMNES, B., MEHLUM, A., GILLOOLY, D. J., D'ARRIGO, A., STANG, E. & STENMARK, H. 2001. FYVE and coiled-coil domains determine the specific localisation of Hrs to early endosomes. *J Cell Sci*, 114, 2255-63.
- RAJA, A. I., BRICKLEY, E. B., TAAFFE, J., TON, T., ZHAO, Z., BOCK, K. W., ORR-GONZALEZ, S., THOMAS, M. L., LAMBERT, L. E., MOORE, I. N. & DUFFY, P. E. 2019. A primate model of severe malarial anaemia: a comparative pathogenesis study. *Scientific Reports*, 9, 18965.
- RENNICK, J. J., JOHNSTON, A. P. R. & PARTON, R. G. 2021. Key principles and methods for studying the endocytosis of biological and nanoparticle therapeutics. *Nature Nanotechnology*, 16, 266-276.
- RICHTER, J., FRANKEN, G., MEHLHORN, H., LABISCH, A. & HÄUSSINGER, D. 2010. What is the evidence for the existence of *Plasmodium ovale* hypnozoites? *Parasitol Res*, 107, 1285-90.
- RINK, J., GHIGO, E., KALAIIDZIDIS, Y. & ZERIAL, M. 2005. Rab Conversion as a Mechanism of Progression from Early to Late Endosomes. *Cell*, 122, 735-749.
- ROBINSON, M. S., SAHLENDER, D. A. & FOSTER, S. D. 2010. Rapid inactivation of proteins by rapamycin-induced rerouting to mitochondria. *Dev Cell*, 18, 324-31.

- ROCAMORA, F., ZHU, L., LIONG, K. Y., DONDORP, A., MIOTTO, O., MOK, S. & BOZDECH, Z. 2018. Oxidative stress and protein damage responses mediate artemisinin resistance in malaria parasites. *PLOS Pathogens*, 14, e1006930.
- ROSENBERG, R., WIRTZ, R. A., SCHNEIDER, I. & BURGE, R. 1990. An estimation of the number of malaria sporozoites ejected by a feeding mosquito. *Trans R Soc Trop Med Hyg*, 84, 209-12.
- ROUX, K. J., KIM, D. I., RAIDA, M. & BURKE, B. 2012. A promiscuous biotin ligase fusion protein identifies proximal and interacting proteins in mammalian cells. *The Journal of cell biology*, 196, 801-810.
- RTS, S. C. T. P. 2015. Efficacy and safety of RTS,S/AS01 malaria vaccine with or without a booster dose in infants and children in Africa: final results of a phase 3, individually randomised, controlled trial. *Lancet*, 386, 31-45.
- SABITZKI, R., SPIELMANN, T., GRAS, S. & MEISSNER, M. 2020. Endocytosis in *Plasmodium* and *Toxoplasma* Parasites. *Trends Parasitol*, 36, 520-532.
- SAGARA, I., DICKO, A., ELLIS, R. D., FAY, M. P., DIAWARA, S. I., ASSADOU, M. H., SISSOKO, M. S., KONE, M., DIALLO, A. I., SAYE, R., GUINDO, M. A., KANTE, O., NIAMBELE, M. B., MIURA, K., MULLEN, G. E. D., PIERCE, M., MARTIN, L. B., DOLO, A., DIALLO, D. A., DOUMBO, O. K., MILLER, L. H. & SAUL, A. 2009. A randomized controlled phase 2 trial of the blood stage AMA1-C1/Alhydrogel malaria vaccine in children in Mali. *Vaccine*, 27, 3090-3098.
- SAHLY, H. M. E., PATEL, S. M., ATMAR, R. L., LANFORD, T. A., DUBE, T., THOMPSON, D., SIM, B. K. L., LONG, C. & KEITEL, W. A. 2010. Safety and Immunogenicity of a Recombinant Nonglycosylated Erythrocyte Binding Antigen 175 Region II Malaria Vaccine in Healthy Adults Living in an Area Where Malaria Is Not Endemic. *Clinical and Vaccine Immunology*, 17, 1552-1559.
- SALA, K. A., ANGRISANO, F., DA, D. F., TAYLOR, I. J., CHURCHER, T. S. & BLAGBOROUGH, A. M. 2018. Immunization with Transgenic Rodent Malaria Parasites Expressing Pfs25 Induces Potent Transmission-Blocking Activity. *Scientific reports*, 8, 1573-1573.
- SALAMANCA, D. R., GÓMEZ, M., CAMARGO, A., CUY-CHAPARRO, L., MOLINA-FRANKY, J., REYES, C., PATARROYO, M. A. & PATARROYO, M. E. 2019. *Plasmodium falciparum* Blood Stage Antimalarial Vaccines: An Analysis of Ongoing Clinical Trials and New Perspectives Related to Synthetic Vaccines. *Frontiers in Microbiology*, 10.
- SANGARE, L. O., ALAYI, T. D., WESTERMANN, B., HOVASSE, A., SINDIKUBWABO, F., CALLEBAUT, I., WERKMEISTER, E., LAFONT, F., SLOMIANNY, C., HAKIMI, M. A., VAN DORSSELAER, A., SCHAEFFER-REISS, C. & TOMAVO, S. 2016. Unconventional endosome-like compartment and retromer complex in *Toxoplasma gondii* govern parasite integrity and host infection. *Nat Commun*, 7, 11191.
- SCHIESS, N., VILLABONA-RUEDA, A., COTTIER, K. E., HUETHER, K., CHIPETA, J. & STINS, M. F. 2020. Pathophysiology and neurologic sequelae of cerebral malaria. *Malar J*, 19, 266.

- SCHMITT, M. 2020. *Functional investigation of unknown malaria proteins in the human malaria parasite Plasmodium falciparum*. Dissertation, University of Hamburg.
- SCHULZE, J., KWIATKOWSKI, M., BORNER, J., SCHLÜTER, H., BRUCHHAUS, I., BURMESTER, T., SPIELMANN, T. & PICK, C. 2015. The *Plasmodium falciparum* exportome contains non-canonical PEXEL/HT proteins. *Molecular Microbiology*, 97, 301-314.
- SHARMA, L. & SHUKLA, G. 2017. Placental Malaria: A New Insight into the Pathophysiology. *Frontiers in medicine*, 4, 117-117.
- SHERMAN, I. W. 1977. Amino acid metabolism and protein synthesis in malarial parasites. *Bull World Health Organ*, 55, 265-76.
- SIDDIQUI, A. A., SAHA, D., IQBAL, M. S., SAHA, S. J., SARKAR, S., BANERJEE, C., NAG, S., MAZUMDER, S., DE, R., PRAMANIK, S., DEBSHARMA, S. & BANDYOPADHYAY, U. 2020. Rab7 of *Plasmodium falciparum* is involved in its retromer complex assembly near the digestive vacuole. *Biochim Biophys Acta Gen Subj*, 1864, 129656.
- SIDHU, A. B. S., UHLEMANN, A.-C., VALDERRAMOS, S. G., VALDERRAMOS, J.-C., KRISHNA, S. & FIDOCK, D. A. 2006. Decreasing pfmdr1 Copy Number in *Plasmodium falciparum* Malaria Heightens Susceptibility to Mefloquine, Lumefantrine, Halofantrine, Quinine, and Artemisinin. *The Journal of Infectious Diseases*, 194, 528-535.
- SIEVERS, F., WILM, A., DINEEN, D., GIBSON, T. J., KARPLUS, K., LI, W., LOPEZ, R., MCWILLIAM, H., REMMERT, M., SÖDING, J., THOMPSON, J. D. & HIGGINS, D. G. 2011. Fast, scalable generation of high-quality protein multiple sequence alignments using Clustal Omega. *Molecular Systems Biology*, 7, 539.
- SIJWALI, P. S. & ROSENTHAL, P. J. 2004. Gene disruption confirms a critical role for the cysteine protease falcipain-2 in hemoglobin hydrolysis by *Plasmodium falciparum*. *Proc Natl Acad Sci U S A*, 101, 4384-9.
- SINGH, S. K., THRANE, S., CHOURASIA, B. K., TELEN, K., GRAUMANS, W., STOTER, R., VAN GEMERT, G. J., VAN DE VEGTE-BOLMER, M. G., NIELSEN, M. A., SALANTI, A., SANDER, A. F., SAUERWEIN, R. W., JORE, M. M. & THEISEN, M. 2019. Pfs230 and Pfs48/45 Fusion Proteins Elicit Strong Transmission-Blocking Antibody Responses Against *Plasmodium falciparum*. *Front Immunol*, 10, 1256.
- SIRIMA, S. B., TIONO, A. B., OUÉDRAOGO, A., DIARRA, A., OUÉDRAOGO, A. L., YARO, J. B., OUÉDRAOGO, E., GANSANÉ, A., BOUGOUMA, E. C., KONATÉ, A. T., KABORÉ, Y., TRAORÉ, A., ROMA, C., SOULAMA, I., LUTY, A. J. F., COUSENS, S. & NÉBIÉ, I. 2009. Safety and Immunogenicity of the Malaria Vaccine Candidate MSP3 Long Synthetic Peptide in 12–24 Months-Old Burkinabe Children. *PLOS ONE*, 4, e7549.
- SLATER, H. C., ROSS, A., FELGER, I., HOFMANN, N. E., ROBINSON, L., COOK, J., GONÇALVES, B. P., BJÖRKMAN, A., OUEDRAOGO, A. L., MORRIS, U., MSELLEM, M., KOEPFLI, C., MUELLER, I., TADESSE, F., GADISA, E., DAS, S., DOMINGO, G., KAPULU, M., MIDEGA, J., OWUSU-AGYEI, S., NABET, C.,

- PIARROUX, R., DOUMBO, O., DOUMBO, S. N., KORAM, K., LUCCHI, N., UDHAYAKUMAR, V., MOSHA, J., TIONO, A., CHANDRAMOHAN, D., GOSLING, R., MWINGIRA, F., SAUERWEIN, R., PAUL, R., RILEY, E. M., WHITE, N. J., NOSTEN, F., IMWONG, M., BOUSEMA, T., DRAKELEY, C. & OKELL, L. C. 2019. The temporal dynamics and infectiousness of subpatent *Plasmodium falciparum* infections in relation to parasite density. *Nature Communications*, 10, 1433.
- SPIELMANN, T., MONTAGNA, G. N., HECHT, L. & MATUSCHEWSKI, K. 2012. Molecular make-up of the *Plasmodium* parasitophorous vacuolar membrane. *International Journal of Medical Microbiology*, 302, 179-186.
- STÄCKER, J. 2021. *Functional analysis of trophozoite- and schizont exported proteins of the human malaria parasite Plasmodium falciparum (Welch 1897)*. University of Hamburg.
- STRAIMER, J., GNÄDIG, N. F., WITKOWSKI, B., AMARATUNGA, C., DURU, V., RAMADANI, A. P., DACHEUX, M., KHIM, N., ZHANG, L., LAM, S., GREGORY, P. D., URNOV, F. D., MERCEREAU-PUJALON, O., BENOIT-VICAL, F., FAIRHURST, R. M., MÉNARD, D. & FIDOCK, D. A. 2015. K13-propeller mutations confer artemisinin resistance in *Plasmodium falciparum* clinical isolates. *Science*, 347, 428-431.
- STROUPE, C. 2018. This Is the End: Regulation of Rab7 Nucleotide Binding in Endolysosomal Trafficking and Autophagy. *Frontiers in Cell and Developmental Biology*, 6.
- STROUPE, C. & BRUNGER, A. T. 2000. Crystal Structures of a Rab Protein in its Inactive and Active Conformations. *Journal of Molecular Biology*, 304, 585-598.
- STRUCK, N. S., DE SOUZA DIAS, S., LANGER, C., MARTI, M., PEARCE, J. A., COWMAN, A. F. & GILBERGER, T. W. 2005. Re-defining the Golgi complex in *Plasmodium falciparum* using the novel Golgi marker PfGRASP. *J Cell Sci*, 118, 5603-13.
- STURM, A., AMINO, R., VAN DE SAND, C., REGEN, T., RETZLAFF, S., RENNENBERG, A., KRUEGER, A., POLLOK, J. M., MENARD, R. & HEUSSLER, V. T. 2006. Manipulation of host hepatocytes by the malaria parasite for delivery into liver sinusoids. *Science*, 313, 1287-90.
- SÜDHOF, T. C. & ROTHMAN, J. E. 2009. Membrane fusion: grappling with SNARE and SM proteins. *Science*, 323, 474-7.
- SULLIVAN, D. J., JR., GLUZMAN, I. Y., RUSSELL, D. G. & GOLDBERG, D. E. 1996. On the molecular mechanism of chloroquine's antimalarial action. *Proc Natl Acad Sci U S A*, 93, 11865-70.
- TAKU, I., HIRAI, T., MAKIUCHI, T., SHINZAWA, N., IWANAGA, S., ANNOURA, T., NAGAMUNE, K., NOZAKI, T. & SAITO-NAKANO, Y. 2021. Rab5b-Associated Arf1 GTPase Regulates Export of N-Myristoylated Adenylate Kinase 2 From the Endoplasmic Reticulum in *Plasmodium falciparum*. *Frontiers in Cellular and Infection Microbiology*, 10.

- TANGPUKDEE, N., DUANGDEE, C., WILAIRATANA, P. & KRUDSOOD, S. 2009. Malaria diagnosis: a brief review. *The Korean journal of parasitology*, 47, 93-102.
- TAWK, L., CHICANNE, G., DUBREMETZ, J.-F., RICHARD, V., PAYRASTRE, B., VIAL, H. J., ROY, C. & WENGELNIK, K. 2010a. Phosphatidylinositol 3-phosphate, an essential lipid in *Plasmodium*, localizes to the food vacuole membrane and the apicoplast. *Eukaryotic cell*, 9, 1519-1530.
- TIAN, J.-H., PATEL, N., HAUPT, R., ZHOU, H., WESTON, S., HAMMOND, H., LOGUE, J., PORTNOFF, A. D., NORTON, J., GUEBRE-XABIER, M., ZHOU, B., JACOBSON, K., MACIEJEWSKI, S., KHATOON, R., WISNIEWSKA, M., MOFFITT, W., KLUEPFEL-STAHN, S., EKECHUKWU, B., PAPIN, J., BODDAPATI, S., JASON WONG, C., PIEDRA, P. A., FRIEMAN, M. B., MASSARE, M. J., FRIES, L., BENGTSSON, K. L., STERTMAN, L., ELLINGSWORTH, L., GLENN, G. & SMITH, G. 2021. SARS-CoV-2 spike glycoprotein vaccine candidate NVX-CoV2373 immunogenicity in baboons and protection in mice. *Nature Communications*, 12, 372.
- TIAN, Y., CHANG, J. C., FAN, E. Y., FLAJOLET, M. & GREENGARD, P. 2013. Adaptor complex AP2/PICALM, through interaction with LC3, targets Alzheimer's APP-CTF for terminal degradation via autophagy. *Proceedings of the National Academy of Sciences*, 110, 17071-17076.
- TOMAVO, S., FORTIER, B., SOETE, M., ANSEL, C., CAMUS, D. & DUBREMETZ, J. F. 1991. Characterization of bradyzoite-specific antigens of *Toxoplasma gondii*. *Infect Immun*, 59, 3750-3.
- TOMAVO, S., SLOMIANNY, C., MEISSNER, M. & CARRUTHERS, V. B. 2013a. Protein Trafficking through the Endosomal System Prepares Intracellular Parasites for a Home Invasion. *PLOS Pathogens*, 9, e1003629.
- TOMLINS, A. M., BEN-RACHED, F., WILLIAMS, R. A., PROTO, W. R., COPPENS, I., RUCH, U., GILBERGER, T. W., COOMBS, G. H., MOTTRAM, J. C., MÜLLER, S. & LANGSLEY, G. 2013. *Plasmodium falciparum* ATG8 implicated in both autophagy and apicoplast formation. *Autophagy*, 9, 1540-52.
- TOMLINSON, A., SEMBLAT, J.-P., GAMAIN, B. & CHÊNE, A. 2021. VAR2CSA-Mediated Host Defense Evasion of *Plasmodium falciparum* Infected Erythrocytes in Placental Malaria. *Frontiers in Immunology*, 11.
- TONKIN, C. J., VAN DOOREN, G. G., SPURCK, T. P., STRUCK, N. S., GOOD, R. T., HANDMAN, E., COWMAN, A. F. & MCFADDEN, G. I. 2004. Localization of organellar proteins in *Plasmodium falciparum* using a novel set of transfection vectors and a new immunofluorescence fixation method. *Mol Biochem Parasitol*, 137, 13-21.
- TRAGER, W. & JENSEN, J. B. 1976. Human malaria parasites in continuous culture. *Science*, 193, 673-5.
- TRAMPUZ, A., JEREB, M., MUZLOVIC, I. & PRABHU, R. M. 2003. Clinical review: Severe malaria. *Crit Care*, 7, 315-23.

- TRAUB, L. M. & BONIFACINO, J. S. 2013. Cargo recognition in clathrin-mediated endocytosis. *Cold Spring Harbor perspectives in biology*, 5, a016790-a016790.
- TURNER, L., LAVSTSEN, T., BERGER, S. S., WANG, C. W., PETERSEN, J. E., AVRIL, M., BRAZIER, A. J., FREETH, J., JESPERSEN, J. S., NIELSEN, M. A., MAGISTRADO, P., LUSINGU, J., SMITH, J. D., HIGGINS, M. K. & THEANDER, T. G. 2013. Severe malaria is associated with parasite binding to endothelial protein C receptor. *Nature*, 498, 502-5.
- VAN DIJK, M. R., JANSE, C. J., THOMPSON, J., WATERS, A. P., BRAKS, J. A., DODEMONT, H. J., STUNNENBERG, H. G., VAN GEMERT, G. J., SAUERWEIN, R. W. & ELING, W. 2001. A central role for P48/45 in malaria parasite male gamete fertility. *Cell*, 104, 153-64.
- VAN DOOREN, G. G., MARTI, M., TONKIN, C. J., STIMMLER, L. M., COWMAN, A. F. & MCFADDEN, G. I. 2005. Development of the endoplasmic reticulum, mitochondrion and apicoplast during the asexual life cycle of *Plasmodium falciparum*. *Mol Microbiol*, 57, 405-19.
- VAN DOOREN, G. G. & STRIEPEN, B. 2013. The algal past and parasite present of the apicoplast. *Annu Rev Microbiol*, 67, 271-89.
- VANLANDINGHAM, P. A. & CERESA, B. P. 2009. Rab7 regulates late endocytic trafficking downstream of multivesicular body biogenesis and cargo sequestration. *J Biol Chem*, 284, 12110-24.
- VENUGOPAL, K., HENTZSCHEL, F., VALKIŪNAS, G. & MARTI, M. 2020. *Plasmodium* asexual growth and sexual development in the haematopoietic niche of the host. *Nat Rev Microbiol*, 18, 177-189.
- VOSS, T. S., MINI, T., JENOE, P. & BECK, H. P. 2002. *Plasmodium falciparum* possesses a cell cycle-regulated short type replication protein A large subunit encoded by an unusual transcript. *J Biol Chem*, 277, 17493-501.
- WANG, C., ZHAO, T., LI, Y., HUANG, G., WHITE, M. A. & GAO, J. 2017. Investigation of endosome and lysosome biology by ultra pH-sensitive nanoprobe. *Advanced Drug Delivery Reviews*, 113, 87-96.
- WANG, W. F. & ZHANG, Y. L. 2020. PfSWIB, a potential chromatin regulator for var gene regulation and parasite development in *Plasmodium falciparum*. *Parasit Vectors*, 13, 48.
- WASSMER, S. C. & GRAU, G. E. R. 2017. Severe malaria: what's new on the pathogenesis front? *International journal for parasitology*, 47, 145-152.
- WHO 2012. *Management of severe malaria: a practical handbook*, Geneva, World Health Organization.
- WHO 2014. Severe malaria. *Trop Med Int Health*, 19 Suppl 1, 7-131.
- WHO 2020a. *The potential impact of health service disruptions on the burden of malaria: a modelling analysis for countries in sub-Saharan Africa*, Geneva, World Health Organization.

- WHO 2020b. *World malaria report 2020: 20 years of global progress and challenges*, Geneva, World Health Organization.
- WHO 2021a. Global Malaria Programme.
- WHO 2021b. Malaria vaccine implementation programme.
- WHO 2021c. Protecting malaria high-risk groups.
- WICHERS, J. S., WUNDERLICH, J., HEINCKE, D., PAZICKY, S., STRAUSS, J., SCHMITT, M., KIMMEL, J., WILCKE, L., SCHARF, S., VON THIEN, H., BURDA, P.-C., SPIELMANN, T., LÖW, C., FILARSKY, M., BACHMANN, A. & GILBERGER, T. W. 2021. Identification of novel inner membrane complex and apical annuli proteins of the malaria parasite *Plasmodium falciparum*. *Cellular Microbiology*, 23, e13341.
- XIE, S. C., DOGOVSKI, C., HANSSSEN, E., CHIU, F., YANG, T., CRESPO, M. P., STAFFORD, C., BATINOVIC, S., TEGUH, S., CHARMAN, S., KLONIS, N. & TILLEY, L. 2016. Haemoglobin degradation underpins the sensitivity of early ring stage *Plasmodium falciparum* to artemisinin. *J Cell Sci*, 129, 406-16.
- YANG, T., YEOH, L. M., TUTOR, M. V., DIXON, M. W., MCMILLAN, P. J., XIE, S. C., BRIDGFORD, J. L., GILLETT, D. L., DUFFY, M. F., RALPH, S. A., MCCONVILLE, M. J., TILLEY, L. & COBBOLD, S. A. 2019. Decreased K13 Abundance Reduces Hemoglobin Catabolism and Proteotoxic Stress, Underpinning Artemisinin Resistance. *Cell Rep*, 29, 2917-2928.e5.
- YEH, E. & DERISI, J. L. 2011. Chemical rescue of malaria parasites lacking an apicoplast defines organelle function in blood-stage *Plasmodium falciparum*. *PLoS Biol*, 9, e1001138.
- ZAKAMA, A. K., OZARSLAN, N. & GAW, S. L. 2020. Placental Malaria. *Current Tropical Medicine Reports*, 7, 162-171.
- ZIMMERMANN, L., STEPHENS, A., NAM, S.-Z., RAU, D., KÜBLER, J., LOZAJIC, M., GABLER, F., SÖDING, J., LUPAS, A. N. & ALVA, V. 2018. A Completely Reimplemented MPI Bioinformatics Toolkit with a New HHpred Server at its Core. *Journal of Molecular Biology*, 430, 2237-2243.

AP2beta fw	ggtgacactatagaataactcgcgccgctaaAAATGCTCATA- TATTTAATTCCAAATAC
AP2beta rv	GCAGATCTTGATCTCAATCCTGAacctaggTGTCTGAGTTACAC- TTAAGGAAAATGC
Rab5b_coloc fw	TATATAAAATATAATTTTTAAAAGTAActcga- gATGATTGATCCGGTTAAAAGAGATTTG
Rab5b_coloc rv	ctggattatcatatggataacttgtCCTAGGAGGATTGTTATAA- TATAAACTTC
VPS45_coloc fw	TATAAAATATAATTTTTAAAAGTAActcgagATGGAGAA- TAATCCTTACGTGTTTTAAAAGC
VPS45_coloc rv	ggattatcatatggataacttgtCCTAGGTTTCTTGATAAGCTGCAAAAC- GTCTG
SLI_NLSmisloc_i nfrontWR fw	ataaatacctaatagaaatataatcaggatccccaaaaaaaaaaaaagaaaagttacgcggtg
SLI_NLSmisloc_i nfrontWR rv	acgatgcagtttagcgaaccatgcatggatccAGGAC- CAGGGTTCTCCTCAACGTCACCGCAAGTAAGAAGTGAAC- CACGACCCTCACCCctttgagattcgtcggaacacAtgataatag
ap2_alpha-loxp ohne 3xha fw	GAGATATACTTAATTA AAAACAACCCCGGGATAACTTCG- TATAGCATACATTATAC gaaaaacgaacattaagctgccatattccCTCGAGTTAGAA- GAACTCGTCAAGAAGGC
ap2_alpha_loxp gfp_n-term fw	GTTGAAGAAAATCCAGGTCCACCTAGGGGTACCatgag- taaaggagaagaacttttactggag
ap2_alpha_loxp gfp_n-term rv	GACCTTTAATTGAGTGCTTTATCATCCTAGGAGCAGCTCTAG- CAGCACCACC
cam5->nmd3 frag1 fw	caaatgatggttttctcaatttcgatatacaattatagaacaaaatatatacttg
cam5- >nmd3frag1 rv	tatatatatatcaatttttcaaaaataaa

<i>cam5'</i> > <i>nmd3</i> frag2 fw	taattatTTTTgaaaaaattgatatatataGTTGAAA- TATAAATTTCAAAAAAATG
<i>cam5'</i> > <i>nmd3</i> frag2 rv	tttctTTTTTTTTggtgccatACTAGTTTATCTTTAAAATGATATAC- GTTATAAATA
<i>sf3a2</i> 'vps_Rbsn_ Rab5b_ eea1 fw	gattatgcAccagttgcaacattaggtaccatggtgagcaagggcgaggagg
<i>sf3a2</i> 'vps_Rbsn_ Rab5b_ eea1 rv	ACATTAAGCTGCCATATCCCTCGACCCGGGTTActt- gtacagctcgccatgccg
1xNLSFRBT2A- dDSM1_F1mfel fw	GTTTTTCTTATTTATATATTTATACCAATTGattgtattataactg- taaaaatgtgatgttg
1xNLS-FRB-T2A- dDSM1_F1_T2A rv	CAAGAACTTGGTAGTTAAACTGGCTGTCATGTCGACAGGAC- CAGGGTTCTCCTCAAC
1xNLS-FRB-T2A- DSM1_F2 dhodh fw	ATGACAGCCAGTTTAACTACCAAGTTC
1xNLS-FRB-T2A- DSM1_F2 dhodh rv	TAATATTTTTAATCTATTATTAATAA- GCTTTTAAATGCTGTTCAACTTCCCACGGAAGTCTG
coloc/misloc_ <i>sf3a2</i> sigma fw	TATATAAAATATAATTTTAAAAGTAActcgagATGTTGAATTTTA- TATTGCTACAAAATAG
col- oc/misloc_ <i>sf3a2</i> sigma rv	tggattatcatatggataactt- gtCCTAGGTATTAACTTTTTTATTTTATTTTATCTAA- TATAATG
col- oc/misloc_ <i>sf3a2</i> KIC7 fw	TAATATATAAAATATAATTTTAAAAGTAActcgagATGTCGTCAG- CAACACAATTGGG
col- oc/misloc_ <i>sf3a2</i>	ctggattatcatatggataacttgtCCTAGGAAATTTTTTGT- GAATCAAAAACAGGATAAC

KIC7 rv	
Rbsn2xFKBP fw	ACAAAGGAATTGCTATATAAGAAAcctaggTCAGGATTGA- GATCAAGATCTGCTG
Rbsn2xFKBP rv	gaaaaacgaacattaagctgccatatccCTCGAGTTAGAA- GAACTCGTCAAGAAGGCGATAG
sli2a+2xFKBP1F_ 2A_AP2S fw	ggtgacactatagaataactcgcgccgctaaCAAATAGACAAGGAAAAACC
sli2a+2xFKBP1F_ 2A_AP2S rv	TATTAAC TTTTTTATTTTATTTATTTTATC
sli2a+2xFKBP2F_ 2A_FKBPfw	GATAAAATAAATAAATAAAAAAGTTAATAC- CTAGGGCCAGGGGAGCAGCCGCA
sli2a+2xFKBP2F_ 2A_FKBP rv	AGTTTCCAGTTTCAAAGTTTCGACATCAAACAC
sli2a+2xFKBP3F_ 2A_msca fw	TTTGATGTCGAACTTTTGAAACTGGAACTATGGTGAG- TAAGGGTGAGGCAGTG
3F_2A mSca rv	AATAAACTTCCTCTTCTCCGTCGACCTTGTA- GCTCATCCATACCACCTG
2a_kic7_2x fw	gtgacactatagaataactcgcgccgctaaGATAGAACAAGAGATA- GAACACGAG
2a_kic7_2x rv	TGCTCCTGCGGCTGCTCCCCTGGCCCTAGGAAATTTTTT- GTTTGAATCAAAAACAGG
2a_sand1_2x fw	gctatttaggtgacactatagaataactcgcgccgctaaTAGATGGATTTGAAC- CTCTAC
2a_sand1_2x rv	CTCCTGCGGCTGCTCCCCTGGCCCTAGGAGATGTTATTT- GCTTTATATTATTAATAAATATC
sf3a2p40 fw	CATAATATATAAAATATAATTTTAAAAGTAAActcga- gATGGCTGTGGCCCAGCAG
sf3a2p40 rv	ctggattatcatatggataactgtCCTAGGGCGGAGTGCCTGGGGCAC

sf3a2- PlasmepsinII- mCh fw	CATAATATATAAAATATAATTTTAAAAGTAActcgagATGGA- TATTACAGTAAGAGAACATG
sf3a2- PlasmepsinII- mCh rv	ctggattatcatatggataacttgtCCTAGGTAAATTCTTTTTAGCAAGAG- CAATAC
farblosRBSN fw	CAAAGGAATTGCTATATAAGAAAcctaggTCAGGATTGA- GATCAAGATCTGC
farblosRBSN rv	TAA- TAAACTTCCTCTTCCTTCTCCGTCGACTGTCTCTAACTTTAACA ATTCAACG
F1msca fw	gattatgcAccagttgcaacattaggtaccATGGTGAGTAAGGGTGAGGC
F1msca rv	CTTGTAAGCTCATCCATACCACC
F2miniturbo_(link er) fw	GTACAGGTGGTATGGATGAGCTTTACAAGGGAA- GAGCTAAAGGTAGTGGATC
F2miniturbo rv	CATTAAGCTGCCATATCCCTCGACCCGGGTTActtttcggcagaccg- cagactg
gbpminiturbo fw	gttttttaatttcttacataTAActcgagATGCGACTTTCTAAAGTATCTG
gbpminiturbo rv	CACTGCCTCACCCCTTACTCACCATggtacctaattgtgcaactggTg- cataatctggattatcatatggataacttgtT- GTTTTCTGCTTACTTTTTCTTAATG
F1p40 fw	gttttttaatttcttacataTAActcgagATGGCTGTGGCCCAGCAG
F1p40 rv	CACTGCCTCACCCCTTACTCACCATggtacctaattgtgcaactggTg- cataatctg
F2msca fw	ATGGTGAGTAAGGGTGAGGC
F2msca rv	GAACATTAAGCTGCCATATCCCTCGACCCGGGTTACTT- GTAAAGCTCATCCATACC
Seq_OR_alpha fw	ATTAAGAACGAGCTTAAGAAGAAGC

Seq_ORalpha_rv	ACTCGCAAGCTCTAGTCTGAAGCTC
seq_OR alpha_2. fw	CATATATAATTGGAAGCTTCGGTTACC
seq_VPS45_fw	TAAGAATGATCATAAATTTATAG
seq Rab5b_rv	CATTTTCTTGTTACAAAACCTTCATG
seq_VPS45_rv	TTATCGTTATTAATATGTTCAATAG
seq_PMII_rv	ACACATAATTCATTTCTACTTTG
seqminiturbo rv	cccactcttcagctcgccgattc
3xHA_seq fw	ACCATGTACCCATACGATGTTC
BirA_75 rv	CTCTTGACATACCTAATGTTTCACC
<i>Crt</i> fw	CCGTTAATAATAAATACACGCAGTC
DHODH_42 rv	GATGCATTCATAAATGGGTTTTTC
DHODH_865 fw	GTCAAGATTTTTGAACGTATCG
DHODH_875 fw	AAAAGACATAATGGAAGCTAAGG
FKBP_253 fw	TCACCAGATTATGCATACGGTG
FKBP_276fw	CAGGCCATCCTGGCATCATC
FKBP_39 rv	TTGACCTCTTTTTGGAAATGTACG
FKBP_82 rv	CTTCCATCTTCAAGCATTCCAG
FKBPcodonad- justed_56 rv	GTAGTGAACACTACGCATGTCTGTC
FRB_216 fw	ccaagagtggcagGaagtac
FRB_251 fw	gaatgtcaaggacctcctccaagc
FRB_42 rv	AAACGAGATGCCTCTTCCAG
FRB_76 rv	tcaaacatGccttcacgttcc
GFP_272 as	CCTTCGGGCATGGCACTC

GFP_541 rv	GGTCTGCTAGTTGAACGCTTCCATCTTC
GFP_633 fw	gcccttcgaaagatccc
hDHFR_seq fw	ACCCAGGTGTTCTCTCTGATGTC
mCherry_620 fw	ctcccacaacgaggactacacc
mCherry_88 rv	GGCCGTTACGGAGCCCTCC
mScarlet_38 rv	CCCTCCATGTGCACCTTAAAACGC
mScarlet_615 fw	GTAAGCTTGATATTACAAGTCAC
Neo_40 rv	CGAATAGCCTCTCCACCCAAG
Neo_693 fw	CTTGGCGGCGAATGGGCTGACC
Neo_746 fw	TGCTTTACGGTATCGCCGCTCC
Neo_75 rv	CAGAGCAGCCGATTGTCTGTTG
pARLminus rv	CAGTTATAAATACAATCAATTGG
pARLsense 55	ggaattgtgagcggataacaattcacacagg
REP83sense	AGAAACCGTTGATTAATAATAC
Sfa32 fw	GAAGAAGCAATAAAATTTTTATG

A.2 Oligonucleotides to assess correct integration

Primer name	Sequence (5'-3')
AP-1/2 β int fw	TGGATTATCGTCACCGAACAAATTTGG
AP-1/2 β int rv	GTTTTTTTTTTGTACAAATTAATTCTCGTC
AP-2 α -3xHAint(1) fw	ATATATAGAATGCTAGCTTTTCCTCC
AP-2 α -3xHAint rv	TTACAATAATAAAAAGAGAACAGATG
AP-2 α int(2) fw	AATAAAAGACACAACAACAATAATTACAC
AP-2 σ int fw	AATTGTATAGAACAATAAATAATGTTG
AP-2 σ int rv	GGAAAAATATATCGGTCAATATGAAC
Rbsn5int fw	GATTGATAGATCGATATCGATGTGTGG
Rbsn5int rv	GAATAACACATCGACATTTTACATTTTAC
KIC7int fw	GATAGAGACAGAGATAAAGATAGAG
KIC7int rv	TACACACATGATATCATAcataAAGG
Sand1int fw	TAAGATATTTATTAGATGGAGCAG
Sand1int rv	GATAATATTAATAGTCTATGTAATATC
Rab7int fw	TAAAAAAAATTATAGGTAATTATATAAC
Rab7int rv	TACTTCTTTGTGTTTAATCCTATAATATG
GFP85 rv	ACCTTCACCCTCTCCACTGAC
pARLsense55	GGAATTGTGAGCGGATAACAATTTACACACAGG
Neo40 rv	CGAATAGCCTCTCCACCCAAG
DHODH42 rv	GATGCATTCATAAATGGGTTTTTC
pARLminus rv	CAGTTATAAATACAATCAATTGG
mSca38 rv	CCCTCCATGTGCACCTTAAAACGC

A.3 Plasmids

Generated plasmid based on the SLI-system:

SLI-based plasmids	integration
AP-1/2 β -2xFKBP-GFP-2xFKBP ^{endo}	Yes
AP-2 α -3xHA ^{endo}	Yes
N-GFP-AP-2 α ^{endo} (loxP)	Yes
N-2xFKBP-GFP-AP-2 α ^{endo} (loxP)	No
AP-2 α -GFP ^{endo}	No
AP-2 α -TGD ^{endo}	No
AP-2 σ -3xHA ^{endo}	Yes
AP-2 σ -GFP ^{endo}	Yes
AP-2 σ -2xFKBP-GFP ^{endo}	Yes
AP-2 σ -TGD ^{endo}	No
Rbsn5-2xFKBP-GFP-2xFKBP ^{endo}	Yes
Rbsn5-2xFKBP-GFP-2xFKBP ^{endo} _ndm3'NLS-FRB-T2A-hDHFR	Yes
Rbsn5-2xFKBP-GFP ^{endo} _ndm3'NLS-FRB-T2A-hDHFR	Yes
Rbsn5-2xFKBP-GFP ^{endo} _ndm3'NLS-FRB-T2A-hDHFR	Yes
KIC7-2xFKBP-mSca ^{endo} (SLI2A-based)	Yes
Sand1-2xFKBP-mSca ^{endo} (SLI2A-based)	Yes
N-2xFKBP-GFP-2xFKBP-Rab7 ^{endo}	Yes

Generated episomal plasmid:**Episomal plasmids**

sf3a2'VPS45-mCh^{epi}

sf3a2'Rab5b-mCh^{epi}

sf3a2'Rab5b-mSca_*nmd3*'NLS-FRB-T2A-DHODH

nmd3'NLS-FRB-mCh^{epi}

sf3a2'P40-mSca_*nmd3*'NLS-FRB-T2A-DHODH

crt'P40-mSca_*nmd3*'NLS-FRB-T2A-DHODH

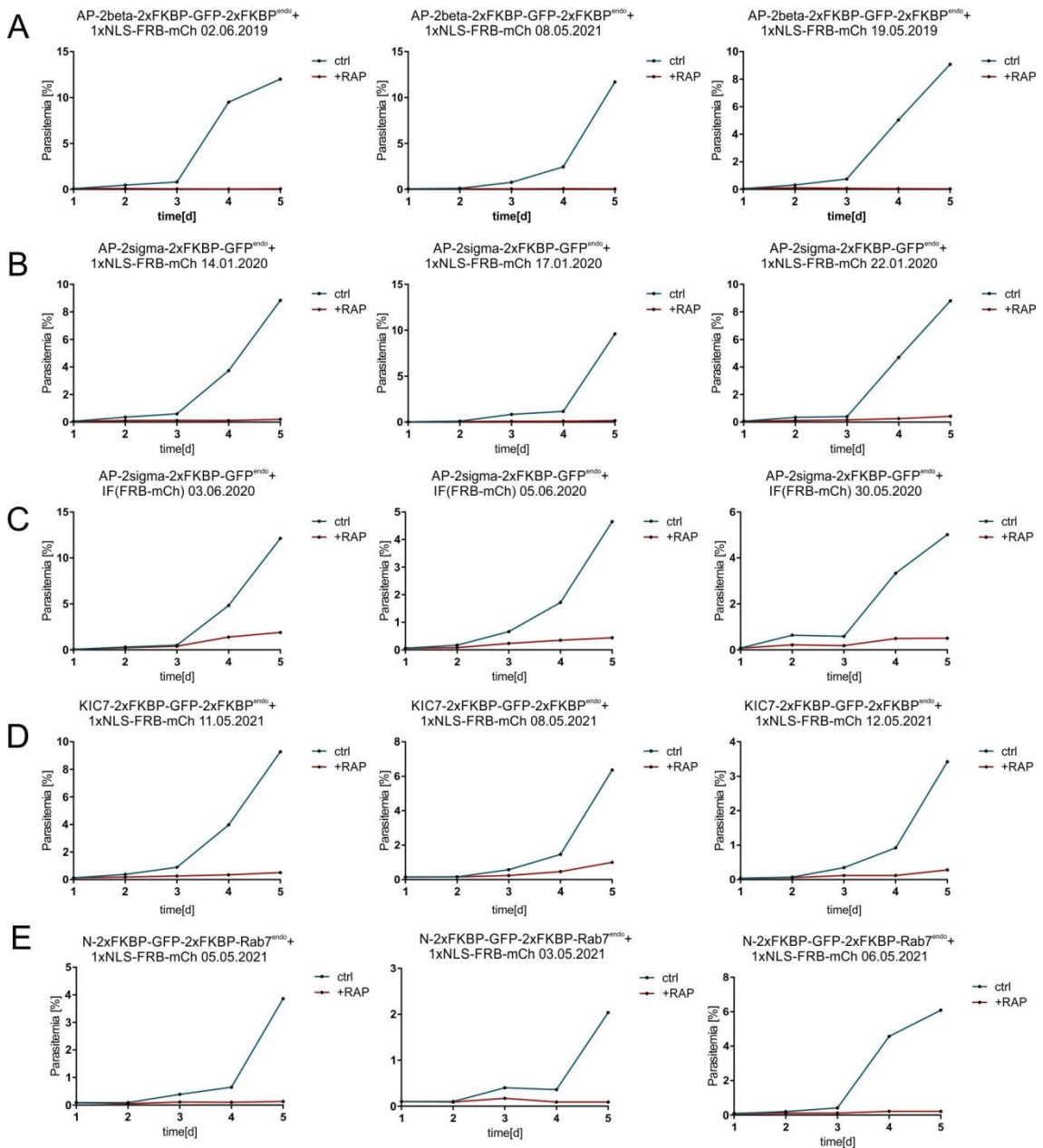
sf3a2'AP-2 σ -mCh_*nmd3*'NLS-FRB-T2A-DHODH^{epi}

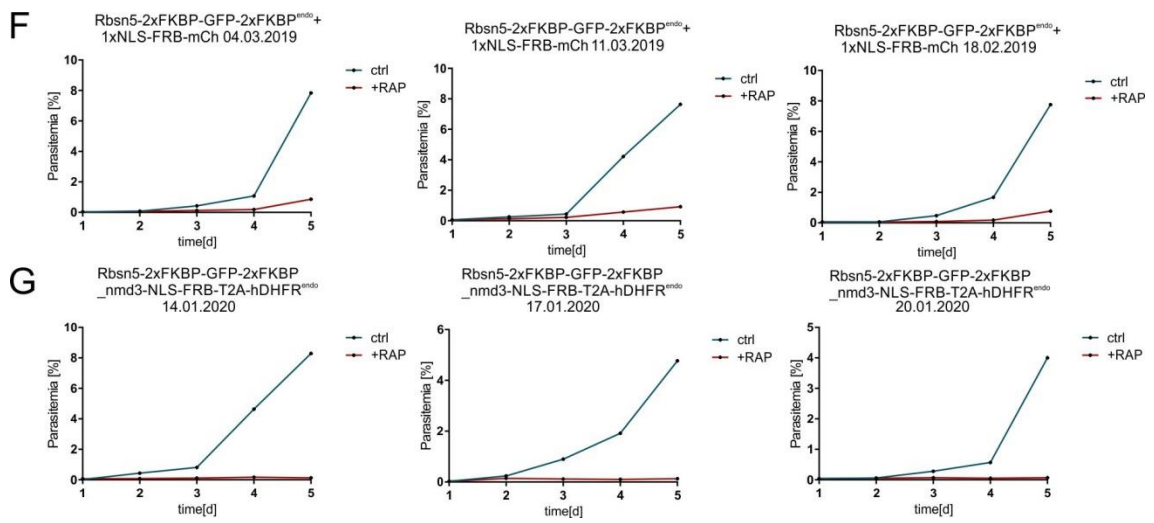
sf3a2'PMII-mCh_*nmd3*'NLS-FRB^{epi}

crt'GBP¹⁻¹⁰⁸-mSca-miniTurbo_*nmd3*'NLS-FRB-T2A-DHODH^{epi}

crt'GBP¹⁻¹⁰⁸-BirA*-mSca

Appendix B- Flow cytometry growth curves





Appendix C- Sequence alignment

Sequence alignment (ClustalOmega) of the Rab5 binding domain of *HsRbsn5* with the entire aa sequence of putative Rbsn5b of *P. falciparum*, *P. berghei*, *P. malariae*, *P. knowlesi*, and *P.vivax*:

```

H.sapiens_Rbsn5-Rab5-BD          SGPEAEFPTEEELL-----LQQIDNIKA----- 23
P.falciparum_Pf3D7_1310300     ---MIDPVKRDLTNLFLEKREMAK EEDPRKDWLKRILLNNTNDRMFLKASELKTKE 56
P.berghei_PBANKA_1408800       ---MDDKMGRDLTTPFMEQRKLAKE-ELNPRKNWLKRILINNNWSDLKLFIKSGDLKKKI 55
P.malariae_PmUG01_14027000     ---MNRISRDLTENFIEKREIAKEEMDPRKDWLKRILMNNNSFDLKMFLRAGDFKKKE 56
P.knowlesi_PKNH_1410700       ---MNDRISRDLTKSFLEKREMAKEEVDPRKNWLKRILMNNNSYDMKMFLKAGELKKKD 56
P.vivax_PVX_122345            ---MNDRISRDLTKSFLEKREMAKDEVDPRKNWLKRILMNNNSYDLKMFLKAGELKTKD 56
                                : : : *                               : : : *

H.sapiens_Rbsn5-Rab5-BD          ----- 23
P.falciparum_Pf3D7_1310300     GDYCMTCKSNVQLLYLHTKKMYCHLCEEIFCAYCVKSIDFMKDEKDYIKIRLCRNCFI 116
P.berghei_PBANKA_1408800       GDSCTNCQRSVKHIYYLSKDKIFCDICEEIIYCLYCTKYIDVMKDNQSKYIKLKLRCDFI 115
P.malariae_PmUG01_14027000     GDYCNSCKSSVNQIYYLNTNKLFCDVCEEIYCMYCVKSIDVMKDNQLKYIKVRLCKKCFI 116
P.knowlesi_PKNH_1410700       GDYCKTCKTSVKQIYYINTSKVFCVECEEIFCIYCVKTIIDVMKDSQLKYIKVRLCKNCFI 116
P.vivax_PVX_122345            GDYCKSCKTSVKQIYYINTSKVFCVECEEIFCMYCVKSIDVMKDSQLKYIKVRLCKNCFI 116

H.sapiens_Rbsn5-Rab5-BD          -----YIFDAKQCGRLDEVEVLTENLRELKHTL 51
P.falciparum_Pf3D7_1310300     YINELKYIINPNLSVDRKAIDLQNSFNDISNRYITCSNISQLNGLIILLCENNFVDF 176
P.berghei_PBANKA_1408800       YINELKCIHNPNTIDKDAIELVNNFNEISNRYITCSNISQLNGLIILLCENNFVDF 175
P.malariae_PmUG01_14027000     YINELKYIINPNLSIDKKAIDLVTNFNEISNRYITCSNVSQNLGLIILLCENNFVDF 176
P.knowlesi_PKNH_1410700       YINELKYIINPNLSIDKKAIDLVAFADEISNRYITMCSNVSQNLGLIILLCENNFVDF 176
P.vivax_PVX_122345            YINELKYIINPNLSIDKKAIDLVAFADEISSRYITMCSNVSQNLGLIILLCENNFVDF 176
                                * .. : * : * * * ..

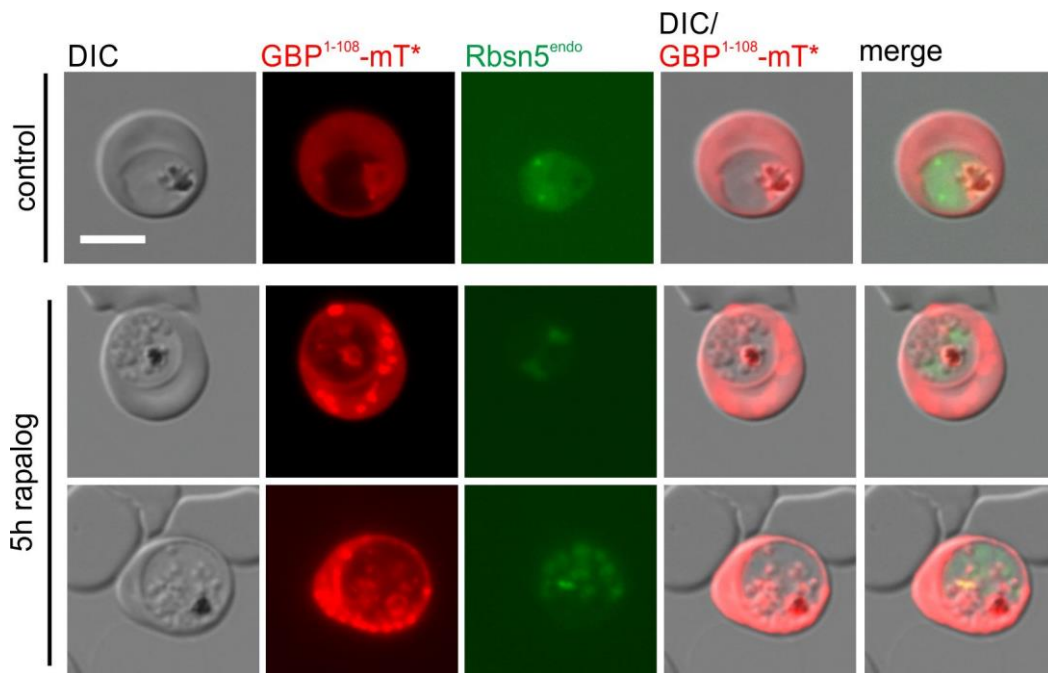
H.sapiens_Rbsn5-Rab5-BD          A-----KQKGGTD----- 59
P.falciparum_Pf3D7_1310300     KSEIKQLEEKIQHVDVFLNIMKKNNFLSDNTLILNKMGNLLLYLKIIRNKIIPSSIEV 236
P.berghei_PBANKA_1408800       KSEIDQLRGIQTDIKFLTTMKKS-KIGVNNNFILNKMKNLSQYLKIIKKNITPVAFDV 234
P.malariae_PmUG01_14027000     KIEINKLVEIIQEDVDFLNTMKKKNNFLSDNNFIINKMGKNLLLYLKIIRNKIIPDAADV 236
P.knowlesi_PKNH_1410700       KTEIKQLMDVIQNDVDFLNAKRRNFAEDNTLILNKMGNLLLYLKIIRNKIIPSSVDV 236
P.vivax_PVX_122345            KTEIKQLMDVIQHDLDLFDAMKKNNFAADNTLILNKMGNLLLYLKIIRNKIIPSAVDV 236
                                : * ..

H.sapiens_Rbsn5-Rab5-BD          ----- 59
P.falciparum_Pf3D7_1310300     LNKTKELLYKK- 247
P.berghei_PBANKA_1408800       LNNTQELLCKNK 246
P.malariae_PmUG01_14027000     LSKTKELLYKKT 248
P.knowlesi_PKNH_1410700       INKTKELLYKKK 248
P.vivax_PVX_122345            MNKTKELLYKKT 248

```

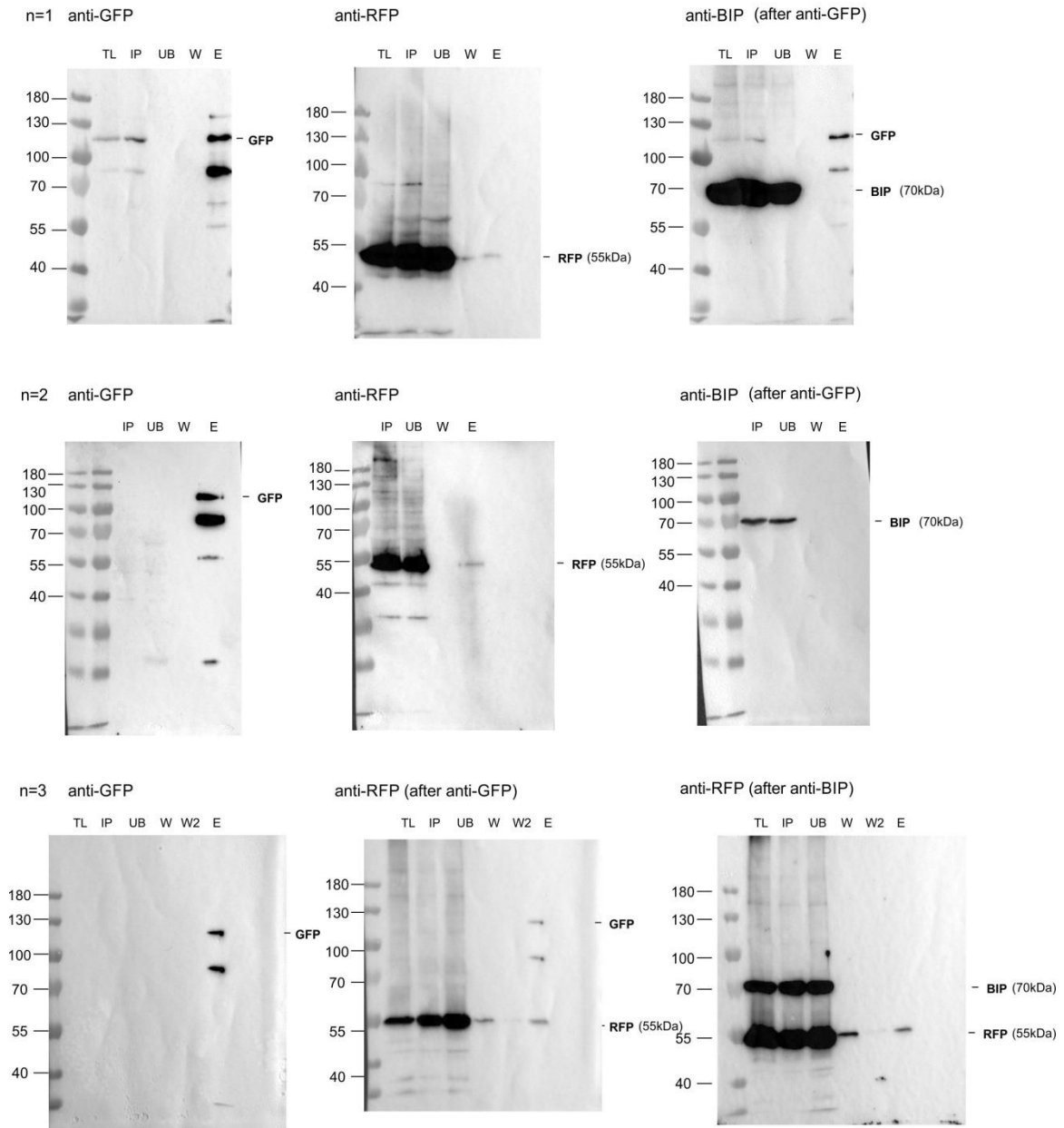
Appendix D- Live cell images

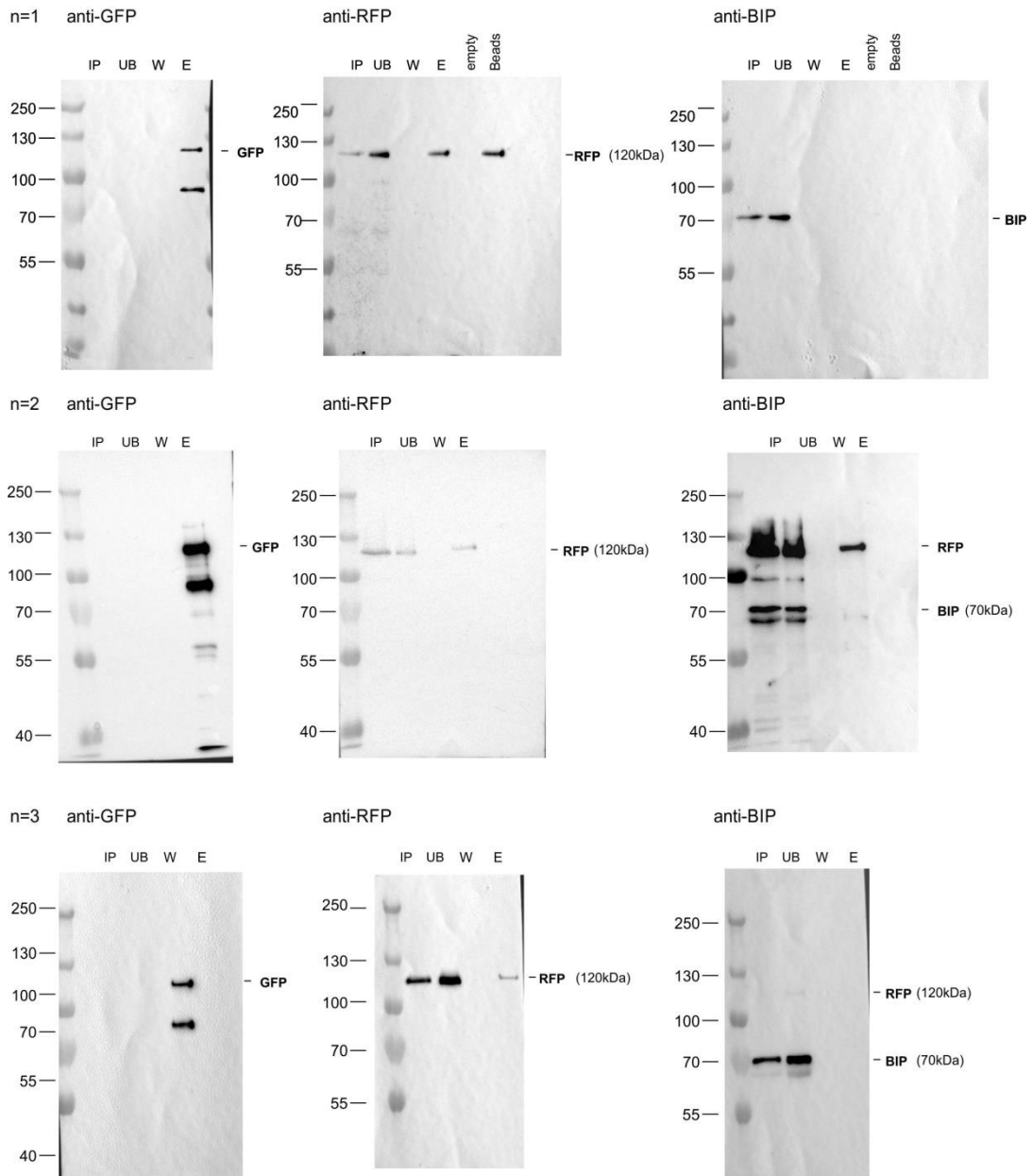
Rbsn5-2xFKBP-GFP^{endo} + *crf* GBP¹⁻¹⁰⁸-mSca-miniTurbo_*nmd3*NLS-FRB-T2A-DHODH^{epi}



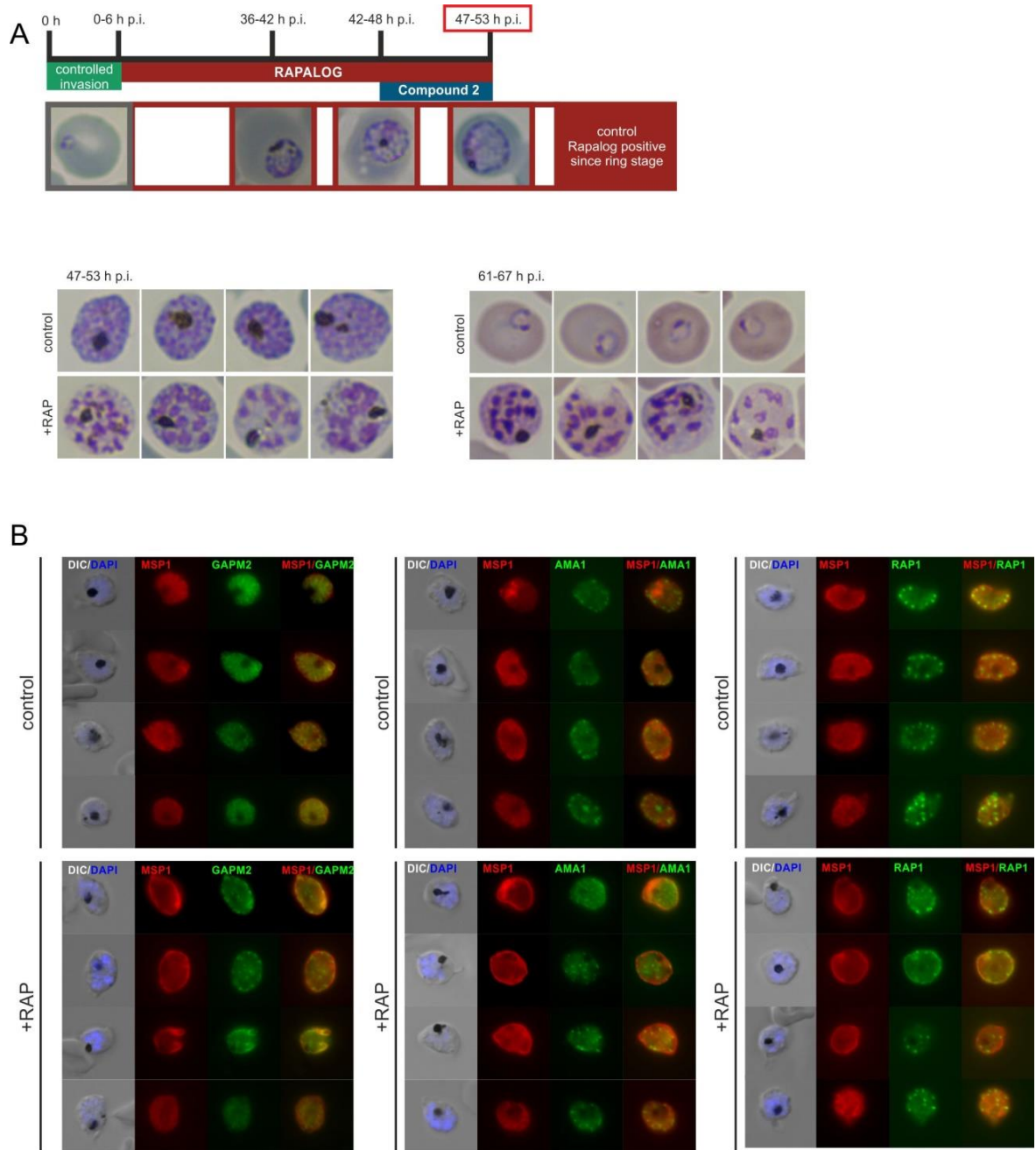
Appendix E- Co-IP

CoIP: Rbsn5-2xFKBP-GFP-2xFKBP^{endo}+Rab5b-mCh^{epi}.



CoIP: Rbsn5-2xFKBP-GFP-2xFKBP^{endo}+VPS45-mCh^{epi}:

Appendix F- Functional analysis of VPS45 in schizonts



List of publications

BISIO, H., CHAABENE, R. B., **SABITZKI, R.**, MACO, B., MARQ, J. B., GILBERGER, T.-W., SPIELMANN, T. & SOLDATI-FAVRE, D. 2020a. **The ZIP Code of Vesicle Trafficking in Apicomplexa: SEC1/Munc18 and SNARE Proteins.** *mBio*, 11, e02092-20.

SABITZKI, R., SPIELMANN, T., GRAS, S. & MEISSNER, M. 2020. **Endocytosis in *Plasmodium* and *Toxoplasma* Parasites.** *Trends Parasitol*, 36, 520-532.

BIRNBAUM, J., SCHARF, S., SCHMIDT, S., JONSCHER, E., HOEIJMAKERS, W. A. M., FLEMMING, S., TOENHAKE, C. G., SCHMITT, M., **SABITZKI, R.**, BERGMANN, B., FROHLKE, U., MESEN-RAMIREZ, P., BLANCKE SOARES, A., HERRMANN, H., BARTFAI, R. & SPIELMANN, T. 2020. **A Kelch13-defined endocytosis pathway mediates artemisinin resistance in malaria parasites.** *Science*, 367, 51-59.

JONSCHER, E., FLEMMING, S., SCHMITT, M., **SABITZKI, R.**, REICHARD, N., BIRNBAUM, J., BERGMANN, B., HOHN, K. & SPIELMANN, T. 2019. **PFVPS45 Is Required for Host Cell Cytosol Uptake by Malaria Blood Stage Parasites.** *Cell Host Microbe*, 25, 166-173.e5.

Danksagung

An erster Stelle möchte ich mich ganz besonders bei Dr. Tobias Spielmann dafür bedanken, dass er mir die Möglichkeit gegeben hat, meine Doktorarbeit in seiner Arbeitsgruppe durchzuführen. Danke, dass du mir ein so spannendes Projekt anvertraut hast.

Die regelmäßigen Treffen, dein stets offenes Ohr, dein umfangreiches Wissen und deine Hilfsbereitschaft waren von enormen Nutzen. Ich schätze es sehr, dass du dir viel Zeit für die Betreuung genommen und gleichzeitig mir große Freiheiten eingeräumt hast. Es war eine sehr lehrreiche und zugleich spannende Erfahrung, in der ich mich weiterentwickeln konnte und durfte.

Des Weiteren möchte ich mich bei meinen Betreuern und Co-Betreuern Herrn Prof. Tim-Wolf Gilberger und Dr. Paul-Christian Burda bedanken für die ergänzenden Anstöße und die motivierenden Worte. Zusätzlich danke ich Tim und Tobi für die Übernahme des Dissertationsgutachtens. Gerade weil ihr wenig Zeit zur Verfügung habt, möchte ich euch umso mehr dafür danken, dass Sie diese Aufgabe übernommen habt.

Zusätzlich möchte ich mich bei Dr. Katharina Höhn für ihre Unterstützung, die netten Gespräche und ihre Arbeit an elektronenmikroskopischen Tätigkeiten bedanken.

Danken möchte ich auch Dr. Sven Flemming, Dr. Ernst Jonscher, Dr. Marius Schmitt und allen weiteren Personen, ohne deren Vorarbeit ein Teil des Projekts heute nicht da stünde, wo es jetzt ist.

Ich bedanke mich auch bei allen ehemaligen und aktuellen Mitarbeitern der AG Spielmann und der AG Gilberger für das kollegiale, produktive und solidarische Miteinander. Durch die exzellente Atmosphäre war es immer eine Freude, zur Arbeit zu kommen. Ohne euch wäre die Zeit nur halb so schön gewesen! Ich werde viele unvergessliche Erinnerungen und Freundschaften aus dieser Zeit mitnehmen.

Abschließend möchte ich mich bei meinen Freunden und insbesondere bei meiner Familie für ihre Unterstützung bedanken. Peter, Karin, Vanessa und Clara, ich danke euch für euer Verständnis und euren Rückhalt, den ihr mir trotz eurer persönlichen Herausforderungen immer gegeben habt.